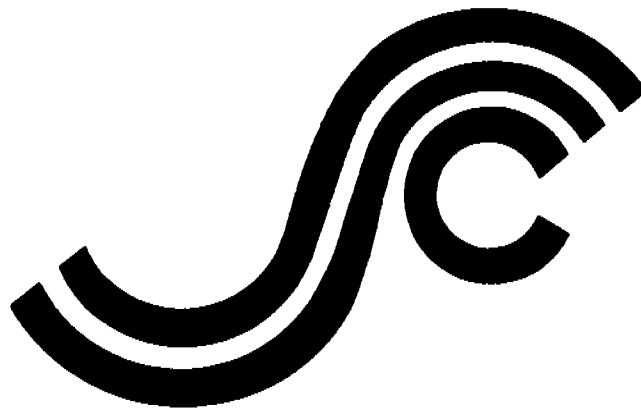


SSC-384

**POST-YIELD STRENGTH OF
ICEBREAKING SHIP
STRUCTURAL MEMBERS**



This document has been approved
for public release and sale; its
distribution is unlimited

SHIP STRUCTURE COMMITTEE

1995

C-1

SHIP STRUCTURE COMMITTEE

The SHIP STRUCTURE COMMITTEE is constituted to prosecute a research program to improve the hull structures of ships and other marine structures by an extension of knowledge pertaining to design, materials, and methods of construction.

RADM J. C. Card, USCG (Chairman)
Chief, Office of Marine Safety, Security
and Environmental Protection
U. S. Coast Guard

Mr. Thomas H. Peirce
Marine Research and Development
Coordinator
Transportation Development Center
Transport Canada

Mr. Edwin B. Schimler
Associate Administrator for Ship-
building and Technology Development
Maritime Administration

Dr. Donald Liu
Senior Vice President
American Bureau of Shipping

Mr. Robert McCarthy
Director, Survivability and Structural
Integrity Group (SEA O3P)
Naval Sea Systems Command

Mr. Thomas Connors
Acting Director of Engineering (N7)
Military Sealift Command

Dr. Ross Grahm
Head, Hydronautics Section
Defence Research Establishment-Atlantic

EXECUTIVE DIRECTOR

CDR Stephen E. Sharpe, USCG
U. S. Coast Guard

CONTRACTING OFFICER TECHNICAL REPRESENTATIVE

Mr. William J. Siekierka
Naval Sea Systems Command

SHIP STRUCTURE SUBCOMMITTEE

The SHIP STRUCTURE SUBCOMMITTEE acts for the Ship Structure Committee on technical matters by providing technical coordination for determining the goals and objectives of the program and by evaluating and interpreting the results in terms of structural design, construction, and operation.

MILITARY SEALIFT COMMAND

Mr. Robert E. Van Jones (Chairman)
Mr. Rickard A. Anderson
Mr. Michael W. Touma
Mr. Jeffrey E. Beach

MARITIME ADMINISTRATION

Mr. Frederick Seibold
Mr. Richard P. Voelker
Mr. Chao H. Lin
Dr. Walter M. Maclean

U. S. COAST GUARD

CAPT George Wright
Mr. Walter Lincoln
Mr. Rubin Sheinberg

AMERICAN BUREAU OF SHIPPING

Mr. Glenn Ashe
Mr. John F. Conlon
Mr. Phillip G. Rynn
Mr. William Hanzelek

NAVAL SEA SYSTEMS COMMAND

Mr. W. Thomas Packard
Mr. Charles L. Null
Mr. Edward Kadala
Mr. Allen H. Engle

TRANSPORT CANADA

Mr. John Grinstead
Mr. Ian Bayly
Mr. David L. Stocks
Mr. Peter Timonin

DEFENCE RESEARCH ESTABLISHMENT ATLANTIC

Dr. Neil Pegg
LCDR Stephen Gibson
Dr. Roger Hollingshead
Mr. John Porter

SHIP STRUCTURE SUBCOMMITTEE LIAISON MEMBERS

SOCIETY OF NAVAL ARCHITECTS AND
MARINE ENGINEERS
Dr. William Sandberg

NATIONAL ACADEMY OF SCIENCES -
MARINE BOARD
Dr. Robert Sielski

CANADA CENTRE FOR MINERALS AND
ENERGY TECHNOLOGIES
Dr. William R. Tyson

NATIONAL ACADEMY OF SCIENCES -
COMMITTEE ON MARINE STRUCTURES
Dr. John Landes

U. S. NAVAL ACADEMY
Dr. Ramswar Bhattacharyya

WELDING RESEARCH COUNCIL
Dr. Martin Prager

U. S. MERCHANT MARINE ACADEMY
Dr. C. B. Kim

AMERICAN IRON AND STEEL INSTITUTE
Mr. Alexander D. Wilson

U. S. COAST GUARD ACADEMY
LCDR Bruce R. Mustain

OFFICE OF NAVAL RESEARCH
Dr. Yapa D. S. Rajapaske

U. S. TECHNICAL ADVISORY GROUP TO THE
INTERNATIONAL STANDARDS ORGANIZATION
CAPT Charles Piersall

MASSACHUSETTS INSTITUTE OF TECHNOLOGY
CAPT Alan J. Brown

STUDENT MEMBER

Mr. Jason Miller
Massachusetts Institute of Technology

SSC-384 Post-Yield Strength of Icebreaking Ship Structural Members

Ship Structure Committee 1995

SD

Member Agencies:

*American Bureau of Shipping
Defence Research Establishment Atlantic
Maritime Administration
Military Sealift Command
Naval Sea Systems Command
Transport Canada
United States Coast Guard*



Address Correspondence to:

Executive Director
Ship Structure Committee
U.S. Coast Guard (G-MMS/SSC)
2100 Second Street, S.W.
Washington, D.C. 20593-0001
Ph:(202) 267-0003
Fax:(202) 267-4816

An Interagency Advisory Committee

SSC-384
SR-1380

23 October, 1995

POST-YIELD STRENGTH OF ICEBREAKING SHIP STRUCTURAL MEMBERS

In this project an icebreaker hull, as modified to meet the requirements of the proposed Canadian Arctic Ship Pollution Prevention Regulations (ASPPR), was modeled. The model was then given a load which was extreme enough to cause some minor plastic deformations of the degree which would be allowed under ASPPR. Through analysis it was determined that the load at which main frame buckling would occur was less than that which had been anticipated. This was interpreted to be due to the progressive yielding of the surrounding structure.

Through this and other work the ASPPR will be reviewed for adequacy. This study will also be used to determine how global effects can be applied to local area models of ship structures to avoid the need to model the entire vessel structure.

This project was funded by the Canadian Transportation Development Centre and given to the Ship Structure Committee to allow a wider distribution of the results.



J. C. CARD
Rear Admiral, U.S. Coast Guard
Chairman, Ship Structure Committee

1. Transport Canada Publication No. TP11837E		2. Project No. 7720		3. Recipient's Catalogue No.	
4. Title and Subtitle SSC-384 Post-Yield Buckling of Icebreaking Ship Structural Members		5. Publication Date February 1994		6. Performing Organization Document No. TR-94-02	
		7. Author(s) C.G. DesRochers, E.J. Crocker, R. Kumar, D.P. Brennan, B. Dick and S. Lantos		8. Transport Canada File No. 1460-310	
9. Performing Organization Name and Address Martec Limited 1888 Brunswick Street Suite 400 Halifax, NS B3J 3J8		10. DSS File No. XSD90-00268-(673)		11. DSS or Transport Canada Contract No. T8200-0-0561/01-XSD	
		12. Sponsoring Agency Name and Address Transport Development Centre (TDC) Guy Faureau Complex 200 Rene Levesque Blvd. West West Tower, Suite 601 Montreal, Quebec H2Z 1X4		13. Type of Publication and Period Covered Final Report	
		14. Project Officer Mr. Ian Bayly			
15. Supplementary Notes (Funding programs, titles of related publications, etc.) Cospponsored by the National Energy Board. Direction from a project committee consisting of representatives from TDC, Coast Guard (Coast Guard Northern, Ship Safety and Fleet Systems), Canadian Navy Defense Research Establishment Atlantic, and the project team.					
16. Abstract The proposed ASPPR regulations allow a certain amount of plastic deformation of the structure under extreme ice loads. The buckling criteria employed in the regulations has factors to take into account some of the nonlinear effects associated with exceeding the linear range of material properties. This project is an exploratory investigation into the post-yield behaviour of icebreaking vessels with the underlying objective to determine whether or not the regulations are adequate in regards to buckling. The project consists of modelling two areas of the MV Arctic under a ASPPR calculated ice load of total magnitude F_{max} . The main frames were redesigned locally to conform to the proposed ASPPR regulations. An analysis was performed using the finite element program ADINA and consisted of a nonlinear static analysis using the arc-length method (load-displacement control). Plasticity was found to initiate in the main frames at a load of about $.7F_{max}$. Buckling was found to occur in the main frames at a load level of approximately $1.2 * F_{max}$. The load required to cause buckling calculated using linear assumptions was significantly higher indicating a substantial degradation of buckling strength associated with the progression of yielding through the structure. The structure was found to be capable of carrying further load through membrane strength in the plating. The analysis accounts for global ship effects in the local area by modelling the entire MV Arctic using the program MAESTRO. Conclusions were drawn as to how the global effects can be included in the local mode without the requirement of modelling the entire ship.					
17. Key Words Post-Yield Buckling, Icebreaking Ship Structures, Nonlinear Analysis, ASPPR, MV Arctic, Main Frames, Imperfections, Arc-Length Method			18. Distribution Statement Distribution is unlimited; available from: National Technical Information Service U. S. Dept of Commerce Springfield, Va 22151		
19. Security Classification (of this publication) Unclassified		20. Security Classification (of this page) Unclassified		21. Declassification (date)	22. No. of Pages 286
				23. Price \$36.50 Paper	



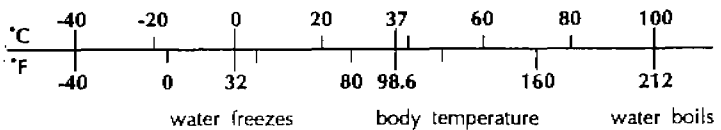
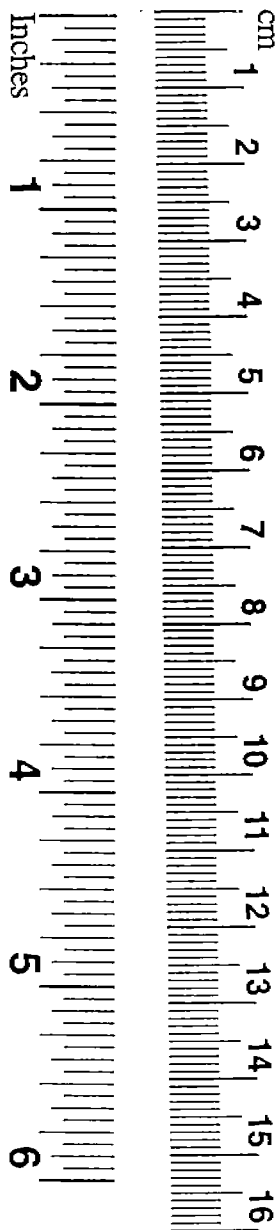
METRIC CONVERSION CARD

Approximate Conversions to Metric Measures

Symbol	When You Know	Multiply by	To Find	Symbol
LENGTH				
in	inches	2.5	centimeters	cm
ft	feet	30	centimeters	cm
yd	yards	0.9	meters	m
mi	miles	1.6	kilometers	km
AREA				
in ²	square inches	6.5	square centimeters	cm ²
ft ²	square feet	0.09	square meters	m ²
yd ²	square yards	0.8	square meters	m ²
mi ²	square miles	2.6	square kilometers	km ²
	acres	0.4	hectares	ha
MASS (weight)				
oz	ounces	28	grams	g
lb	pounds	0.45	kilograms	kg
	short tons (2000 lb)	0.9	metric ton	t
VOLUME				
tsp	teaspoons	5	milliliters	mL
Tbsp	tablespoons	15	milliliters	mL
in ³	cubic inches	16	milliliters	mL
fl oz	fluid ounces	30	milliliters	mL
c	cups	0.24	liters	L
pt	pints	0.47	liters	L
qt	quarts	0.95	liters	L
gal	gallons	3.8	liters	L
ft ³	cubic feet	0.03	cubic meters	m ³
yd ³	cubic yards	0.76	cubic meters	m ³
TEMPERATURE (exact)				
°F	degrees Fahrenheit	subtract 32, multiply by 5/9	degrees Celsius	°C

Approximate Conversions from Metric Measures

Symbol	When You Know	Multiply by	To Find	Symbol
LENGTH				
mm	millimeters	0.04	inches	in
cm	centimeters	0.4	inches	in
m	meters	3.3	feet	ft
m	meters	1.1	yards	yd
km	kilometers	0.6	miles	mi
AREA				
cm ²	square centimeters	0.16	square inches	in ²
m ²	square meters	1.2	square yards	yd ²
km ²	square kilometers	0.4	square miles	mi ²
ha	hectares (10,000 m ²)	2.5	acres	
MASS (weight)				
g	grams	0.035	ounces	oz
kg	kilograms	2.2	pounds	lb
t	metric ton (1,000 kg)	1.1	short tons	
VOLUME				
mL	milliliters	0.03	fluid ounces	fl oz
mL	milliliters	0.06	cubic inches	in ³
L	liters	2.1	pints	pt
L	liters	1.06	quarts	qt
L	liters	0.26	gallons	gal
m ³	cubic meters	35	cubic feet	ft ³
m ³	cubic meters	1.3	cubic yards	yd ³
TEMPERATURE (exact)				
°C	degrees Celsius	multiply by 9/5, add 32	degrees Fahrenheit	°F



4

TABLE OF CONTENTS

VOLUME I

1.	INTRODUCTION	1-1
2.	LITERATURE REVIEW OF POST-YIELD BUCKLING	2-1
2.1	Sources of Information	2-1
2.2	List of References	2-2
2.3	Overall Observations on Ship Structural Stability	2-4
2.4	Material Relevant to Post-Yield Buckling	2-7
2.4.1	Type of Failure	2-8
2.4.2	The Yield Criteria	2-8
2.4.3	Effect of Slenderness Ratios	2-9
2.4.4	Effect of Stiffener/Plate Area Ratio	2-9
2.4.5	Effect of Imperfections on the Strength of Ship Hulls	2-11
2.4.6	Effect of Residual Stresses on the Strength of Ship Hulls	2-11
2.4.7	Effect of Different Load Components	2-14
2.4.8	Numerical Analysis Techniques	2-14
2.5	Summary and Conclusions	2-17
3.	SURVEY OF TYPICAL ICE DAMAGE AND SELECTION OF CANDIDATE SHIP	3-1
3.1	Sources of Information	3-1
3.2	Selection of Candidate Ship for Modelling	3-1
4.	METHODOLOGY FOR THE ANALYSIS OF THE M.V. ARCTIC	4-1
4.1	Overall Description of the M.V. Arctic Structure	4-1
4.1.1	Material and Elastic Properties	4-1
4.2	Loads	4-3
4.3	Overall Modelling Philosophy	4-3
4.3.1	MAESTRO Analysis Procedure	4-6
4.3.2	ADINA Analysis Procedure	4-7
4.3.3	Top-Down Method of Analysis	4-12
4.4	Boundary Conditions	4-14
4.4.1	Boundary Conditions Applied To The Overall Model	4-14
4.4.2	Boundary Conditions Applied To The Local Models	4-19
4.5	Benchmark and Test Problems	4-20
4.5.1	Conclusions	4-27
5.	MIDBODY ANALYSIS	5-1
5.1	Description of Structure	5-1
5.2	MAESTRO Analysis	5-1
5.2.1	Description of Model	5-1
5.2.2	Boundary Conditions	5-4
5.2.3	Loads	5-6
5.2.4	Analysis and Results	5-8

TABLE OF CONTENTS - Continued

5.3	ADINA Analysis of Existing Structure	5-14
	5.3.1 Description of the Model	5-14
	5.3.2 Boundary Conditions	5-14
	5.3.3 Loads	5-16
	5.3.4 Linear Analysis Results	5-16
	5.3.5 Nonlinear Analysis Results	5-20
5.4	ADINA Analysis of the Revised ASPPR Redesigned Structure	5-27
	5.4.1 Description of the Model	5-27
	5.4.2 Boundary Conditions	5-27
	5.4.3 Loads	5-27
	5.4.4 Nonlinear Analysis Results	5-30
	5.4.5 Nonlinear Analysis using a Modified Grid	5-41
5.5	Summary and Conclusions	5-48
6.	BOW ANALYSIS	6-1
	6.1 Description of Structure	6-1
	6.2 Modelling the Ship Inertial Effects in the Bow Area	6-2
	6.3 MAESTRO Analysis	6-7
	6.3.1 Description of Model	6-7
	6.3.2 Boundary Conditions	6-10
	6.3.3 Loads	6-11
	6.3.4 Results	6-14
	6.4 ADINA Analysis	6-19
	6.4.1 Description of Model	6-19
	6.4.2 Boundary Conditions	6-22
	6.4.3 Loads	6-22
	6.4.4 Linear Analysis Results	6-22
	6.4.5 Non-Linear Analysis Results	6-26
	6.5 Summary and Conclusions	6-34
7.	PARAMETRIC STUDY OF THE MIDBODY REGION	7-1
	7.1 Selection of Region for Further Study	7-1
	7.2 Selection of Parameters to be Studied	7-2
	7.3 MAESTRO Analysis	7-2
	7.4 Nonlinear Analysis Results using ADINA	7-3
	7.4.1 Mainframes Modelled as Tee Sections	7-3
	7.4.2 Mainframes Modelled as Angle Sections	7-10
	7.4.3 Mainframes Modelled as 70° Flat Bar Sections	7-16
	7.4.4 Modified Slenderness Ratios of Flat Bar Sections	7-26
	7.4.5 Modified Slenderness Ratios of Canted Flat Bar Sections	7-34
	7.5 Summary and Conclusions from the Parametric Study	7-39
8.	EVALUATION OF THE COMPUTATIONAL IMPACT OF INCORPORATING STRAIN HARDENING MODULUS	8-1
	8.1 Angle Model Using MAESTRO Boundary Conditions	8-3
	8.2 Flat Bar Model Using MAESTRO Boundary Conditions	8-7
	8.3 Summary and Conclusions	8-11

6

TABLE OF CONTENTS - Continued

9.	STUDY OF BUCKLING SENSITIVITY TO BOUNDARY CONDITIONS AT THE MIDBODY	9-1
9.1	Overall Midbody FE Model Boundary Condition Study	9-1
	9.1.1 Summary of Overall Model Boundary Condition Study	9-7
9.2	Center Bay Model Boundary Condition Study	9-9
	9.2.1 Summary of Center Bay Model Boundary Condition Study	9-20
9.3	Summary of Boundary Condition Study	9-20
10.	EVALUATION OF THE EFFECT OF IMPERFECTIONS ON THE MODEL	10-1
10.1	Midpanel Model Using Fixed Rotations with In-plane Load	10-2
	10.1.1 Nonlinear Analysis of Midpanel Model with Imperfections	10-3
10.2	Overall Model Using Fixed Rotations With In-plane Load	10-8
10.3	Residual Stress Effects due to Welding	10-10
10.4	Summary of Imperfection Study	10-10
11.	SUMMARY, CONCLUSIONS AND RECOMMENDATIONS	11-1

REFERENCES

APPENDIX A: ASPPR ICE LOAD DETERMINATION FOR THE BOW AND MIDBODY REGIONS OF THE M.V. ARCTIC

APPENDIX B: BENCHMARK AND TEST PROBLEMS

APPENDIX C: RESIDUAL STRESS IN T-BUTT WELDMENT

LIST OF TABLES

- TABLE 2.1: Plate and Stiffener Initial Imperfections and Residual Stresses
- TABLE 4.1: Properties of Mild Steel
- TABLE 4.2: Recommended Integration Order for ADINA Shell Element
- TABLE 5.1: Sizes and Plate Thicknesses of Existing M.V. Arctic Midbody Scantli
- TABLE 5.2: ADINA Load Fractions for the Nonlinear Analysis
- TABLE 5.3: Sizes and Plate Thicknesses of ASPPR Redesigned Midbody Scantlings
- TABLE 5.4: ADINA Load Fractions for the Nonlinear Analysis of the ASPPR (Flat Bar) Redesigned Midbody Scantlings
- TABLE 6.1: Factored Weights for MAESTRO Modules
- TABLE 6.2: Sizes and Plate Thickness of Redesigned ASPPR Bow Scantlings
- TABLE 6.3: ADINA Load Fractions for the Nonlinear Analysis of the M.V. ASPPR Redesigned Bow Scantlings
- TABLE 7.1: Comparison of Results of Parametric Study

8

LIST OF FIGURES

- FIGURE 2.1: Types of Buckling
FIGURE 2.2: Weld-Induced Residual Stress in Cross-Section of Stiffened Plating
FIGURE 2.3: Methods of Modelling Material Nonlinearities
- FIGURE 4.1: ASPPR Ice Loads on the M.V. Arctic
FIGURE 4.2: Location of Midbody and Bow FE Models on the MV Arctic
FIGURE 4.3: Top-down Method of FE Analysis
FIGURE 4.4: Modelling Implications of Assuming Transverse Symmetry
FIGURE 4.5: Analysis Check on the Assumption of Longitudinal Symmetry About Midship
FIGURE 4.6: SXX Stress Plots for Symmetric and Antisymmetric Boundary Conditions
FIGURE 4.7: Sketch of ADINA Test Problem #1
FIGURE 4.8: Plot of FE Model and Results of Analysis of Test Problem #1
FIGURE 4.9: Sketch of ADINA Test Problem #2
FIGURE 4.10: Plot of FE Model and Load Displacement Curve for Test Problem #2
FIGURE 4.11: Line Stress Plots at the Top and Bottom of the Beam of Example Problem #2
FIGURE 4.12: Sketch of ADINA Test Problem #3
FIGURE 4.13: FE Model and Resulting Load Displacement Curve for Test Problem #3
FIGURE 4.14: SXX Stress Along a Line on the Top and Bottom of the Beam for Test Problem #3
- FIGURE 5.1: MAESTRO Model of the M.V. ARCTIC (Showing the Main Bulkheads Locations)
FIGURE 5.2: Substructuring Scheme for the MAESTRO Model Showing Locations to be Modelled in Detail
FIGURE 5.3: Symmetry Boundary Conditions for the Midbody Analysis
FIGURE 5.4: Location of the Ice Loads
FIGURE 5.5: Procedure to Apply Ice Loads to the MAESTRO Model
FIGURE 5.6: Displaced Shape of MAESTRO Model from Midbody Loads
FIGURE 5.7: Longitudinal Stress Distribution due to Still Water Bending Moment and Ice Loads Acting at the Midbody
FIGURE 5.8: Transverse Stress Distribution due to Still Water Bending Moment and Ice Loads Acting at the Midbody
FIGURE 5.9: Finite Element Model of M.V. Arctic Existing Midbody Structure Showing ASPPR Load
FIGURE 5.10: Stress Distribution from the Linear Analysis of the Existing Midbody FE Model
FIGURE 5.11: Scantling Stresses from the Linear Analysis of the Existing Midbody FE Model
FIGURE 5.12: Inside View of Displaced Shape of Outer Skin and Mainframes - Linear Analysis of the Existing Midbody FE Model
FIGURE 5.13: SYY Stress Near F_{max} - Nonlinear Analysis of the Existing Midbody FE Model
FIGURE 5.14: Displacement versus Load Fraction - Nonlinear Analysis of Existing Midbody FE Model
FIGURE 5.15: Displaced Shape Plot of the FE Model Without the Inner Skin - Nonlinear Analysis of the Existing Midbody FE Model
FIGURE 5.16: SYY Stress Distribution at Various Percentages of F_{max} - Nonlinear Analysis of Existing Midbody FE Model
FIGURE 5.17: FE Model of Redesigned Midbody Structure with Flat Bars

LIST OF FIGURES - Continued

- FIGURE 5.18: Displacement versus Load Fraction - Nonlinear Analysis of ASPPR Redesigned Midbody FE Model
- FIGURE 5.19: Progression of Yield at Various Percentages of F_{max} - Nonlinear Analysis of ASPPR Redesigned Midbody Structure
- FIGURE 5.20: Progression of Yield in the Top Stringer - Nonlinear Analysis of the ASPPR Redesigned Midbody FE Model
- FIGURE 5.21: Displaced Shape of Stringers - Nonlinear Analysis of Redesigned ASPPR Midbody FE Model
- FIGURE 5.22: SYY Stress at 140% of F_{max} - Nonlinear Analysis of ASPPR Redesigned Midbody FE Model
- FIGURE 5.23: SYY Stress on the Center Bay at Various Load Levels - Nonlinear Analysis of ASPPR Redesigned Midbody FE Model
- FIGURE 5.24: Displaced Shape of the Center Bay at Various Load Levels - Nonlinear Analysis of ASPPR Redesigned Midbody FE Model
- FIGURE 5.25: Modified Stringer Mesh - Nonlinear Analysis of ASPPR Redesigned FE Model
- FIGURE 5.26: Displacement versus Load Fraction - Nonlinear Analysis of Redesigned FE Midbody Model With a Modified Stringer Mesh
- FIGURE 5.27: Progression of Yield - Nonlinear Analysis of ASPPR Redesigned FE Model With Modified Stringer Mesh
- FIGURE 5.28: Progression of Yield in the Top Stringer - Nonlinear Analysis of ASPPR Redesigned FE Model With Modified Stringer Mesh
- FIGURE 5.29: SYY on the Center Bay at Various Load Levels - Nonlinear Analysis of ASPPR Redesigned FE Model With Modified Stringer Mesh
- FIGURE 6.1: Location of Bow Area Being Modelled
- FIGURE 6.2: MAESTRO Displaced Shape Plot; Station Sections 180 to 186
- FIGURE 6.3: MAESTRO Model Showing Modules of MV Arctic
- FIGURE 6.4: Illustration of the Distance from the Midship to the Centroid of Each Module
- FIGURE 6.5: Qualitative Illustration of the Assumption of Transverse Symmetry
- FIGURE 6.6: Ice Pressure Load as Calculated Using the Proposed ASPPR Regulations
- FIGURE 6.7: Longitudinal Stress Distribution in Outer and Inner Shells -- MAESTRO Analysis
- FIGURE 6.8: Vertical Stress in the Outer and Inner Shells -- MAESTRO Analysis Web Frame Stresses
- FIGURE 6.9: Superposition of the Bending and In-Plane Stress Components Along a Typical Web Frame
- FIGURE 6.10: ADINA Finite Element Model of Bow Panel
- FIGURE 6.11: Applied Load on ADINA Model
- FIGURE 6.12: Linear Analysis Results for Bow Panel
- FIGURE 6.13: SYY Stress Contours in Panel Structure
- FIGURE 6.14: SYY Stress in Outer Shell Plating
- FIGURE 6.15: Progression of Yielding Through the Structure
- FIGURE 6.16: SYY Stress in Mainframes at Center Bay

LIST OF FIGURES - Continued

- FIGURE 7.1: Redesigned ASPPR FE Model of the Midbody Panel Using TEE Stiffeners
- FIGURE 7.2: Displacement versus Applied Load Curves - Nonlinear Analysis of the ASPPR Redesigned TEE Section Model
- FIGURE 7.3: Displaced Shape - Nonlinear Analysis of the ASPPR Redesigned TEE Section Model
- FIGURE 7.4: Overall SYX Stress at Various Load Levels - Nonlinear Analysis of the ASPPR Redesigned TEE Section Model
- FIGURE 7.5: Center Bay SYX Stress at Various Load Levels - Nonlinear Analysis of the ASPPR Redesigned TEE Section Model
- FIGURE 7.6: Progression of Yield - Nonlinear Analysis of the ASPPR Redesigned TEE Section Model
- FIGURE 7.7.: Redesigned ASPPR FE Model of the Midbody Panel Using ANGLE Stiffeners
- FIGURE 7.8: Displacement versus Applied Load Curves - Nonlinear Analysis of the ASPPR Redesigned Angle Section Model
- FIGURE 7.9: Overall and Center Bay Displaced Shapes- Nonlinear Analysis of the ASPPR Redesigned Angle Section Model
- FIGURE 7.10: Overall SXX and SYX Stresses - Nonlinear Analysis of the ASPPR Redesigned Angle Section Model
- FIGURE 7.11: Center Bay SYX Stresses - Nonlinear Analysis of the ASPPR Redesigned Angle Section Model
- FIGURE 7.12: Progression of Yield - Nonlinear Analysis of the ASPPR Redesigned Angle Section Model
- FIGURE 7.13: Redesigned ASPPR FE Model of the Midbody Panel Using Canted 70° Flat Bars
- FIGURE 7.14: Displacement versus Applied Load Curves - Nonlinear Analysis of the ASPPR Redesigned Canted 70° Flat Bar Model
- FIGURE 7.15: Overall SXX and SYX Stresses - Nonlinear Analysis of the ASPPR Redesigned Canted 70° Flat Bar Model
- FIGURE 7.16: Progression of Yield - Nonlinear Analysis of the ASPPR Redesigned Canted 70° Flat Bar Model
- FIGURE 7.17: Displaced Shape - Nonlinear Analysis of the ASPPR Redesigned Canted 70° Flat Bar Model
- FIGURE 7.18: Redesigned ASPPR FE Model of the Midbody Panel Using Flat Bars With Increased Slenderness
- FIGURE 7.19: Displacement versus Applied Load Curves - Nonlinear Analysis of the ASPPR Redesigned Increased Slenderness Flat Bar Model
- FIGURE 7.20: Progression of Yield - Nonlinear Analysis of the ASPPR Redesigned Increased Slenderness Flat Bar Model
- FIGURE 7.21: Center Bay Displaced Shape - Nonlinear Analysis of the ASPPR Redesigned Increased Slenderness Flat Bar Model
- FIGURE 7.22: Stringer Displaced Shape - Nonlinear Analysis of the ASPPR Redesigned Increased Slenderness Flat Bar Model
- FIGURE 7.23: FE Model of Midbody Panel Using Canted Flat Bars With Increased Slenderness
- FIGURE 7.24: Displacement versus Applied Load Curves - Nonlinear Analysis of Increased Slenderness 70° Canted Flat Bar Model
- FIGURE 7.25: Overall SXX and SYX Stresses - Nonlinear Analysis of Increased Slenderness 70° Canted Flat Bar Model

LIST OF FIGURES - Continued

- FIGURE 7.26: Progression of Yield - Nonlinear Analysis of Increased Slenderness 70° Canted Flat Bar Model
- FIGURE 7.27: Displaced Shape - Nonlinear Analysis of Increased Slenderness 70° Canted Flat Bar Model
- FIGURE 8.1: Types of Modelling Methods for the Nonlinear Material Properties of Steel
- FIGURE 8.2: Redesigned ASPPR FE Model of the Midbody Panel Using ANGLE Stiffeners
- FIGURE 8.3: X Displacement vs. Applied Load Curves - Nonlinear Analysis of ASPPR Redesigned Angle Section With and Without Strain Hardening
- FIGURE 8.4: SYY at Center Bay - Nonlinear Analysis of ASPPR Redesigned Angle Section With and Without Strain Hardening
- FIGURE 8.5: FE Model of Redesigned Midbody Structure with Flat Bars
- FIGURE 8.6: X Displacement vs. Applied Load Curve - Nonlinear Analysis of ASPPR Redesigned Flat Bar Section With and Without Strain Hardening
- FIGURE 8.7: Overall SYY Stresses - Nonlinear Analysis of ASPPR Redesigned Flat Bar Section With and Without Strain Hardening
- FIGURE 9.1: Boundary Conditions Used in Sensitivity Study of Midbody FE Model With Angle Stiffeners
- FIGURE 9.2: X Displacement vs. Load Curves - Nonlinear Analysis of ASPPR Redesigned Midbody Model Comparing Angle Sections With MAESTRO and Fixed Boundary Conditions
- FIGURE 9.3: SYY Stresses on the Center Bay - Nonlinear Analysis of ASPPR Redesigned Midbody Model Comparing Angle Sections With MAESTRO and Fixed Boundary Conditions
- FIGURE 9.4: Angle Section Deformed Shape - Nonlinear Analysis of ASPPR Redesigned Model With Fixed Boundary Conditions
- FIGURE 9.5: Angle Section Deformed Shape - Nonlinear Analysis of ASPPR Redesigned Model With Pinned Boundary Conditions
- FIGURE 9.6: FE Model of Center Bay Section of Midbody Model Using the Redesigned ASPPR Angle Section
- FIGURE 9.7: Boundary Conditions Used in the Sensitivity Study of the Midbody Center Bay FE Model
- FIGURE 9.8: Applied Load at Each Time Step - Nonlinear Analysis of Center Bay FE Model
- FIGURE 9.9: SYY at Various Load STEPS - Nonlinear Analysis of Center Bay FE Model
- FIGURE 9.10: Mainframe Displaced Shape Plots - Nonlinear Analysis of Center Bay FE Model
- FIGURE 9.11: Applied Load at Each Time Step - Nonlinear Analysis of Center Bay FE Model With an In-Plane Load
- FIGURE 9.12: X Displacement vs. Load at the Midspan of the Mainframe - Nonlinear Analysis of Center Bay FE Model With an In-Plane Load
- FIGURE 9.13: Mainframe Displaced Shape Plots - Nonlinear Analysis of Center Bay FE Model With an In-Plane Load
- FIGURE 9.14: First Buckling Mode-Linear Eigenvalue Buckling Analysis of Center Bay FE Model With an In-Plane Load

LIST OF FIGURES - Continued

FIGURE 10.1: Second Buckling Mode Shape- Nonlinear Analysis of Midpanel Model Using Fixed Rotations and an In-Plane Load

FIGURE 10.2: Load Fraction vs. X Displacement - Nonlinear Analysis of Midpanel Model With Imperfections

FIGURE 10.3: Load Step Multiplier for Midpanel Model With Imperfections

FIGURE 10.4: Comparison of Mainframe Deflected Cross-Sections With and Without Imperfections

(THIS PAGE INTENTIONALLY LEFT BLANK)

ACKNOWLEDGEMENTS

The work carried out on this project was assisted by the advice and direction of a project committee consisting of technical representatives from TDC, Coast Guard (Coast Guard Northern, Ship Safety and Fleet Systems), the Canadian Navy, Defence Research Establishment Atlantic, and the project team (Martec and Melville Shipping). The project committee met approximately once per month for the duration of the project and discussed detailed technical issues as the analysis work progressed.

The project committee concept was found to be extremely effective. With a project such as this where the physical process modelled is complex and is subject to some interpretation, the contribution from these individuals was invaluable. The direction of study was altered somewhat throughout the project as the analysis results revealed areas of potential concern. This would not have been possible without the input of the committee. The project committee provided a vehicle which enabled Martec and Melville Shipping to ensure that the work which was produced addressed the requirements of the different organizations involved.

The authors express their thanks to the individuals who provided their time and effort to be involved in the committee and especially to Mr. Ian Bayly, project Scientific Authority and chairman of the project committee.

Project Committee Members

Ian Bayly (chairperson)	Transport Development Centre
Peter Timonin	Coast Guard Northern, Arctic Ship Safety
David Stocks	Coast Guard, Fleet Systems
Victor Santos-Pedros	Coast Guard Northern, Arctic Ship Safety
Dr. Neil Pegg	Defence Research Establishment Atlantic
Steven Yang	DND, DSE 5-4-3
Bob Dick	Melville Shipping Limited
Claude DesRochers	Martec Limited

Finally, the authors would like to express their appreciation to Ms. Barbara Campbell for her work in the preparation of an extensive amount of very detailed color figures.

(THIS PAGE INTENTIONALLY LEFT BLANK)

SUMMARY

This work presents the results of an investigation into the post-yield buckling response of ship structures. The principal objective of this work is to gain an understanding of post-yield buckling of primary structure. A secondary objective is to check the proposed Canadian Arctic Shipping Pollution Prevention Regulations (ASPPR) with regards to the adequacy of the design of primary structure.

A literature review was first performed to determine the most recent work (post 1987) carried out with respect to the post-yield buckling of ship structures. Most papers regarding ship structural instability have little information specifically on post-yield buckling. However, because other types of instabilities such as post-buckling have response parameters common to post-yield buckling, much of the information was pertinent to this study.

The bulk of the work involved a numerical investigation into the post-yield buckling response of ship structure to an iceload. The icebreaker, M.V. Arctic, was chosen for this investigation. The post-yield buckling response is determined by performing numerical analyses of both the original M.V. Arctic structure and M.V. Arctic structure redesigned to the proposed ASPPR. The numerical analyses consisted of a linear finite element (FE) analysis of a global model of the M.V. Arctic, and a series of nonlinear FE analyses of models of local structure of two regions (midbody and bow) of the M.V. Arctic.

The global FE model of the M.V. Arctic includes all the principal structural members which contribute to the hull structural stiffness. Transverse symmetry is assumed about a bow to stern vertical plane and longitudinal symmetry is assumed about a lateral symmetry plane located at the midship section of the vessel. A boundary condition is applied to the midship keel to prevent unconstrained rigid body vertical translation of the vessel.

The applied loads consist of three components; a still water bending moment, a hydrostatic pressure load, and an iceload of total magnitude, F_{max} . The worst case for ice damage due to buckling is when the structural members above the neutral axis are in compression. This condition is achieved when the vessel is subjected to a sagging hull girder bending moment and the hold where the ice load is acting is empty. A draft of 35.85 ft is used to calculate the hydrostatic loading. The sagging still water bending moment applied to the M.V. Arctic is 0.48×10^6 Ft LTons at the midship of the vessel. The ice loads were calculated using the proposed ASPPR regulations.

The global FE analysis of the M.V. Arctic was performed using the FE program, MAESTRO. The predicted longitudinal stress is approximately -9550 lb/in^2 . The transverse stress is predicted to be between -9550 lb/in^2 and $-13000.00 \text{ lb/in}^2$.

The nonlinear FE analyses of the local midbody structure of the M.V. Arctic was then performed using a procedure called the "top-down" method. In this procedure a nonlinear model of the M.V. Arctic local structure is created using the FE program, ADINA. The local model is analyzed using the applied iceload and the displacements predicted from the global model (MAESTRO) as boundary conditions. The local response therefore incorporates the effects of the global response of the ship. The method of solution used for the ADINA nonlinear analyses is the Load Displacement Control (LDC) method. The steel is assumed to behave as elastic-perfectly plastic using von Mises failure criteria.

The boundaries of the local ADINA model are defined with one web frame spacing forward and aft beyond the bay of interest, and one stringer spacing above and below the bay. This results in a 3x3 grid of panel bays to accurately model the response of the center bay.

In the nonlinear analysis of the original M.V. Arctic structure, yielding begins at approximately at $0.70 F_{max}$. This occurs at the (midspan) intersection of the web and flange of the main frames which is directly under the ice load. The structure continues to carry incremental load until, at $1.06 F_{max}$, this frame buckles through tripping.

Following the analysis of the original M.V. Arctic scantlings, an analysis was carried out on the same midbody region with the scantlings redesigned according to the proposed ASPPR. To make it easier to understand the reasons for departure from the response of the original midbody structure, as few changes as possible were made to the structure. This decision resulted in changes the main frames only. Flat bars were used as the main frame section with the same frame spacing as the original frames. The stringers and deep webs were not changed from the original scantlings. The extent of the top-down model, iceload, and boundary conditions are the same as for the FE model of the original structure.

In the nonlinear analysis of the the proposed ASPPR redesigned model, yielding starts at approximately at $0.70 F_{max}$ at the extreme fibre of the flat bar main frame under the maximum applied iceload. The yielding in the main frame progresses toward the outer hull until, at $1.70 F_{max}$, an instability appears in a stringer at the point where it intersects with the frame to which the maximum iceload is applied. The flat bar main frames remain very stable throughout the entire load sequence.

Following the midbody analysis, a nonlinear FE analysis was carried out on a model of the local bow structure of the M.V. Arctic. The bow main frames were redesigned to the proposed ASPPR, and the same "top-down" procedure was used to include the global ship response from the MAESTRO analysis. Inertial effects were also modelled.

The nonlinear analysis of the bow model does not predict failure due to buckling. It was found that a large decrease in stiffness occurs in the whole panel near $0.8 F_{max}$. This is associated with extensive yielding. Following this, yielding progresses quickly until at approximately $1.05 F_{max}$ almost all of the panel is plastic.

The final aspect of the investigation was performing a limited parametric study on the midbody structure. Nonlinear analyses were carried out to study the differences in the response from : using different cross-sections designed to the proposed ASPPR; including a strain hardening modulus; including imperfections, and; varying the global ship response on the local panel.

Based upon the results of the parametric study of the main frame sections, all ASPPR designed sections are stable at F_{max} . Flat bar frame sections are predicted to provide the best stability and carry the greatest load before failure. Angle sections were determined to be the least stable. Increasing the slenderness of uncanted flat bar main frames reduces the post-yield stability of the frames, and the maximum load that the structure can carry. Finally, when flat bars are canted their post-yield stability increases, however, the maximum load that the structure can carry does not change significantly.

The effect of the global ship response upon the local response was studied. It was found that the post-yield buckling response of the main frames of the M.V. Arctic is greatly effected by the contribution from the global ship response. This response does not seem to significantly depend upon

the stiffness of the structure outside of the deep webs and stringers that immediately bound the local bay in which the main frames are located.

The use of a strain hardening modulus has a visible effect on the stresses in a model with stiffeners modelled as flat bars and a much less visible effect on the stresses in a model with stiffeners modelled as angle sections. The buckling response of both models (flat bars and angles) is not significantly affected by using a strain hardening modulus.

The use of imperfections derived from a linear eigenvalue buckling analysis do not produce any significant changes in the nonlinear response of the main frames in the midbody FE model of the M.V. Arctic. Instabilities appear at approximately the same load levels with and without imperfections. The response and maximum loads after the development of the instability are very similar.

In general, the results of this investigation show that all main frame sections designed to the proposed ASPPR regulations remain stable up to the design ice load of F_{max} . This is after substantial yielding of the main frames (starting at approximately $0.7 F_{max}$).

The type of main frame section that seems to be of most interest with respect to possible use in the design of ships scantlings (that are expected to experience yielding) is the flat bar. Flat bars increased their stability through yielding and are most likely the least expensive section to fabricate. All other analyzed sections decreased their stability through yielding.

One of the most important conclusions from this investigation is that the local response of the ship is significantly affected by the global response resulting from the iceload.

(THIS PAGE INTENTIONALLY LEFT BLANK)

1. INTRODUCTION

In 1972 the Arctic Shipping Pollution Prevention Regulations were first published. This was partly in response to two Arctic voyages of the Manhattan during 1969 and 1970. Subsequent revisions and amendments to these regulations did not radically change the structural requirements.

During the late 1970s and early to mid 1980s there was a substantial construction boom for ships to be involved in Arctic icebreaking. These ships included the MV ARCTIC, KIGORIAK, ROBERT LEMEUR, TERRY FOX, and IKALUK as well as several Canadian Coast Guard (CCG) icebreakers. The experience gained from the activities of these icebreaking ships showed that the ASPPR structural requirements were inadequate and required substantial modification.

In 1985 the commission of the Coast Guard formed a committee composed of government and industrial representatives to review the existing regulations (ASPPR) and to propose revisions. In 1989 the revisions proposed by the committee were published.

The proposed ASPPR requirements lean heavily on a specific design approach which recognizes that the material properties, defined loads, and design philosophy must be interlinked. In addition, while global structure is important, it has been found through the inspection of ice damaged vessels that failure occurs consistently in the supporting structure rather than the hull plating. This failure demonstrates itself in the form of tripping or buckling which typically escalates into major collapse of a large structural panel. An important focus of the proposed ASPPR regulations is to design the supporting structure for the prevention of tripping or buckling.

The proposed ASPPR regulations recognize that a certain amount of plastic deformation of the structure should be permissible to meet design requirements under extreme ice loads. Consequently, the buckling criterion employed in the regulations has factors to take into account some nonlinear effects associated with exceeding the linear range of material properties. The methods employed in the regulations can now be used to design a structure which would previously have been unacceptable. It is a requirement that an understanding of the failure mechanism be developed such

that confidence in the regulations can be realized. Developing this understanding was the primary objective of this project.

Consider the case where an ice load encountered by an icebreaker is of sufficient magnitude to cause yielding in the area of load application. As the materials experience local yielding, the structure becomes unable to support additional loads by the same mechanism and the incremental loads are redistributed to other areas of the structure. This has two effects: 1) the yielding causes changes in the local stiffness of the structure; and 2) the load distribution on the structure changes.

Among other effects, ship structures are designed such that buckling of scantlings does not occur. For example, in a conventional ship design, mainframes would be designed such that they do not buckle under design loads. The problem that we wish to address in this project comes from the fact that the stiffness of the mainframes undergoes changes as yielding occurs. Combined with this, the incremental loads normally carried by the mainframes are redistributed to other parts of the structure, which could result in an increase in compressive forces in the plating to which the frames are attached. The end result is that the mainframes could be much less stiff than in their original design and could be subjected to a set of loads substantially different from the design loads. One result of these changes is that the structure could experience nonlinear buckling even though it has been designed to resist linear buckling.

The main objective of this project was to model the post-yield buckling behaviour of a stiffened hull structure subjected to ice loading and to determine the effect of yielding on its buckling characteristics. The secondary objective was to establish simplified modelling procedures for post-yield buckling of ship stiffened panel structures.

The first step in the project was to conduct a literature review of current methods employed in the post-yield buckling analysis of ship structures. The results of this review are presented in Chapter 2 along with a list of references.

The next step in the project was to select a candidate ship for modelling. This selection was prefaced by a survey of typical ice damage which has been encountered in Canadian waters over the past 15 years. The survey and selection process are described in Chapter 3.

In Chapter 4 of this report the analysis methodology is described. This chapter details the steps undertaken in performing the analysis and describes the assumptions made.

Two local areas of the ship are analyzed — a midbody area and an area in the bow. The midbody analysis is described in Chapter 5 and the bow analysis is described in Chapter 6.

A parametric study was undertaken to determine the effect of varying certain parameters on the stability of the structure following the onset of yielding. This study is presented in Chapter 7.

Chapter 8 describes the effect of incorporating a strain hardening modulus into the numerical finite element model during the yielding process.

In achieving the secondary objective of the project (that is in establishing a simplified modelling procedure) several different modelling procedures were attempted. Effective boundary conditions are described in Chapter 9. These allow simplified modelling which yields results with reasonable accuracy.

2. LITERATURE REVIEW OF POST-YIELD BUCKLING

Prior to the commencement of the analytical component of this study, it was necessary to identify the most recent developments in the study of ship plastic stability. This was done through a literature search and review of the state-of-the-art of ship structural stability. The focus of the survey was on plastic design methodologies, buckling and tripping as it relates to a range of structural configurations. Post 1987 reports and technical papers were considered to be a primary interest.

In the project start-up meeting, it was concluded that researching information on ice loads was not required. The analysis would use the magnitudes and extent of ice loads as specified in the proposed revisions to the Arctic Shipping Pollution Prevention Regulations (ASPPR).

2.1 Sources of Information

The following sources were contacted directly or indirectly (via computer database searches) during the survey:

TRANSPORT CANADA
Library and Information Centre
2nd Floor, Place de Ville, Tower C
Ottawa, Ontario

TRANSPORT CANADA
Coast Guard Library - Fleet Systems
Canada Building
344 Slater Street, 7th Floor
Ottawa, Ontario

CISTI: CANADIAN INSTITUTE FOR SCIENTIFIC AND TECHNICAL INFORMATION
National Research Council
Montreal Road, Building M-55
Ottawa, Ontario

CISTI BRANCH AERONAUTICAL/MECHANICAL ENGINEERING
National Research Council
Montreal Road, Building M-2
Ottawa, Ontario

CISTI BRANCH INSTITUTE FOR MARINE DYNAMICS
National Research Council
Kerwin Place
St. John's, Newfoundland

ADMIRALTY RESEARCH ESTABLISHMENT
Dunfermline, Scotland

MELVILLE SHIPPING LTD. LIBRARY
Inhouse reports and documents

2.2 List of References

From the sources listed in the previous section a list of references was compiled and are as follows:

- Smith, C.S.; "Influence of Local Compressive Failure on Ultimate Longitudinal Strength of a Ship Hull", PRADS '77, Tokyo, 1977.
- Smith, C.S., Davidson, P.C., Chapman, J.C. and Dowling, P.J.; "Strength and Stiffness of Ships' Plating under In-Plane Compression and Tension", Trans. RINA, Vol. 130, 1988.
- Dow, R.S. and Smith, C.S.; "Effects on Localized Imperfections on Compressive Strength of Long Rectangular Plates", Journal Construction Steel Research, Vol. 4, No. 1, 1984.
- Chen, W.F. and Sohal, I.S.; "Cylindrical Members in Offshore Structures", Thin-Walled Structures 6, Elsevier Applied Sciences Publishers Ltd., 1988.
- Caridis, P.A. and Frieze, P.A.; "Flexural-Torsional Elasto-plastic Buckling Analysis of Stiffened Plates using Dynamic Relaxation. Part 1: Theory" Thin-Walled Structures 6, Elsevier Applied Sciences Publishers Ltd., 1988.
- Caridis, P.A. and Frieze, P.A.; "Flexural-Torsional Elasto-plastic Buckling Analysis of Stiffened Plates using Dynamic Relaxation. Part 2: Comparison with Test Results and Other Formulations" Thin-Walled Structures 7, Elsevier Applied Sciences Publishers Ltd., 1989.
- Duan, L. and Chen, W.F.; "Effective Length Factor for Columns in Unbraced Frames", Journal of Structural Engineering, Vol. 115, No. 1, 1989.
- Duan, L. and Chen, W.F.; "Design Rules of Built-Up Members in Load and Resistance Factor Design", Journal of Structural Engineering, Vol. 114, No. 11, 1988.
- Duan, L. and Chen, W.F.; "Design Interaction Equation for Steel Beam-Columns", Journal of Structural Engineering, Vol. 115, No. 5, 1989.

- Graves Smith, T.R.; "The Finite Strip Analysis of Thin-Walled Structures", Developments in Thin-Walled Structure - 3, Elsevier Applied Science Publishers Ltd., 1987.
- Reis, A.J.; "Interactive Buckling in Thin-Walled Structures", Developments in Thin-Walled Structures - 3, Elsevier Applied Science Publishers Ltd., 1987.
- Iyengar, N.G.R.; "Structural Stability of Columns and Plates", published by Ellis Horwood Limited, 1988.
- "Post-Buckling of Elastic Structures", Proceedings of the Euromech Colloquium, No. 200, Hungary, October 1985.
- "Buckling and Post-Buckling - Four Lectures in Experimental, Numerical and Theoretical Solid Mechanics", CISM Meeting, Italy, October 1985.
- Bazant, Z.P.; "Stability of Structures - Elastic, Inelastic, Fracture and Damage Theories", Oxford University Press, 1991.
- "Buckling of Structures Theory and Experiment", The Josef Singer Anniversary Volume, Elsevier Science Publishing Company, 1988.
- Barbero, E. and Raftoyiannis, I.; "Buckling Analysis of Pultruded Composite Beams", Impact and Buckling of Structures - ASME Annual Meeting, Nov. 1990.
- Chen, V.L., Wu, X.X. and Sun, C.T.; "Prediction of Buckling Loads of Stiffened Composite Panels", Impact and Buckling of Structures - ASME Annual Meeting, Nov. 1990.
- Guran, A. and Shirazi-Adl, A.; "Some Remarks Concerning the Post-Buckling Behaviour of a Compressible Column", Impact and Buckling of Structures - ASME Annual Meeting, Nov. 1990.
- Delan, Y. and Dongsheng, Q.; "The Ultimate Capacity of Stiffened Plates Loaded in Plane", Proceedings of 4th International Colloquium on Structural Stability, Beijing China, October 1989.
- Guo-Liang, Z. and Xiang, Z.J.; "Post-buckling Behaviour of Stiffened Plate", Proceedings of 4th International Colloquium on Structural Stability, Beijing China, October 1989.
- Karnikova, I., Skaloud, M. and Janus, K.; "Ultimate Load Behaviour of Longitudinally Stiffened Steel Plate Girders Subject to Stationary or Variable Repeated Patch Loading", Proceedings of 4th International Colloquium on Structural Stability, Beijing China, October 1989.
- Caridis, P.A. and Frieze, P.A.; "Torsional Buckling of Stringers of Flat Stiffened Plating and Ring-Frames of Ring-Stiffened Cylinders, Report 1", Department of Naval Architecture and Ocean Engineering, University of Glasgow, June 1982.

- Caridis, P.A. and Frieze, P.A.; "Torsional Buckling of Stiffeners in Flat Panels - Correlation Studies for Lateral Pressure and Combined Loading Tests", Department of Naval Architecture and Ocean Engineering, University of Glasgow, Sept. 1986.
- Caridis, P.A. and Frieze, P.A.; "Torsional Buckling of Stiffeners in Flat Panels - Numerical Analysis and Correlation with Results for Axial Compression Tests on Stiffened Panels", Department of Naval Architecture and Ocean Engineering, University of Glasgow, May 1985.
- Sands, G. and Caridis, P.A.; "Torsional Buckling of Flat Bar Stiffeners, Report 2", Department of Naval Architecture and Ocean Engineering, University of Glasgow, Nov. 1983.
- Caridis, P.A. and Frieze, P.A.; "Elasto-Plastic Response of Stiffened Panels in Compression using Dynamic Relaxation", Department of Naval Architecture and Ocean Engineering, University of Glasgow, 1984.
- Birman, V.; "On the Post-Buckling Behaviour of Reinforced Composite Shells", Journal of Ship Research, Vol. 34, Sept. 1990.
- Bhat, S.U.; "On the Plastic Tripping of Flatbar Stiffeners", Thin-Walled Structures 7, Elsevier Science Publishers Ltd., 1989.
- Mansour-Tehrani, F. and Graves Smith, T.R.; "A Mixed-Mode Method for Analyzing the Buckling of Partially Prismatic Thin-Walled Structures", Thin-Walled Structures 12, Elsevier Science Publishers Ltd., 1991.
- Kakol, W.; "Stability Analysis of Stiffened Plates by Finite Strips", Thin-Walled Structures 10, Elsevier Science Publishers Ltd., 1990.
- Ming, S.X. and Wenda, L.; "Post-buckling and Imperfection Sensitivity Analysis of Structures in the Plastic Range, Part I: Model Analysis", Thin-Walled Structures 10, Elsevier Science Publishers Ltd., 1990.

2.3 Overall Observations on Ship Structural Stability

Traditional allowable stress methods permit design based upon yield stress or linear buckling loads. Since the safe response of a structure ultimately depends upon the magnitude and combination of loads which cause failure, and most causes of failure are nonlinear [1], this method does not reliably predict the safe limits of all structures. A more rigorous approach, using a method called limit state design, checks the structural response against various limiting conditions. Since these conditions include the response between the elastic limit and failure (in post-yield buckling), both the mode of failure and

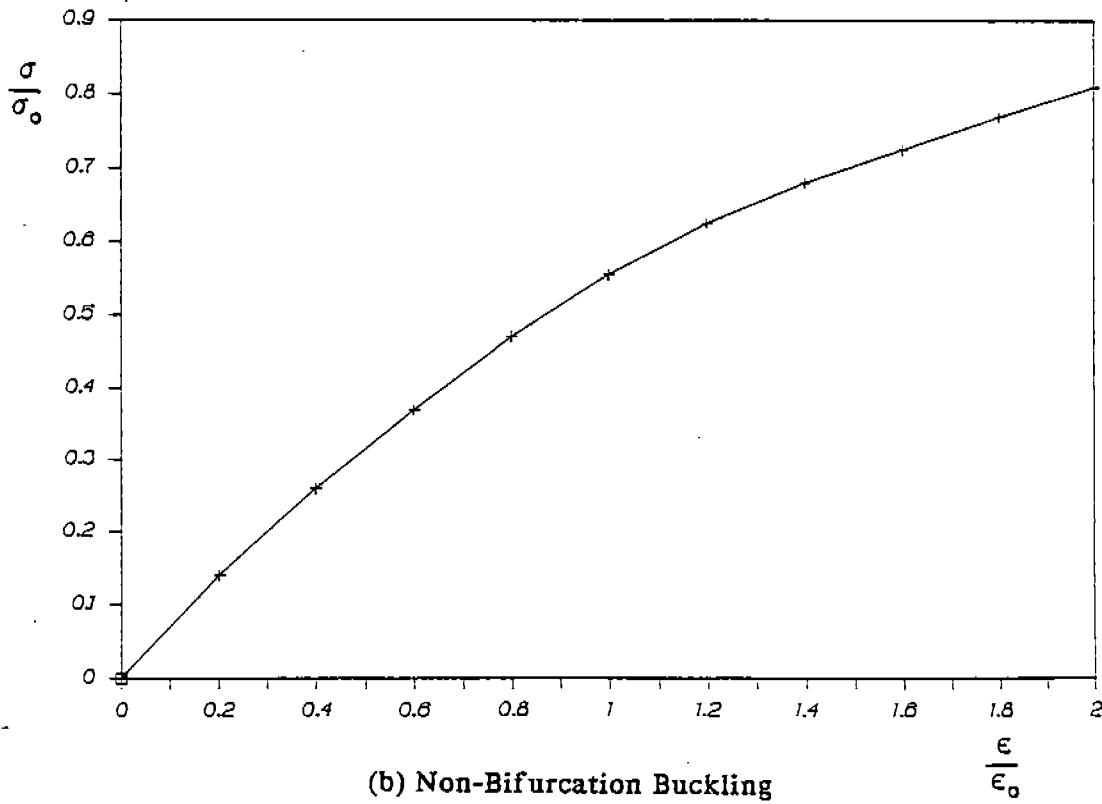
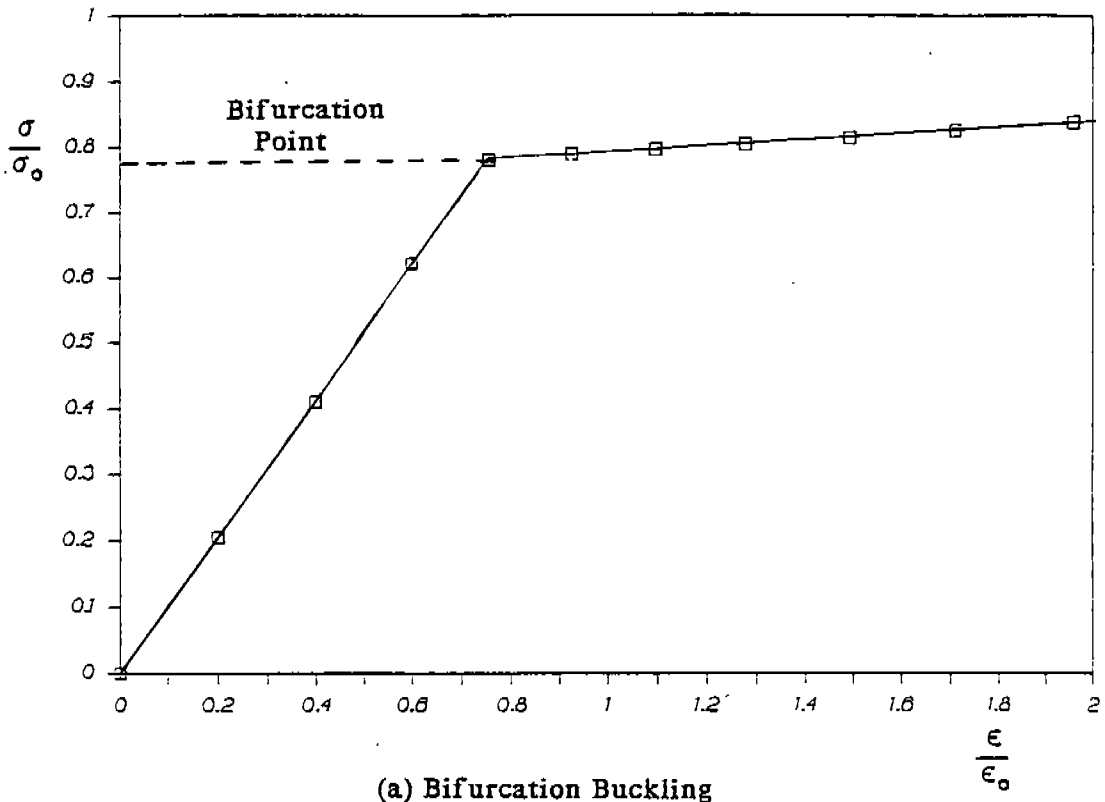


FIGURE 2.1: Types of Buckling

the response in the inelastic and large displacement range are important in determining the strength of ship hulls.

Post-yield buckling (i.e. plastic behaviour prior to buckling) and post-buckling (i.e. only elastic behaviour prior to buckling) are similar nonlinear inelastic behaviours in that two kinds of structural failure occur: material failure, and form failure [2]. Material failure results when the stresses exceed the safe load limit (usually the material yield stress) of the structure. Form failure — commonly known as buckling — results when a structure cannot maintain its original shape under a load which may also produce material failure.

Two types of buckling (form failure) exist:

- a. Bifurcation buckling; and
- b. Non-bifurcation buckling.

Bifurcation buckling is best described by a sudden departure from a linear load path. The most common example of this is the buckling of a simple column. When an axial load is gradually applied to an imperfect elastic column, the lateral stiffness of the column decreases and lateral displacement increases. For small loads these lateral deflections are relatively small and the system is linear. However, a load level is eventually reached where the lateral stiffness becomes negligible, and lateral deflections increase rapidly. This load is called the critical buckling or bifurcation load of the structure and is characterized by the point of dramatic change of slope on the effective stress-strain curve as shown in Figure 2.1(a).

Non-bifurcation buckling can most easily be described by studying the curve of Figure 2.1(b). Conversely to bifurcation buckling where both a sudden loss in lateral stiffness and a large increase in lateral displacement occur, non-bifurcation buckling exhibits a steady nonlinear (large displacement) response during the complete load range. This progressive loss in lateral stiffness and increase in lateral displacement produces no identifiable bifurcation point. However, the structure still reaches a point where the lateral stiffness is small and the structure becomes unstable and buckles.

There is much information available on ship structural stability as evidenced by the volume of information accumulated during the literature search. Although the thrust of the search was oriented towards post-yield buckling -- for which very little information was explicitly discovered -- the majority of papers dealt with either the buckling or post-buckling response of structures, with the most relevant of these from Admiralty Research Establishment (ARE), Dunfermline. Consequently, the state-of-the-art of post-yield buckling of ships structures was determined by identifying the information found in these papers which is significant to post-yield buckling. This was done by identifying parameters which have been studied that are common to buckling, post-buckling, and post-yield buckling and examining the effect of each parameter on the strength of ship hulls.

In most papers, the strength of ship hulls (including the effects of these parameters on this strength) is presented using comprehensive plots of effective stress-strain curves. Figure 2.1 illustrates typical examples of these curves.

2.4 Material Relevant to Post-Yield Buckling

Post-yield buckling and post-buckling differ in that the first nonlinear effect to occur in post-buckling is the large displacement associated with buckling, while the first nonlinear effect to occur in post-yield buckling is material yielding (which may or may not be accompanied by large displacements). Both types of nonlinear structural failure (i.e. material and form failure) take place; however, in post-yield buckling, yielding occurs first. The onset of yielding reduces both the load carrying capability and stability (stiffness) of the structure which then leads to buckling upon further loading.

Most of the papers covering nonlinear structural response study the post-buckling of plates, columns, and stiffened panels. However, many post-buckling parameters that have significant effects on the strength of ships hulls are also common to post-yield buckling. The most commonly studied parameters discovered in the survey are:

- a. Type of failure;
- b. Yield criteria;
- c. Slenderness ratios;

- d. Ratio of stiffener/plate areas;
- e. Imperfections;
- f. Residual stress;
- g. Loading types; and
- h. Numerical analysis techniques.

The effect that each of these has on the strength of ship hulls is discussed in more detail in the following sections.

2.4.1 Type of Failure

Smith [3] classifies four types of collapse for stiffened panels under compressive loads as follows:

- a. Plate failure (between stiffeners);
- b. Interframe flexural buckling;
- c. Lateral-torsional stiffener buckling (tripping); and
- d. Overall grillage buckling.

In this paper, he concludes that plating failure will most likely occur in structures with near perfect plating or with high strength stiffeners, and if tripping and overall grillage buckling are avoided, collapse will probably occur due to interframe flexural buckling. He reinforces this in a more recent paper [4] where he also concludes that interframe flexural buckling may be influenced by pre-collapse loss of plating stiffness.

Tripping is prevented by limiting the stiffener proportions to ensure that material failure occurs first [5], and overall grillage buckling is prevented by utilizing both stiff transverse frames and support from minor bulkheads [4].

2.4.2 The Yield Criteria

Most papers studied structures under longitudinal loads and, consequently, failure (yield) is based directly on the yield strength of the material. However, for structures subjected to biaxial loads, the von Mises yield criterion ([5],[7]) seemed most common.

The effect of varying the yield strength was studied by Caridis [9], who found that the relative strength (stress at failure divided by the material yield strength) of short stiffened plates reduces as the yield strength increases. Smith [4] concludes that although yield has a significant effect on collapse behaviour, the relative strengths increase slightly due to increases in the yield stress.

2.4.3 Effect of Slenderness Ratios

The slenderness of stiffened panels — defined by nondimensional ratios based on the dimensions of the plating and stiffeners — influence both the type and behaviour of buckling.

Tanaka and Endo [6] show that at critical values of slenderness, flat bar stiffener response changes from local to overall collapse.

Carlsen [14] presents similar findings for tee-bar stiffeners with low stiffener slenderness and concludes that they fail due to plastic crushing of the cross-section (i.e. local response), and further concludes that stocky stiffeners have up to 10% additional strength after initial yielding at the top of the stiffener. Stiffeners with high slenderness were shown to yield at the top of the stiffener closely followed by failure with rapid load relaxation (it is assumed that the load relaxes due to transfer to adjacent spans).

Evidence is also presented by Smith [4] that tee-bar stiffened panels with widely spaced slender columns exhibit a fast and significant loss in post-collapse load carrying ability under compressive load. The paper then suggests (through quantitative guidelines) that relatively low plate and stiffener slenderness ratios provide the highest strength and therefore should be used for primary hull structure. The disadvantage of low plate slenderness may be significant penalties in weight and fabrication costs.

2.4.4 Effect of Stiffener/Plate Area Ratio

A common conclusion was reached in studies of the effect of the ratio of the stiffener area to the plating area on the strength of ship hulls by Smith [4], Carlsen [14], and Caridis [9]: increasing

TABLE 2.1: Plate and Stiffener Initial Imperfections and Residual Stresses

Level	Plate		Stiffener			
	Maximum Initial Deformation (W_o/t)	Reduced Stress (σ_{RC}/σ_o)	$\lambda = 0.2$		$\lambda = 0.4$	
			δ_{01}/a	δ_{02}/δ_{01}	δ_{01}/a	δ_{02}/σ_{01}
Slight	$0.025 \beta^2$	0.05	0.00025	.025	0.00025	0.25
Average	$0.10 \beta^2$	0.15	0.0008	0.25	0.0012	0.25
Severe	$0.30 \beta^2$	0.30	0.0020	-1.0	0.0015	0.25

- σ_o = yield stress
- σ_{RC} = compressive stress in plating
- W_o = out-of-plane plate distortion
- a = plate long dimension
- b = plate short dimension
- t = plate thickness
- r = radius of gyration of a representative stringer acting with a strip of plating of width b
- E = modulus of elasticity
- δ_{01} = out-of-plane stiffener distortion
- δ_{02} = out-of-plane adjacent stiffener distortion
- β = plate slenderness ratio
- $\beta = b/t \sqrt{\sigma_o/E}$
- λ = column slenderness ratio
- $\lambda = \frac{a}{r\pi} \sqrt{\frac{\sigma_o}{E}}$

2-10

34

the ratio of stiffener area to plating area generally increases the strength of the stiffened panel. For lower ratios Caridis also observed that increasing the stiffener size increases the stiffener strength but reduces the plate strength.

2.4.5 Effect of Imperfections on the Strength of Ship Hulls

Deformations, caused by welding, fabrication and in-service loads, can strongly influence the compressive strength of ship hulls. These deformations are usually in the form of out-of-plane one-half sinewaves for weld-induced imperfections (in both the lateral and lengthwise plate directions) with smaller wavelengths for fabrication and in-service imperfections [8].

Imperfections can be modelled using Fourier components corresponding to elastic buckling modes generated from a Fourier analysis of actual ship plating distortions; however, Dow [10] and Smith [8] consider this unsatisfactory because it does not include local imperfections. Smith further concludes that although there is presently no satisfactory procedure to describe ship plating distortions, the deformations should be based upon actual ship distortions and accordingly defines "slight", "average", and "severe" initial imperfections as a function of plate and stiffener slenderness based upon extensive surveys of actual ship deformations. The plate and stiffener initial imperfections used by Smith are shown in Table 2.1.

Smith [3] presents evidence that initial deformations generally reduce the compressive strength of stiffened panels and modify rapid failure modes to gradual ones. He also studies the effect of adjacent bay imperfections on stiffened panels [4].

2.4.6 Effect of Residual Stresses on the Strength of Ship Hulls

Residual stresses in ship plating are typically the result of welding stringers or frames to the hull. The distribution of stresses, as shown by Smith ([3],[4],[8]), is characterized by a region of high plate tensile stresses near stiffener attachments (see Figure 2.2) balanced by lower compressive stresses in the rest of the plate. A region of stiffener tensile stress also exists near the web-hull interface. This rapidly changes to a zone of compressive stress that reduces linearly towards the stiffener flange.

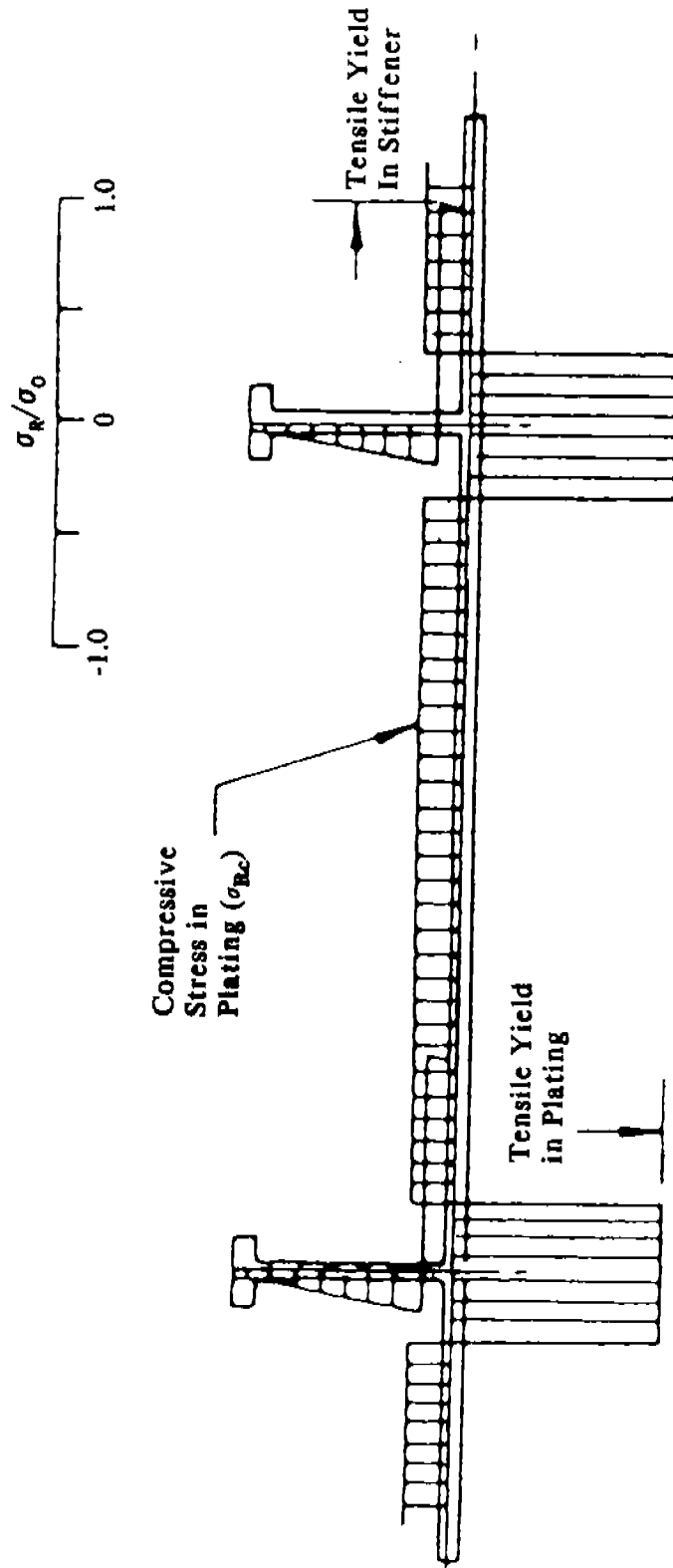


FIGURE 2.2: Weld-Induced Residual Stress in Cross-Section of Stiffened Plating

As with the initial imperfections, Smith [8] also uses "slight", "average", and "severe" levels of residual stresses based upon extensive ship surveys (see Table 2.1) to determine effective stress-strain curves. He then modifies these curves (in the tensile region) because of the presence of a discontinuity due to the effect of the tensile yield residual stress in the plate. This modification is rationalised by arguing that real life residual stresses are "shaken out" as a result of cyclic wave-induced straining. This brings up a question (to which the answer was not discovered) of whether residual stresses, if they are actually "shaken out", should be included in determining the compressive region of effective stress-strain curves.

In another paper Smith [3] concludes that residual stresses typically have little effect on the strength of plates with low or very high slenderness; cause pre-collapse loss of stiffness due to premature yielding in low and moderately slender plates; and generally reduce the compressive strength of stiffened panels.

Carlsen [14] also studied the effect of welding stresses on the lateral collapse only (i.e. excluding tripping) of stiffened panels and concludes:

- a. The plating strength is influenced by both the plate and stiffener residual stresses;
- b. The primary effect of plate residual stress is to magnify stiffener bending due to a reduction in plate stiffness;
- c. Collapse occurs near the onset of yielding at the top of stiffeners in slender stiffeners;
- d. Welding stresses above 10-15% of yield have no further effect on the strength of stocky plates, and more explicitly;
- e. Welding stresses have no effect at all on stocky plates with slender stiffeners.

Because yielding and collapse occur near the top of stiffeners (except for stocky stiffeners), he assumes that only the residual stresses in that region influence the strength. The stress (residual) distribution in the stiffener is then simplified to a constant compressive stress and numerically modelled by reducing the yield strength of the stiffener.

2.4.7 Effect of Different Load Components

The buckling response of stiffened panels has been studied using individual or combined application of in-plane (longitudinal and transverse) and lateral loads. While most studies provide effective stress-strain curves for longitudinal loads, Smith [8] also produces curves for transverse loads, and combined longitudinal and transverse (biaxial) loads.

Smith [4] also shows that lateral loads reduce the compressive strength of tee-bar stiffened panels with the most dramatic losses occurring in structures with high plate and column slenderness. If the lateral loads are concentrated, shear lag effects (for effective breadth determination) must also be included [8].

2.4.8 Numerical Analysis Techniques

Three different numerical methods are consistently used to determine the buckling response of stiffened panels. They are:

- a. Finite difference ([5],[9],[14]);
- b. Finite strip method ([11],[12]); and
- c. Finite element method ([3],[4],[8],[10]).

A combined finite element-finite strip method is also employed in one paper [13]. The present study is primarily concerned with the numerical determination of the buckling response of ship hulls using the finite element (FE) method, therefore only information pertaining to the FE method is presented.

Post-yield buckling includes both material and geometric nonlinearities. Of the papers that provided specific details of FE analyses, geometric nonlinearities are typically modelled using an updated Lagrangian formulation ([10],[15]) including the geometric stiffness terms at each load step. Equilibrium iterations are typically performed using a modified Newton-Raphson method.

The three stress-strain curves of Figure 2.3 demonstrate how material nonlinearities are modelled in most papers. In these cases the material response is modelled in one of three ways: elastic-perfectly plastic (curve 1), bilinear elasto-plastic (curve 2), or nonlinear elasto-plastic (curve 3).

For bifurcation buckling, most papers assume the pre-yield material response to be linear (pre-yield of curves 1 and 2). The post-yield response is modelled as either perfectly plastic (post-yield of curve 1) or linear plastic (post-yield of curve 2). Effective stress-strain curves similar to curve 3, which model material response throughout the full strain range, are also numerically entered into FE programs ([4], [8]). ADINA is capable of modelling the material nonlinearities of all three curves of Figure 3.

Most FE analyses that attempt to predict the structural response in the post-buckled region by using applied forces encounter numerical problems either due to a non-positive definite stiffness matrix following bifurcation or an inability to maintain equilibrium near failure. Smith [4] eliminates these numerical problems in the post-buckled range by first utilizing displacements instead of loads. If failure is dramatic then the response further into the post-collapse region is determined by applying lateral displacements along the stiffener.

Dr. Neil Pegg, of Defense Research Establishment Atlantic, has taken a different approach in performing a series of buckling analyses of ring stiffened cylindrical shells under an impulsive load (using ADINA). He has discovered that the solution progresses well into the post-collapse region using a large displacement nonlinear elasto-plastic solution. Dr. Pegg does not induce buckling by lateral displacements since he suspects lateral displacements may force an incorrect response due to the nature of the load. The results, which have been verified experimentally, have been found to be sensitive to the assumed imperfections.

Many commercial FE packages now provide a nonlinear solution method that does not encounter numerical problems in regions of high nonlinearity. This method is called the arc-length method and uses load-displacement control parameters for the solution. A more in-depth discussion of the load-displacement control method is presented in Section 4.3.2.

2-16
2/0

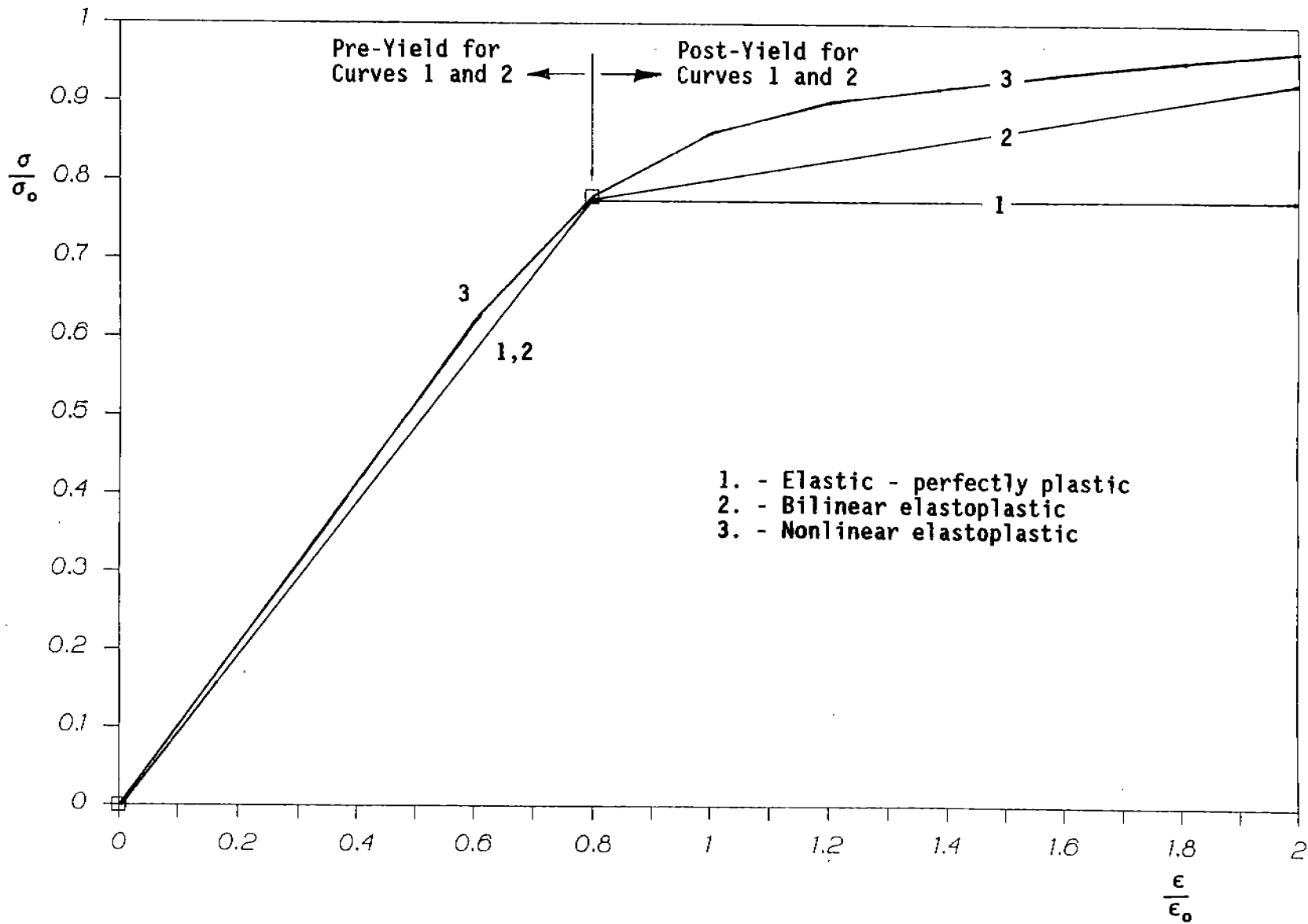


FIGURE 2.3: Methods of Modelling Material Nonlinearities

2.5 Summary and Conclusions

Most papers regarding ship structural instability have little information specifically on post-yield buckling. However, because other types of instabilities such as post-buckling have response parameters common to post-yield buckling, much of the information was pertinent to this study. The most relevant information was found in papers from Admiralty Research Establishment (ARE), Dunfermline.

From the details of the literature review, it seems that varying any of several parameters can produce significant effects on the structural response of stiffened panels. This is compounded by the different response obtained by varying the type of stiffeners. Therefore, any parametric studies carried out during this work should be conducted such that the response changes from varying any one parameter can be isolated.

None of the papers refer to the effects of the global response of a ship on the structural instability of a local stiffened panel. This is considered to be a very important part of this study, therefore, the effects should be understood and well documented in the post yield buckling investigation.

The area of study which seems to be the least understood is the effect of imperfections (geometric and welding) on the stability of a ship's primary structure. This seems mostly due to an incomplete understanding of the types of imperfections found in ships. This is important for any numerical analysis in this area. If an imperfection is used that does not accurately simulate an actual imperfection, then the results of any analysis using this imperfection will most likely not correspond to the actual ship response. The conclusions from any imperfection study should therefore be directly related to the type of imperfection used in the analysis.

3. SURVEY OF TYPICAL ICE DAMAGE AND SELECTION OF CANDIDATE SHIP

As part of this study, it was necessary to select a candidate ship which had documented cases of hull damage, particularly damage due to post-yield buckling of support structure. This selection process involved surveying ship operators and reviewing reports to determine potential candidate ships. The sources of information in this investigation and the rationale behind the selection of the candidate ship are presented in the following sections.

3.1 Sources of Information

Listed below are the owners/operators surveyed, and the published reports reviewed in order to identify the best ship for the study.

Owners/Operators:

Arctic Transportation Ltd.
Gulf Canada Resources Ltd.
Canarctic Shipping Ltd.
Canadian Marine Drilling Ltd.

3.2 Selection of Candidate Ship for Modelling

During the project start-up meeting, emphasis was placed on the M.V. Arctic and the M.V. Robert Lemeur as the most likely ships for further analysis. To be considered suitable, the candidate ship must have experienced hull damage due to operations in ice and this damage must have been well documented. A further requirement was the access to information on the ship, particularly structural details.

The post-yield buckling analysis carried out during this project could be performed on a structure that has been totally designed to the proposed ASPPR. Alternatively, the analysis could be performed by initially using the structure of an existing ship (designed to ASPPR but not designed to

the revised ASPPR), then modifying this structure to include the revised ASPPR redesigned structure at specific regions of interest.

The first approach allows flexibility to design a nominal structure without any ship specific constraints (since no vessels designed to the revised regulations exist). The second constrains the analysis to ship specific structure, but has several benefits:

- Ship details are available to realistically set the boundary conditions;
- The structure is known to be practical with regard to construction;
- The structural performance history is known; and
- Details of ice damages are available for possible validation of the buckling model.

These benefits weigh heavily in favour of this approach.

Several Canadian ships have been designed and constructed to the existing ASPPR requirements but none to the proposed ASPPR amendments. Therefore, by selecting an existing ship that is known to have sustained ice damage it may be possible to validate the analysis results for the existing ASPPR.

Several Canadian ships have been built to the existing ASPPR. From a review of damage history it is apparent that two ships stand out with regard to ice damage. The first is Robert Lemeur, an Arctic Class 4 offshore supply vessel built in 1983 for operation in the Beaufort Sea. The second is the M.V. Arctic, an Arctic Class 3 OBO built in 1978 for operation in the eastern Arctic. Both ships have sustained significant structural damage. However, the M.V. Arctic stands out with regard to documentation and previous analysis of the damage.

A number of the publicly available reports of structural design and damage history of the M.V. Arctic are listed below.

- "M.V. Arctic Midbody Damage Analysis", prepared by CANMAR for Transport Canada, TP 6224E, March, 1985.
- "M.V. Arctic Structural Performance", prepared by Arctec Canada Ltd. for Transportation Development Centre, TP 5680E, April, 1985.

- "M.V. Arctic Structural Performance — Summary Report", prepared by Arctec Canada Ltd. for Transportation Development Centre, TP 5681E, February, 1985.
- "Assessment of the Strength of the Bow Hull Structure of M.V. Arctic under Ice Loads caused by Multiyear Ice", VTT Report LAI-348A/82, October 1982.
- "Nonlinear Analysis of M.V. Arctic Stringer", VTT Report LAI-348F/83. Feb. 1983.
- "M.V. Arctic Midbody Structure Design", prepared by Melville Shipping Ltd. for Canarctic Shipping Ltd., Feb. 1985.
- "Port Weller Dry Dock Damage Survey of the M.V. Arctic", prepared for Canadian Coast Guard, Jan. 1984.
- "Mathematical Model of M.V. Arctic Ramming Multi-year Ice Floes", VTT Report LAI-335B/82, July 1982.
- "Measurement of Hull Girder Bending Strain and Vibration on the M.V. Arctic in Admiralty Inlet", prepared by Melville Shipping Ltd. for Department of Supply and Services, March 1983.
- "Final Report on Midbody Damage Analysis of the M.V. Robert Lemeur and the M.V. CANMAR Kigoriak", CANMAR, TP 5376E, March 1984.

From this list it is clear that the M.V. Arctic has more publicly available documentation than any other ship with regard to its structure and damage history. Damage is located in the bow and midbody areas and exact locations and extent are known. Some photographic information is available although this is not extensive.

The damage that has been sustained by the M.V. Arctic has been of two principal types:

- Denting of the outer shell combined with buckling of the internal support members, vertical frames, vertical webs and horizontal stringers. This type of damage has been located from the aft section of the bow through to the aft section of the mid body areas at or near the waterline.
- Rupture of the outer shell in the form of a tear/crack causing a narrow band of damage to the internal support structure in way of the rupture.

The predominant form of damage is denting. The area around the shoulder, either immediately forward or aft of the point of maximum beam, has seen a substantial number of these

occurrences. Although the M.V. Arctic was selected for analysis, this type of damage can also be seen from the historical review of other icebreaking ships. Similarly, with the other ships the point of maximum beam is where such damages may be found.

4. METHODOLOGY FOR THE ANALYSIS OF THE M.V. ARCTIC

This chapter describes the methodology behind the FE analysis of the M.V. Arctic and provides information on the structural and physical details of the ship that pertain to the analysis methodology. This includes information on the physical structure, loads, and boundary conditions and on how the numerical models (MAESTRO and ADINA) are employed to replicate the response of the actual structure and its physical mechanisms.

4.1 Overall Description of the M.V. Arctic Structure

The M.V. Arctic was built at Port Weller Dry Dock, St. Catherines, Canada in 1978. The vessel is owned by the Royal Trust Company of Canada and operated by Canasic Shipping Company Limited.

In May 1986, the M.V. Arctic's ice class was upgraded from Class 2 to Class 4 equivalent and the vessel was converted to carry bulk oil cargo as well as dry bulk. The M.V. Arctic has a double hull throughout the length of its cargo holds and engine room. The vessel has three levels of support: mainframes; stringers; and deep webs. All framing and stiffening for the inner and outer skin is arranged within the double skin space. The M.V. Arctic is classed by Lloyds' Register of Shipping. The present hull of the vessel has seven cargo holds. The middle five are used for oil cargo, whereas the first and the seventh holds are used for dry cargo only.

The principal dimensions of the vessel are as follows:

Length O.A.	724.00 feet
Length B.P.	675.56 feet
Breadth Moulded	74.95 feet
Depth Moulded	50.00 feet
Summer Draft	36.28 feet

4.1.1 Material and Elastic Properties

All scantlings in both the midbody and bow regions of the M.V. Arctic are modelled using the properties of mild steel. These values are provided in Table 4.1. The post-yield modulus (strain

TABLE 4.1: Properties of Mild Steel	
Modulus of elasticity	30,000,000 psi
Poisson's Ratio	0.3
Yield strength	34,000 psi

hardening modulus) applies only to the ADINA analysis since MAESTRO assumes linear response (in the elastic material range).

4.2 Loads

The M.V. Arctic loading condition for this investigation consists of three components: a still water bending moment, a hydrostatic pressure load, and an iceload.

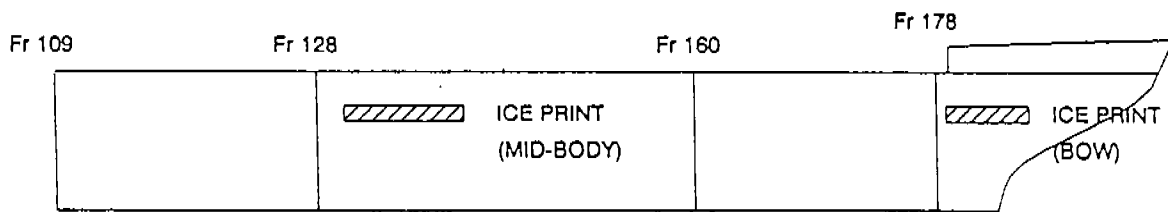
Since the primary objective of this study is to determine the post-yield buckling response of the ship scantlings during ice interaction, it is important to obtain the worst case still water bending moment condition for ice damage. Since buckling only occurs under compression, the worst case is when the hull is in compression. This condition is achieved when the vessel is subjected to a sagging hull girder bending moment and the hold, where the ice load is acting, is empty. This implies that there will be no pressure from the cargo to counteract the external iceloads.

The effect of the still water bending moment is much greater at the midbody region of the ship than at the bow. On the other hand, the effects of the vertical component of the iceload, which is nonexistent at the midbody, is very significant at the bow. Since the loading conditions for each region of the ship have unique components, they are not covered in detail in this section. The midbody loading condition is detailed in Section 5.2.3, and the bow loads are detailed in Sections 6.2 and 6.3.3.

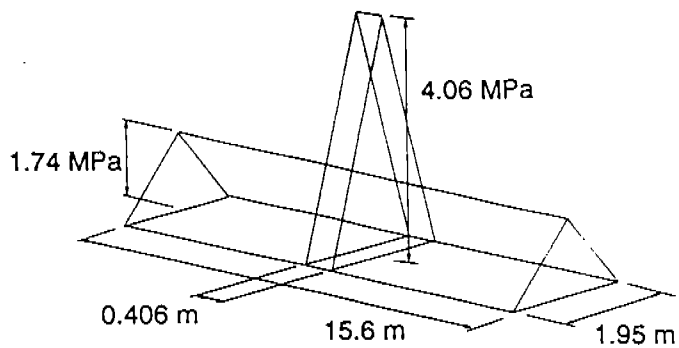
The iceloads have been determined according to the revised ASPPR regulations with the distribution of the average ice pressure on the ice print being triangular. This distribution for the M.V. Arctic is illustrated in Figure 4.1(b) for the midbody region and Figure 4.1(c) for the bow. A more detailed presentation of the ASPPR iceloads is found in Appendix A.

4.3 Overall Modelling Philosophy

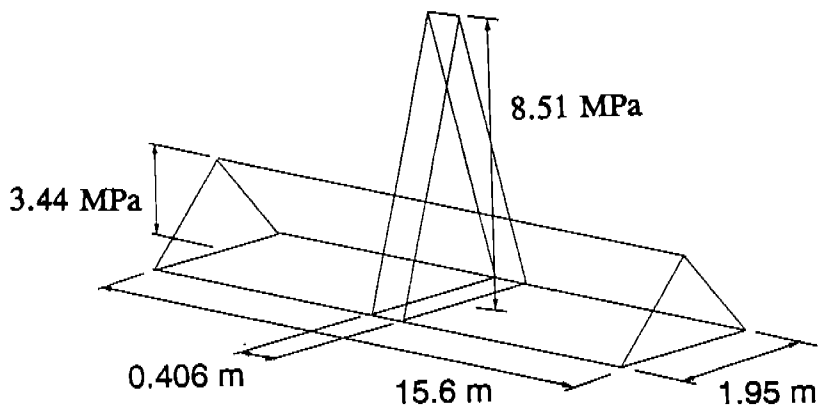
The primary objective of this project is to study the post-yield buckling response of two local areas of the ship to an ice load. The main interest in the study is to determine whether or not the local structure (hereafter referred to as the "local panel" which is an area framed by two stringers and two



(a) Locations of ASPPR ice loads



(b) Midbody pressure distribution ASPPR ice load



(c) Bow pressure distribution ASPPR ice load

FIGURE 4.1: ASPPR Ice Loads on the M.V. Arctic

deep webs and encompassing two mainframes) buckles under the applied ice load. It is apparent that the response of the local panel is affected by the response of the overall ship; however, the sensitivity of the local response to the overall ship response is not apparent.

If it were practical, the easiest way to get accurate results in the local panel would be to develop a model of the entire ship which contains sufficient refinement in the local panel area to allow an accurate prediction of local response. One problem with this approach is that the local response is highly nonlinear (since buckling is of interest locally) whereas the response of the overall ship will remain linear. If one model were used to predict the response, then the entire model would have to be analyzed using nonlinear methods. Due to model size limitations and time constraints it is not practical to adopt this approach directly. However, it is possible to model the response in a two step procedure called "top-down" analysis, which allows for the accurate determination of both local and overall response with two separate models.

The method consists of first developing a coarse, "overall" model of the structure which can be used to determine the overall response of the ship but which will not be capable of accurately predicting the local response. A local model is then developed independently with boundaries extending far enough away from the local panel to allow accurate prediction of the response at model boundaries, using the overall ship linear analysis. The overall model is analyzed and the response (displacements) at the location corresponding to the local model is determined. The local model is then analyzed by applying the local loads to the outer skin and the displacements predicted from the overall model to its boundaries. Using this method, the local response incorporates the effects of the global response of the ship. The local model is analyzed using nonlinear methods and the overall model is analyzed using linear assumptions. The local response will be accurate if the boundaries extend far enough away from the local area to ensure that the response at the boundaries is linear and accurate.

The two finite element programs MAESTRO and ADINA were used in the analysis of the M.V. Arctic. MAESTRO was used to model the linear response of the overall ship and to provide an understanding of the ship response to an ice load. The MAESTRO model was then used to provide the boundary conditions to be applied to a more refined ADINA model. The ADINA model was analyzed using the program's nonlinear capability. This analysis was performed to determine the nonlinear

buckling response of the local panel. The MAESTRO and ADINA models are developed to model different responses and hence the geometry, loads, and boundary conditions employed with the models are also quite different. A general description of these differences and how they are modelled in this study is provided in the following sections. More details are provided in the sections specific to each region of the ship studied.

The procedure used to transfer the overall boundary conditions from the MAESTRO analysis to the ADINA models is called the top-down method. A more detailed description of this method is provided in Section 4.3.3.

Version 5.4_4 of MAESTRO was used to create and analyze the overall models of the M.V. Arctic. All ADINA FE models were created using Version 6.0 of the program VASGEN [16] and translated by the program ADIDAT [12] to a format that would permit analysis by the FE package ADINA [18]. After translation from VASGEN, the models were recreated using Version 3.0 of the program ADINA-IN, analysis was performed using Version 6.0 of ADINA, and the post-processing performed using Version 4.0 of ADINAPLOT.

4.3.1 MAESTRO Analysis Procedure

The purpose of the MAESTRO analysis is to determine the linear response of the overall ship. The emphasis on the analysis is to accurately determine the displacements which occur on a 3x3 bay area in the midbody and bow areas of the ship when it is subjected to ice loading. This allows for the introduction of global effects into the local model and allows for accurate calculation of nonlinear post-yield buckling response in the detailed ADINA models. The loading and boundary conditions used in the analysis and the extent of the M.V. Arctic structure used in the MAESTRO model are outlined in Sections 4.2, 4.4, and 4.3.2 respectively.

MAESTRO uses a 4-noded quadrilateral element called a "STRAKE" to model stiffened panel structures. The strake element is basically a shell element with stiffener properties accounted for by smearing them into the plating. The element possesses bending stiffness; however, the stiffeners

contribute in axial stiffness only. The normal stresses in a strake element are assumed to vary linearly while the shear stress is assumed to be constant in either of the two principal directions of the element.

MAESTRO was used to provide a mesh refinement such that individual frames were modelled with typically one strake element between each web frame. Because nodal displacements from the MAESTRO model will be used as boundary conditions for the detailed ADINA models, it is important to obtain these displacements at a sufficient number of nodes to ensure valid boundary conditions in the local model. With the degree of refinement of the MAESTRO model known, the mesh of the detailed ADINA models was created such that nodal displacements supplied at each frame location were sufficient to obtain valid boundary conditions.




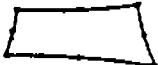




4.3.2 ADINA Analysis Procedure

The refined ADINA models of the M.V. Arctic midship and bow regions must be large enough to predict the local web, stringer and mainframe response to the iceload, but small enough to minimize potential file storage and analysis time problems. Since several mainframes are located between the region bounded by one stringer spacing and one web frame spacing, the local response can be isolated to this region provided the boundary conditions can be properly applied.

When applying boundary conditions to a top-down model, several considerations are important. First, the boundary conditions should be determined from a region in the overall model where relatively small stress gradients exist. By determining the boundary conditions in regions of low stress gradients, the possibility of not including the correct overall response in the top-down model is minimized. If the overall model has not been sufficiently refined to predict the response in the region where the top-down model boundary conditions are being determined, then incorrect boundary conditions will be applied to the top-down model. Second, the boundary conditions should be applied as far as possible from the area of interest to minimize both the effects from round off error in the application of the boundary conditions and the nonlinear response of the region of interest.

To satisfy these considerations, the boundaries of the detailed model were defined such that one web frame spacing forward and aft and one extra spacing above and below an individual stiffened

TABLE 4.2: Recommended Integration Order for ADINA Shell Element

ELEMENT		RELIABLE (DEFAULT) INTEGRATION ORDER	REDUCED INTEGRATION USED IN PRACTICE (WITH SPURIOUS ZERO ENERGY MODE(S))
4-NODE		2 x 2	
4-NODE DISTORTED		2 x 2	
8-NODE		3 x 3	2 x 2
8-NODE DISTORTED		3 x 3	2 x 2
9-NODE		3 x 3	2 x 2
9-NODE DISTORTED		3 x 3	2 x 2
16-NODE		4 x 4	3 x 3
16-NODE DISTORTED		4 x 4	3 x 3

GAUSS NUMERICAL
INTEGRATION
ORDERS FOR
QUADRILATERAL
SHELL ELEMENTS

is also capable of multiple types of plastic material properties. Even though the use of the 4-noded shell element could result in a smaller model, it is felt that the results would be compromised.

The method of solution used for the ADINA nonlinear analyses is a procedure called the Load Displacement Control (LDC) method [19]. When conventional applied force methods are used in the solution of large displacement nonlinear analyses, the solution often fails at regions of high nonlinearity (for example at the bifurcation point of buckled structures) due to non-positive definite (or very small) stiffness terms in the stiffness matrix. This results in an inability of the algorithm to converge to a unique solution.

The LDC method eliminates this problem by using displacements to control the solution. A load vector must be provided; however, the algorithm is started at the first load step with an initial nodal displacement in the desired direction instead of a force. The program automatically determines the load factor (a constant multiplied by the load vector) necessary to displace the structure by the initial displacement while maintaining equilibrium. The program then automatically determines the next incremental displacement and continues to the next load step. This procedure continues until either the maximum specified displacement is reached, the maximum number of time steps is reached, or the nonlinearity is extreme enough to prevent convergence within four iterations (maximum) of repeatedly reducing the incremental load. The advantage of using displacement control occurs when a large displacement results from a very small force (due to small stiffness). Without LDC, if a force is applied, the program has difficulty converging to a displacement.

The LDC method is a nonlinear solution algorithm where all of the loads and initial conditions are incrementally increased at each load step. In the actual structural response, the still water bending moment is fairly constant during the ice loading procedure (which sees the ice load applied incrementally from 0 to F_{max}) — particularly at the midbody. However, a method of simultaneously applying a constant load (i.e. still water bending) and an increasing load (i.e. ice load) is not available using the LDC method. Therefore, all of the load components (the prescribed displacements that define the still water bending moment, the hydrostatic pressure load, and the ice load) are incrementally increased together. While this may seem likely to generate potentially invalid responses (because the loads are not exactly applied as they should be), in actuality the source of error will be small for the

region of the response of interest and will be exact at the ice load magnitude equal to F_{\max} (i.e. at full ice load). Since the load application has no error at F_{\max} where all of the load components are totally applied, and the response at or near F_{\max} is of most importance, the correct response will be predicted. The error expected during the application of the load is minimal due to the domination of the ice loading in the response.

4.3.3 Top-Down Method of Analysis

A common procedure to obtain more accurate results at specific regions of FE models is to refine the grid near the area of interest and reanalyse the whole model. However, when the models are very large, repeated refinement may be restricted by either limited storage requirements or excessive analysis times. To overcome these problems a procedure called the top-down method is available.

The top-down method of FE analysis is a procedure by which the response of specific regions of large numerical models can be accurately predicted without performing a re-analysis of the whole structure. This procedure is shown in more detail in Figure 4.3. Top-down modelling involves isolating a specific region of the whole FE model as shown in Figure 4.3(b). The geometry of this region and the results of a previous analysis of the whole model are then used to generate both the refined top-down model as shown in Figure 4.3(c) with the boundary conditions (prescribed displacements determined from the overall model analysis) as shown in the figure. Provided the response at the boundaries of the top-down model is accurately predicted, the top-down method is a very effective and accurate tool in predicting the local response of various structures.

With the overall linear response of the M.V. Arctic known from the MAESTRO analysis using the revised ASPPR predicted ice loads, the detailed midship response — which incorporates the effects of the overall response — can now be determined. This is done by isolating a midship region of the M.V. Arctic for further analysis using the top-down method.

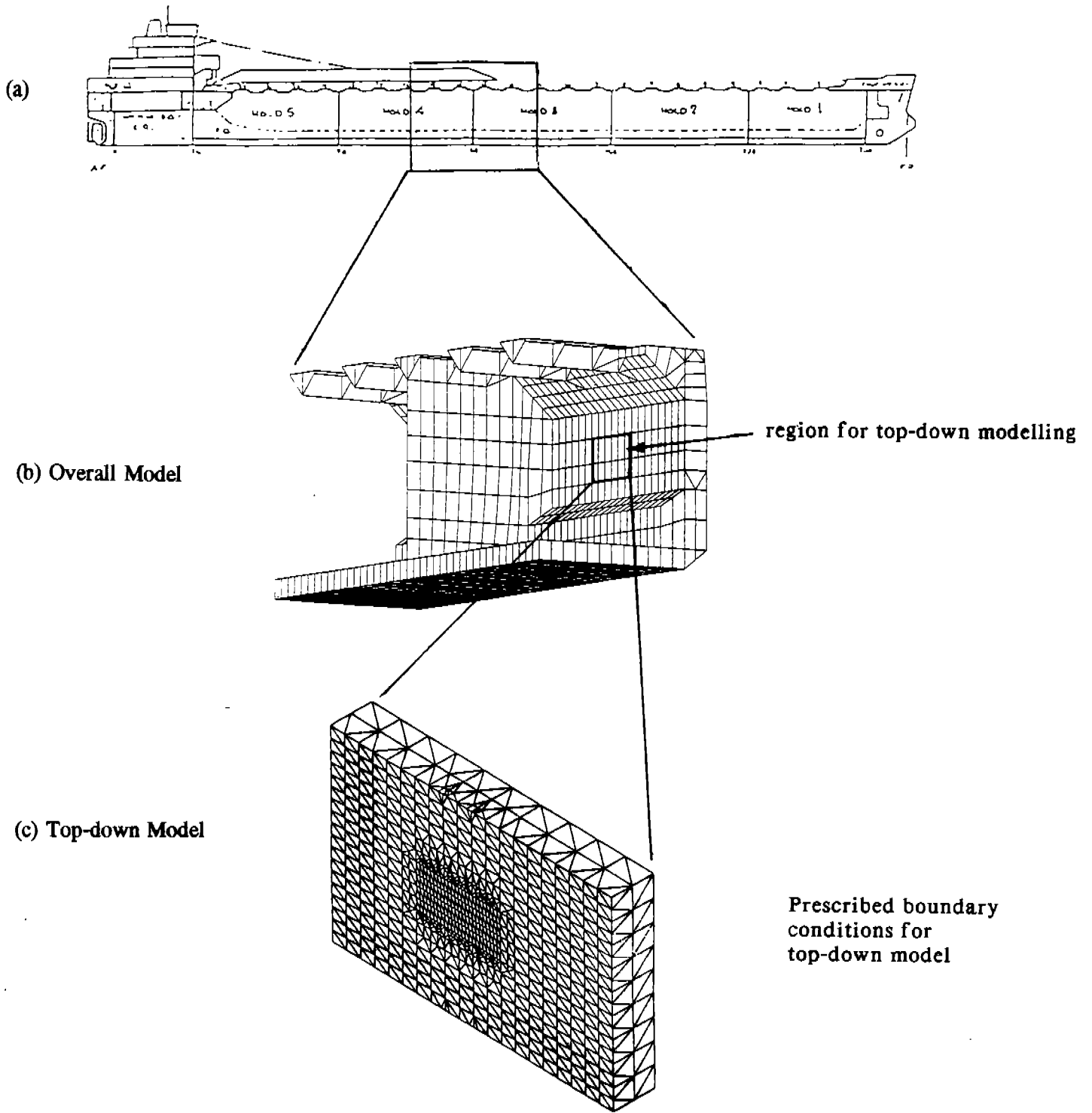


FIGURE 4.3: Top-down Method of FE Analysis

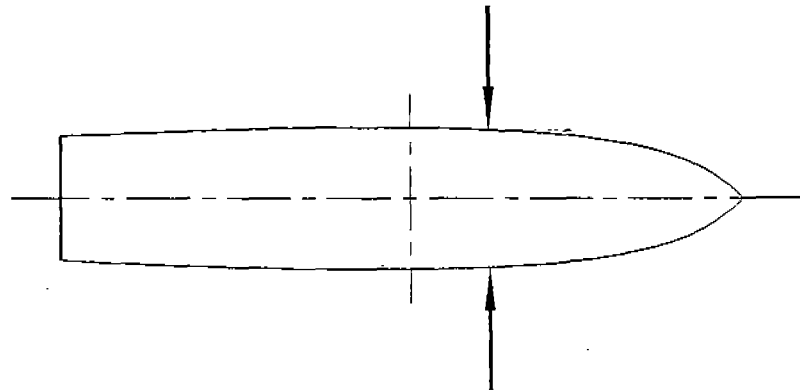
4.4 Boundary Conditions

The "top-down" method described in the previous section was employed to perform the local analysis. This requires two types of numerical models to be generated; a MAESTRO model of the overall ship scantlings; and detailed ADINA models of local regions. These models are very different in their structural detail and also in the expected response; therefore, the boundary conditions for each are unique and must be defined separately. The following sections describe the boundary conditions which were employed in the analyses for both the global and local models.

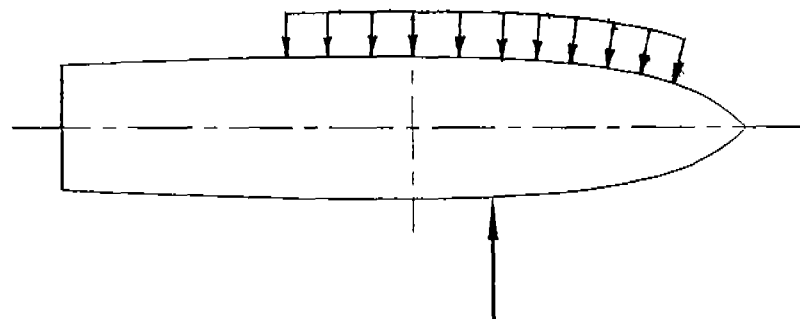
4.4.1 Boundary Conditions Applied To The Overall Model

Three types of boundary conditions are imposed on the overall model of the ship: two regarding structural/loading symmetry; and the other to prevent the rigid body motion in response to the loads. The first structural/loading boundary condition assumes that the ship is symmetric about a bow to stern vertical symmetry plane. This allows for modelling of only one side of the vessel and assumes that the geometry, response, applied loading, etc. of the other side of the ship are identical. This assumption is not quite valid. The geometry is identical; however, in regard to the loads, this assumption implies that identical loads are applied to both the port and starboard sides of the vessel simultaneously. This is not the case, as the applied load is an ice load which is applied to one side of the vessel only. This applied ice load is reacted on the other side of the vessel by a water pressure which is created as the vessel tries to accelerate in response to the ice load. This reaction should be a more-or-less uniformly distributed pressure load on the opposite side of the ship. The actual load and expected reactions versus the modelling assumptions are shown schematically in Figure 4.4. It is assumed that the results of these two different scenarios will not be significantly different near the point of load application. One factor which helps to minimize the effect of this assumption is that the load is applied in the center of a hold. This means that the load path from the starboard to port side of the ship must be the same (i.e. through the transverse bulkheads) regardless of whether or not it is reacted as a point load or as a uniform pressure load.

The second structural/loading symmetry condition assumes longitudinal symmetry about a lateral symmetry plane located at the midship section of the vessel. Again the assumption of symmetry



(b) Modelling assumption inherent in transverse symmetry



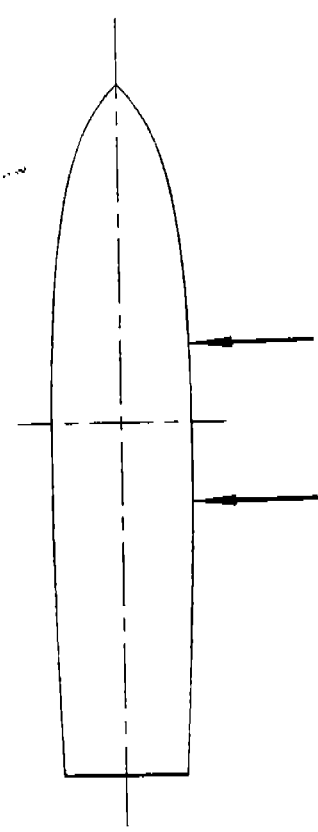
(a) Expected actual load distribution on ship

FIGURE 4.4: Modelling Implications of Assuming Transverse Symmetry

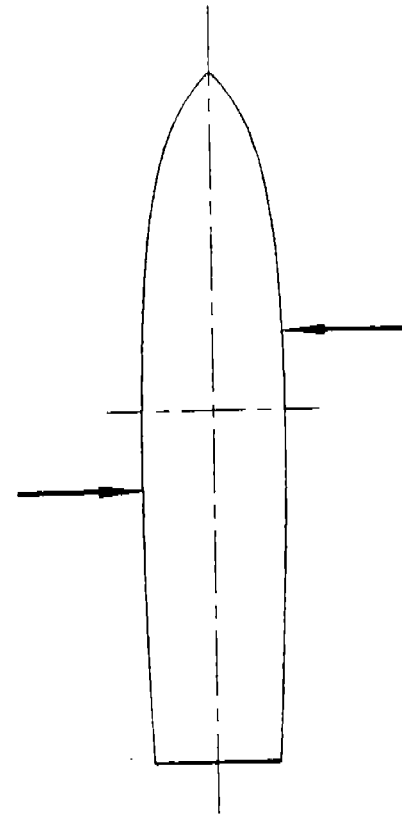
implies that the geometry, loading and response are identical on either side of the assumed plane of symmetry. The reaction to the applied load will be a pressure load on the opposite side of the ship. This is not shown in these sketches. The after and forward geometries of the vessel are different in the areas of the bow and stern; however, the ship has a large parallel midbody and the still water bending moment is approximately symmetric about midship. The response of the vessel (both locally and globally) will be unaffected forward of midship by the differences in geometry in the stern of the vessel. Therefore, in regard to the geometry, the still water bending moment, and hydrostatic pressure load, the assumption of longitudinal symmetry about midship is valid. However, the ice load is applied physically to the ship in the forward portion of the ship only as shown in Figure 4.5(c) and the assumption of symmetry implies that the load is applied both forward and aft of midship, as shown in Figure 4.5(a). A more rigorous treatment of the problem, which would eliminate any assumptions as to the symmetry of the loading, would be to develop two separate models: one assuming symmetry about midship; and the other assuming antisymmetry about midship. The condition of antisymmetry is shown in Figure 4.5(b). If half of the load is applied in the symmetric model (Figure 4.5(a)) and half of the load is applied in the antisymmetric model (Figure 4.5(b)) and the two results are summed, then the condition shown in Figure 4.5(c) for this vessel is achieved. The only simplifying assumption in this modelling procedure is that the geometry is symmetric about midship (shown as a dotted line in the figure) which has already been discussed.

The summation of the results from modelling using the assumptions of Figures 4.5(a) and 4.5(b) will produce the response predicted by explicitly modelling as shown in Figure 4.5(c). It is also true then that if the identical response were predicted using the assumptions of either Figures 4.5(a) or 4.5(b), then the results could be predicted by employing the assumptions of Figure 4.5(a) and using the full load (i.e. twice the symmetric load). Therefore, if the model of Figures 4.5(a) and 4.5(b) are run independently and the results compared and they show no significant difference, then the assumption of longitudinal symmetry about midship is valid. This procedure was undertaken using the MAESTRO model and little difference in results was observed between the two responses, indicating that the assumption of longitudinal symmetry is valid. The results of the two runs are shown in Figure 4.6. A complete description of the MAESTRO model and analysis is presented in Section 5.3. The results have been presented here only to justify the selection of boundary conditions.

(a) Implied modelling assumption
with condition of symmetry at midship

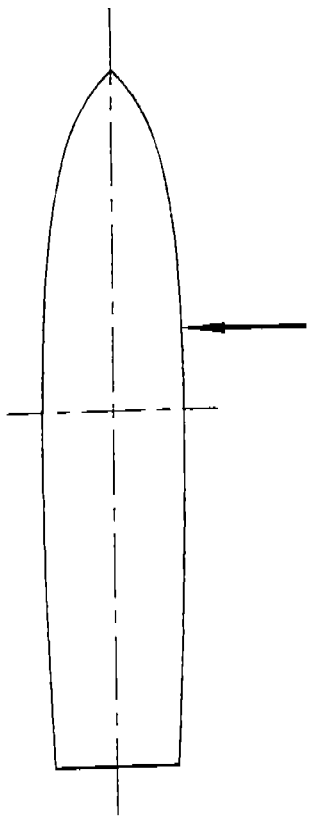


+



=

(c) Actual ship loading condition



(b) Implied modelling assumption
with condition of antisymmetry at midship

FIGURE 4.5: Analysis Check on the Assumption of Longitudinal Symmetry About Midship

The last boundary condition that is applied to the structural model is to prevent unconstrained rigid body vertical translation of the vessel. The boundary condition is applied to the midship keel position and consists of fixing all translations. This boundary condition has little physical significance. It is applied only to prevent ill-conditioning of the stiffness matrix.

4.4.2 Boundary Conditions Applied To The Local Models

For the local analyses, the boundary conditions used in the ADINA model are prescribed displacements at all nodes along the outer boundaries of the detailed FE model. These prescribed displacements force the boundaries of the local model into the same shape which is predicted from the global model. The results from the global effect of applying the ice load to the overall ship are thus incorporated into the local model. They are used to account for the still water bending moment effects, the hydrostatic pressure load effects, and the overall ice load effects which are being modelled in the MAESTRO global model. This involves using a procedure called the top-down method which is described in detail in Section 4.3.3.

Details of the boundary conditions applied to the local models for each region of the ship are found in the sections which deal specifically with the midbody (Section 5) and bow (Section 6) analyses.

There is some question as to the importance of incorporating the global effects of the ship response into the local analysis and it may be possible to achieve sufficiently accurate results by making some simplifying assumptions as to the constraints which the ship imposes on the local model without actually using prescribed displacements from MAESTRO. The best way to evaluate the importance of the boundary conditions on the local panel response is to compare results predicted using "simplified boundary condition assumptions" to the "correct response" predicted using explicitly defined boundary conditions (predicted using MAESTRO) which employ as few assumptions as possible. Chapter 9 describes the results of a study in which simplified boundary conditions were applied to a local panel model to determine what assumptions yield favourable results.

4.5 Benchmark and Test Problems

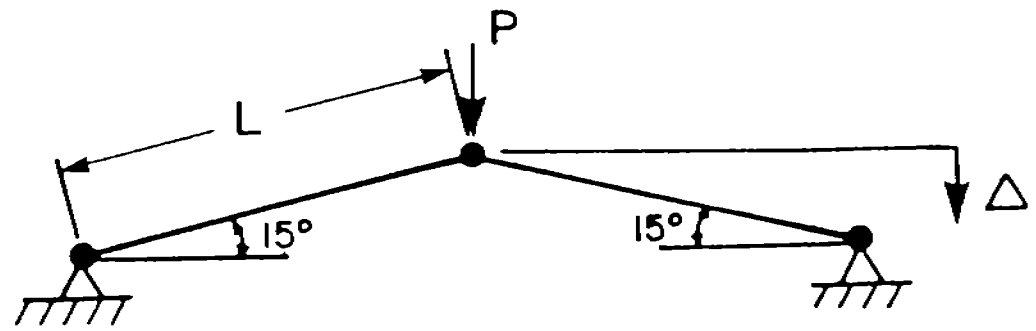
Whenever a complicated FE analysis is to be performed on a complex structure, a series of simple benchmark problems should almost always be performed first. The greatest benefit from doing this is the potential of gaining some understanding of the response of the detailed model. However, if the detailed FE model is very complicated (as in the M.V. Arctic), then the simplified problems may not be able to provide any insight into the global response. Such being the case, these problems can be designed to provide an understanding and demonstration of the analysis methods and possibly any local response that is considered important. This is the approach used in this investigation.

Since the overall analysis will involve both geometric and material nonlinearities, it was necessary to design the test problems around the nonlinear techniques that will be used to analyse the M.V. Arctic. It was also decided to create one model that was similar in geometry to a mainframe of the M.V. Arctic. This is the region of the model where the greatest instability is anticipated and will provide some understanding of how the progression of plasticity affects the response of the mainframes.

The first problem is an ADINA benchmark problem that checks the nonlinear solution algorithm that is used extensively in this study of the M.V. Arctic -- the LDC method. This is example B.40 of the verification problems [20]. Details of the ADINA files required to generate the model and plot the results are found in Appendix B. The results are presented below.

A sketch of the physical problem is shown in Figure 4.7. This is a snap-through problem that involves a nonlinear solution of large displacements using the LDC method. A pin exists at the point of applied load and at the boundaries. Therefore, the load taken by each member is completely axial, and one bar element can be used (per member) to predict the response. The geometry and loading is symmetric; therefore, one-half of the structure is modelled. The FE model is shown in Figure 4.8(a).

An initial displacement of 0.1 units is applied at node 2 in the negative z direction and the ADINA solution using the LDC method is performed. The resulting load displacement curve for the ADINA analysis is compared with the analytical solution in Figure 4.8(b). Very good agreement exists throughout the entire load range.



$L = 10$
 $E = 2.1 \times 10^6$
 $AREA = 1.0$
 $k = 2.1 \times 10^5$

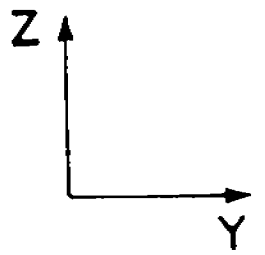


FIGURE 4.7: Sketch of ADINA Test Problem #1

4-21

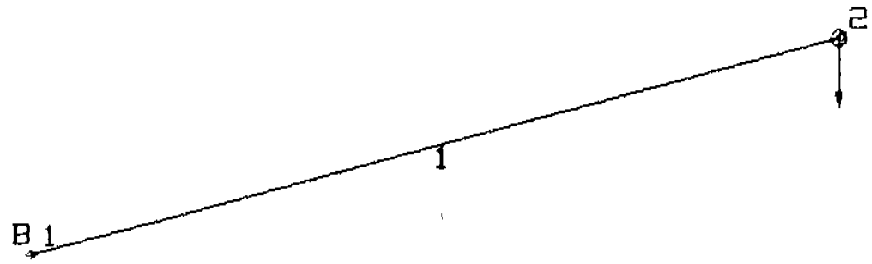
67

ADINA-PLOT VERSION 4.0.3 3 MARCH 1992
 B.40 ANALYSIS OF SNAP THROUGH OF AN ARCH STRUCTURE

ADINA ORIGINAL UNIT: 0.000
 XUMAX: 0.659
 0.7430 YUMIN: 0.000
 YUMAX: 0.588

Z
 Y

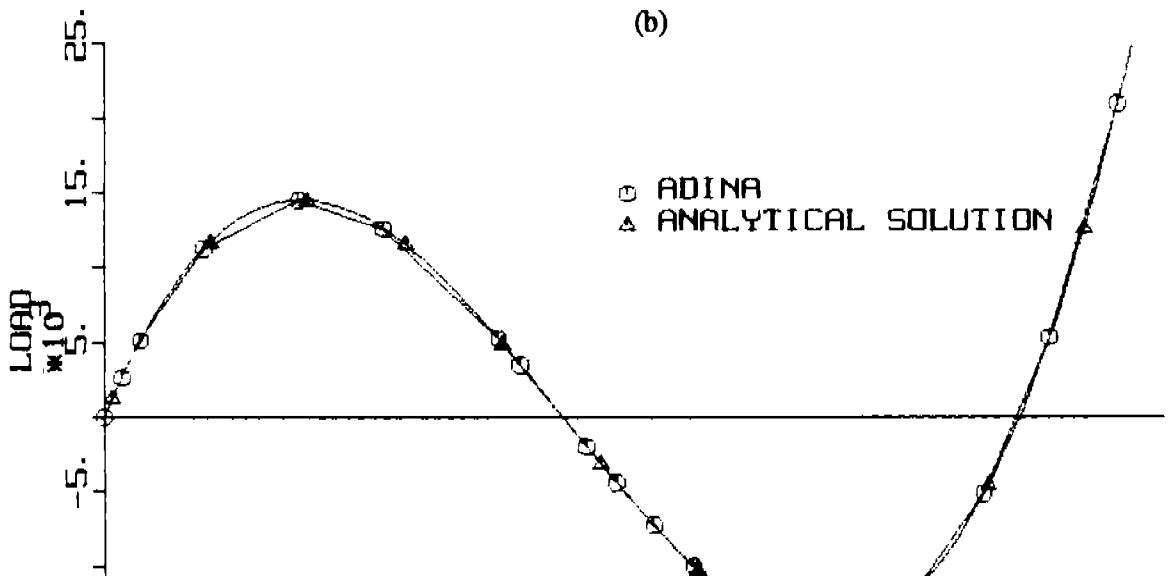
PRESCRIBED
 FORCE
 TIME: 19.00
 10505.



(a)

U₃
 B -

(b)



This problem provides a successful check of the LDC method in ADINA. An added benefit is the familiarization with performing this type of analysis.

The second problem was a test problem to study the nonlinear response of a structure that includes both large displacement and elastic perfectly plastic material properties. These types of nonlinearities are similar to those expected when studying post-yield buckling. To make the test problem seem more representative, it resembles a ship mainframe under an applied lateral load.

The physical problem is illustrated in the sketch of Figure 4.9. The geometry consists of a plate that is pinned at one boundary, with a pinned roller at the other boundary, and an applied lateral load at midspan. The beam is modelled with 8-noded shell elements. This is the same element that is used in the M.V. Arctic FE model. The measured response is the in-plane bending. The 8-noded shell element predicts linear bending very well, therefore, only one element is required through the depth, h .

The FE model is shown in Figure 4.10(a). One variation between the sketch of Figure 4.9 and the FE model is that the boundary conditions are applied at mid-depth in the FE model (i.e., a pin at node 2 and a roller at node 32).

The model was analyzed using ADINA with the LDC solution algorithm. The resulting load displacement curve is shown in Figure 4.10(b). The response is linear up to step 2; however, above step 2, a highly nonlinear response is predicted. The reason for this can be explained by studying the SXX stress along a line at the top and bottom of the beam as shown in Figure 4.11. At load levels above step 2, yielding occurs and a plastic hinge forms at midspan. The load remains virtually the same for subsequent time steps. The displacement continues to increase; however, the SXX stresses do not. This is evidenced by the same stress curves from steps 4 to 6.

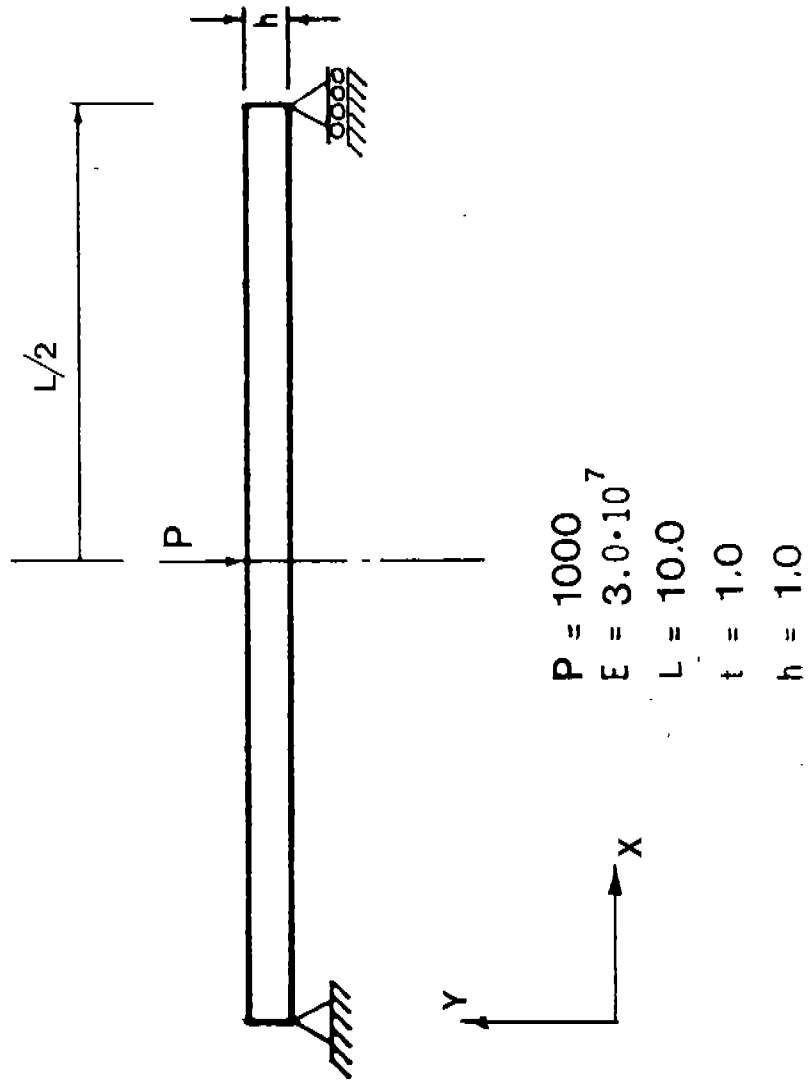


FIGURE 4.9: Sketch of ADINA Test Problem #2

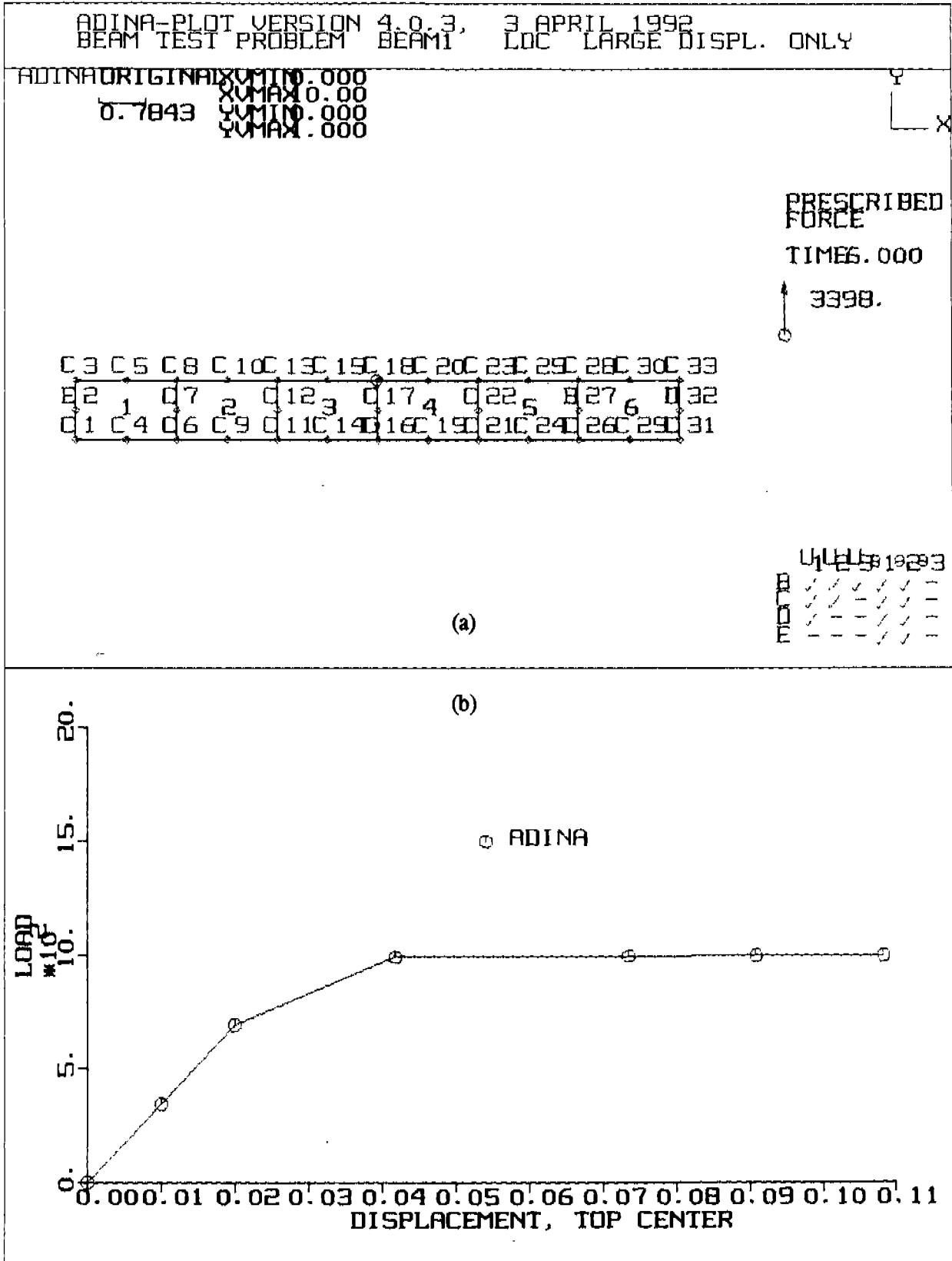


FIGURE 4.10: Plot of FE Model and Load Displacement Curve for Test Problem #2

ADINA-PLOT VERSION 4.0.3, 3 APRIL 1992
 BEAM TEST PROBLEM BEAM1 LOC LARGE DISPL.

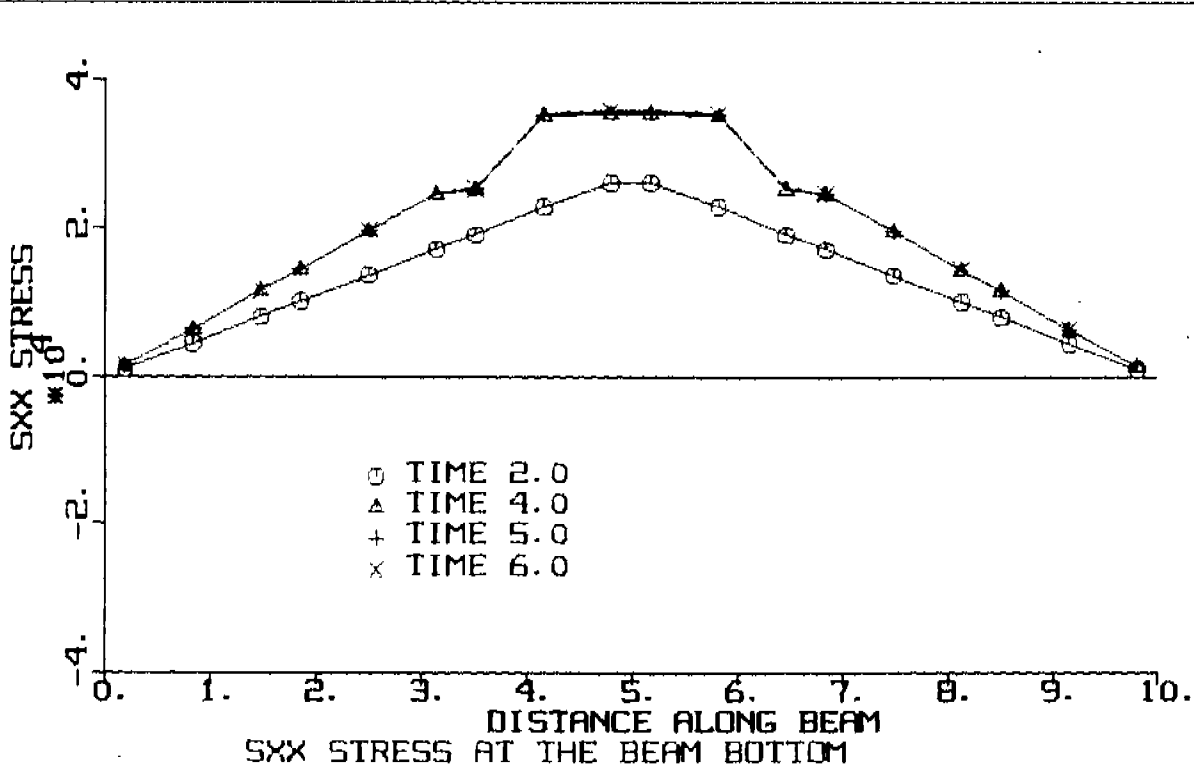
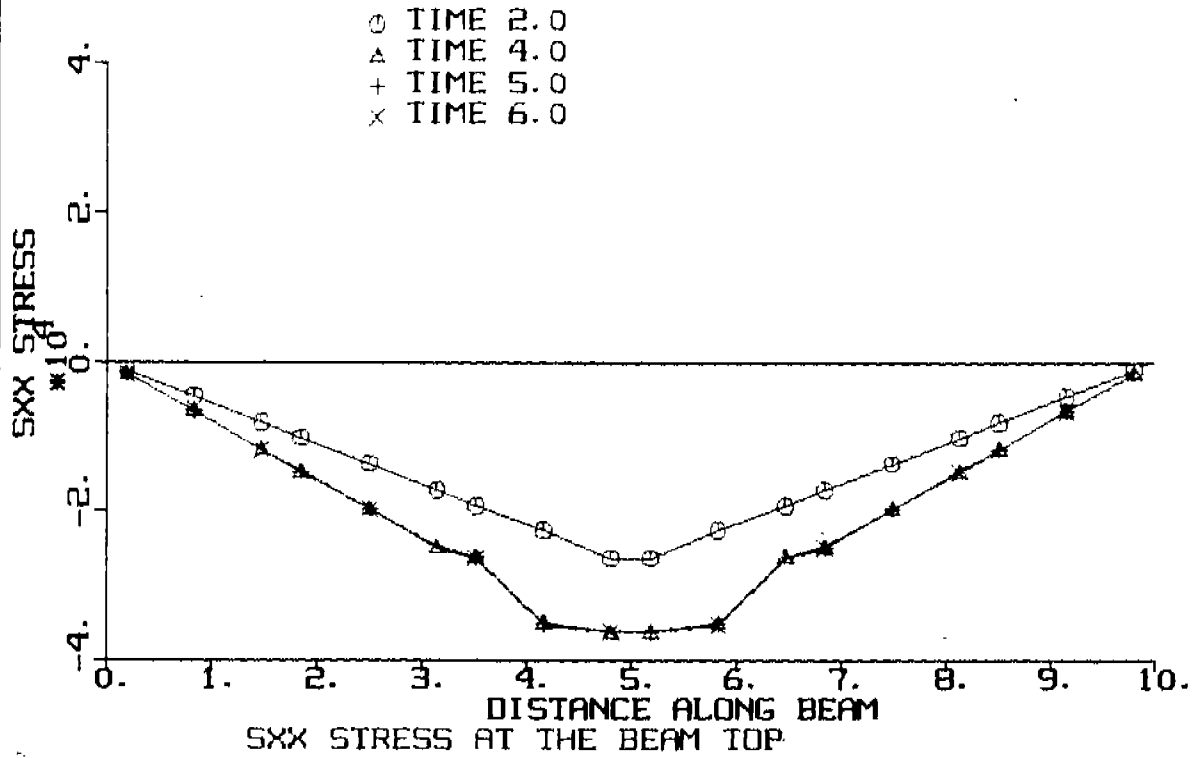


FIGURE 4.11: Line Stress Plots at the Top and Bottom of the Beam of Example Problem #2

Based upon this, the third and final test problem was created. This problem has the same geometry and loading as test problem #2; however, the roller boundary condition has been changed to a pinned boundary condition. This enables membrane stresses to exist after the plastic hinge occurs.

The physical setup for test problem #3 is illustrated in Figure 4.12. The FE model is shown in Figure 4.13(a). The resulting load displacement curve is shown in Figure 4.13(b) and the SXX stress plots along a line at the top and bottom of the beam are shown in Figure 4.14.

The load displacement curve looks similar to the previous model; however, the change in response due to having two pinned boundary conditions is evident. In problem 2, the applied load and resulting stresses remain fairly constant after the plastic hinge is established. In problem 3, the loads and stresses continue to expand outward from the beam midspan. This is because the structure can now handle membrane loads.

The membrane effects are shown in Figure 4.14. The flatness of the curves at midspan shows that the plastic hinge is established at step 3. As the load increases, the membrane effects increase and plasticity expands outward from midspan. This is evident in the increasing SXX stresses from steps 4 to 6 away from midspan. This increasing stress results in an increasing plastic zone spreading outward from the midspan region.

4.5.1 Conclusions

The test problems show that the boundary conditions are important in the prediction of the extent of plasticity of a simple plate problem. This may be important in the analysis of the M.V. Arctic since the plate problem resembles a ship mainframe. The objective of the M.V. Arctic investigation is to study post-yield buckling. If the extent of plasticity in the mainframes of the M.V. Arctic is as affected by boundary conditions as in the test problem, then the boundary conditions may have a significant effect on the buckling response.

The test problems also show that the load displacement control (LDC) solution method is quite capable of predicting the response of highly unstable structures.

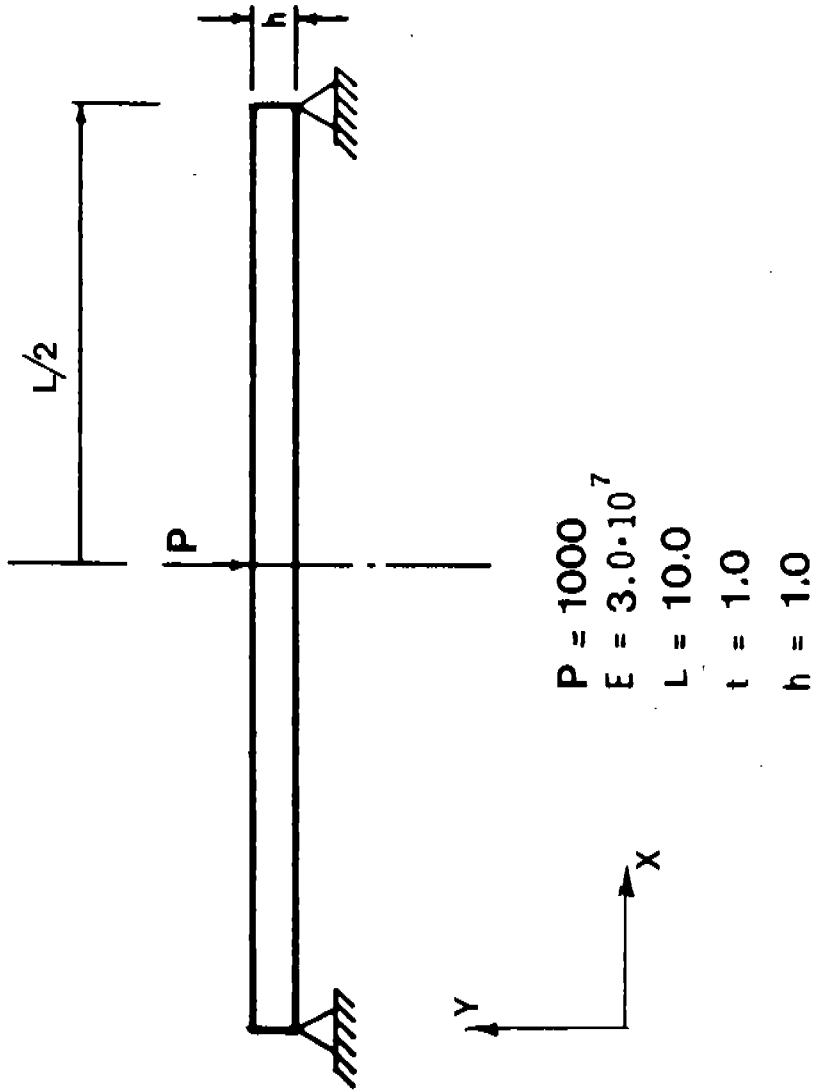
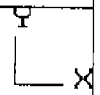


FIGURE 4.12: Sketch of ADINA Test Problem #3

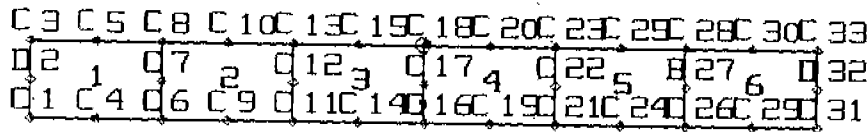
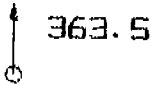
ADINA-PLOT VERSION 4.0.3, 5 APRIL 1992
 BEAM TEST PROBLEM BEAM2, LOC LARGE DISPL AND ELASTIC

ADINA ORIGINAL XUMIN: 0.000
 XUMAX: 0.000
 0.7843 YUMIN: 0.000
 YUMAX: 0.000



PRESCRIBED FORCE

TIME: 6.000



U1 U2 U3 U4 U5 U6 U7 U8 U9 U10 U11 U12 U13 U14 U15 U16 U17 U18 U19 U20 U21 U22 U23 U24 U25 U26 U27 U28 U29 U30 U31 U32 U33

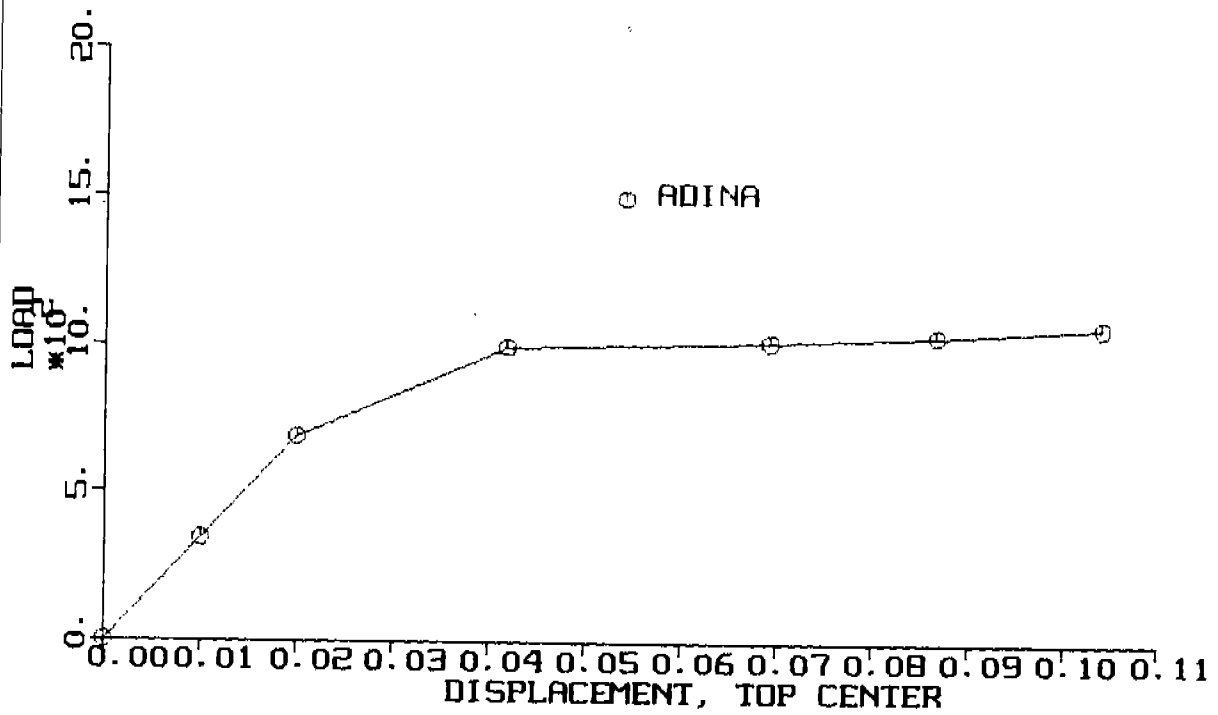


FIGURE 4.13: FE Model and Resulting Load Displacement Curve for Test Problem #3

75

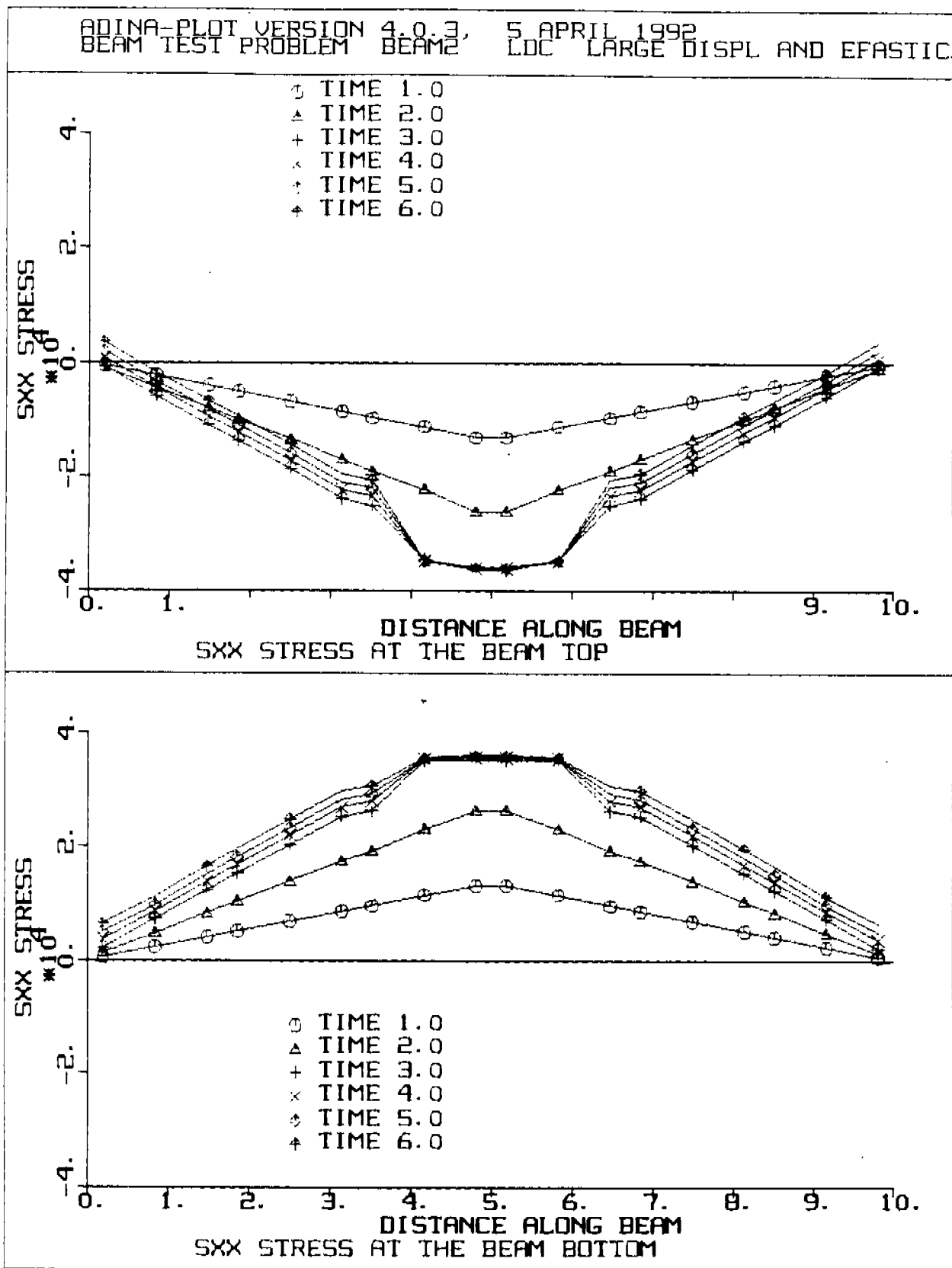


FIGURE 4.14: SXX Stress Along a Line on the Top and Bottom of the Beam for Test Problem #3

5. MIDBODY ANALYSIS

The results presented in this chapter are based upon a global ship coordinate system. This system is coincident with the axis shown on the plots from both the MAESTRO and ADINA analyses. The global x direction is positive in the forward direction, the global y direction is positive vertical and the global z direction is positive in the starboard direction of the ship.

5.1 Description of Structure

The extent of the midbody model is from frame stations 135 to 138 and 258AB (inches Above Base) to 438AB. This region of the ship corresponds to a documented ice damaged region of the M.V. Arctic as outlined in Section 3.2. The mainframes are angle sections with a spacing equal to 0.41m (16 inches), the web frame spacing is equal to 1.22m (48 inches) and the depth between stringers is 1.52m (60 inches). The sizes of all scantlings in this region of the ship are provided in Table 5.1.

5.2 MAESTRO Analysis

One MAESTRO model was developed for the analysis of the M.V. Arctic. This model predicts the overall response of the M.V. Arctic, which is used to determine the boundary conditions for the ADINA top-down models. A description is provided in the following section of the whole model even though the analysis of the bow is presented in Chapter 6. When reading Chapter 6 the reader can refer back to this chapter for a description of the MAESTRO model.

5.2.1 Description of Model

A global course mesh, finite element model of the M.V. Arctic was generated. As illustrated in Figure 5.1 this model extended from the midship to the bow. Due to the transverse symmetry only one side of the vessel has been modeled (see Section 4.4.1). The global model includes all the principal structural members which contribute to the hull structural stiffness. The outline of the top-down midbody and bow models are shown in this figure with arrows indicating the location of each model.

TABLE 5.1: Sizes and Plate Thicknesses of Existing M.V. Arctic Midbody Scantlings		
Part	Description	Dimension(s)
Outer shell	Plate	0.9449 in (24 mm)
Web frames	Plate	0.4331 in (11 mm)
Stringers	Plate	0.4921 in (12.5 mm)
Mainframes	Angles	9 x 4 x ½ in (228.6 x 101.6 x 12.7 mm)
Inner skin	Plate	0.7480 in (19 mm)

TABLE 5.2: ADINA Load Fractions for the Nonlinear Analysis of the Existing M.V. Arctic Structure	
Time Step	Load Level (Fraction of F_{max})
1	.147
2	.295
3	.578
4	.814
5	.915
6	.976
7	1.023
8	1.063

TABLE 5.3: Sizes and Plate Thicknesses of ASPPR Redesigned Midbody Scantlings		
Part	Description	Dimension(s)
Outer shell	Plate	0.9449 in (24 mm)
Web frames	Plate	0.4331 in (11 mm)
Stringers	Plate	0.4921 in (12.5 mm)
Mainframes	Flat bar	11.81 x 0.7087 in (300 x 18 mm)
Inner skin	Plate	0.7480 in (19 mm)

The MAESTRO model of the M.V. Arctic is composed of the 15 modules shown in Figure 5.2. These modules are combined into the following three substructures defining the full global FE model for the vessel.

- Substructure No. 1 - Fr109 to Fr160
- Substructure No. 2 - Fr160 to Fr 178
- Substructure No. 3 - Fr178 to Stem

There are 3,435 nodes used in modelling the M.V. Arctic which yield a total of 19,158 degrees-of-freedom for the entire model.

The principal longitudinal structural members of the vessel (deck, side shell, tank top, bottom, inner bottom, inner shell, stringers and double bottom girders) are included into the MAESTRO model as strake elements. These elements represent a unit made of a stiffened panel and its associated longitudinal girder (optional) and transverse frame. The strake elements are four noded quadrilateral elements with six degrees-of-freedom per node. The stiffeners in a MAESTRO model are smeared into the plating of the strake and they do not provide any local bending stiffness. On the other hand the longitudinal girders and transverse frames associated with a strake element have six degrees-of-freedom and they provide both membrane and bending stiffness.

The principal transverse structural members (transverse bulkhead, heavy brackets and solid floors) for the M.V. Arctic are included into the global FE model as superelements. MAESTRO's superelement is a membrane type of element providing three degrees-of-freedom per node. For the M.V. Arctic, within a superelement the plating of the transverse structure is modeled as membrane elements and its associated stiffeners as bar elements.

5.2.2 Boundary Conditions

There are two types of boundary conditions imposed on the MAESTRO model; one pertaining to the structural symmetry, and the other to prevent the rigid body motion.

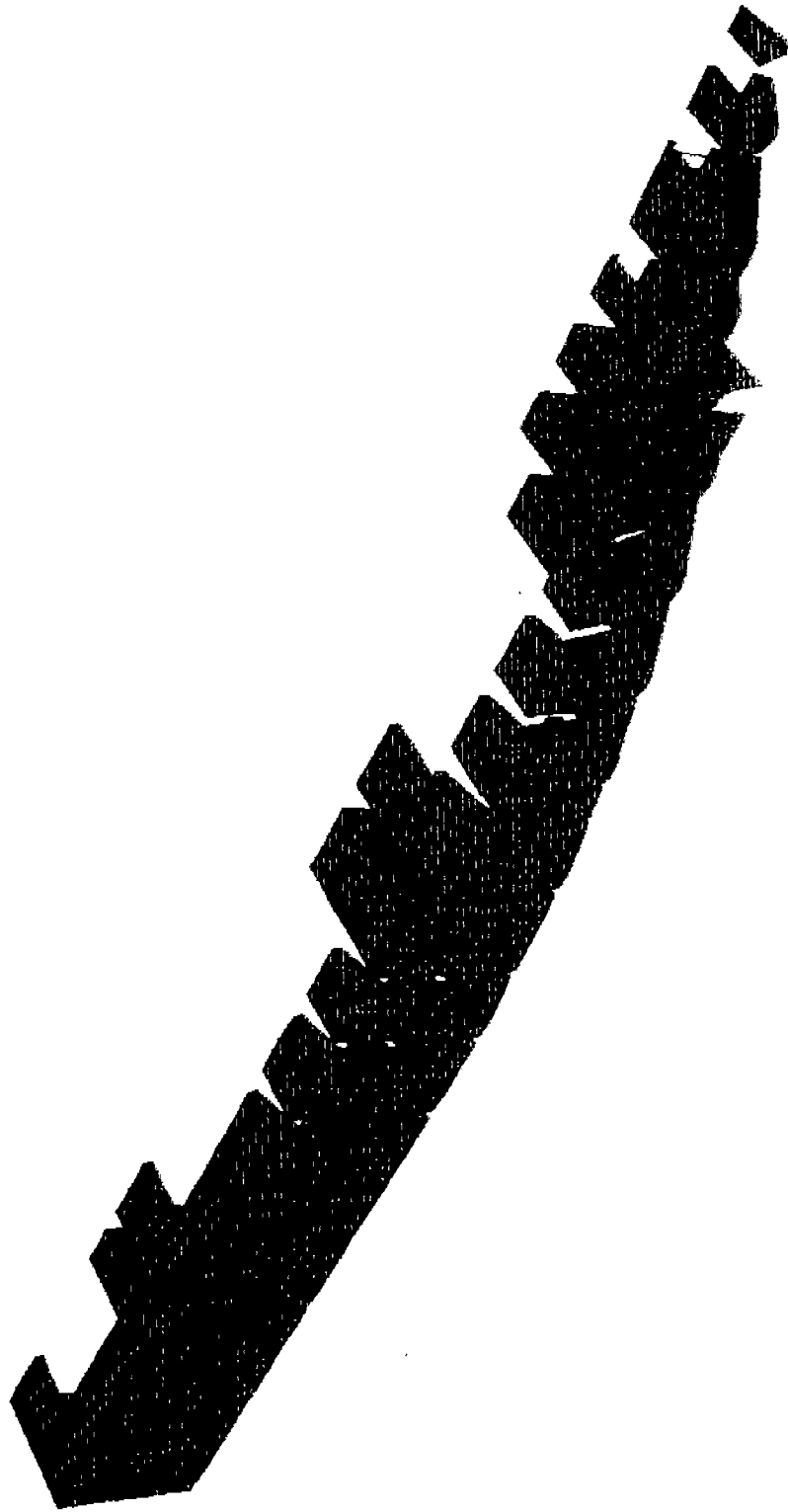


FIGURE 5.2: Substructuring Scheme for the MAESTRO Model
Showing Locations to be Modelled in Detail

As mentioned in Section 5.2.1 the structural members on the M.V. Arctic are symmetrical with respect to the centerline plane of the vessel. Hence, symmetry has been imposed and only one side of the vessel has been modelled. The boundary conditions applied to the nodes located on this plane of symmetry are illustrated in Figure 5.3(b). A detailed justification of this symmetry assumption with respect to geometry and loading is contained in Section 4.4.1.

Symmetry has also been imposed on the nodes located at the midship section of the vessel (Fr109). Due to the difference in the after and forward body of the vessel this assumption is not fully true. However, due to the approximate symmetry of the still water bending moment and large parallel midbody of the vessel this assumption is justified. Figure 5.3(a) illustrates the constraints applied to the nodes located at the midship. Section 4.4.1 provided a detailed justification for this assumption.

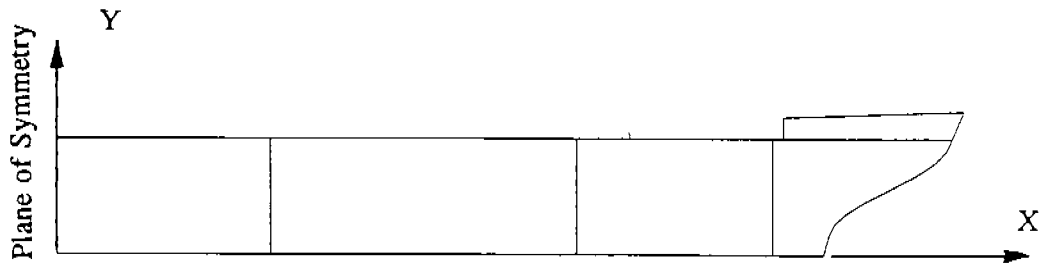
In addition to the constraints from the symmetry condition, the M.V. Arctic is subjected to a boundary condition to prevent any rigid body motion. In order to satisfy this condition the node located on the keel at the midship is fixed from translating. This constraint is applied to prevent ill-conditioning of the stiffness matrix. It has no effect on the response at the region of interest.

5.2.3 Loads

For the global analysis, the M.V. Arctic is subjected to the combination of still water bending moment, hydrostatic pressure load, and the ice loads.

The worst case for ice damage is when the structural members above the neutral axis are in compression. This condition is achieved when the vessel is subjected to a sagging hull girder bending moment and the hold where the ice load is acting is empty. This implies that there will be no pressure from the cargo to counteract the external iceloads.

The loading conditions provided by the shipyard from the original stability booklet did not satisfy the scenario discussed above. Due to this, an artificial loading condition was formed by increasing the weight density of the cargo bay structural members to represent the weight of the cargo. This condition represents a sagging moment on the vessel. All the holds for this condition are kept



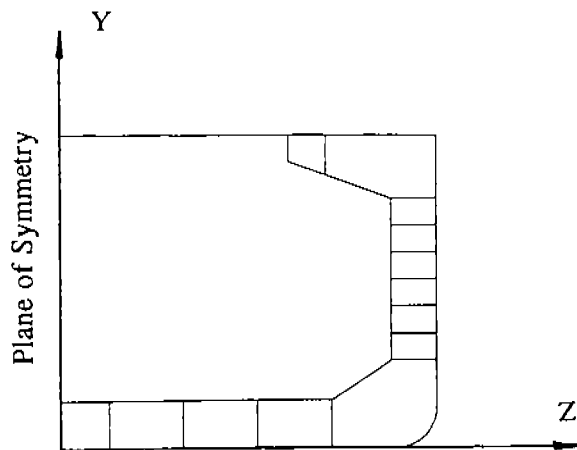
B.C.'s:

$$X = 0$$

$$\theta_y = 0$$

$$\theta_x = 0$$

(a) Symmetry Boundary Conditions (Transverse)



B.C.'s:

$$Z = 0$$

$$\theta_x = 0$$

$$\theta_y = 0$$

(b) Symmetry Boundary Conditions (Longitudinal)

FIGURE 5.3: Symmetry Boundary Conditions for the Midbody Analysis

empty, since the full weight is represented by structural weight density factor. For the hydrostatic loading a draft of 10.93m (35.85 ft) is used for the analysis. This draft correspond to the most common displacement at which the vessel operates. The combination of weight distribution and buoyancy applied to the M.V. Arctic resulted in a sagging still water bending moment with its maximum value of 0.48×10^6 Ft LTons at the midship of the vessel. The ice loads for the midbody and the bow area are determined according to the revised ASPPR regulations. The details of the calculated ice pressure and ice print are given in Appendix A.

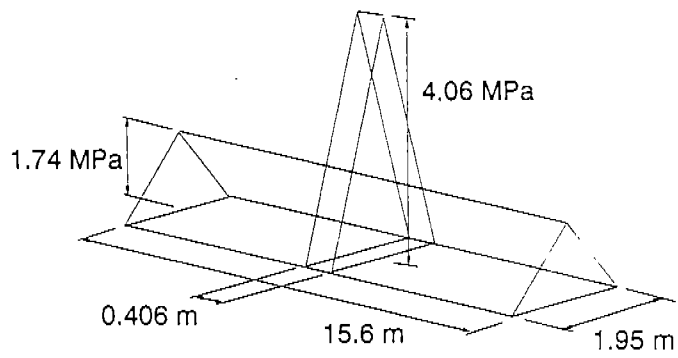
According to the revised ASPPR regulations, the distribution of the average ice pressure on the ice print is triangular. This distribution for the M.V. Arctic is illustrated in Figure 5.4 and described in more detail in Appendix A. The ice print for the midbody is located between Fr133 to Fr140.

The program MAESTRO does not allow a variation in the pressure distribution over an element. Hence, for the global analysis the triangular pressure distribution due to ice was approximated by point loads and applied to the appropriate nodes. The total load is the same as if the pressure distribution was used, therefore, the effect of using point loads instead of pressure loads on the response is expected to be minimal. The details of the calculation of point loads is presented in Figure 5.5.

5.2.4 Analysis and Results

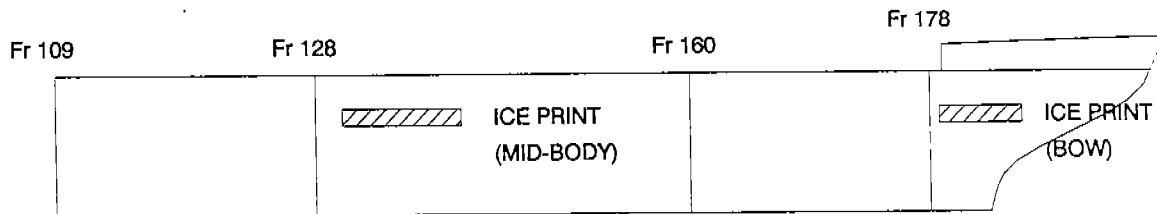
The global analysis of the M.V. Arctic was performed on a VAX3100 workstation using MAESTRO Version 5.4. The analysis was conducted in two phases. First, the structural response was determined when the vessel was subjected to the still water bending moment only. Secondly, the ice loads were applied to simulate the condition that produces midbody damage.

The deformed shape and the stresses due to the combination of still water bending moment and ice load at the midbody location are presented in Figures 5.6 to 5.8. As discussed in Section 5.2.3, the weight of the cargo in the holds has been modelled by increasing the weight density of the structure. Hence, the holds are kept empty to maximize the ice load effect. This can be seen by the



Ice Loads at Mid-body

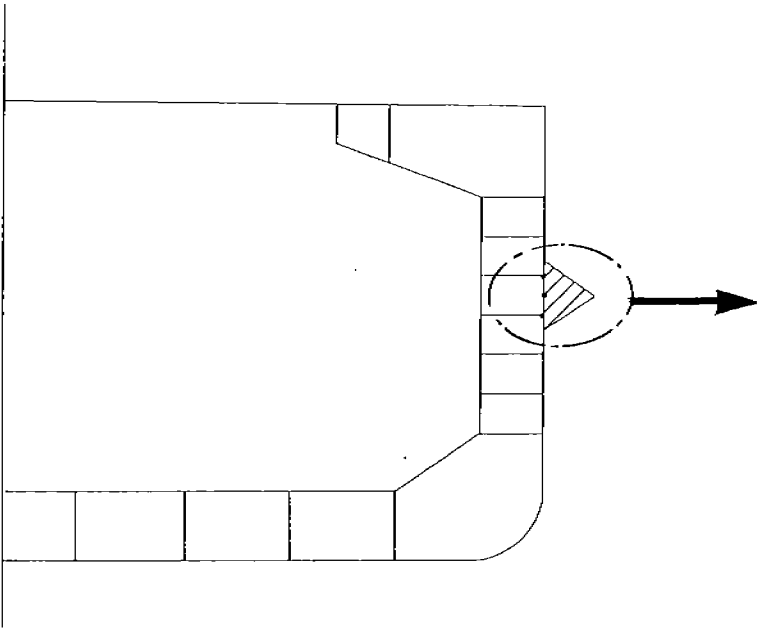
(a) Pressure Distribution of ASPPR Ice Load



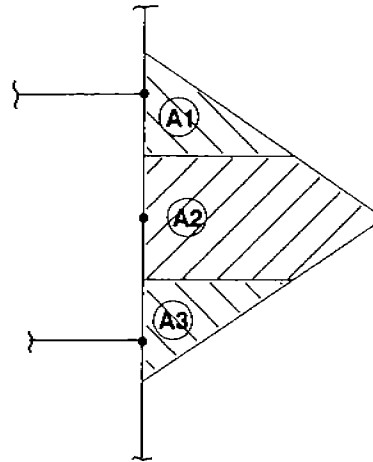
(b) Location of Ice Print on M.V. Arctic

FIGURE 5.4: Location of the Ice Loads

5-10



Ice Pressure
Distribution



Ice Pressure
approximated as
point loads

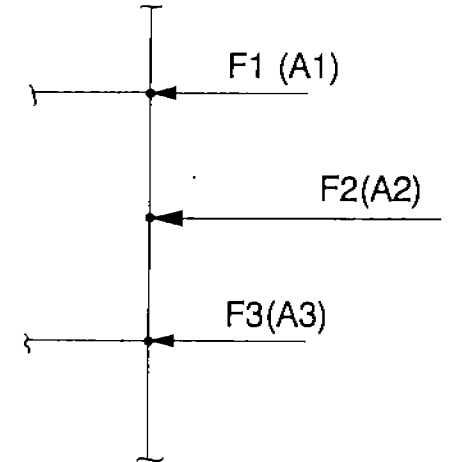
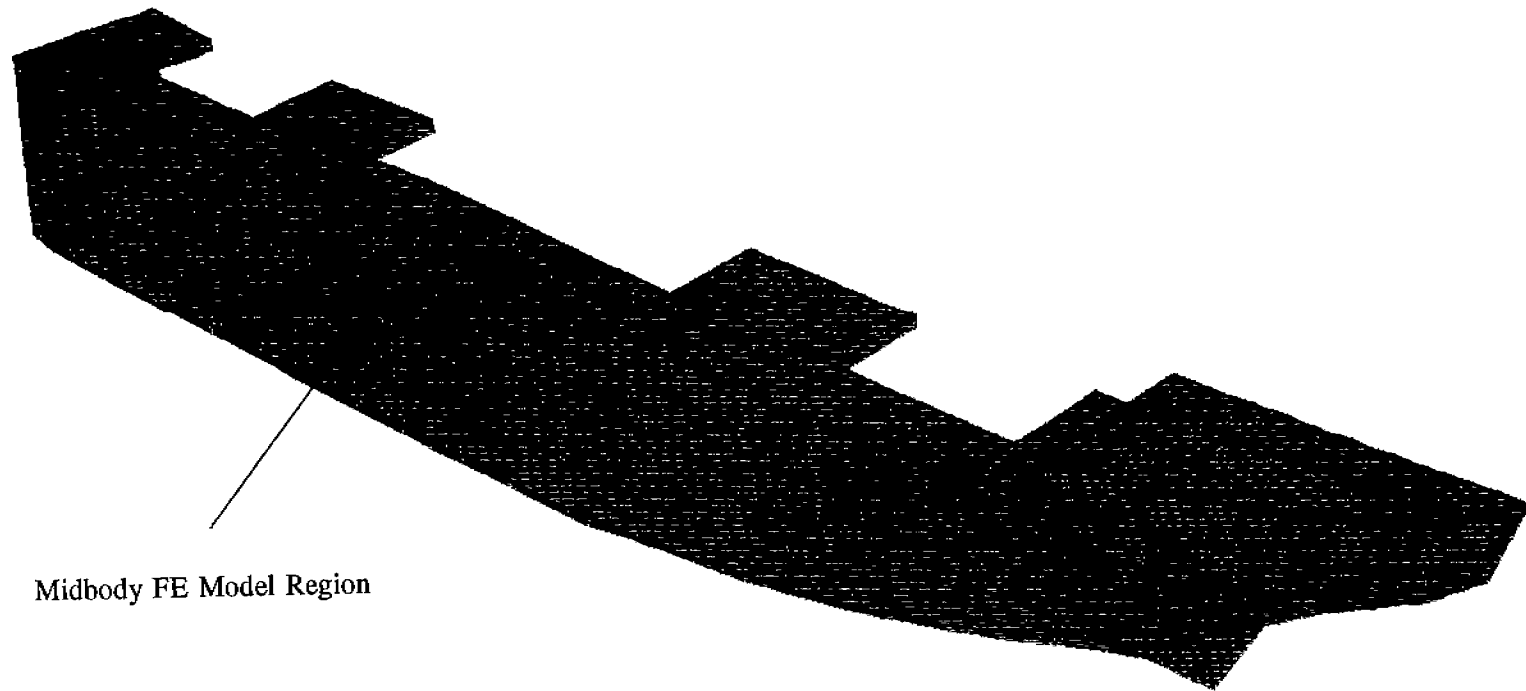


FIGURE 5.5: Procedure to Apply Ice Loads to the MAESTRO Model

98



Midbody FE Model Region

DEFORMATIONS LOAD CASE 1

87

FIGURE 5.6: Displaced Shape of MAESTRO Model from Midbody Loads

amount of inward displacement (maximum of approximately 1.0 inch) of the outer skin in Figure 5.6. As illustrated in Figure 5.7 the longitudinal stress (SXX) for this load case at the ice print location is of a compressive nature with a value of approximately 9550 lb/in². The transverse stress (SYY) for the same location is given in Figure 5.8, and its value is between 9550 lb/in² and 13000.00 lb/in² (compressive stress). The boundaries of the top-down model are outlined by the rectangular boxes sketched on both of these stress plots. This allows for much easier comparison of the stresses between the MAESTRO analysis and the ADINA linear top-down analysis at F_{max} .

5.3 ADINA Analysis of Existing Structure

The ADINA analysis of the existing structure is performed using the top-down modelling procedure outlined in Section 4.3.3. A description of the FE model plus the results of a linear and nonlinear analysis is presented in the following sections. A description of the scantlings for the model is provided in Section 5.1.

5.3.1 Description of the Model

The FE model, which has 2500 nodes and 750 elements, utilizes all 8-node shell elements with a coarse grid near all boundaries and a finer grid only near the center bay. Specifically, the more refined regions are; the outer shell plating bounded by the center bay, the upper and lower stringer sections adjacent to the center bay, the aft web frame section adjacent to the center bay, and the primary loaded mainframe which is on the aft side of the center bay. A plot of the FE model is shown in Figure 5.9(a).

5.3.2 Boundary Conditions

The boundary conditions for the top-down model have been derived from the MAESTRO

analysis to the top-down model was automated, through the creation of a Fortran program, to minimize any potential errors in prescribing the displacements on the top-down FE model boundaries.

Because the MAESTRO results are strictly linear, the procedure employs the assumption that the response at the panel boundaries is linear and that the nonlinear effects are local to the interior of the panel. This is felt to be a good assumption since the application of the ice load is quite local. For the nonlinear ADINA analysis, the MAESTRO boundary conditions are scaled according to the percentage of load which is applied to the structure at the load step in question. The still water bending moment is also scaled since it forms part of the MAESTRO total load. This is not strictly correct since the still water bending moment is present at its full value during the entire application of the ice load and therefore the total load will only be completely accurate at the magnitude F_{\max} . This is not felt to be a significant drawback in the procedure since the results are most important at F_{\max} where the load application will be accurate.

The prescribed displacements are placed on all nodes of the FE model boundaries where the outer and inner shells, the webs, frames, and the stringers have been cut away from the overall MAESTRO model. Since these displacements are linear, the results from the nonlinear analysis are also linear at these boundaries.

5.3.3 Loads

The prescribed displacements from the MAESTRO analysis represent a combination of the still water bending moment, hydrostatic pressure, and the ice load. When applying loads to a model in a "top-down" approach, the global effect of the load on the structure is brought into the local analysis by the prescribed boundary conditions employed from the MAESTRO analysis. The local effect of the load is determined by applying the local load to the model in the presence of the prescribed boundary conditions. It is imperative to employ the local load in the model as well as the prescribed boundary conditions since this is the load condition required to establish equilibrium in the structure.

The distribution and magnitude of the applied ice load (F_{\max}) is as detailed in Appendix A and as presented in Section 5.2.3 for the MAESTRO model. The still water bending moment does not have

an external load component and is transferred to the top-down model through the MAESTRO prescribed displacements. The local loading on this particular model does not include the hydrostatic pressure load, however, this is such a small component of the load (0.5% of the maximum ice pressure load at the frame midspan), that it is not expected to have a significant effect on the response. A plot of the applied load is shown in Figure 5.9(b).

5.3.4 Linear Analysis Results

The results of the linear analysis are presented in Figures 5.10 to 5.14. Figure 5.10 shows the global SXX and SYY stresses. These compare well with the MAESTRO results (Figures 5.7 and 5.8). Both show outer skin compressive stresses and inner skin tensile stresses with values ranging from approximately 8000 psi to 16000 psi. This indicates that the applied loads are the same for both models and that the boundary conditions (prescribed displacements) are being properly transferred to the top-down model.

In general, the structure acts similar to a simple beam under the applied load, with the outer shell going into compression and the inner skin going into tension. This is shown in Figures 5.10(a) and 5.10(b). This response is also demonstrated for the vertical stress component, SYY, in the mainframes and the deep webs in Figures 5.11(a) and 5.11(b) respectively. The mainframes, since they are close to the outer shell, are generally in compression. However, this changes on the mainframe flanges near midlength where the maximum load is applied. At this location on all mainframes, the stresses change to tension. This is a local effect due to the application of the highest peak in the ice load triangular distribution at this location on the mainframes. This is most evident on the mainframe with the highest peak load where the tensile stresses extend over a larger region of the flange. The deep webs in Figure 5.11 (b) show the simple beam effect with the plating near the outer skin in compression, the plating near the inner skin in tension, and the neutral axis running vertically at approximately mid-depth.

The only region of the structure in which the linear analysis shows that plasticity may be a problem (at F_{max}) is in the stringers above the center bay where they intersect with the mainframes. As shown in Figure 5.11(c), the SZZ compressive stresses are very high. This is due to the inward

displacement of the web of the mainframes being resisted by the stringers. This region will have to be studied in more detail in the nonlinear analysis.

A displaced shape plot of the outer skin and mainframes is shown in Figure 5.12. Because this analysis is linear and does not account for geometric or material nonlinearities, no definite conclusions can be made as to the failure of the panel, however, the displaced shape of the mainframes resembles tripping.

5.3.5 Nonlinear Analysis Results

The same load vector used in the linear analysis was also used to perform the nonlinear analysis using the load displacement control method. A very small initial z displacement was used to start the solution, and ADINA automatically determined the new loads for each subsequent load step until the program failed to converge at a load level equal to 106% F_{max} . This solution took eight time steps with the load fractions for each step provided in Table 5.2.

The following was found to occur during the nonlinear buckling process for the existing structure. At approximately 70% of F_{max} , yielding begins to occur at the point of intersection of the mainframe web and flange at about the center of the span between stringers. As the load is increased, yielding progresses through the web of the frame until, as shown in Figure 5.13, at about F_{max} , the area of intersection of the web and the flange is completely yielded. Since the frames are steel, which is assumed to behave as elastic-perfectly plastic, this yielded material now has no strength under further incremental loading which leaves a small ribbon of material in the outer flange which is essentially suspended in space and under increasing tensile loads. This ribbon of material is very unstable and tries to align with the frame web as the load increases. At 106% of F_{max} the frame, which is directly under the ice load, buckles through tripping.

This mechanism can be more easily seen from Figure 5.14. This plot shows the displacements at two points on the center bay mainframe with the highest applied load. Node 1166 is at the intersection of the mainframe web and flange and node 466 is at a point where the mainframe web

ADINA-PLOT VERSION 4.0.3, 10 APRIL 1992
M.V. ARCTIC

ADINA DEFORMED UMIN 6019.
LOAD-STEP XUMAX 5847.
TIME 1.000.5156 UMIN 199.2
YUMAX 372.5

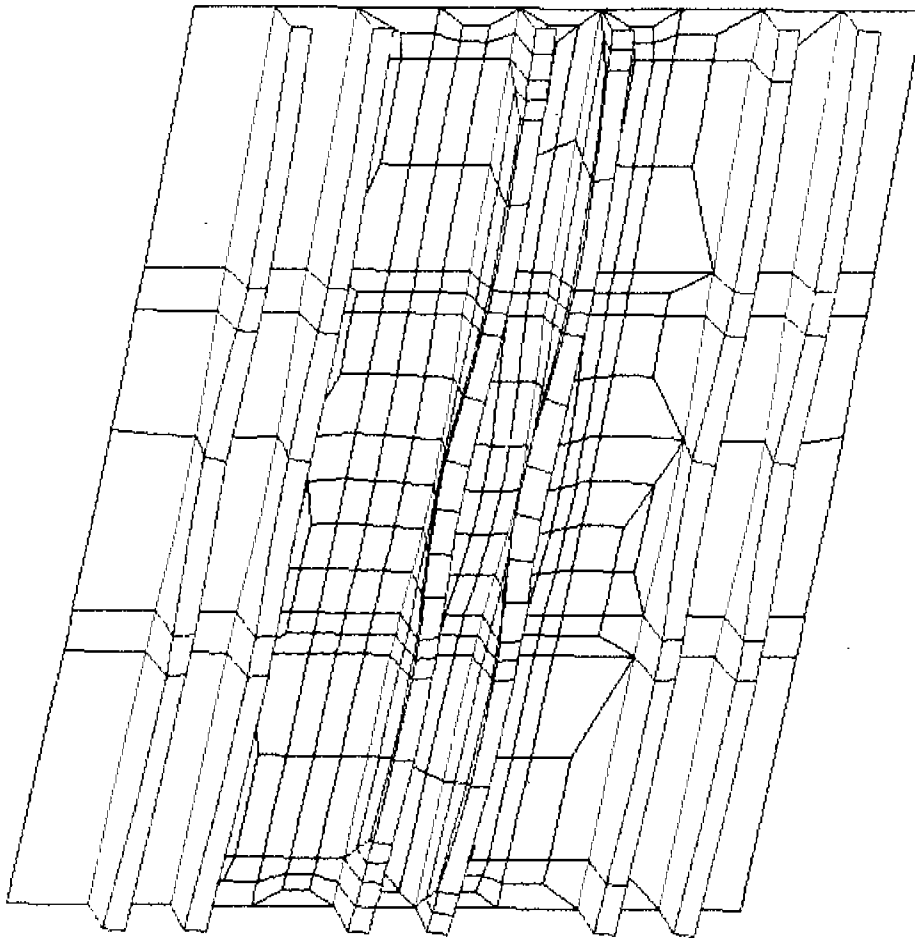
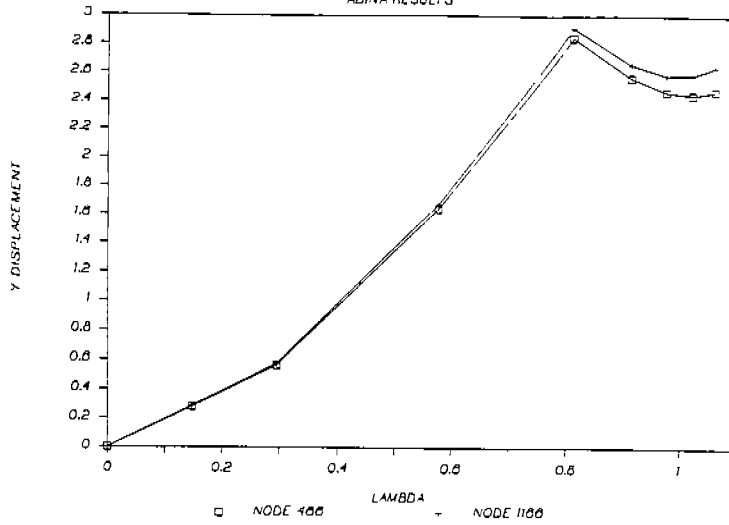


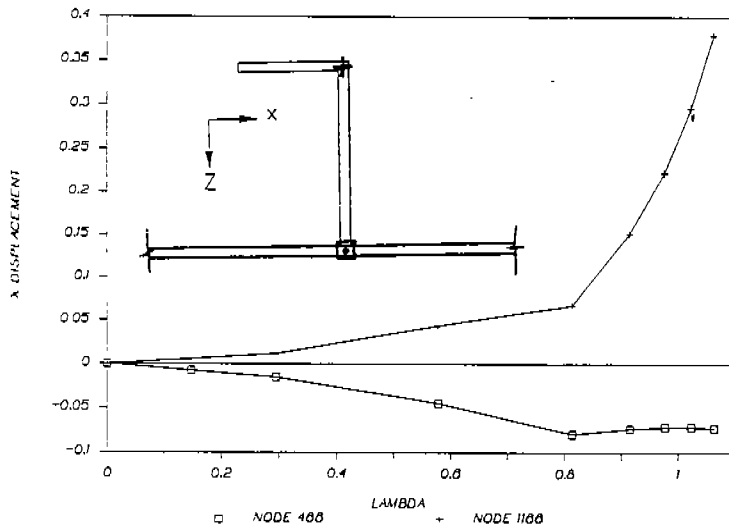
FIGURE 5.12: Inside View of Displaced Shape of Outer Skin and Main Frames
- Linear Analysis of the Existing Midbody FE Model

MV5NL2 - LDC EXISTING STRUCTURE

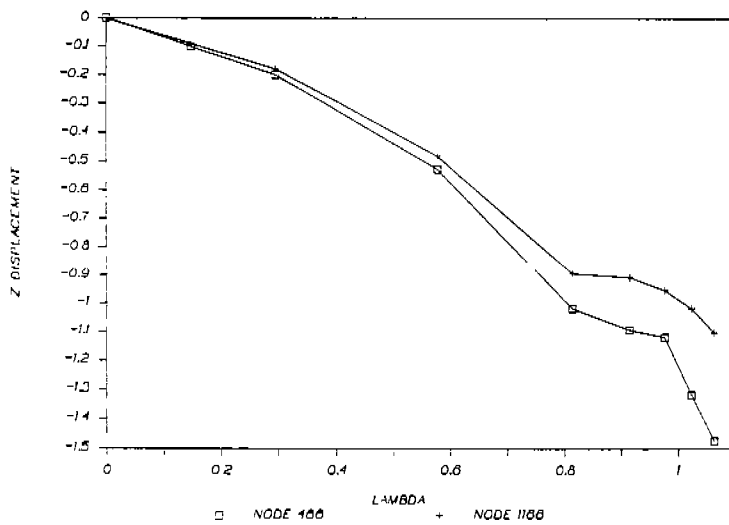
ADINA RESULTS



(a) Y Displacement



(b) X Displacement



(c) Z Displacement

FIGURE 5.14: Displacement vs. Load Fraction
- Nonlinear Analysis of Existing Midbody FE Model

intersects with the hull plating just above midlength of the mainframe. The purpose of presenting the results of these two points is to illustrate the relative movements between the two points.

The y and z displacement at the different applied loads is shown in Figures 5.14(a) and 5.14(c) respectively. The y displacement is vertical and the z displacement is the displacement normal to the hull. At $\Lambda=1.0$ the applied load is equal to F_{max} . For both plots, the two points can be seen to follow the same displacement pattern, indicating that as the load is increased, the hull, and the mainframe displace upward and inward. At load step 4, it can be seen that a substantial change in the response occurs. This corresponds to the point where the mainframe begins to trip. This can be seen in Figure 5.14(b) where at load step 4, the node on the flange starts to displace significantly more in the lateral (x) direction than the node on the outer shell.

Following this point, the load increases to a maximum of about $1.06 F_{max}$ at load step 8, after which the analysis fails to converge. As explained in Section 4.3.2, the LDC method will stop if four iterations of repeatedly reducing the incremental load fails to produce convergence. This is what happened at load step 8 where the mainframe under the maximum applied iceload becomes very unstable. This instability is assumed to be due to the tripping. The analysis could be continued past this point, if the LDC method was restarted at load step 9 with an initial z displacement small enough to produce convergence. However, this would be a very computationally expensive procedure. It is also not necessary. The analysis up to load step 8 has established that post-yield buckling occurs. There is no need to proceed past this point.

The final displaced shape of the model, without the inner skin, is shown in Figure 5.15. The mainframe buckling is quite evident.

At the highest load level, the hull plating is supporting some of the applied loads through membrane action. This is apparent in the SYY stress results of Figure 5.16. Above load step 4, the overall outer skin compressive stresses are reducing. This indicates that nonlinear effects are taking over the response and eventually tensile stresses will be set up in an area of the ship which is globally in compression.

5.4 ADINA Analysis of the Revised ASPPR Redesigned Structure

Following the linear and nonlinear analysis of the existing M.V. Arctic scantlings, an analysis was carried out on the same midbody region with the scantlings redesigned according to the ASPPR regulations. Several possible scenarios were presented for the new mainframe sections and spacing, however, it was felt that the fewer changes that were made to the structure, the easier it would be to understand the new response and the reasons for deviation from the original response. Based upon this, it was decided to maintain the same mainframe spacing and to use flat bars as the mainframe section. Other mainframe sections are analyzed later in the report. The stringers and deep webs were not changed from the original design.

5.4.1 Description of the Model

The extent of the top-down model is the same as for the previous model (i.e. 3x3 bays from frame stations 135 to 138 and 258AB to 438AB). The redesigned mainframes are flat bar sections with the original spacing of 16 inches. All other scantling sizes and model dimensions are the same as for the existing structure. The dimensions of all scantlings are provided in Table 5.3 and the FE model is shown in Figure 5.17.

5.4.2 Boundary Conditions

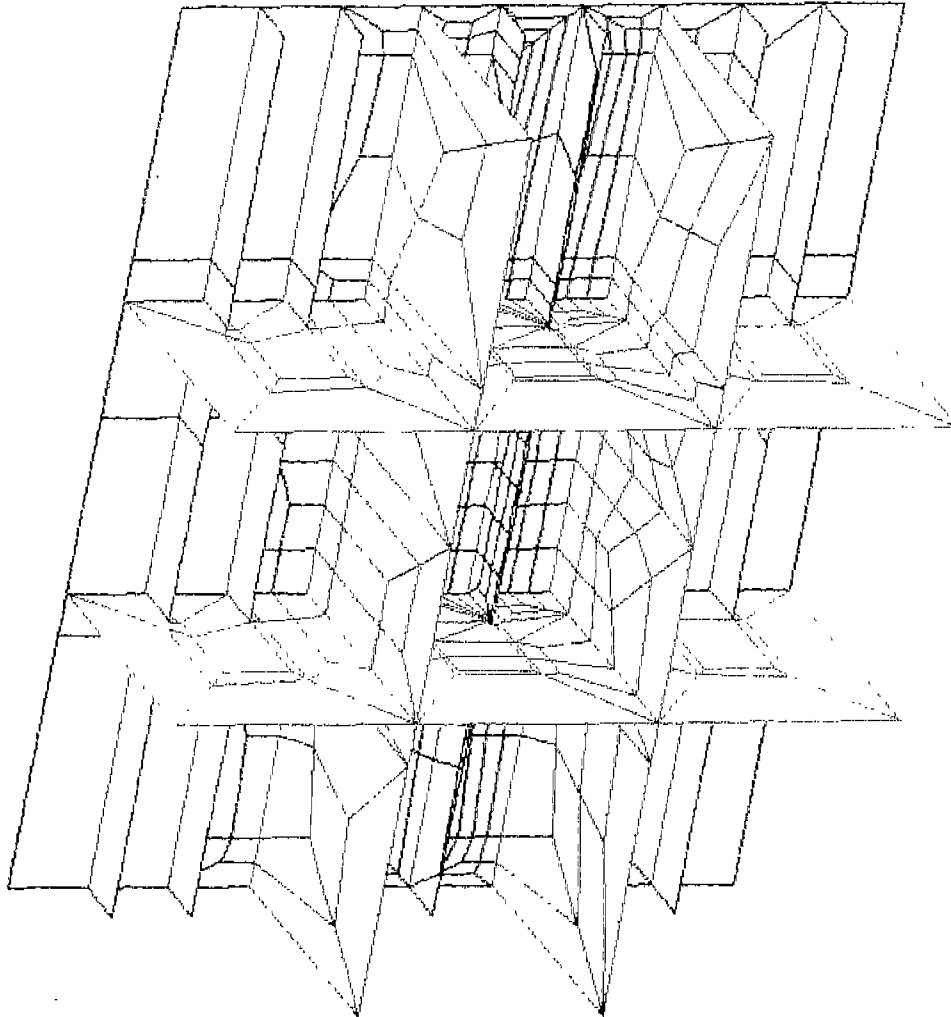
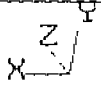
The boundary conditions for the redesigned FE top-down model are the same prescribed displacements determined from the MAESTRO analysis of the overall M.V. Arctic and used in the analysis of the model of the existing structure. A new MAESTRO analysis with the redesigned mainframes was not performed since it was felt that the overall ship response would not change significantly with the new redesigned ASPPR mainframes.

5.4.3 Loads

The applied ice load is the same as detailed in Section 5.3.3 for the existing structural model. The local loading on this particular model also includes the hydrostatic pressure load.

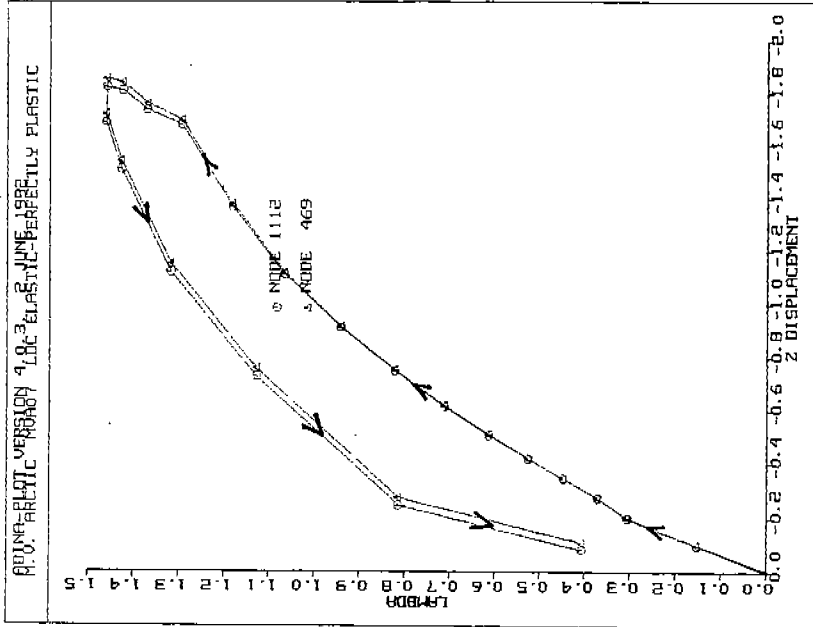
ADINA-PLOT VERSION 4.0.3, 8 JUNE 1992
M.V. ARCTIC MVA07 LDC ELASTIC-PERFECTLY PLASTIC

ADINA DEFORMED XUMIN 6023.
LOAD-STEP XUMAX 5851.
TIME 21.001.26 YUMIN 149.4
YUMAX 336.1

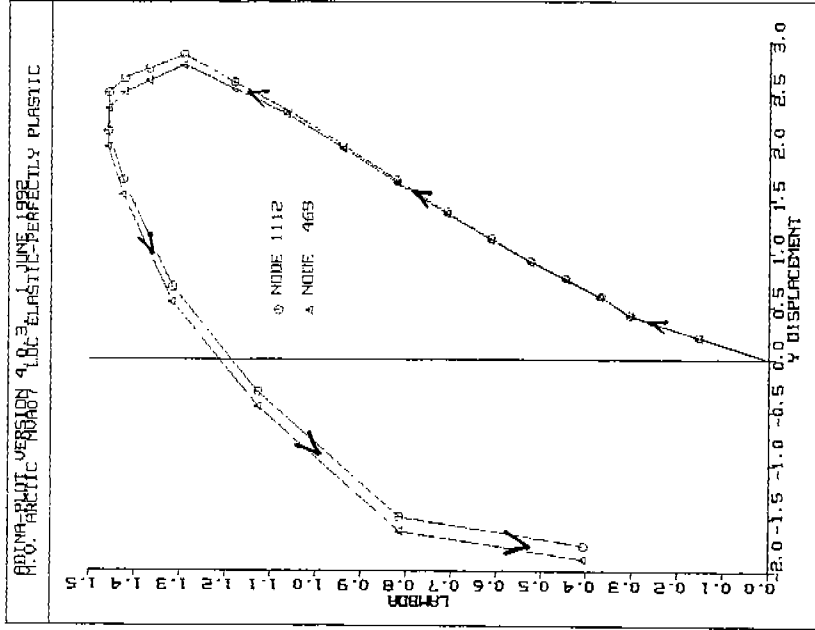


M.V. ARCTIC - WITHOUT INNER SKIN

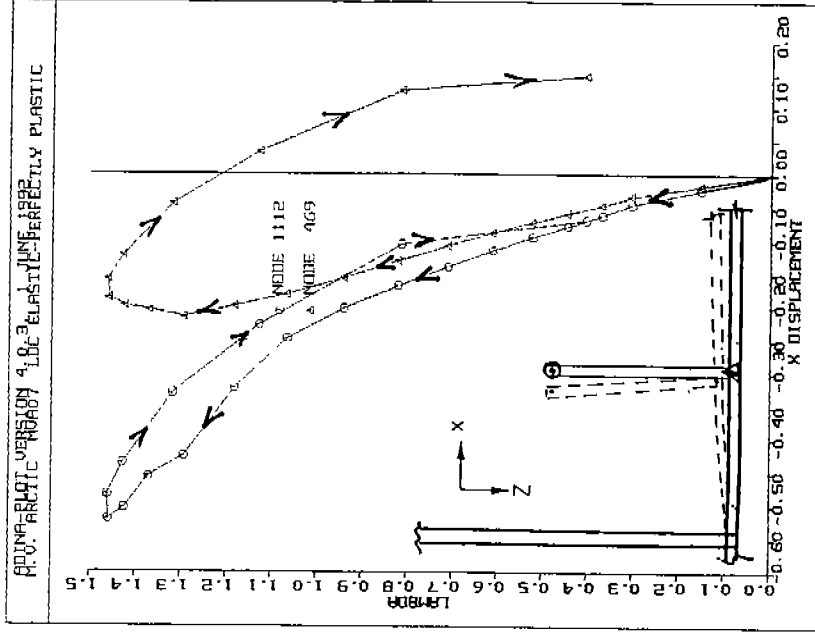
FIGURE 5.17: F.E. Model of Redesigned Midbody Structure with Flat Bars



(a) Z Displacement



(b) Y Displacement



(c) X Displacement

FIGURE 5.18: Displacement versus Load Fraction - Nonlinear Analysis of ASPPR Redesigned Midbody FE Model

5.4.4 Nonlinear Analysis Results

A linear analysis was not performed for this model. Since the linear analysis of the existing midbody FE model confirmed that the top-down modelling procedure is correct (Section 5.3.4), and the boundary conditions from the MAESTRO analysis have not changed in the redesigned model, there is no need to perform the linear analysis. Locally there will be differences in the response due to the change in the mainframes; however, globally there will be little change.

The same load vector used in the analysis of the existing midbody structure was also used to perform the nonlinear analysis of the redesigned ASPPR model. The load displacement control method was used which determines the new loads for each load step from an initial specified z displacement. Using this option, ADINA automatically determines the correct load increment to use to establish equilibrium and uses smaller load fractions as convergence becomes difficult to achieve. (Some user control is required in setting up an initial displacement size). The solution took 21 time steps with the load fractions for each step provided in Table 5.4.

Figure 5.18 shows the displacements of two points at midlength on the maximum loaded mainframe in the center bay. Node 1112 is a point on the mainframe at the point furthest from the hull plating and node 469 is at a point where the frame intersects with the hull plating. The purpose of presenting the results of these two points is to illustrate the relative movements between the two points.

The z displacement (normal to the hull) versus the applied load is shown in Figure 5.18(a). At $\Lambda=1.0$ the applied load is equal to F_{max} . The two points can be seen to follow the same displacement pattern, indicating that as the load is increased, the hull, and the mainframe displace inward. At load step 12, it can be seen that a substantial change in the response occurs. This corresponds to the point where local buckling is beginning to occur elsewhere in the structure. Following this point, the load increases to a maximum of about 150% of F_{max} at load step 15, after which it is steadily decreased until the analysis is terminated at about step 21 at 40% of F_{max} .

**TABLE 5.4: ADINA Load Fractions for the
Nonlinear Analysis of the ASPPR (Flat
Bar) Redesigned Midbody Scantlings**

Time Step	Load Level (Fraction of F_{max})
1	0.15
2	0.31
3	0.38
4	0.45
5	0.53
6	0.61
7	0.71
8	0.82
9	0.94
10	1.07
11	1.16
12	1.28
13	1.36
14	1.42
15	1.45
16	1.45
17	1.40
18	1.32
19	1.12
20	0.82
21	0.40

The decrease in the applied load is a result of the analytical technique which is employed in the analysis. The arc-length method is selected as the solution technique for this problem. In the arc-length method, buckling can be modelled as it occurs by changing from a load controlled solution to a displacement controlled solution. During the buckling procedure, the structure becomes unstable and cannot support the load which it was capable of supporting prior to buckling. Equilibrium can only be achieved by decreasing the load to a point where the structure is capable of supporting the load.

The buckling in this case is not a buckling of the mainframes, as was experienced prior to the application of F_{max} in the existing structure, but a local buckling in an area of a stringer, where the stringer intersects with the frame to which the ice load is applied. This buckling is unlikely to result in a collapse of the entire structure, and perhaps if the solution were continued, the structure may be found to be capable of carrying a larger load. However, numerically, it is difficult to continue past this point in the analysis. The solution was terminated due to an excessive number of iterations being required to establish convergence. This is generally indicative of collapse. To restart the problem, a sequence of runs would be necessary to define a small enough increment in order to establish equilibrium. This would be a very time consuming procedure. Approximately 36 hours of CPU time were used to complete the solution on a supercomputer. This took a period of about four days.

Figure 5.18(b) shows the y displacement for the same two points. The y displacement is a displacement in the longitudinal direction of the frames (i.e. vertical). The two points can be seen to displace together, showing very little deviation as the load is increased. At time step 11 (i.e. about 120% of F_{max}), the two points start to show some deviation, indicating a nonsymmetric response of the frame. This would correspond to a rotation of the frames about a fore-aft axis, as would be expected if substantial bending were taking place. The only interesting point to observe about the plot is that the two points show virtually an identical response during the early, and linear, phases of the response, and only show some deviation at large load levels, where the stresses in a substantial part of the structure have exceeded yield stresses. No significance can be placed upon the results past load step 15.

Figure 5.18(c) is the most interesting of the three plots. It shows the displacement in the x direction (i.e. in the fore-aft direction). The two points in the plot can be seen to show a difference in

displacement from the early stages of response which increases fairly linearly until about time step 11. After this point, the two curves diverge and at the point of maximum load application show a difference in displacement of about 0.5 inches. As the load level is decreased, this difference in displacement does not disappear, indicating a permanent deformation in the forward direction. The interesting point to note is that the displacement at the outer fibre of the frame disappears completely when the load is removed; however, the displacement at the hull plating does not. This is due to permanent plastic deformation at the intersection of the frame and hull. The frame is showing some tripping, which does not appear to be severe enough to completely buckle, however it is severe enough to remain as a permanent deformation.

The progression of yielding in the model is shown in Figure 5.19 where it is first observed at time step 7 (70% of F_{max}) in two locations. The first location is the stringers at the point where they intersect the mainframe (about which the ice load is centered) and the second location is the outer fibre of the same mainframe. Since the stringers provide the boundary conditions on the frame, they experience large stresses where this constraint is applied and since the mainframe is trying to trip, this rotation is resisted by the stringers. The mainframe is attached to the stringer on one side only by means of a gusset plate. This means that the cut which has been made through the stringer to allow the frame to pass through has been "repaired" on one side only, resulting in a discontinuity in the stringer at this point.

The yielding in the frame is due to local bending stresses which are set up in the frames to carry the applied ice load. The applied load is carried globally by the overall bending of the ship hull/web/stringer combination, however it is carried locally (between webs) by the mainframe/hull plating structure. At low load levels, the mainframes are capable of carrying the local load and the stresses which exist in the hull plating are the global stresses which result from the overall bending action of the hull/web/stringer. As the load is increased, the bending stresses in the mainframes increase to the point of yielding. As the yielding progresses through the frame, the frames become no longer capable of carrying additional load and the hull plating is forced to carry this load through a membrane action which is accompanied by large normal hull plate displacements.

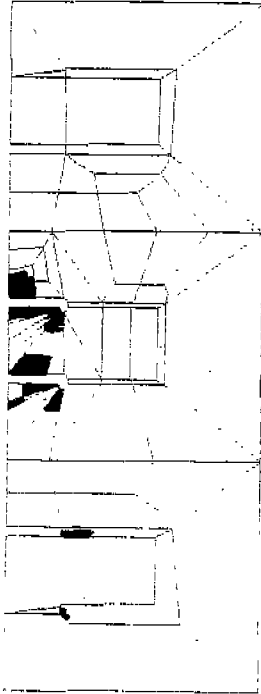
At the point where yielding initiates in the mainframes, the stresses in the hull plating are predominately compressive in both the x and y directions. The compressive stresses in the plating are relatively large; in the order of -20 ksi. As the load is increased, the compressive stresses in the plate increase. If the plating is looked at independently of the frames, a band of high compressive stress exists in the plating which reaches a level of -30 to -40 ksi at a load corresponding to F_{max} (at load step 9). However, as the load is increased, the yielding in the frames progresses further and the additional load must be carried by the membrane action in the plating. This shows up as a local decrease in the compressive stresses and an eventual tension being set up in the plating. This will be shown in the stress plots which are discussed later in this section.

Observing the progression of yield through the structure, Figure 5.19 shows that at time step 9 there is yielding being experienced in the plating at a location corresponding to the intersection of the hull plating and the deep web. Between time steps 11 and 13, it can be seen that the mainframe is completely yielded and no longer capable of carrying any increased load, however, the frame still continues to carry the load which it carried at yield.

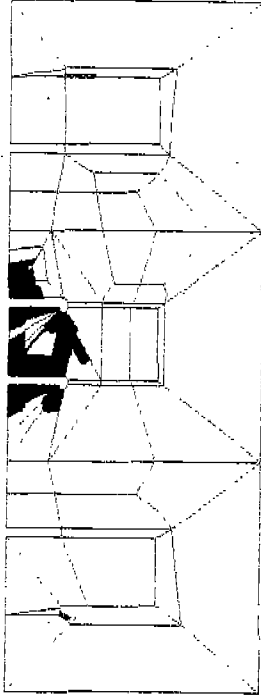
The load level decreases slightly from time step 15 to time step 17 and from the plot it can be seen that there is substantially less material experiencing yielding at step 17. The decrease in the amount of structure which is experiencing yielding is a direct result of the decrease in applied load. Since the material is modelled as elastic-perfectly plastic, a small decrease in applied load can result in complete recovery of the linear properties. (If one considers a uniform bar subjected to tensile stresses, the bar will see progressively larger stresses until yielding occurs. Further increase in load will result in increased strain with no increase in stress. A small decrease in applied load at this point results in a corresponding decrease in stress. The stress is once again in the linear range - below the yield stress.)

As the load level continues to decrease (time step 19) little change occurs. At load step 21, there is a redistribution of yielded areas but it is fairly minor.

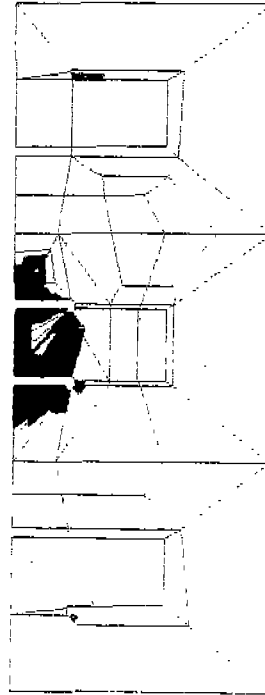
Figure 5.20 shows a more detailed look at the progression of yielding through the top stringer. It can be seen in this plot that the yielding occurs at the intersection of the frames and the stringer. As



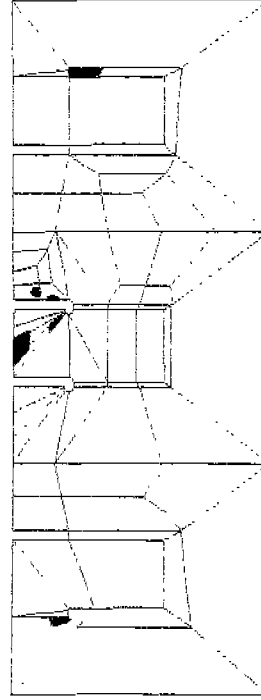
PLASTIC FLAG T=11.0 118%



PLASTIC FLAG T=13.0 138%



PLASTIC FLAG T=15.0 145%



PLASTIC FLAG T=17.0 140%



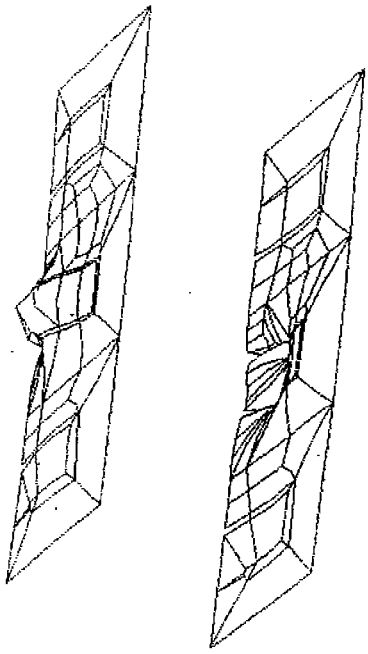
112

FIGURE 5.20: Progression of Yield in the Top Stringer - Nonlinear Analysis of the ASPPR Redesigned Midbody FE Model

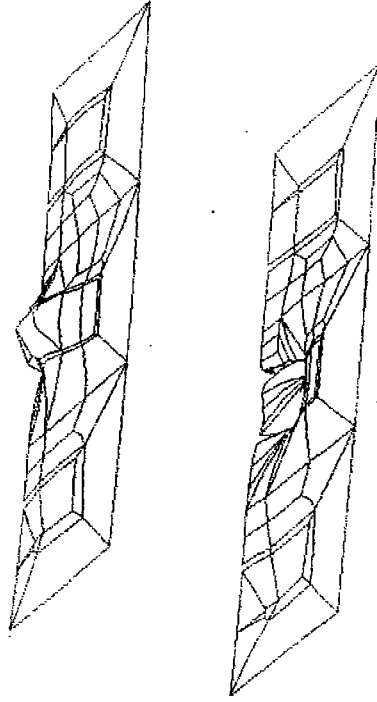
the load is increased, the yielding advances until, at load step 15, the area between the two adjacent frames is completely yielded. This area now becomes unstable and, as plotted in Figure 5.21, the large distortions at load step 16 show where the structure buckles under the increased load. At load step 17, the yielded areas in the plot of the stringer (Figure 5.20) can be seen to have decreased substantially. This corresponds to the decrease in applied load.

Figure 5.22 shows the stress present in the structure at load step 15 where the maximum load is applied (140% of F_{max}). The S_{YY} stresses at the exterior boundaries of the detailed model can be seen to be about -15000 psi. At F_{max} the MAESTRO analysis (Figure 5.8) shows this component to be about -10000 psi. With a difference of 1.5 in the magnitude of the stress for a corresponding difference of 1.4 in the applied load, these numbers can be considered to show good agreement. A band of stress of approximately -30000 psi is present in the FE model outer shell over the area of applied load. This stress is a result of the bending action of the hull/stringer/deep web structure. However, the outer shell stress, close to the point of load application, shows a significant change due to the membrane action being set up in the plating. This ultimately results in the local plate stress changing from a compressive stress to a tensile stress of about 20000 psi. This is not easily seen in Figure 5.22 but is presented in detail in Figure 5.23 where the S_{YY} stress in the center bay is shown from steps 4 to 21.

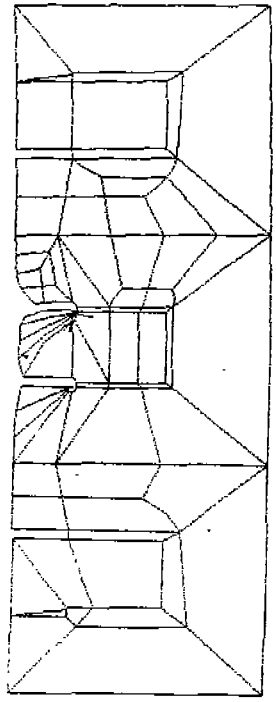
Figure 5.23 shows an increase in the outer shell local compressive S_{YY} stresses up to load step 10. At load step 12 the compressive stress begins to drop and during load steps 14 to 17 — where the structure becomes unstable — a tensile region develops and enlarges. The plate stresses vary over these load steps even though the applied load changes very little and the high compression area of stress present at the aft region of the panel decreases in magnitude from -40000 psi to -30000 psi due to a superimposed tensile stress in the plating. Above time step 17, the load is decreased. This results in the structure attempting to return to its original shape as the prescribed displacements are decreased along the linear boundaries of the model (corresponding to MAESTRO displacements). Since the structure has experienced permanent deformation, it resists returning to its original shape. This results in residual tensile stresses being set up in the plating.



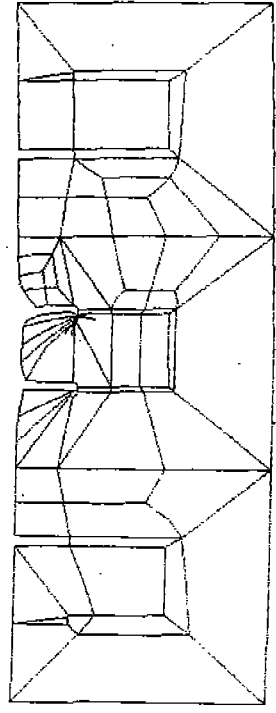
STRINGERS I=16.0 145%



STRINGERS I=17.0 140%



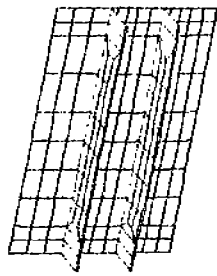
STRINGERS I=16.0 145%



STRINGERS I=17.0 140%

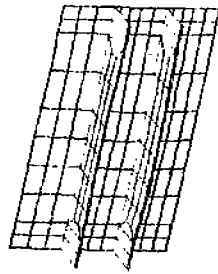


FIGURE 5.21: Displaced Shape of Stringers - Nonlinear Analysis of Redesigned ASPPR Midbody FE Model



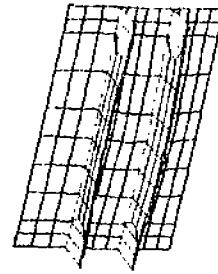
45%

MODEL CENTER PANEL T=4.0



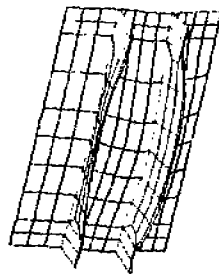
82%

MODEL CENTER PANEL T=8.0



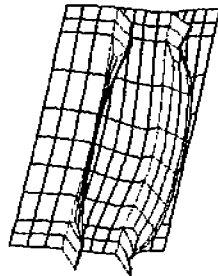
107%

MODEL CENTER PANEL T=10.0



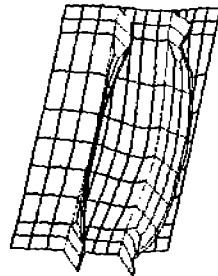
142%

MODEL CENTER PANEL T=14.0



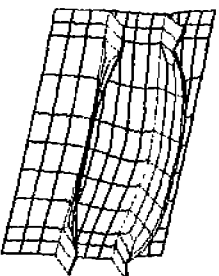
145%

MODEL CENTER PANEL T=15.0



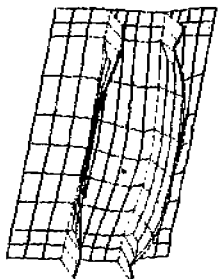
145%

MODEL CENTER PANEL T=16.0



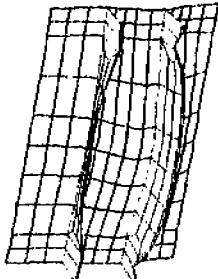
132%

MODEL CENTER PANEL T=18.0



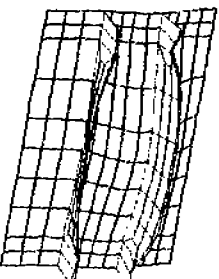
112%

MODEL CENTER PANEL T=19.0



82%

MODEL CENTER PANEL T=20.0



MODEL CENTER PANEL T=20.0

FIGURE 5.23: SY_Y Stress on the Center Bay at Various Load Levels
- Nonlinear Analysis of ASPPR Redesigned Midbody FE Model

5-40

116

Figure 5.24 shows the displaced shape of the outer shell and frames in the center bay from load steps 4 to 21. The mainframe under the local area of load application shows large displacements, and to show this a high magnification factor has been used. The large twisting action of the frames must be supported by the stringers. This puts large loads on the stringers which cause large distortions. Figure 5.21 showed the displaced shape plots of the stringers. The stringers can be seen to be displaying large out-of-plane displacements at load steps 16 and 17. These are believed to be the result of local buckling of the stringers.

5.4.5 Nonlinear Analysis using a Modified Grid

The analyses carried out under this project were initially performed on a supercomputer. Because of the anticipated high level of computing power, little restriction was placed on the size of the initial midbody FE model. However, when the analyses were started, very high solution times (four hours per load step) were encountered for models with approximately 3800 nodes. The supercomputer and the program ADINA were eventually "tuned" such that these times were reduced, however, with future expected load step requirements in the range of 15 to 20, it was decided to reduce the model size to keep analysis times at a manageable level. Unfortunately, the modelling scheme used to develop the initial model was not conducive to a coarse grid. Therefore, the grid of the midbody FE model had some elements (particularly in the stringers) with distorted shapes and high aspect ratios. This was a concern in the results detailed in the previous section since it was concluded that the structure failed at the stringers.

To determine if a more regular stringer grid would result in a different response, a new midbody FE model was developed. The mesh used in the model is exactly the same as the previous model except for the stringer mesh. The new stringer mesh is shown in Figure 5.25. The location of the intersection of the mainframes with the stringer is highlighted by the darker lines. In the previous model (see Figure 5.20), the material removed from the stringers at this location was explicitly modelled in detail. In the new model this material has not been removed. However, the gap between the stringer and frame has been modelled by disconnecting the nodes of the stringer from the nodes of the mainframes along the aft side of this interface line. This effectively produces the same effect as the removed material in the previous model.

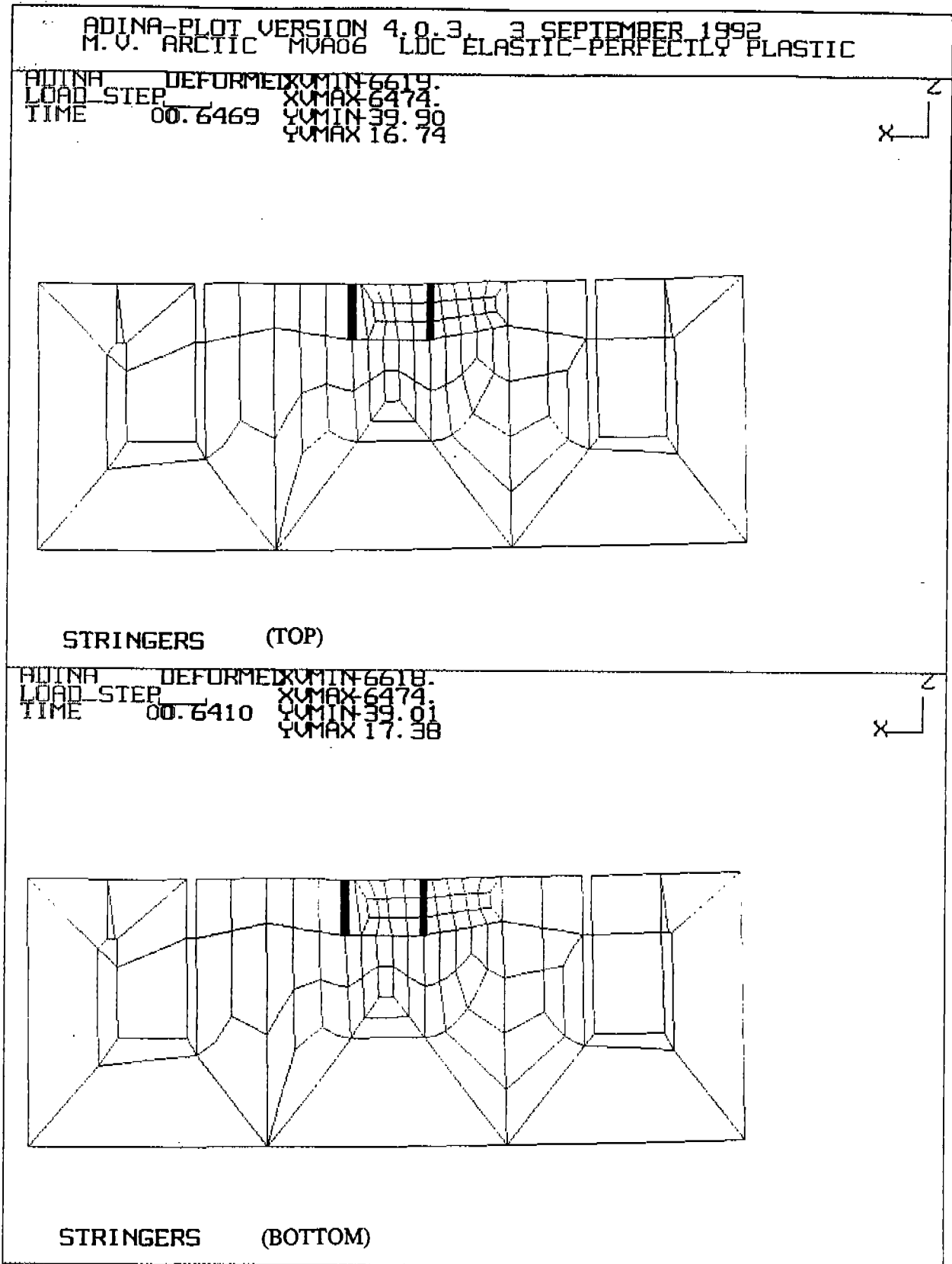


FIGURE 5.25: Modified Stringer Mesh - Nonlinear Analysis of ASPPR Redesigned FE Model

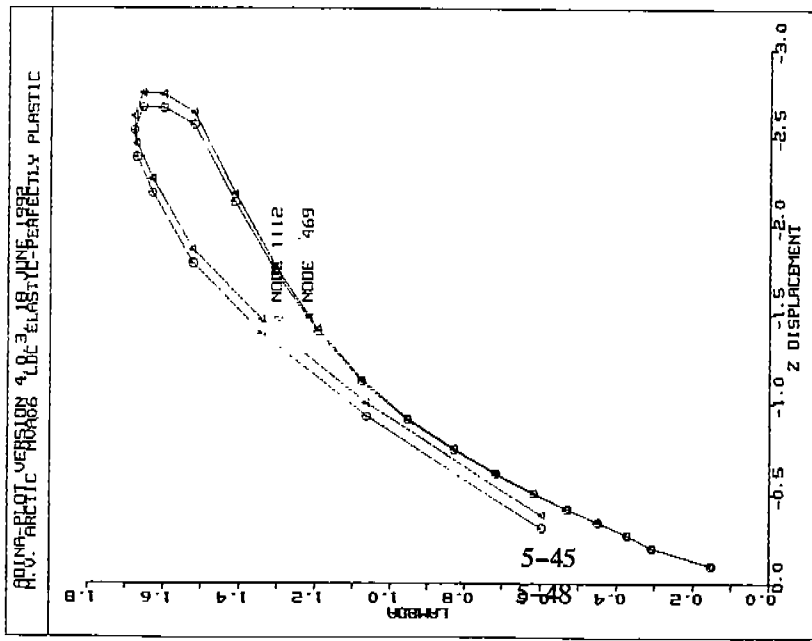
Comparison of this grid with the stringer grid used in the previous midbody FE model (Figure 5.17) shows a much more regular grid on the stringers. Therefore, any numerical problems which may be associated with stringer elements having distorted shapes and high aspect ratios should be eliminated.

To isolate the problems associated with element distortion, the response of the modified grid model is compared with the response of the model detailed in the previous Section 5.4.4. For purposes of comparison the model of Section 5.4.4 is addressed as model 1. The modified stringer grid model is addressed as model 2.

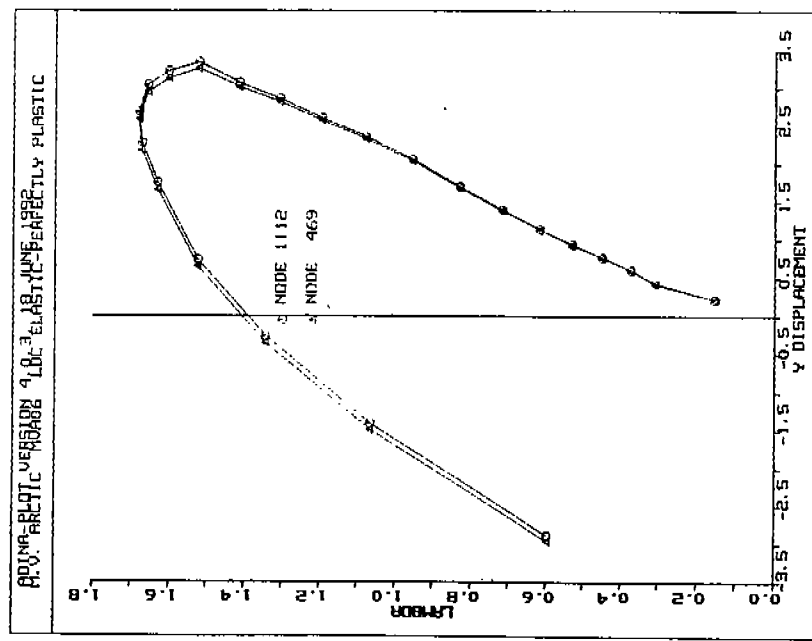
Figure 5.26 shows the displacement versus the applied load of model 2 at the same two mainframe nodal points as presented for model 1 (see Figure 5.18). These points are located at midlength on the maximum loaded mainframe in the center bay. Node 1112 is a point on the mainframe at the point furthestmost from the hull plating and node 469 is at a point where the frame intersects with the hull plating.

There are some apparent differences when comparing the results in Figure 5.26 to the results in Figure 5.18. The maximum applied load has increased from the model 1 value approximately 150% of F_{\max} to 170% of F_{\max} for model 2. The magnitude of the displacements also change. As a result of modifying the grid, the maximum z displacement increases by approximately 50%. The maximum x and y displacements change by approximately 10%. During unloading the x displacements at the outer fibre of the frame are different. In model 1, the x displacement disappears. However, in model 2, permanent deformation occurs. This corresponds to the lateral frame displacement at the frame outer fibre.

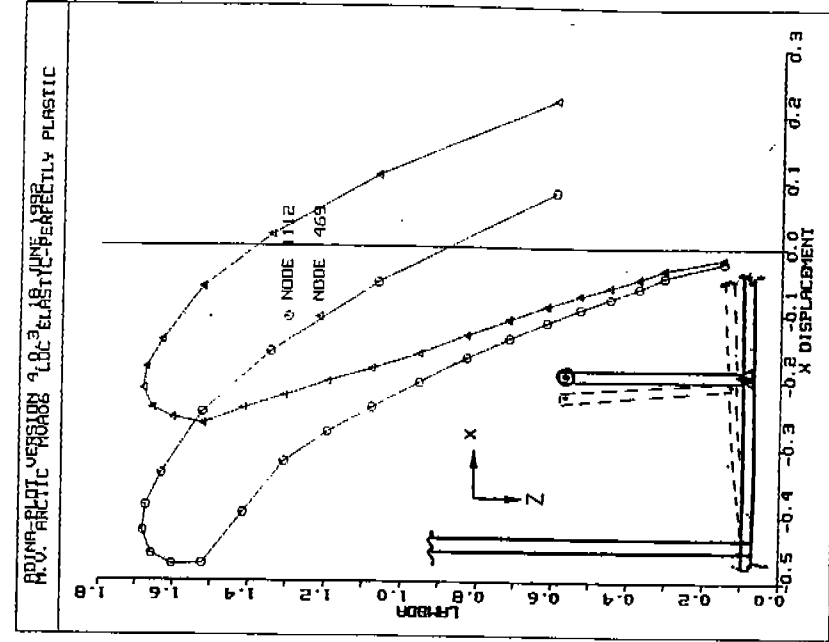
The progression of yielding in model 2 (near the maximum applied load) is shown in Figure 5.27. The magnitude of the load and the progression of yield is very similar to model 1 (see Figure 5.19) at time steps 11 and 13. However, closer inspection of model 2 at time step 13 shows that the section of stringer near the intersection of the mainframe has not yielded nearly as much as model 1. This is shown in more detail in Figure 5.28 for model 2. At time step 15, however, the stringer shows substantial yielding similar to the extent of yielding that produces failure of the stringer in model 1.



(a) Z Displacement



(b) Y Displacement



(c) X Displacement

FIGURE 5.26: Displacement vs. Load Fraction
 - Nonlinear Analysis of Redesigned FE Midbody Model With a Modified Stringer Mesh

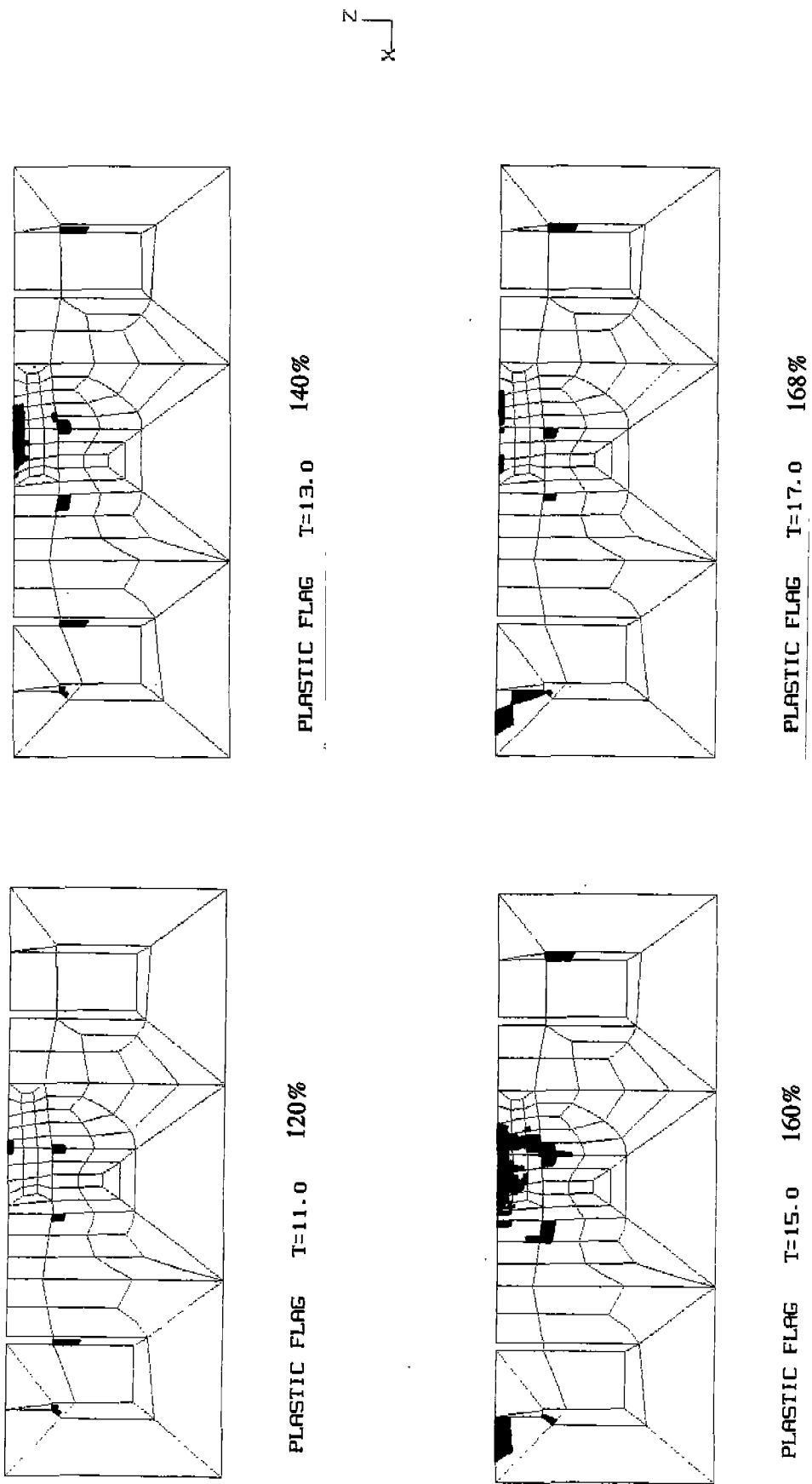


FIGURE 5.28: Progression of Yield in the Top Stringer
 - Nonlinear Analysis of ASPPR Redesigned FE Model With Modified Stringer Mesh

Therefore, a similar response is expected to occur in both models, but at slightly different load levels. The progression of yielding in the stringer of model 1 is shown in Figure 5.20.

Figure 5.29 presents the SYY stresses on the center bay from steps 10 to 15 for model 2. Up to a load fraction of approximately 130% of F_{max} the stress distribution in model 2 is approximately the same as for model 1 (see Figure 5.23). Comparison of model 2 stresses at time step 14 (150% of F_{max}) with model 1 stresses at time step 16 (145% of F_{max}) shows that the bending stresses in the outer skin of both models are reducing. This is shown by the increased tensile stresses in the outer skin of both models. At loads above 168% of F_{max} , membrane stresses become well established in the outer skin of model 2. This is very similar to the response of model 1, even though the load level in model 1 does not exceed 145% of F_{max} .

The comparison of the results of models 1 and 2 show that the high aspect ratios and irregular shapes of the elements used in the stringers of model 1 have an effect on the response. When the element aspect ratios are reduced to near unity and elements are very regular in shape, plasticity does not develop as quickly. This enables the model to carry greater loads before failure. Regardless of this, both models are predicted to fail at the stringer.

Based upon these results, the grid used in model 2 is a better grid and will be used for any subsequent investigations.

5.5 Summary and Conclusions

When the load (F_{max}) is applied to the ASPPR redesigned midbody structure of the M.V. Arctic (using flat bar and mainframes), longitudinal and lateral compressive stresses result in the outer skin of the hull of approximately 8000 psi. The area of highest stress is directly under the peak applied load and covers an area encompassed by the loaded panel and the two adjacent panels in the longitudinal direction. (A panel is defined as an area of plate bounded by stringers and deep webs and stiffened with mainframes.) The load is supported by a bending action in the hull/stringer/web structure. The structure is designed linearly such that the local load is supported by the mainframes which have an effective span equal to the distance between stringers. The load is then transferred from

the mainframes to the stringers and from the stringers to the deep webs. At low load levels, all of the local load is supported by the mainframes and the hull plating is not capable of carrying any load, other than through its small bending stiffness.

As the local load level is increased, the bending stresses in the mainframes, which must support the local load, increase. When the load levels reach a level of about 70% of F_{max} the stresses in the mainframe reach the yield point. As the applied load is increased the yielding progresses through the frame until, at a load level of about 150% of F_{max} , the mainframe reaches a point where it is completely yielded and can no longer carry any additional applied load. Any additional applied load must now be carried by the plating which is capable of supporting a normal applied load chiefly through a tensile membrane action as large out-of-plane deflections become present in the plating. This tensile stress in the plate becomes superimposed on a large existing compressive stress in the plating and actually serves to temporarily decrease the stress levels in the plating. As the load level increases, the local tensile membrane stresses in the plating begin to dominate the response. These tensile stresses have the effect of stabilizing the response and the mainframes do not appear to buckle. As the load is increased, the stresses in the stringers increase to the point of yield and eventually it is an instability in the stringers, rather than in the mainframes that result in the failure of the structure.

Failure of the structure is characterized in our analysis as failure to converge to a unique solution. This presents itself as the number of equilibrium iterations exceeding a selected maximum. Numerically, it is impractical to proceed past this point in the analysis. The load has reached a sufficient level that it is of little use to try to proceed beyond this point and the time required to extend the analysis is significant. If it is desirable to increase the load further, the present design may have to be modified to strengthen the structure.

This response is quite different from the response of the existing M.V. Arctic midbody structure. While yielding initiates at approximately 70% of F_{max} for both models, the existing structure fails due to tripping of the mainframe. The load level at which tripping begins is approximately 80% of F_{max} . This is well below the calculated maximum ice load, F_{max} .

The initial ASPPR redesigned midbody FE model included some areas where the mesh detail included elements with distorted shapes and high aspect ratios. These regions were remeshed with very regular element shapes. This did not affect the type of failure. However, the response up to failure changed as a result of the improved mesh details. The modified mesh resulted in a higher load carrying capability for the FE model. The modified mesh will be used in all subsequent FE models.

(THIS PAGE INTENTIONALLY LEFT BLANK)

6. BOW ANALYSIS

The results presented in this chapter are based upon a global ship coordinate system. This system is coincident with the axis shown on the plots from both the MAESTRO and ADINA analyses. The global x direction is positive in the forward direction, the global y direction is positive vertical and the global z direction is positive in the starboard direction.

6.1 Description of Structure

Figure 6.1 shows a representation of the MAESTRO model of the M.V. Arctic detailing the location of the bow area under study. The area being modelled is located between stations 180 and 186 and between elevations 318AB and 471AB (inches above base). The area being modelled will be referred to throughout this discussion as the "panel".

The structure consists of an inner and outer skin which are connected by a gridwork of deep web frames spaced at 1.22m (48 inches) intervals and large stringers spaced at 1.30m (51 inches) intervals. Between each of the deep webs are three mainframes which pass through the stringers.

There is a fundamental difference between the structure in this panel and the midbody structure which was previously analyzed, in that the bow panel has very stiff boundary conditions. Figure 6.2 shows the MAESTRO plots of various stations along the length of the area under consideration in their displaced positions. The deep webs at stations 180, 182, 184, and 186 are seen to develop into floors immediately below the boundaries of the panel. This is very different from the geometry at the midbody where the deep webs do not intersect any other primary structure from the upper deck to the keel. Therefore, at the bow, this results in stiff rotational supports at the panel boundaries where the deep webs develop into floors. The deep webs behave essentially as stiff beams which are built in at each end and subjected to a normal load.

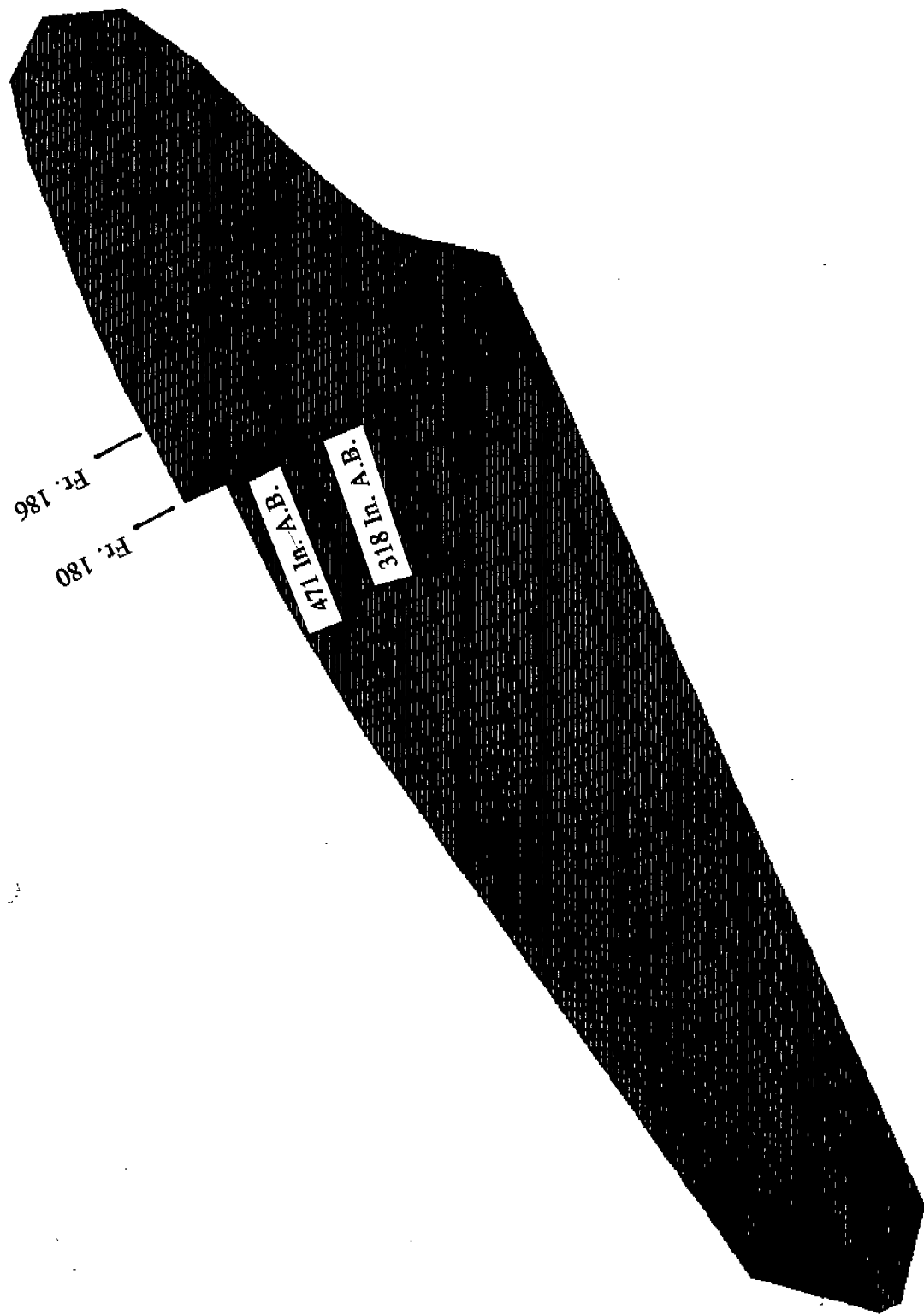


FIGURE 6.1: Location of Bow Area Being Modelled

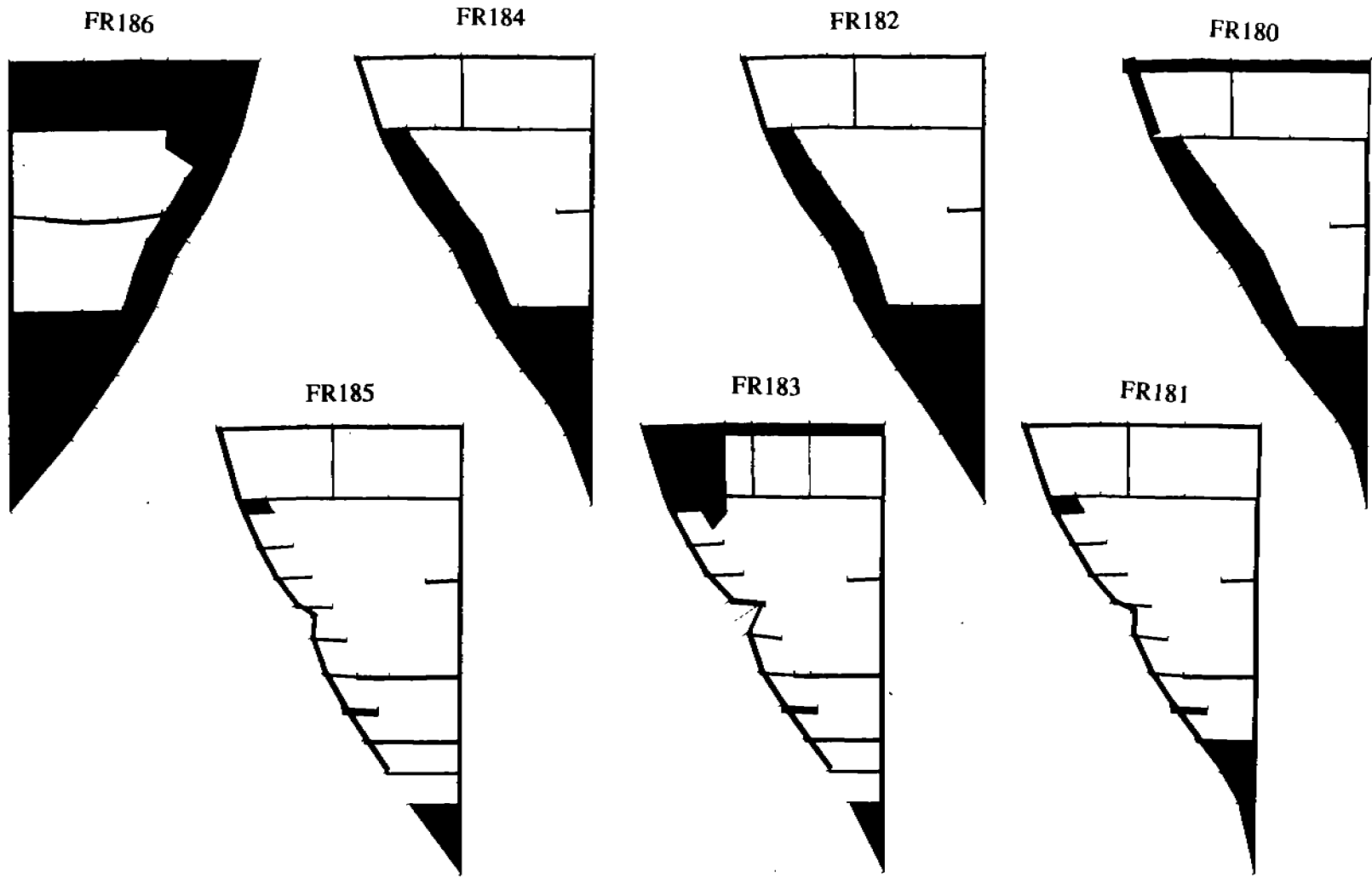


FIGURE 6.2: MAESTRO Displaced Shape Plot; Station Sections 180 to 186

6.2 Modelling the Ship Inertial Effects in the Bow Area

When the ice load impacts the bow area of the vessel there is a substantial vertical component of force applied to the vessel. (This is unlike the midbody area where the hull plating is perpendicular to the waterplane and the applied load.) Prior to application of the ice load, the ship is in static equilibrium with the weight of the ship being counteracted by the hydrostatic forces applied to it by the water. The vertical component due to ice impact creates an out of balance vertical load and the ship is no longer in static equilibrium. The out of balance load component (which is the vertical component of F_{max}) starts to accelerate the ship because static equilibrium no longer exists. This acceleration is resisted by the inertia of the ship which creates a reaction force equal to $F=ma$. The force which the bow area sees as a result of application of the ice load is the same as if the ship weight were increased by an amount equal to the vertical component of F_{max} , and if the ship was in static equilibrium with this increased mass. Therefore, this effect can be modelled in a static analysis if the increased mass could be distributed properly to duplicate the inertia effects resisting the acceleration of the ship. The distribution of the mass should be such that more mass is distributed in areas which will be accelerated the most and no mass added to those areas where there would be no acceleration.

The acceleration which the ship will experience is a rotational acceleration which is about a point close to midship. Also, the acceleration of any point on the deck of the ship is proportional to the distance from midship. Therefore it should be valid to increase the mass of the ship in proportion to its distance from midship. This is performed by changing the material density at various stations of the ship until static equilibrium is achieved with the applied ice load.

In the initial development of the MAESTRO model, the ship was subdivided into 15 modules as shown in Figure 6.3. Each module consists of the combination of all members contained in a volume of the ship between two specified cross-sections. Within each ship module, the user has control over various parameters. One of these parameters is mass density. If the mass density of a module is altered, such that the weight of the module is increased, then, when the force due to self weight is calculated by MAESTRO it will also be increased. In this manner, the mass density of individual members is adjusted until a condition of static equilibrium is reached.

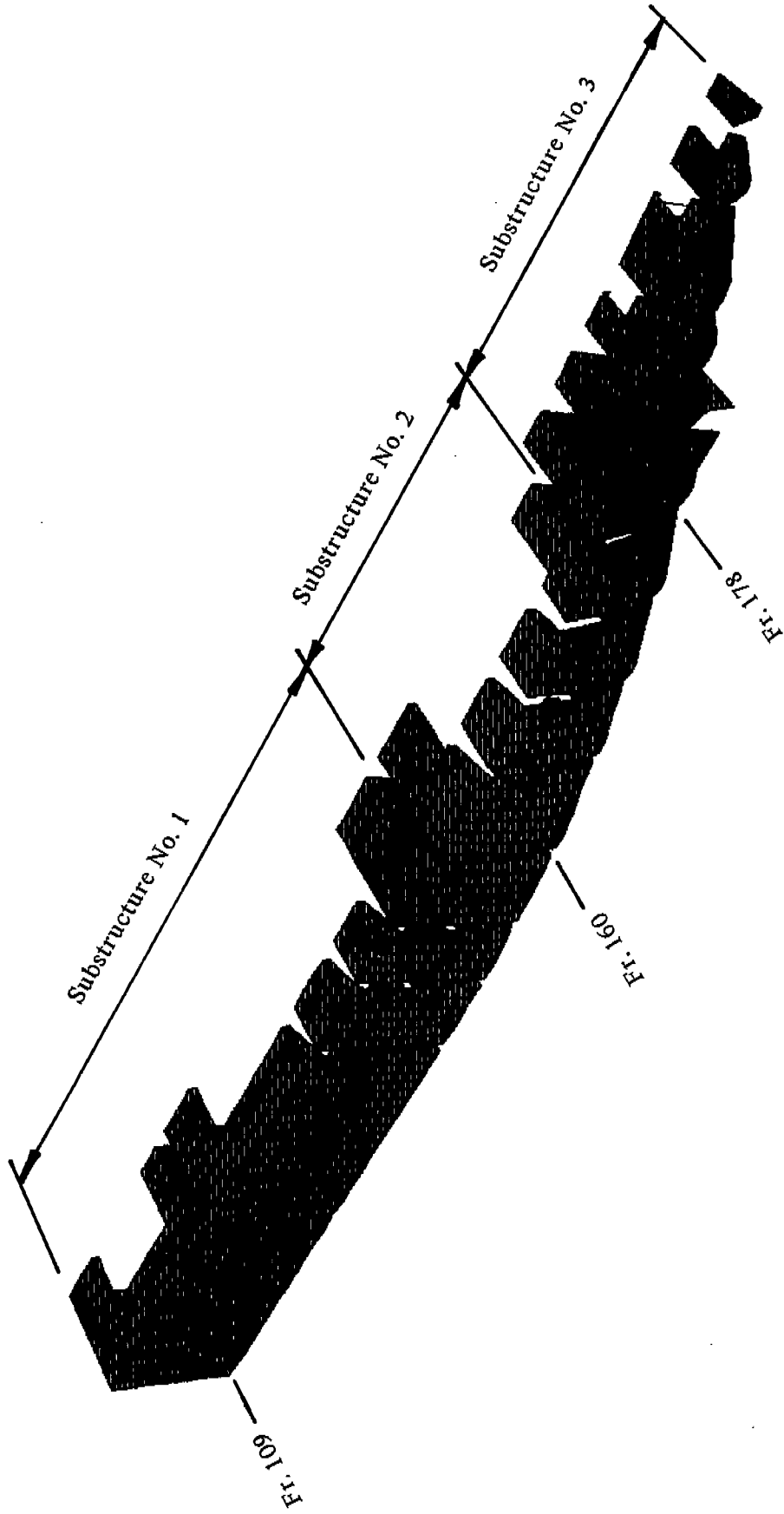


FIGURE 6.3: MAESTRO Model Showing Modules of M.V. Arctic

The increase in mass density is proportional to the distance of the centroid of each module from the center of rotation of the ship. Since the center of rotation is at the center of flotation, and for this vessel, the center of flotation is close to midship, it is assumed that the center of rotation for the M.V. Arctic is also at midship. Based upon this, the mass of each module is determined such that the cumulative increase in weight is equal to the vertical component of F_{\max} (since the ship was in static equilibrium prior to the application of F_{\max}) as follows:

$$\sum_{i=1,13} \Delta M_i \cdot g = F_{v_{\max}} \quad (6.1)$$

where:

$F_{v_{\max}}$ is the vertical component of F_{\max}

ΔM_i is the total mass change for module i

g is the acceleration due to gravity.

Let α be a constant used to multiply the mass of the ship by to increase the self weight of the ship by $F_{v_{\max}}$.

Then:

$$F_{v_{\max}} = \alpha \left(\sum_{i=1,13} \left(1 + \frac{d_i}{3792} \right) \rho V_i \right) \quad (6.2)$$

where:

ρ is the mass density of the ship material (average)

V_i is the volume of material in module i

d_i is the distance from midship of module i

3792 is the distance from midship to the location of the applied load

and,

$$Fv_{\max} = \sum_{i=1,13} \rho_i V_i \quad (6.3)$$

where:

ρ_i is the artificial mass density required for module i in order to establish static equilibrium. By the manipulation of Equations 6.1 and 6.2:

$$\rho_i = \alpha \left(1 + \frac{d_i}{3792} \right) \rho. \quad (6.4)$$

The easiest way to determine the value of α is to perform a finite element static analysis with $\alpha = 1$ and the mass density of each module factored by $(1 + d_i/3792)$ and determine the out-of-balance load. The mass density in each module is then scaled by α to eliminate the out-of-balance load. Note that any cargo weights, concentrated masses, etc. must also be scaled by the factor of $\alpha (1 + d_i/3792)$, depending upon the location (d_i) of the mass.

The values of d_i are provided in Table 6.1 and are referenced to the MAESTRO module plot in Figure 6.4. Table 6.1 gives the factored weights for each of the 15 MAESTRO modules.

6.3 MAESTRO Analysis

6.3.1 Description of Model

The MAESTRO model of the M.V. Arctic is described in Section 5.2.1. The model is the same as that used for the analysis of the midbody region and provides an overall representation of the stiffness of the ship. The main purpose of the MAESTRO model is to provide boundary conditions to apply to the detailed ADINA model of the panel. It is also very useful in providing an understanding of the overall response of the ship.

The model includes all significant structure in the bow (stringers, webs, frames, decks, the inner shell, and the outer shell). In the bow area there are three mainframes between deep webs. The

TABLE 6.1: Factored Weights for MAESTRO Modules						
$F_{max} = 1.23E+07$ lbs $\text{Alpha} = 0.8653$ $F_{vmax} = 6246994$						
Station Number	SS	MO	Weight (lbs.)	(di) Distance From Mid.	Mass Den. Mult.	Factored Weight
1	1	1	7.78E+06	456	0.980	7.63E+06
2	1	2	7.18E+06	1344	1.204	8.65E+06
3	1	3	1.68E+06	1896	1.343	2.26E+06
4	1	4	1.39E+06	2112	1.398	1.94E+06
5	1	5	2.84E+06	2328	1.452	4.12E+06
6	2	1	3.43E+06	2592	1.519	5.22E+06
7	2	2	1.88E+05	2832	1.579	2.98E+05
8	2	3	1.83E+05	3024	1.628	2.97E+05
9	2	4	2.01E+05	3216	1.676	3.36E+05
10	3	1	1.89E+05	3384	1.718	3.24E+05
11	3	2	1.02E+05	3516	1.752	1.78E+05
12	3	3	7.48E+04	3636	1.782	1.33E+05
13	3	4	9.68E+04	3770	1.816	1.76E+05
14	3	5	3.06E+04	3995	1.873	5.73E+04
15	3	6	4.01E+03	4098	1.899	7.60E+03
TOTALS			2.54E+07 lbs.			3.16E+07
			New weight - ship weight =		6.25E+06	

where: SS = Substructure Number
 MO = Module Number

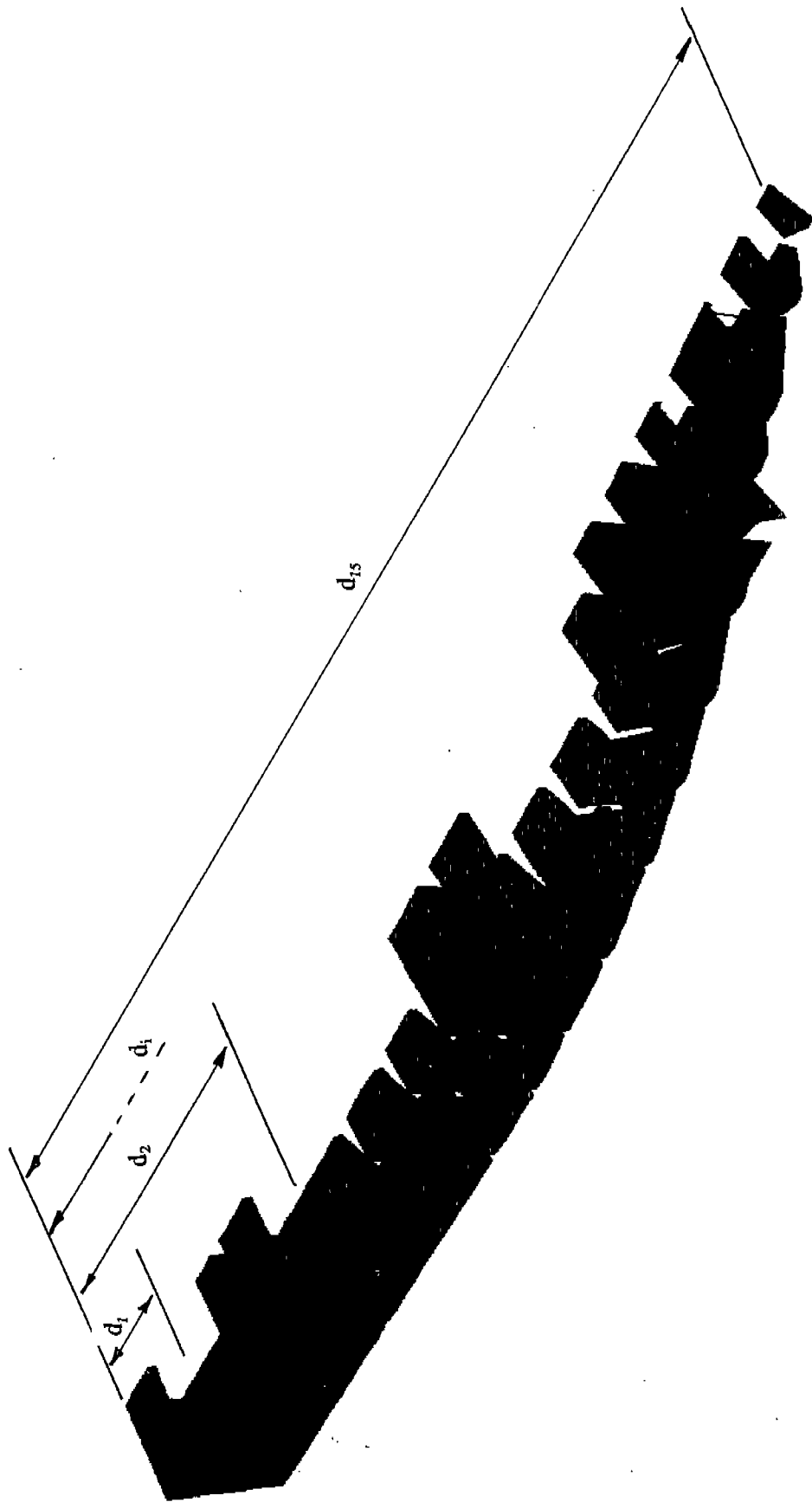


FIGURE 6.4: Illustration of the Distance from the Midship to the Centroid of Each Module

center mainframe is modelled explicitly and the two adjacent frames have their properties smeared into MAESTRO strake elements.

6.3.2 Boundary Conditions

As discussed in Section 5.1.2, transverse symmetry has been assumed in the bow analysis and only half of the ship has been modelled. The implication associated with this assumption is that the identical phenomena occurs on both the port and starboard sides of the ship at the same time. This assumption applies to both the geometry and the loads and hence it is assumed that the ice impacts both the port and starboard sides of the ship simultaneously, and impacts with a load equal to F_{\max} on both sides.

In reality, it is possible for the situation to occur where an ice load is applied to one side of the ship only and the implications on the results should be considered. If the load is applied to one side of the ship only, then a bending of the ship will result and the bow will displace in a transverse direction. (If the ice is assumed to act on both sides of the ship, then the transverse response is symmetric and the bow will not displace transversely other than to compress the bow in the transverse direction.) Applying the load to one side only results in a moment being applied to the ship which is zero at the point of application of the load and increases linearly to a maximum value at the midship section. The resulting moment will therefore be zero in the bow area and will result in no additional longitudinal stresses in this region. Therefore, in this regard, the assumption of transverse symmetry would have little or no effect on the results in the bow.

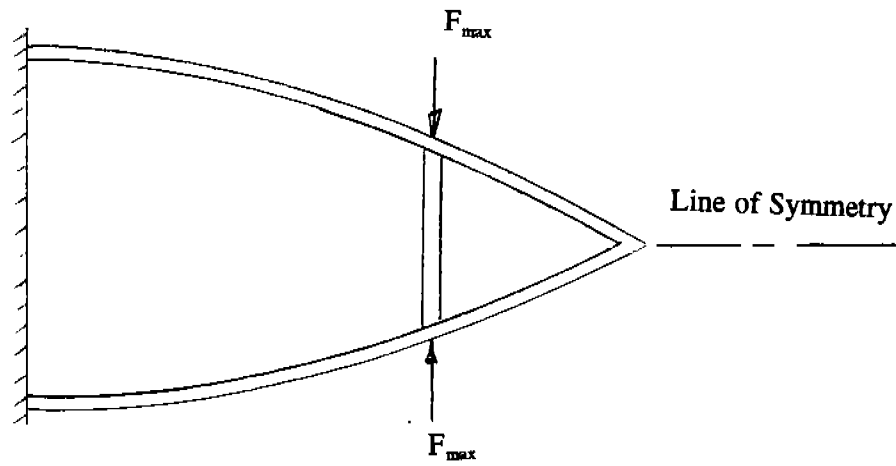
The phenomena which has more potential to affect the results in the bow area is the compression of the bow in the transverse direction. If the load is applied to both sides simultaneously, then the bow is subjected to a transverse compression which is reacted within the bow region by two equal and opposing loads. In this case, the load path is directly from the port side to the starboard side of the ship. If, however, the load is applied only to the port side of the ship, the load path does not go directly from the port to starboard sides. The stress in the transverse direction would have to go from a maximum value at the point of application of the load (i.e. at the outer shell) to zero at the free

face on the other side of the ship. This means that the applied load must be transferred to the internal structure of the ship which is capable of reacting a transverse load.

In reality, the load which is applied to the starboard side of the ship is reacted by the forces which act on the opposing side of the ship. These forces are a result of phenomena which try to oppose displacement of the ship including inertia effects of the water (i.e. added mass) and inertia effects of the ship itself. By a phenomena similar to that described in Section 6.2, the ship must stay in a state of equilibrium. This state of equilibrium is achieved by the water exerting a force on the opposite side of the ship as it tries to move. Therefore, the only difference in applying the load to one side rather than to both sides, would be that the forces reacting the applied load will be more distributed if the load is applied to one side only. The difference between these two conditions is shown in Figure 6.5. The response of the ship hull is found to be quite local and will not be significantly effected by reacting the applied load as a point load rather than as distributed load. Hence, the assumption of transverse symmetry is valid.

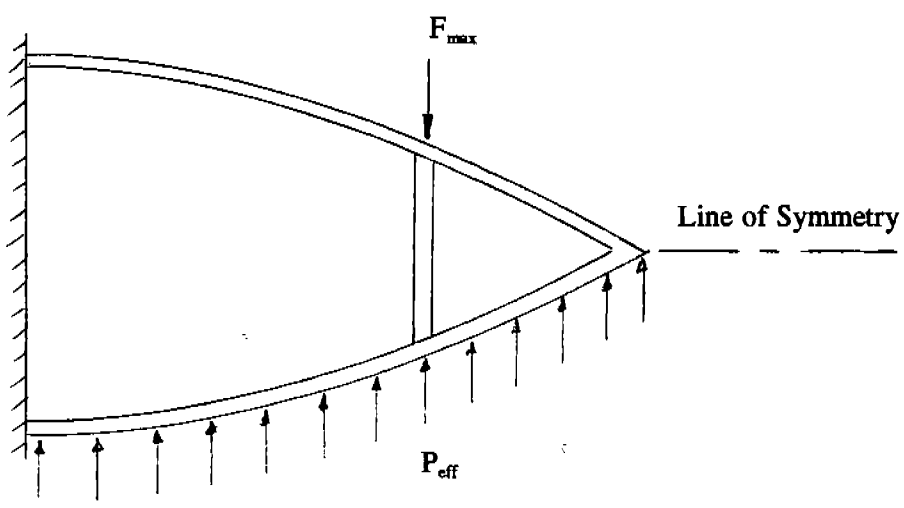
6.3.3 Loads

The load which is applied to the MAESTRO model is a combination of the still water bending moment, the hydrostatic water pressure, and the ice load. The still water bending moment is applied as described in Section 5.2.3. The hydrostatic pressure starts at a value of zero at 471AB and increases linearly with water depth. The ice load is calculated according to the procedure laid out in the proposed ASPPR regulations. According to the regulations, the impact of the ice results in a triangular distribution of pressure over an ice print area on the hull. The calculation of the magnitude of the ice pressure and the size of the ice print area for the bow region are contained in Appendix A. Figure 6.6 shows the calculated ice pressure load and ice print area which are applied to the MAESTRO model. As discussed in Section 5.2.3, in the MAESTRO analysis, the applied ice load was approximated as point loads to achieve the appropriate pressure distribution over the panel.



(a) Ice Load on Port and Starboard Sides

$P_{eff} = F_{max} A_{eff}$, where A_{eff} = effective area of pressure



(b) Ice Load on Port Side Only

FIGURE 6.5: Qualitative Illustration of the Assumption of Transverse Symmetry
6-12

190

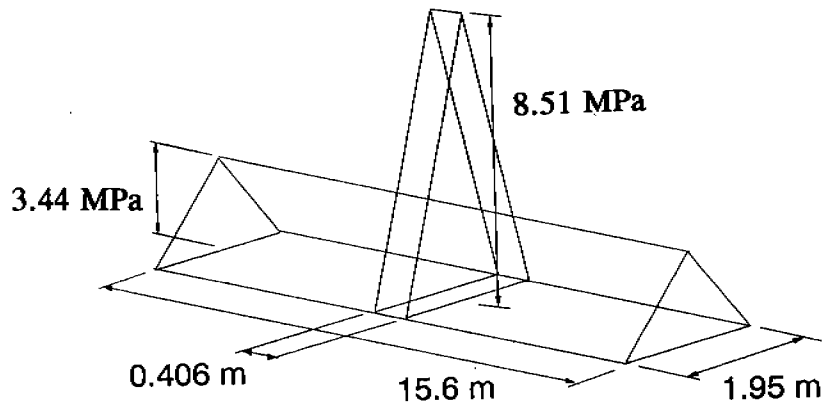
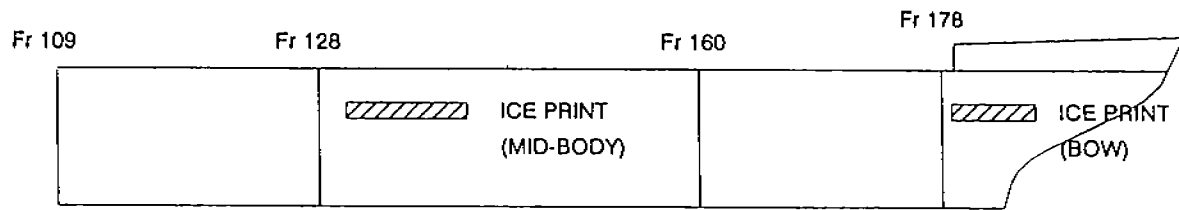


FIGURE 6.6: Ice Pressure Load as Calculated Using the Proposed ASPPR Regulations

6-13

141

6.3.4 Results

Figure 6.7 shows the longitudinal stress (SXX) distribution in the outer and inner shells of the M.V. Arctic. The global stress can be seen to be a bending stress which increases from a stress of zero in the bow area to a maximum stress at the midship section. The bending component is caused by the vertical component of F_{max} which tries to lift the bow of the vessel. Consequently, the stress at the midship section is primarily a bending stress which puts the keel of the ship in tension (approximately 35 ksi.) and the upper deck in compression (approximately -40 ksi). Figure 6.8 shows the vertical component stresses (SYY) in the outer and inner shells. The global stress component of the SYY stress away from the panel is very small and is not of any interest. The local SYY stress in the panel is due to local bending and is very similar in sign and magnitude to the local transverse (SXX) stress in the panel.

In Figures 6.7 and 6.8, closeups of the bow area have been presented for both the inner and outer shells. In the Figures it can be seen that directly under the load, the outer shell goes into compression and the inner shell goes into tension. Near the boundaries of the panel (indicated in the Figure by the dark line) there is a change in the sign of the stress such that the outer shell goes into tension below the applied load and into a reduced compression above the load. The explanation for this is described below.

The results from the MAESTRO linear static analysis of the bow, under the influence of an ice load F_{max} , is shown in the form of a displaced shape plot in Figure 6.2. Since the results being presented here are for a linear analysis, they will be valid locally only for small loads. The results can, however, give insight into the local response even at larger load levels and will be valid globally for all load levels.

At the line of intersection of any of the webs (Frames 180, 182, 184 or 186) with the outer shell of the ship, the webs are found to be in tension at the upper and lower panel boundaries and in compression at the midspan. The curvature of the line of intersection of the webs and outer shell which causes this state of stress can be seen in the deflected shape plot shown in Figure 6.2.

The stress situation in the webs at the bow panel is very different from that of a web in the midbody panel. The webs at the bow develop into floors immediately below the boundaries of the panel. This provides a very stiff boundary condition which effectively fixes the webs at this boundary. In the midbody area, this condition does not exist and the deflection of the panel is much more of a global indentation of the shell and, consequently, no stress reversal takes place.

One way of trying to understand the overall bow response is to look at the response to the different iceload components. Since F_{\max} is applied normal to the outer shell, it has both a transverse and a vertical force component. Because of the angle of application of the iceload, the transverse load has a tendency to cause bending in the structure. The vertical component tries to lift the bow out of the water. It is applied over a relatively small iceprint and results in a tensile stress below the point of application of the load and a compressive stress above this point. Therefore, the total state of stress is the combination of the bending due to the transverse force and the inplane stresses due to the vertical force. This is illustrated qualitatively in Figure 6.9 which shows the approximate state of stress at the upper, lower and midsection of the web at frame 186.

At the lower boundary of the panel (point I in Figure 6.9) the stress in the web and the outer shell will have two components:

- a. A bending stress due to the local bending of the panel of approximately 25 ksi. This results in a tensile stress in the outer hull of 25 ksi and a compressive stress in the inner shell of 25 ksi; and
- b. A tensile stress below the ice load of approximately 15 ksi. This is caused by the vertical component of the ice load lifting the ship.

When these two components are superimposed, the result is a tensile stress of about 40 ksi in the outer shell and a compressive stress of approximately -10 ksi in the inner shell.

At the upper boundary of the panel (point II in Figure 6.9) the stress is again composed of two components:

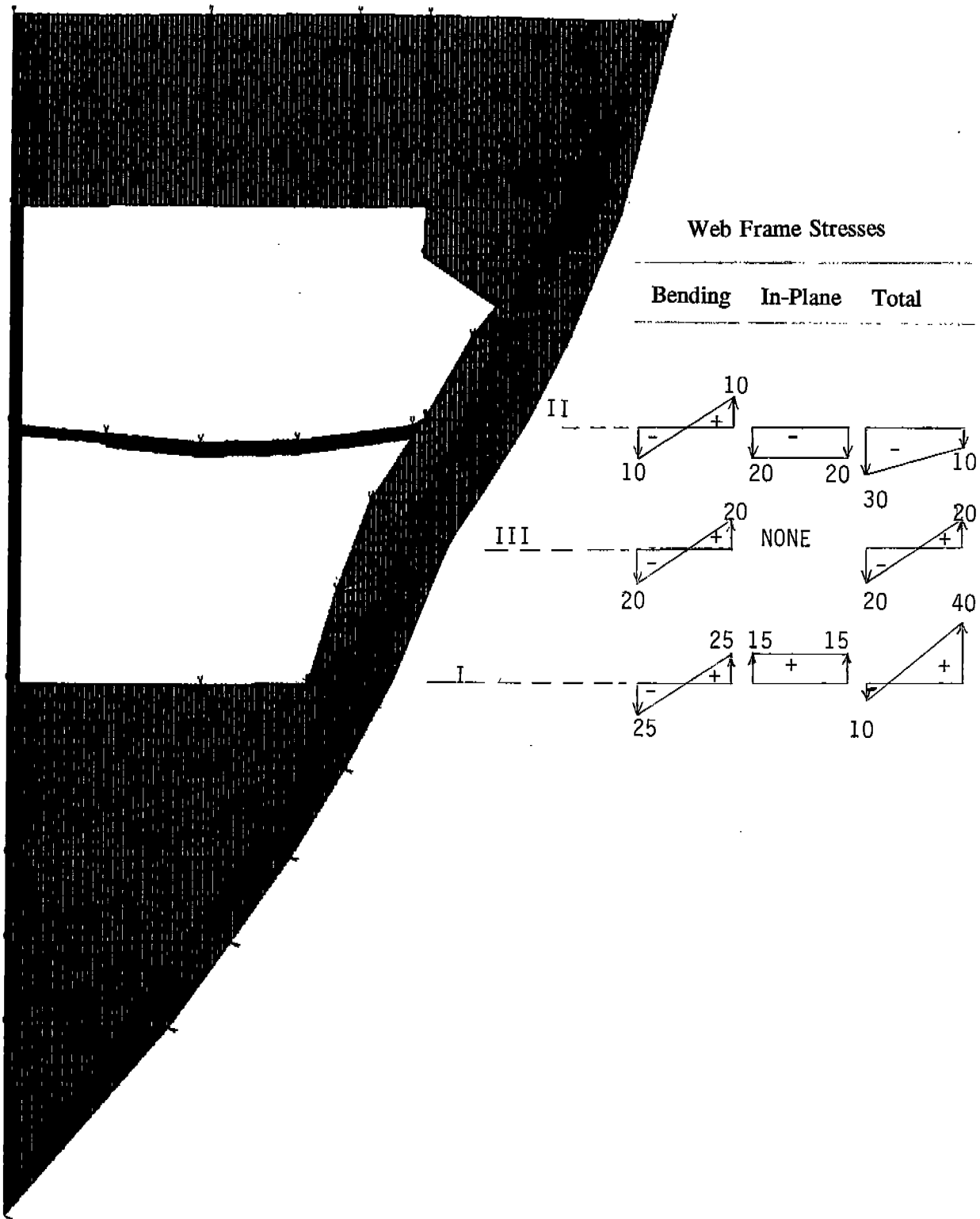


FIGURE 6.9: Superposition of the Bending and In-Plane Stress Components Along a Typical Web Frame

- a. A bending stress due to the local bending of the plate of approximately 10 ksi. This is lower than the bending stress at the lower boundary of the plate because the boundary condition is not near as rigid. (In the limit, where the boundary condition would be pinned, the stress would be zero. The stress therefore has to be somewhere between the 25 ksi present at the lower boundary and zero.) This results in a tensile stress in the outer shell of about 10 ksi and a compressive stress in the inner shell of the about -10 ksi; and
- b. A compressive stress of approximately 20 ksi is caused by the load pushing up on the bow material above the point of application of the ice load.

Superimposing these two stress components results in a compressive state of stress in both the inner and outer shells of -30 ksi and -10 ksi, respectively. The stress in the outer shell will be low since the two stress components will always act in opposite directions and will tend to cancel each other out.

At the center of the panel (point III in Figure 6.9) the stress has only one component which is the bending component. At this point the vertical forces are balanced by a tension below the ice load and a compression above the ice load. The bending component has a magnitude of approximately 20 ksi which results in a compressive stress of -20 ksi in the outer shell and a tensile stress of 20 ksi in the inner shell.

6.4 ADINA Analysis

6.4.1 Description of Model

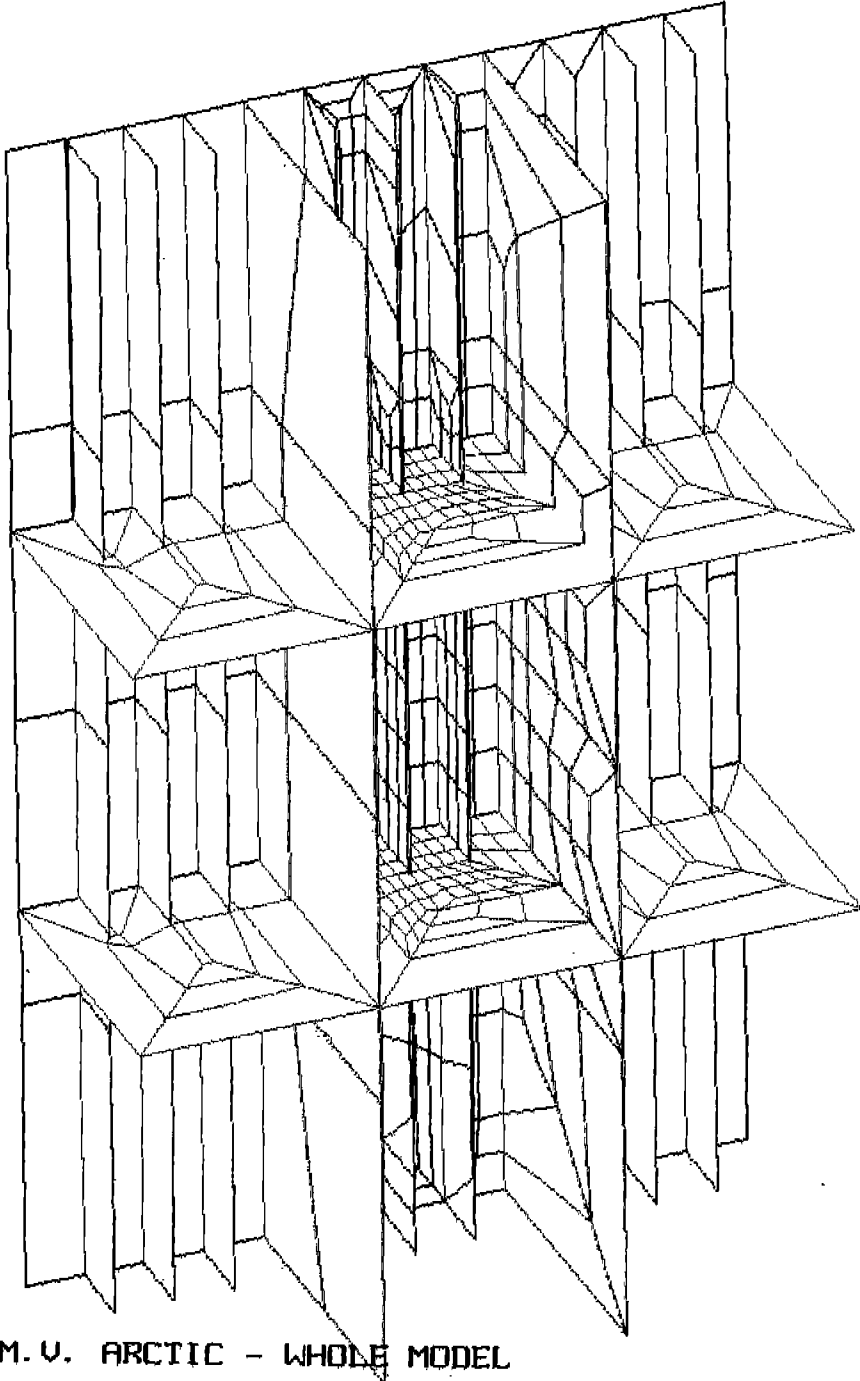
The ADINA model of the panel is shown in Figure 6.10. The model has approximately 3200 nodes and 1000 elements. The figure shows a view of the FE model looking from the inside of the ship with the inner shell removed. A small inset in the figure shows the same view with the inner shell included. Although not shown in the plot, the model is bounded by the webs at stations 180 and 186 and by the stringers at 318AB and 471AB. All of the structure which exists between these boundaries has been included in the FE model. The only difference between the existing structure and the FE model is that the FE model mainframes have been redesigned to flat bars that conform to the proposed ASPPR regulations. The spacing, span and scantlings of the redesigned stringers and webs are the same as the existing structure. The sizes of the redesigned scantlings are provided in Table 6.2.

TABLE 6.2: Sizes and Plate Thickness of Redesigned ASPPR Bow Scantlings	
Part	Bow
Flat bar frames	15.75 x 0.866 in (400 x 22 mm)
Outer skin	1.063 in (27 mm)
Stringers	0.4921 in (12.5 mm)
Webs	0.4921 in (12.5 mm)
Inner skin	0.4331 in (11 mm)

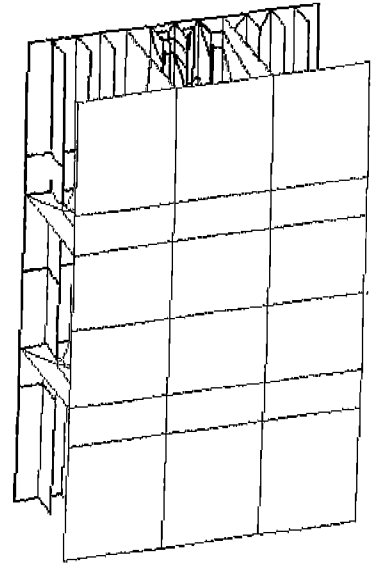
TABLE 6.3: ADINA Load Fractions for the Nonlinear Analysis of the M.V. ASPPR Redesigned Bow Scantlings	
Time Step	Load Level (Fraction of F_{max})
1	.13
2	.27
3	.52
4	.67
5	.79
6	.80
7	.81
8	.82
9	.82
10	.83
11	.84
12	.85
13	.86
14	.87
15	.89
16	.90
17	.92
18	.94
19	.96
20	.99
21	1.02
22	1.05

148

ADINA DEFORMED KUMIN 6159.
LOAD STEP XUMAX 6026.
TIME 7.009.514 YUMIN 405.9
YUMAX 620.4



KUMIN 6140.
XUMAX 5993.
YUMIN 511.0
YUMAX 743.5



M. U. ARCTIC - WHOLE MODEL

FIGURE 6.10: ADINA Finite Element Model of Bow Panel

6.4.2 Boundary Conditions

As with the midbody analysis, the boundary conditions used for the linear and nonlinear analysis of the bow panel have been derived from the MAESTRO displacement results at locations corresponding to the boundaries of the panel. The MAESTRO results are applied as prescribed displacements around the perimeter of the model. This provides a boundary condition which accurately represents the effect of the entire structure on the panel.

6.4.3 Loads

The still water bending moment is not applied explicitly to the panel model since it is not a local load however, its effects are included in the response by employing the prescribed displacement boundary conditions from MAESTRO. The ice load is applied directly to the local model as a triangular distribution of load which is calculated using the procedure defined in the proposed ASPPR regulations. Details on the calculation of the ice load are contained in Appendix A. The hydrostatic pressure is superimposed as a linearly varying pressure load. Figure 6.11 shows the loading applied to the ADINA model.

6.4.4 Linear Analysis Results

The results of the linear analysis are shown in Figure 6.12 in the form of stress contour plots for the stress components SXX (longitudinal) and SYX (vertical). The SYX component of stress is the most important for the purposes of this study in that it is the stress component which has the potential to cause buckling of the mainframes. The stresses in the outer shell can be seen to be consistent with the MAESTRO results. In the outer shell a tensile SYX stress is present at the boundaries of the panel with a small region of compressive stress present in the center area of the panel, directly under the ice load. The magnitudes of the stresses agree with the MAESTRO analysis results.

In the deep webs, the same phenomena is observed as in the MAESTRO analysis. At the lower panel boundary, the webs experience a tensile stress at the outer edge of the web (i.e. line of intersection of the web and the outer hull) and a compressive stress at the inner edge of the web;

similar to what would be expected from a beam built in at two ends with a center load. The longitudinal stresses resulting in a beam from such a load are bending stresses only. In the M.V. Arctic, there is also a tensile stress component which is superimposed on the bending stresses due to the vertical component of the ice load which attempts to lift the ship at the water line. This results in a shifting of the neutral axis to a point close to the inner shell, thereby leaving almost the entire web cross-section at the lower boundary of the panel in tension.

At the upper panel boundary, a bending stress is present, however, the boundary condition is less rigid and the magnitude of the bending component is smaller than at the lower boundary. A compressive stress is superimposed on the bending stress due to the vertical component of the ice load which acts at the water line and attempts to lift the ship. All points above the application of this load will experience a compressive stress component. The combination of the two stresses results in a near zero value of stress at the outer edge of the web and a fairly large compressive component at the inner edge of the web.

There is a third component of stress which also acts on the members of the panel. The inner shell, outer shell, webs and stringers form a box type structure which can sustain loads on a global level as a beam. When exposed to an external load, the entire structure deflects inward as a beam with the inner and outer shells forming inner and outer beam flanges. When subjected to a normal load, the beam resists displacement by compressing the outer flange (outer shell) and elongating the inner flange (inner shell). This causes the mainframes to be compressed as they are an integral part of the outer shell. This phenomena is the predominate response in the midbody region where the entire panel is not restrained from inward deformation, however, in the bow area the structure is significantly stiffer and the global deflection of the cross section is resisted by the boundary conditions imposed on the panel. Whereas in the midbody region this phenomena causes buckling problems at high load levels, in the bow area the effect is minimal. This effect represents the largest difference in results between the bow and midbody.

The three mainframes in the center (longitudinal) bay are seen to be in a very low tensile state of stress in the two outer (top and bottom vertical) bays of the panel. In the center span of the frames, directly under the point of application of the load, the load is supported by the mainframes which

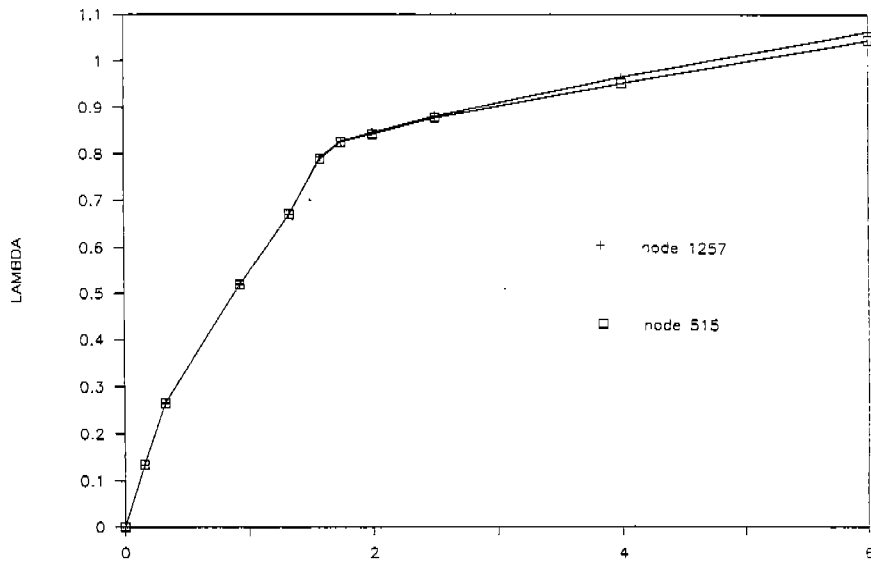
transfer the load to the stringers and in turn to the deep webs. Therefore, the mainframes under the load act as simply supported beams with a center load and experience large bending moments at their centers. The result is a large compressive stress at the inner edge of the frame (i.e. where the frame intersects the outer shell) and a large tensile stress at the outer edge of the frame. The stresses at the ends of the frame (i.e. where the frame is attached to the stringers) change sign. This is due to a change in the bending moments where the frames pass the stringers. Because the center bay is directly under the point of load application, the vertical component of the ice load does not result in any vertical component of stress since the lifting action of the ship is balanced by a tensile stress below the point of load application and a compressive stress above. At the point of load application, this component must be zero.

The results of the linear analysis predict a high degree of mainframe stability in the structure. The mainframes are seen to be largely in tension except for the area of the frame which is attached to the hull, which is in compression. If the load levels were increased to the point of yield, we could expect to see tensile yielding being experienced at the outer edge of the frame web. As the load increases, the nonlinear effect of out-of-plane displacements will result in a tensile component of membrane stress being set up in the outer shell and inner frame boundary to carry the normal ice load. We should expect, therefore, to see a decrease in the compressive stress rather than an increase.

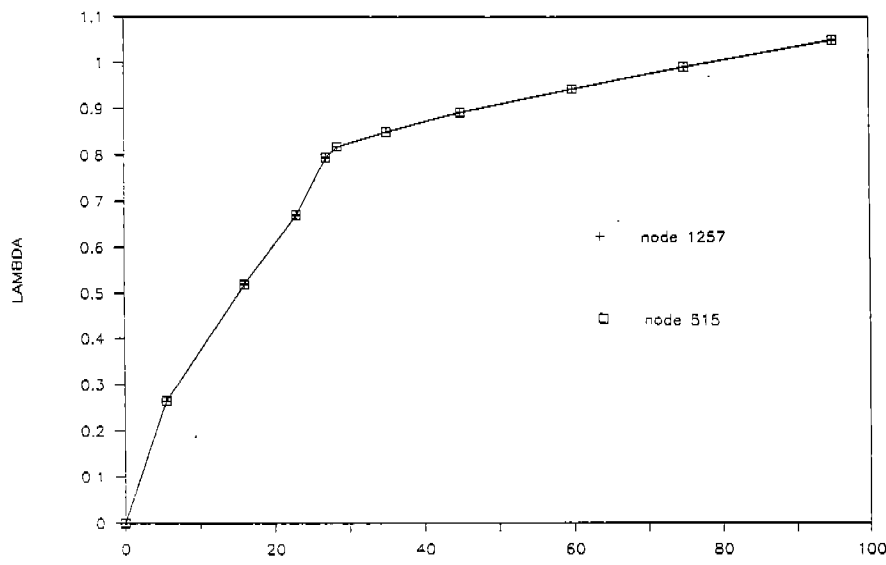
6.4.5 Non-Linear Analysis Results

The nonlinear analysis was performed for the same load, F_{max} , using the load displacement control option available within ADINA. The analysis was permitted to continue until the structure failed at a load level of 105% of F_{max} . The load fractions set up by ADINA are shown in Table 6.3. The failure was determined to be a buckling failure similar to that of the midbody.

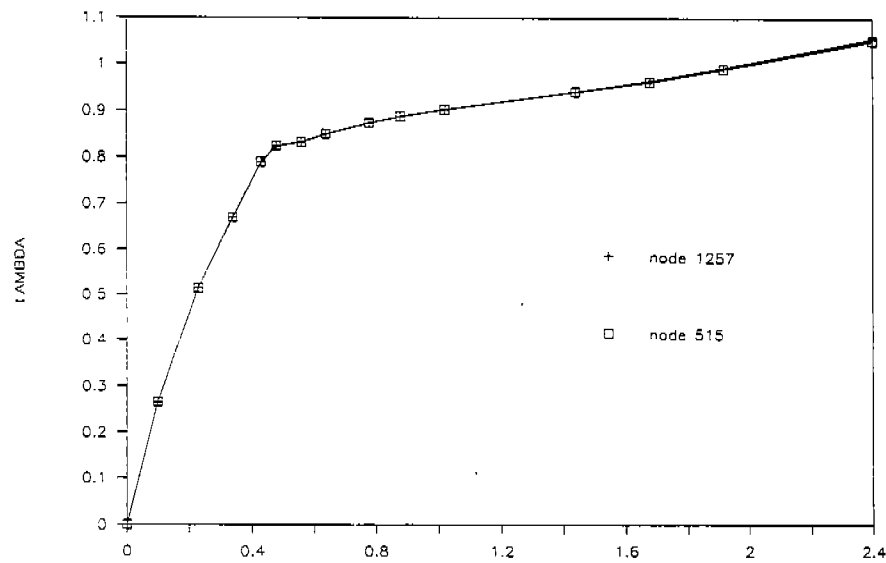
Figure 6.13 shows the displacement of two points at midlength on the maximum loaded mainframe in the center bay. Node 515 is the point where the frame intersects with the hull plating. Node 1257 is a point on the mainframe furthest from the hull plating.



(a) X Displacement



(b) Y Displacement



(c) Z Displacement

FIGURE 6.13: Displacement versus Load Fraction
- Nonlinear Analysis of Bow Model

155

The displacements increase linearly in the three directions until approximately 80% of F_{max} . The maximum lateral (x) displacement at this point is approximately 1.75 inches. This is over twice the lateral displacement that the midbody analysis predicts at the same load (see Figure 5.26). The reason for the increased lateral displacement at the bow region is two-fold. Firstly, the frames are not orthogonal to the outer skin. Because of this, the frames start to displace laterally as soon as the load is applied. The second reason is that the MAESTRO boundary conditions have larger x prescribed displacements than the x prescribed displacements at the midbody. The maximum y displacement is also significantly larger at the bow region. This can be seen by comparing the displacements in Figure 5.26(b) and Figure 6.13(b). This is expected since the vertical displacement at the bow region from the MAESTRO analysis (from which the prescribed displacements are determined) is much larger than from the MAESTRO midbody analysis. This displacement is largely rigid body motion.

At approximately 80% of F_{max} , the frames exhibit substantial increases in displacements in all directions. This is due to the extensive yielding that has occurred in both the mainframes and the stringers (where the mainframes attach). The large displacements (Figure 6.13) at this load level indicate the start of failure.

Figure 6.14 shows the SYY (vertical) component of stress in the panel model with the inner shell removed. Figure 6.15 shows the SYY stress in the outer shell as the load is increased from 27% to 105% of F_{max} . The results up to about 80% of the total load are essentially the same as the linear results presented in Section 6.4.4. At load levels above this point the nonlinear effects begin to dominate the response as yielding and geometric nonlinearities become more significant in the response. Directly under the point of load application, the stress can be seen to start as a compressive stress and then to change to a tensile stress as the geometric nonlinear effect takes over and the incremental load is carried largely as local membrane stresses in the plating.

Figure 6.16 shows the progression of yield through the structure. The structure can be seen to experience some local yielding at 67% of the total load, which progresses through the structure until at approximately 80% of F_{max} . The three center bay mainframes and the stringers attachments above and below these frames experience extensive yielding. This extent of yielding occurs well below the load levels of that of the midbody analysis where load levels of approximately 130% of F_{max} produced

the same degree of yielding. Figure 6.13 showed that the structure becomes unstable just above 80% of F_{max} . At 105% of the load, the structure is essentially totally plastic. At this point in the analysis, the structure is no longer capable of carrying the load and the analysis terminates. This corresponds physically to the point where the structure would be completely yielded and no further increase in stress could result.

Physically the structure is still capable of carrying additional load by "changing its geometry" to provide a larger out-of-plane load component while maintaining the same internal stresses. The structure would ultimately fail when the strain rupture modulus is exceeded but this occurs at very large strain values. Numerically, this is very difficult to predict and the solution algorithms have problems as the stiffness matrix has many terms very close to zero. Because the structure has already failed, there is little merit in continuing the analysis past this point.

Figure 6.17 shows the three mainframes in the center bay of the panel. The stress can be seen to start as in the linear analysis, with tensile stresses in the outer web and compressive stresses in the inner web along the line where it intersects with the outer shell. As the load is increased, the tensile stress in the mainframe grows and is accompanied by tensile yielding in the mainframe. At a load level of 50%, the mainframe directly under the load has experienced some yielding. As the frame experiences yielding, the incremental load which is applied to the structure must be supported by a frame which is, in effect, slightly shallower. The local incremental load is still supported by bending action in the mainframe which results in an increased tension in the outer fibres of the web and a compressive stress being set up in the inner fibres of the web. Since the outermost fibres have yielded and are essentially nonexistent for any incremental load, the tensile stress set up to carry the load migrates towards the base of the frame. At a load level of 79%, the mainframe is found to be largely in a state of tension and has experienced yielding through most of the depth of the frame. At this point, the out-of-plane displacements have increased significantly and the incremental load is now carried largely through tensile membrane stresses being set up in the outer shell rather than through a bending action in the mainframes. This is evident by the change in the condition of stress in the outer shell. At a load level of 79%, the state of stress in the outer shell, directly under the point of load application, is compressive with a level of about -10,000 psi. At a load level of 105%, this state of stress has changed significantly and the stress in the outer shell has changed to a small tensile stress.

6.5 Summary and Conclusions

The analysis results show a substantially different response at the bow when compared to the results at the midbody area. The bow panel designed to the proposed ASPPR does not fail as a result of an instability, whereas the ASPPR designed midbody panel fails due to an instability in the stringer. The bow panel predicts almost complete yielding following the onset of plasticity at 70% of F_{max} and a large decrease in stiffness at 80% of F_{max} . Following this large decrease in stiffness, the internal stresses in the plate became predominantly tensile as the incremental local stresses are carried through membrane action in the plating. As a result, the bow members are found to have stresses reaching tensile yield throughout virtually the entire panel at a load level of 105% of F_{max} . The reasons for the difference between the response of the bow and midbody panels are most likely due to the differences in geometry and applied loads. Since most of the investigation was concentrated on the midbody panel (see Section 7.1), very specific conclusions are not possible, based upon one analysis of the bow panel. Further work is necessary to completely understand the response of the bow region of the M.V. Arctic.

7. PARAMETRIC STUDY OF THE MIDBODY REGION

One of the objectives of this study was to determine the effects of varying certain structural parameters on the stability of the ship structures. Many parameters were presented in the literature review, which affect the stability of ships structures. A few of these are examined in this phase of the study. These parameters are the mainframe slenderness ratios, the mainframe sectional properties, and the residual stresses from welding.

The choice of the region (midbody or bow) of the M.V. Arctic to be used in the parametric study is presented in Section 7.1. The results of the study are presented in Sections 7.2 to 7.4. The conclusions are presented in Section 7.5.

7.1 Selection of Region for Further Study

The analyses of the ASPPR redesigned midbody model predicted that this region of the ship fails due to an instability. The midbody model predicted yielding to occur at approximately 70% of F_{max} ; however, the structure was able to carry substantially more load before failure occurred at a stringer at approximately 130% of F_{max} . The analysis of the ASPPR redesigned bow model predicted that the structure does not buckle. At 105% of F_{max} , the panel has essentially completely yielded. This follows a large decrease in stiffness at approximately 80% of F_{max} .

Based upon these results, the midbody region was chosen for the region to be studied further. It exhibits failure due to buckling, whereas the bow model does not. The midbody model also shows a mainframe instability when the mainframes are modelled as angle sections. Since mainframe angle sections will be widely used for further study, the midbody will most likely exhibit mainframe instability. Finally, the midbody structure is much less complex than the bow structure with no assumptions regarding inertial effects. This means that the results of an analysis of the midbody geometry will be much easier to interpret than that of the bow.

7.2 Selection of Parameters to be Studied

Since the proposed ASPPR regulations allow for several options in the design of an icebreaking vessel, it was decided that it is important to work within the restrictions of these regulations and to check some of the options to ensure that they result in a design which is predicted to maintain stability after yielding. It is not important to have exact values of buckling loads, but much more important to evaluate trends which result from configuration changes.

Consequently, the following modifications were performed to vary the parameters for the analysis of the midbody model:

- a. Modify the mainframes to employ T-bar stiffeners. Although this is not a likely design for an icebreaker, it will provide the navy with an indication of stability after yield for a typical warship configuration;
- b. Modify the redesigned structure to employ angle stiffeners which conform to the revised ASPPR;
- c. For the redesigned ASPPR model of the midbody area employing flat bar stiffeners, evaluate the response when the mainframes are manufactured at a 70° angle to the hull plating;
- d. Increase the slenderness ratio of the redesigned flat bar configuration;
- e. Employ an increase in slenderness ratio for the flat bars orientated at 70° to the hull plating; and
- f. Incorporate residual stresses from welding.

The results of these analysis are presented in the following sections.

7.3 MAESTRO Analysis

MAESTRO was used in this project to ensure that both the ship global and local response were included in the boundary conditions for the FE analysis of the local panel. Since the global response is much more affected by the webs and stringers than the mainframes, modifying the mainframes will have little effect on the MAESTRO boundary conditions of the local panel. Therefore, since the

parameters that will be varied in this part of the study only affect the mainframes, the boundary conditions used for the previous analysis of the midbody panel can be used as boundary conditions for the different models in the parametric study, and it is not necessary to perform a new MAESTRO analysis. The results of the MAESTRO analysis described in Section 5.2 were used as boundary conditions for the local panel models in this chapter.

7.4 Nonlinear Analysis Results using ADINA

It is usually recommended that before any nonlinear analysis is performed, a linear analysis be performed first. This was the procedure used in the previous analyses of both the midbody and bow FE models. However, since a good overall understanding of the linear response has already been achieved for the existing configuration, it was decided to go directly to the nonlinear analysis for the parametric study.

As detailed in the last section, a new MAESTRO analysis was not necessary to determine the boundary conditions for the FE models in the parametric study. Therefore, the applied loads and boundary conditions used in the previous midbody analysis (Sections 5.4.2 and 5.4.3) are also used in this phase of the study.

Similar to the other ADINA nonlinear analyses, the load displacement control method is used as the solution procedure.

7.4.1 Mainframes Modelled as Tee Sections

The tee section used for this analysis was designed to the ASPPR regulations with the following dimensions:

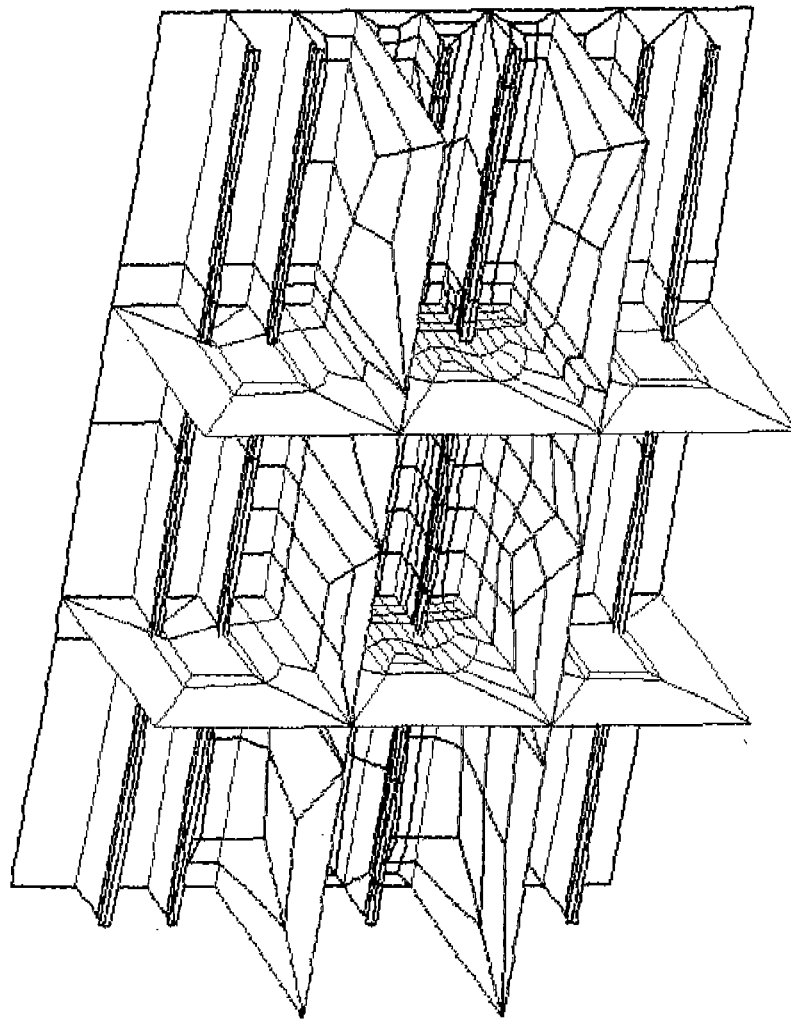
$$\begin{aligned} &15.35 \times 0.47 + 2.36 \times 0.47 \text{ (in)} \\ &390 \times 12 + 60 \times 12 \text{ (mm)} \end{aligned}$$

The FE model of the midbody panel using tee stiffeners is shown in Figure 7.1. The results of the nonlinear analysis of the midbody panel using tee stiffeners are shown in Figures 7.2 to 7.6.

ADINA-PLOT VERSION 4.0.3, 14 SEPTEMBER 1992
M.V. ARCTIC MVA06 LDC ELASTIC-PERFECTLY PLASTIC

ADINA DEFORMED MIN 6022
LOAD STEP XMAX 5849
TIME 14.001.30 YMIN 153.0
YMAX 339.2

Z
x



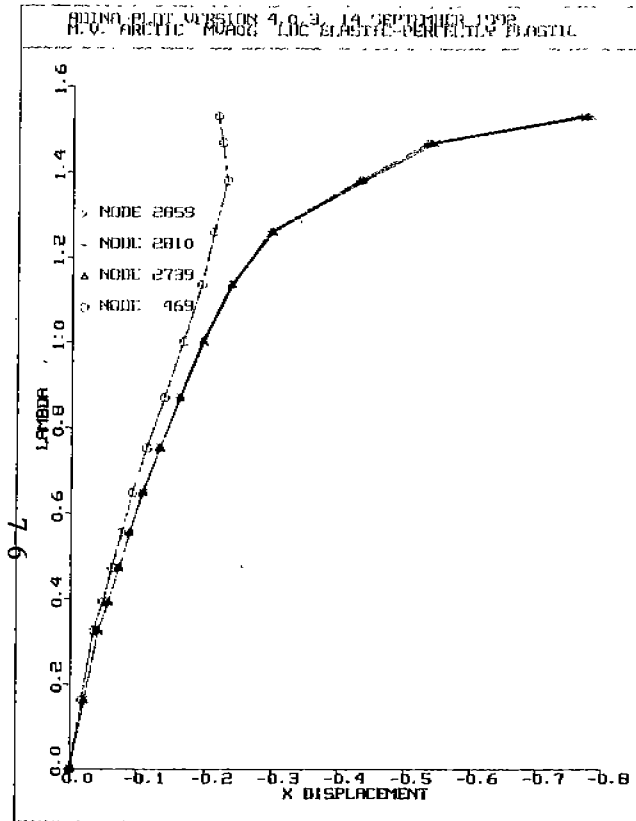
M.V. ARCTIC - WITHOUT INNER SKIN

FIGURE 7.1: Redesigned ASPPR FE Model of the Midbody Panel Using TEE Stiffeners

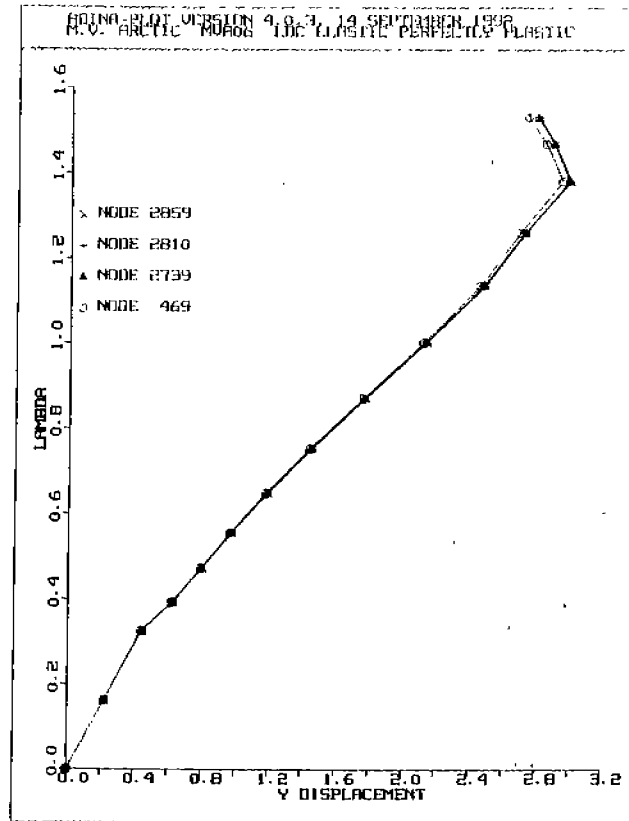
Figure 7.2 shows the response of four nodes of a cross-section at midlength of the tee stiffener which experiences the maximum applied load. Node 469 is located at the intersection of the tee web and the outer plating. The other three nodes (2810, 2739, and 2859) are at the aft, mid and forward positions on the flange respectively. Figure 7.2(a), which shows the lateral frame displacement, predicts that the response will remain fairly linear until about F_{max} . This occurs even though the mainframe plasticity was found to occur at 75% of F_{max} . At approximately 120% of F_{max} , the x displacement at the nodes on the flange increases substantially with respect to the outer shell. The structure fails at 153% of F_{max} due to tripping of the mainframe directly under the maximum applied ice load. This can be seen in Figure 7.3 where the overall displaced shape plot (magnified) shows the tripping of the mainframe.

Figure 7.4 presents a view with the inner skin removed showing the S_{YY} stresses (vertical component) and the S_{XX} stresses (longitudinal component) at various load levels. The results up to about F_{max} are essentially what is predicted from the linear analysis. At load levels above this point, the nonlinear effects begin to dominate the response as yielding and geometric nonlinearities become more significant. Directly under the point of load application, the stress in the outer shell can be seen to start as a compressive stress. As the load gets larger the geometric nonlinear effect takes over and at 153% of F_{max} the stresses near the point of maximum load application change to tensile as local membrane stresses begin to dominate in the plating. This is more clearly illustrated in Figure 7.5 which isolates the mainframes in the center bay of the panel.

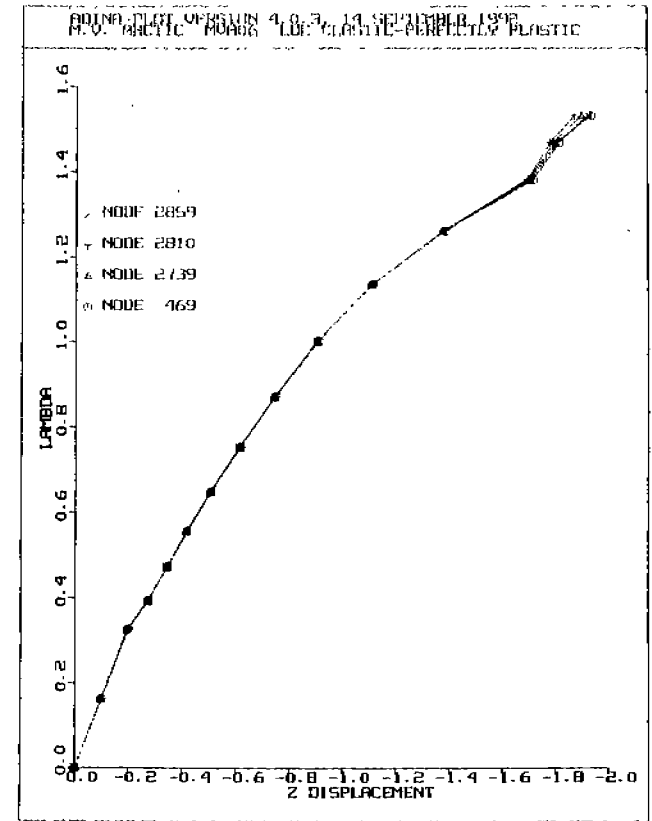
Figure 7.5 also shows the response of the mainframe under the maximum applied load. The stress in the mainframe can be seen to start as tensile stresses in the outer web and compressive stresses in the inner web along the line where it intersects with the outer shell. As the load is increased, the tensile stress in the mainframe grows until, at a load level of 56%, the mainframe has experienced some yielding. As the frame experiences yielding, the incremental load which is applied must be supported by a frame which is slightly shallower. The local incremental load is still supported by a bending action in the mainframe which results in an increased tension in the outer fibres of the web and a compressive stress being set up in the inner fibres of the web. Since the outermost fibres have yielded and are, in essence, nonexistent for any incremental load, the tensile stress set up to carry the load migrates towards the base of the frame. At F_{max} , the mainframe is found to be largely in a state



(a)



(b)



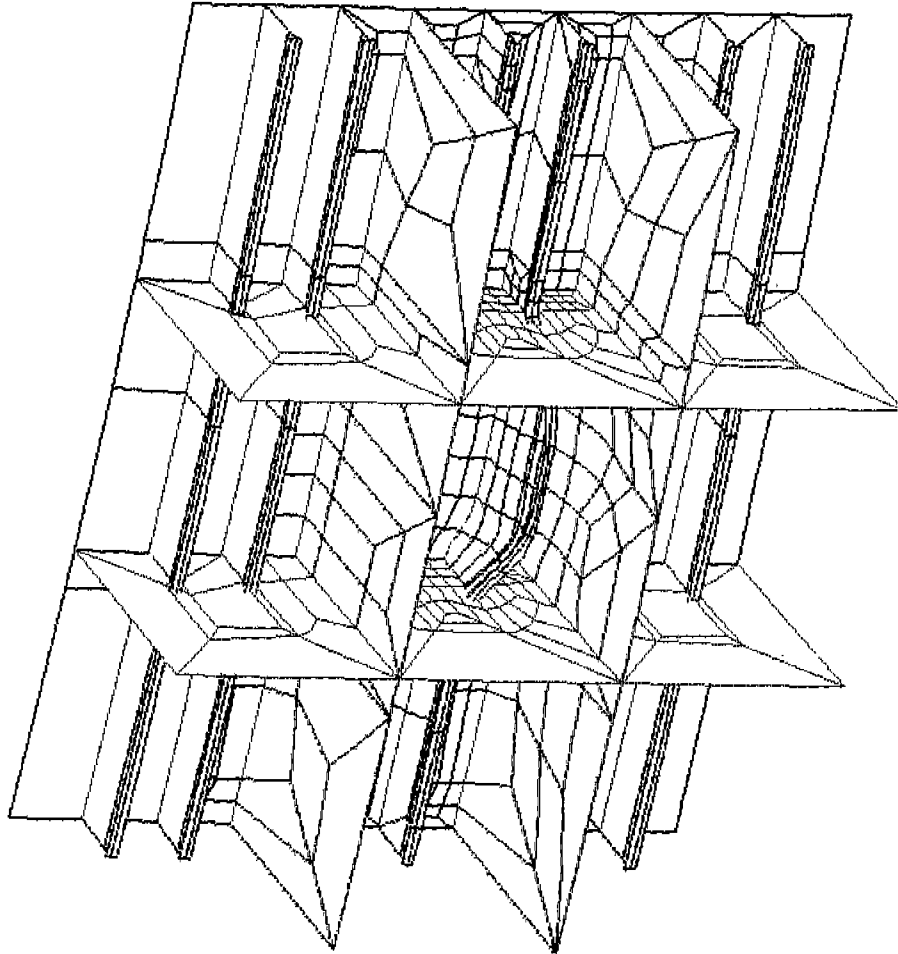
(c)

FIGURE 7.2: Displacement versus Applied Load Curves
 - Nonlinear Analysis of the ASPPR Redesigned TEE Section Model

168

ADINA-PLOT VERSION 4.0.3, 14 SEPTEMBER 1992
M.V. ARCTIC MVA06 LDC ELASTIC-PERFECTLY PLASTIC

ADINA DEFORMED UMIN 6016.
LOAD STEP XMAX 5831.
TIME 14.00.226 YMIN 166.3
YMAX 361.6



of tension and has experienced yielding through most of the depth of the frame. At this point, the outer shell out-of-plane displacements have increased significantly and the incremental load is now being carried largely through to plate tensile membrane stresses rather than through a bending action in the mainframes. This is evident by the change in the condition of stress in the outer shell. As the load level is increased from F_{max} to $153\% F_{max}$, the state of stress in the outer shell, close to the point of load application, reduces from a region of about -25,000 psi compressive stress to a region of either low compressive stresses or tensile stresses.

Tripping occurs as the outer shell out-of-plane displacement continues to increase. This displacement creates an inward slope in the outer shell that increases from the intersection of the web frame and plating to the intersection of the mainframe and plating. This results in the flange of the mainframe rotating about a vertical axis in the aft direction. With most of the mainframe now yielded, the small web section that remains below yield is under a compressive load. With the rotation toward the aft direction increasing substantially, the mainframe trips under this load.

Figure 7.6 shows the progression of yield through the structure. The structure starts to yield at about 75% of F_{max} which progresses until, at 126% of F_{max} , the mainframe is essentially totally plastic. It is at this point in the analysis that the mainframe tripping initiates. At this load level it is also seen that the top of both webs are quite plastic. Since this nonlinear response is quite close to boundaries that are restrained by linear MAESTRO boundary conditions, it is questionable as to whether or not the response is valid and tripping actually occurs. However, at this load level the outer skin has already started to yield, meaning large out-of-plane displacements, and a continuation of the tripping that has already initiated.

7.4.2 Mainframes Modelled as Angle Sections

The angle section used in this analysis was designed to the ASPPR regulations with the following dimensions:

15.35 x 2.36 x 0.47 (in)
390 x 60 x 12 (mm)

The FE model of the midbody panel using angle stiffeners is shown in Figure 7.7

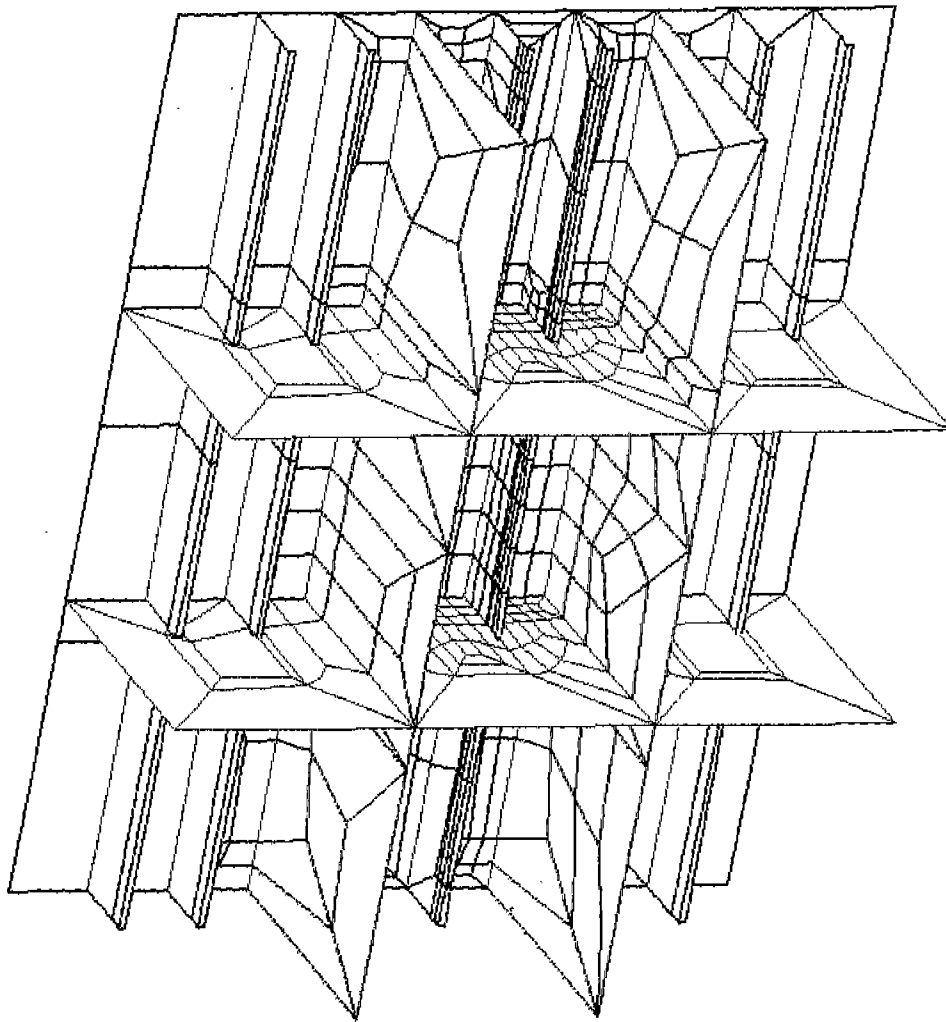
The response of the angle section is quite similar to that of the tee section. The frame displacements remain fairly linear with increasing load until a load level of about F_{max} . The mainframe plasticity starts at about 75% of F_{max} , is quite extensive at F_{max} , and the structure fails at 124% of F_{max} due to tripping of the mainframe directly under the maximum applied ice load.

Figure 7.8 shows the response of three nodes of a cross-section at midspan of the angle stiffener which experiences the largest load. Node 469 is at the intersection of the angle web and the outer plating. The other two nodes (2810 and 2739) are at the aft and forward positions on the flange respectively. Figure 7.8(a) shows that at a load level of approximately F_{max} the x displacement at the nodes on the flange increases substantially with respect to the outer shell. As with the tee frames this shows that the frame is tripping. This can be seen in Figure 7.9 where an overall displaced shape plot shows the buckling of the mainframe at a load of 124% of F_{max} . Also shown in Figure 7.9 are displaced shape plots of the center bay of the panel at various time steps.

One significant difference between the tripping response of the tee section and the angle section is the direction of tripping. While the tee section tripped in the aft direction (-x), the angle section trips in the forward (+x) direction. This is despite an initial response in the aft (-x) direction. The reason for this is the asymmetry of the angle section. As with the tee section, under low loads the slope of the outer shell causes the flange of the angle to rotate in the aft direction. However, as the load increases the region of the flange near the intersection with the web goes plastic. The yielding then progresses towards the outer shell as the load increases. At a load near F_{max} , with most of the mainframe yielded, the remaining non-yielded flange material is now eccentric to the applied tensile forces which are predominantly in the web. This will draw the flange back towards and past the web until the eccentricity disappears. This happens when the centroid of the flange and web coincide. At this point the intersection of the flange and web is at a point in the positive x side of the web. Now as the load increases, the remaining flange material yields leaving only a small section of frame material near the outer shell. The compressive stresses in the outer shell side of the mainframe compress the mainframe resulting in a tripping response towards the forward (+x) direction.

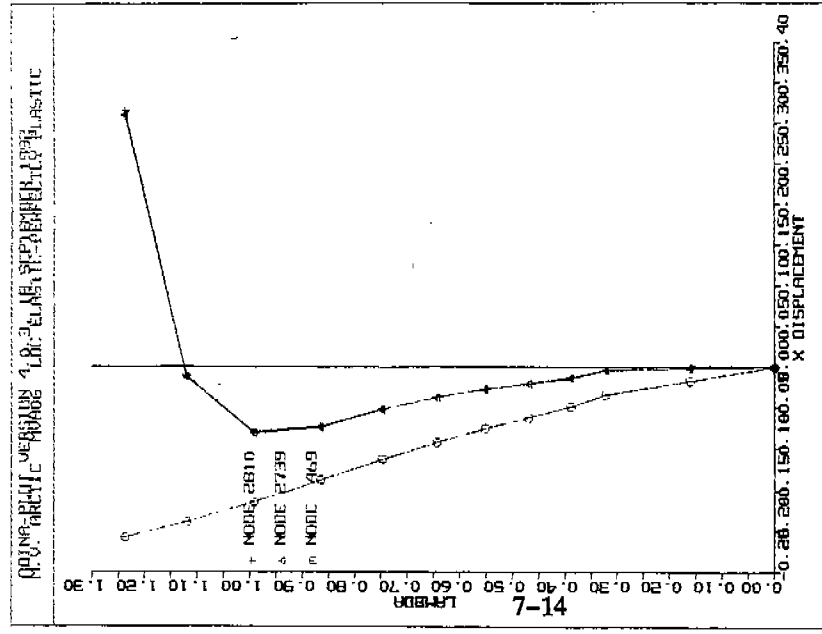
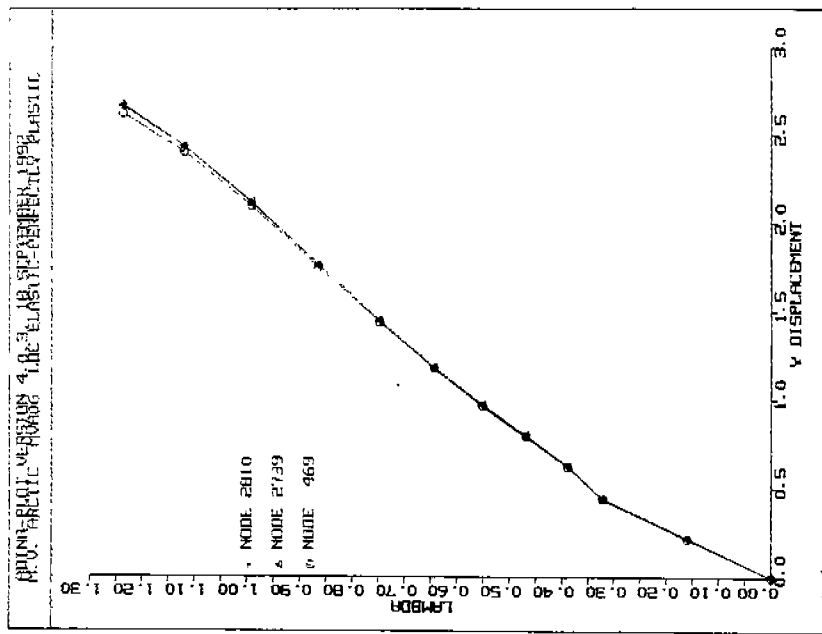
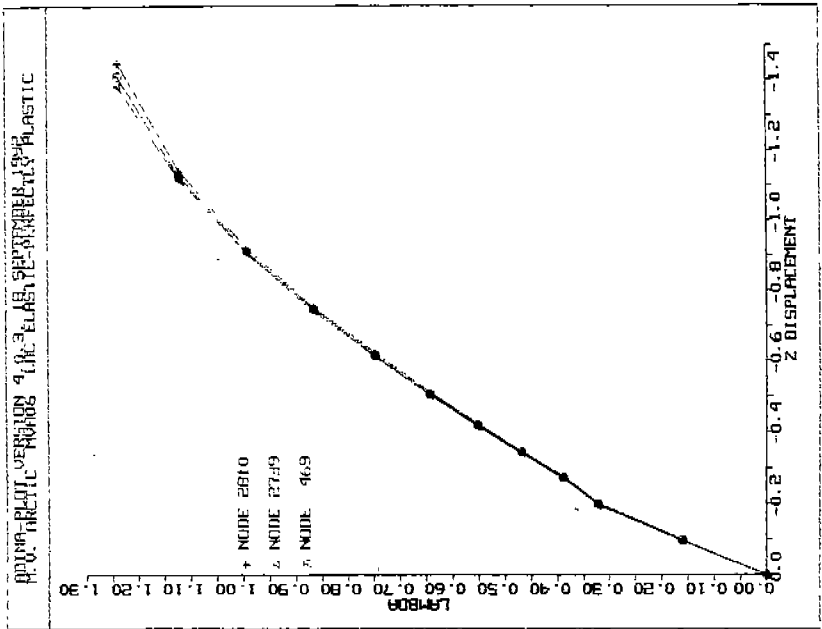
ADINA-PLOT VERSION 4.0.3 18 SEPTEMBER 1992
M.V. ARCTIC MVA06 LDC ELASTIC-PERFECTLY PLASTIC

ADINA DEFORMED XUMIN 6022.
LOAD_STEP XUMAX 5849.
TIME 11.001.30 YUMIN 152.9
YUMAX 339.1



M.V. ARCTIC - WITHOUT INNER SKIN

FIGURE 7.7.: Redesigned ASPPR FE Model of the Midbody Panel Using ANGLE Stiffeners

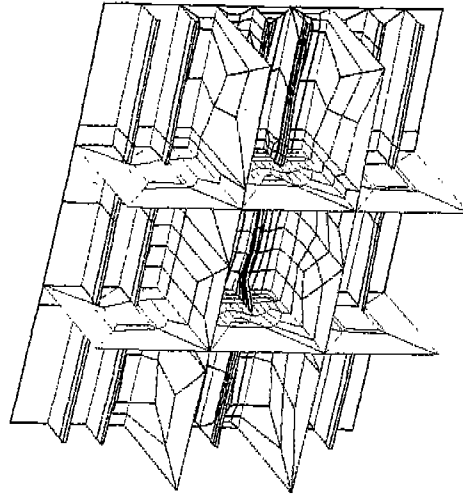


(a)

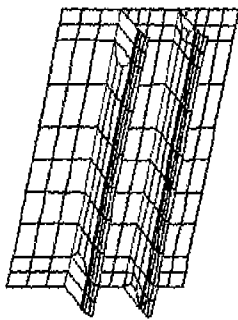
(b)

(c)

FIGURE 7.8: Displacement versus Applied Load Curves
 - Nonlinear Analysis of the ASPPR Redesigned Angle Section Model

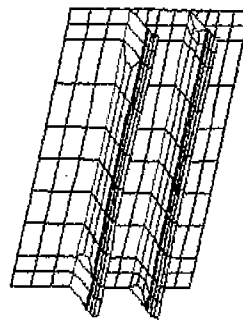


M.O. ARCTIC - WITHOUT INNER SKIN



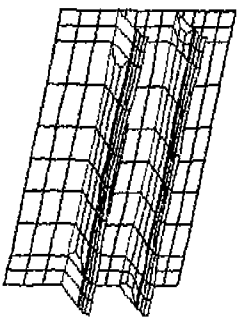
55%

MODEL CENTER PANEL T=5.0



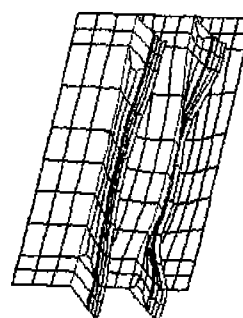
75%

MODEL CENTER PANEL T=7.0



100%

MODEL CENTER PANEL T=9.0



124%

MODEL CENTER PANEL T=11.0

FIGURE 7.9: Overall and Center Bay Displaced Shapes
- Nonlinear Analysis of the ASPPR Redesigned Angle Section Model

Other than this variation, the response of the angle section is very similar to the tee section. Figure 7.10 shows the SYY stresses (vertical component) and the SXX stresses (longitudinal component) of the overall model. The plot is a view with the inner skin removed and has been constructed at various load levels. Up to about F_{max} the response is generally linear, however, above this point the nonlinear effects begin to dominate. Directly under the point of load application, the stress in the outer shell can be seen to start as a compressive stress, but at 124% of F_{max} the compressive stresses near the point of maximum load application start to reduce. This signifies the change to tensile stresses as local bending stresses begin to transform to plate membrane stresses. This is more clearly illustrated in Figure 7.11 which isolates the mainframes in the center bay of the panel.

Also detailed in Figure 7.11 is the response of the mainframe under the maximum applied load. Except for the magnitudes and the final tripping mechanism — which was detailed earlier — the stress distribution of the angle mainframe is very similar to that of the tee section as discussed in Section 7.4.1. This is also true for the progression of yield shown in Figure 7.12. The reader can refer to the previous section for this description.

7.4.3 Mainframes Modelled as 70° Flat Bar Sections

The flat bar section used for this analysis was designed to the ASPPR regulations with the following dimensions:

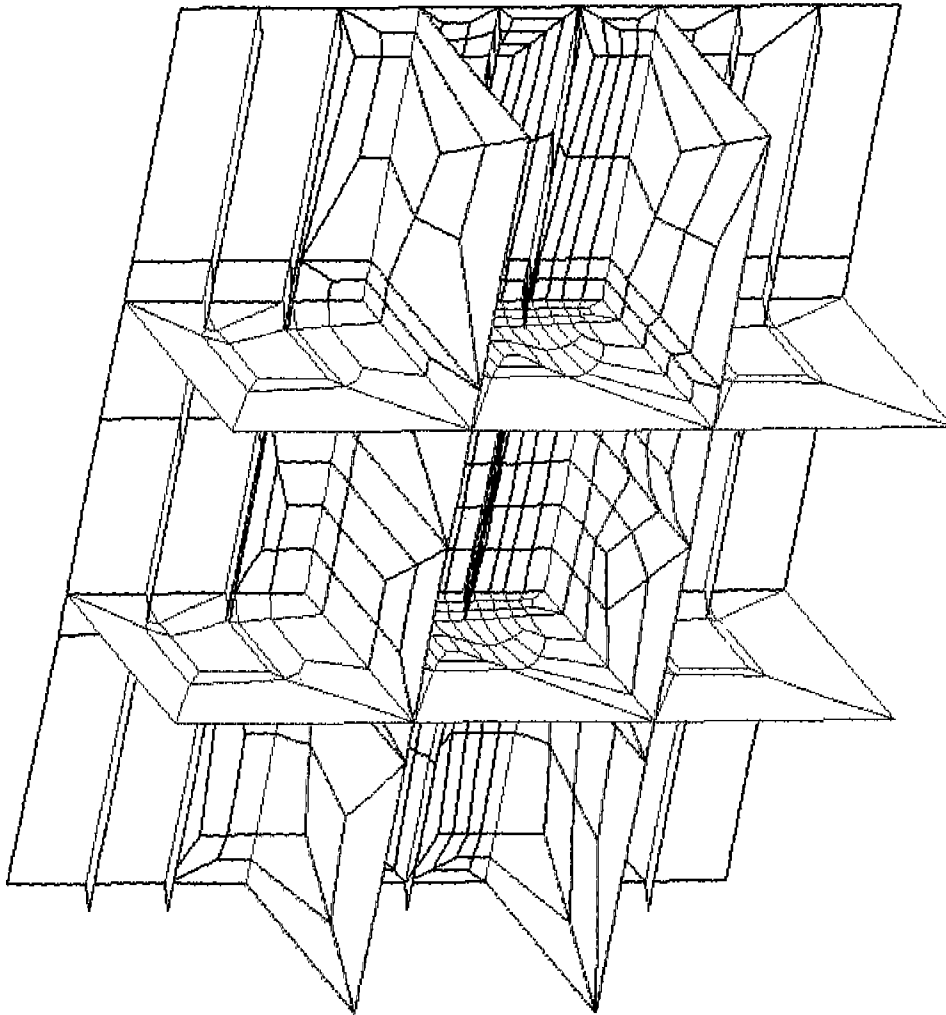
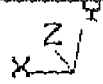
12.0 x 0.95 (in)
305 x 24 (mm)

The flat bars are canted at 70° (forward) to the outer shell. The FE model of this structure is shown in Figure 7.13.

Both of the previous panels (tee and angle) collapsed due to buckling of the mainframes and although the mainframes of the canted flat bar model start to exhibit buckling, it is not the primary collapse mechanism. This is because the type of buckling is non-bifurcation. As shown in Figure 7.14, the initial change in slope of the load-displacement curves indicate a steady nonlinear increase in displacement that gradually decreases to a more linear response (up to 120% of F_{max}). This is quite

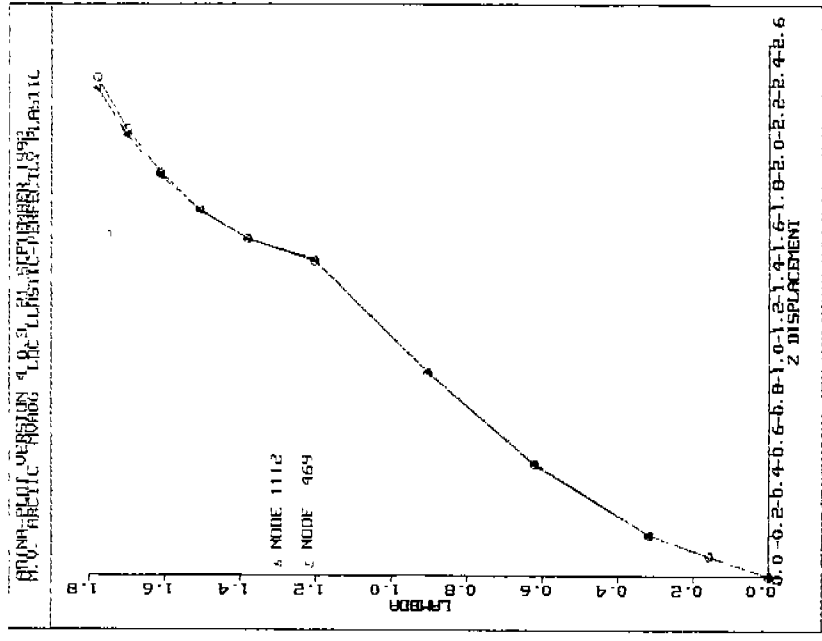
ADINA-PLOT VERSION 4.0.3, 21 SEPTEMBER 1992
M.V. ARCTIC MVA06 LOC ELASTIC-PERFECTLY PLASTIC

ADINA DEFORMED XUMIN 6021.
LOAD STEP XUMAX 5849.
TIME 10.001.30 YUMIN 153.6
YUMAX 339.7

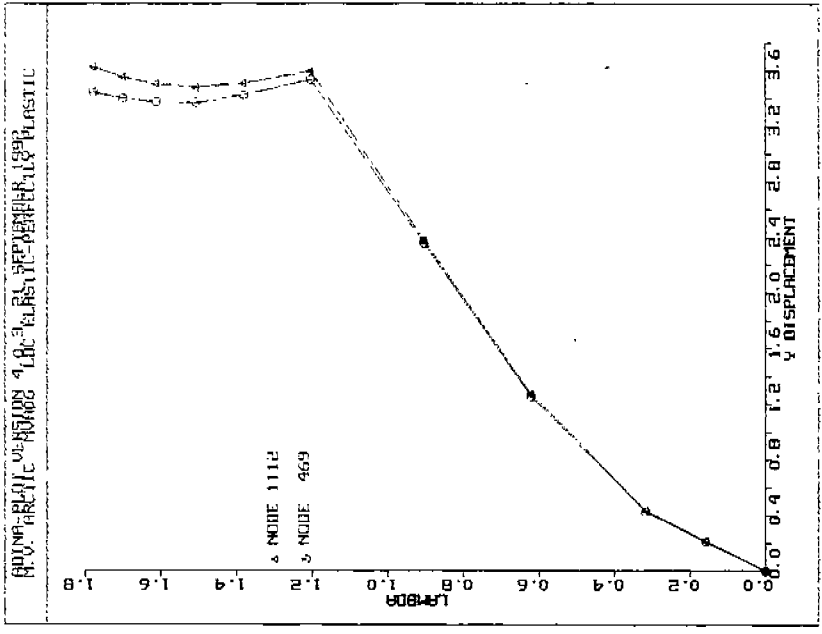


M.V. ARCTIC - WITHOUT INNER SKIN

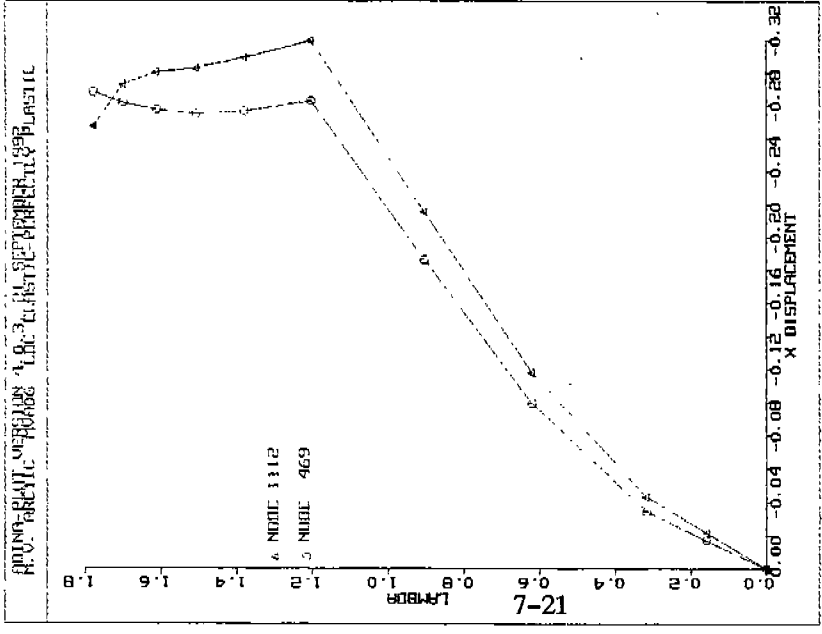
FIGURE 7.13: Redesigned ASPPR FE Model of the Midbody Panel Using Canted 70° Flat Bars



(a)



(b)



(c)

FIGURE 7.14: Displacement versus Applied Load Curves
- Nonlinear Analysis of the ASPPR Redesigned Canted 70° Flat Bar Model

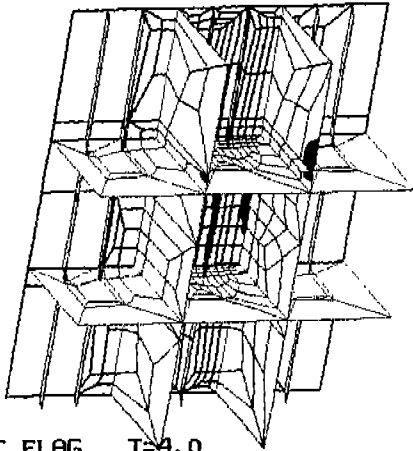
different from the previous analyses. The tee and angle sections exhibited a fairly linear increase in lateral displacement followed by a sudden nonlinear jump. This is typical of bifurcation buckling of which tripping is a primary example. The deep webs in the canted flat bar model seem to take most of the load in bending until 120% of F_{max} where extensive yielding in the deep webs causes collapse.

Figure 7.15 shows the $SY Y$ (vertical component) and SXX stresses (longitudinal component) for the overall model for a view with the inner skin removed. As the load increases from 90% to 138% of F_{max} , the compressive component of the bending stress increases at the outer shell and in the deep web close to the outer shell. This is accompanied by an increase in the tensile component in the deep webs near the inner skin. Above 138% of F_{max} , these stress components show insignificant change except locally at the point on the mainframe which sees the maximum applied load. The reason for this is shown in Figure 7.16. At and above 138% of F_{max} the top and bottom sections of both deep webs have yielded. In fact, as Figure 7.14 shows, this happens at approximately 120% where a dramatic decrease in x and y displacement occurs. When the top and bottom of the deep webs go plastic, the center bay goes through a global translation in the z direction. This means that the z displacement still increases in the mainframes, but the x and y displacements changed very little under the increased load.

The progression of yield through the structure is shown in Figure 7.16. The mainframes and deep webs start to yield near 90% of the total load until at 138% of the load, the mainframe, part of the outer shell, and the tops and bottoms of both deep webs are essentially totally plastic. Above this load no reasonable conclusions can be made about the response. This is because the deep webs show an extensive plastic region that is quite close to boundaries which have been assumed to be linear.

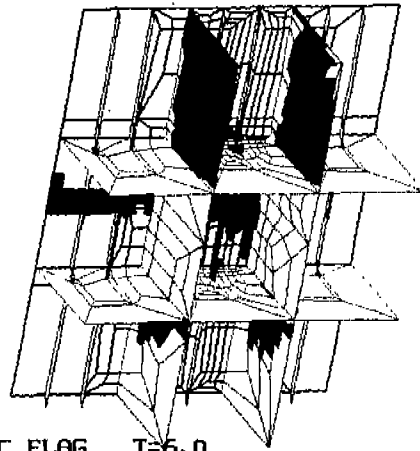
The displaced shape plot at the highest load is shown in Figure 7.17. This plot shows a substantial deflection in the outer skin and the stringers above and below the center bay, and also an extremely deformed center section of the aft deep web. Since most of the structure is plastic at this load level (including the model boundaries), very little can be concluded from the response. This plot is presented only to show the relative displacement of the outer shell and mainframe under the maximum applied load.

90%



PLASTIC FLAG T=4.0

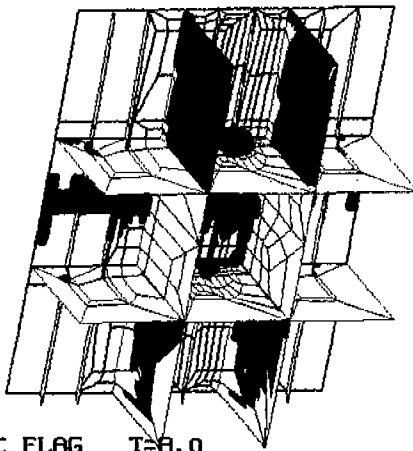
138%



PLASTIC FLAG T=6.0

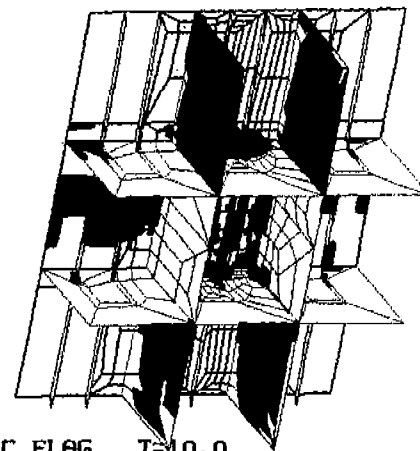


156%



PLASTIC FLAG T=8.0

178%

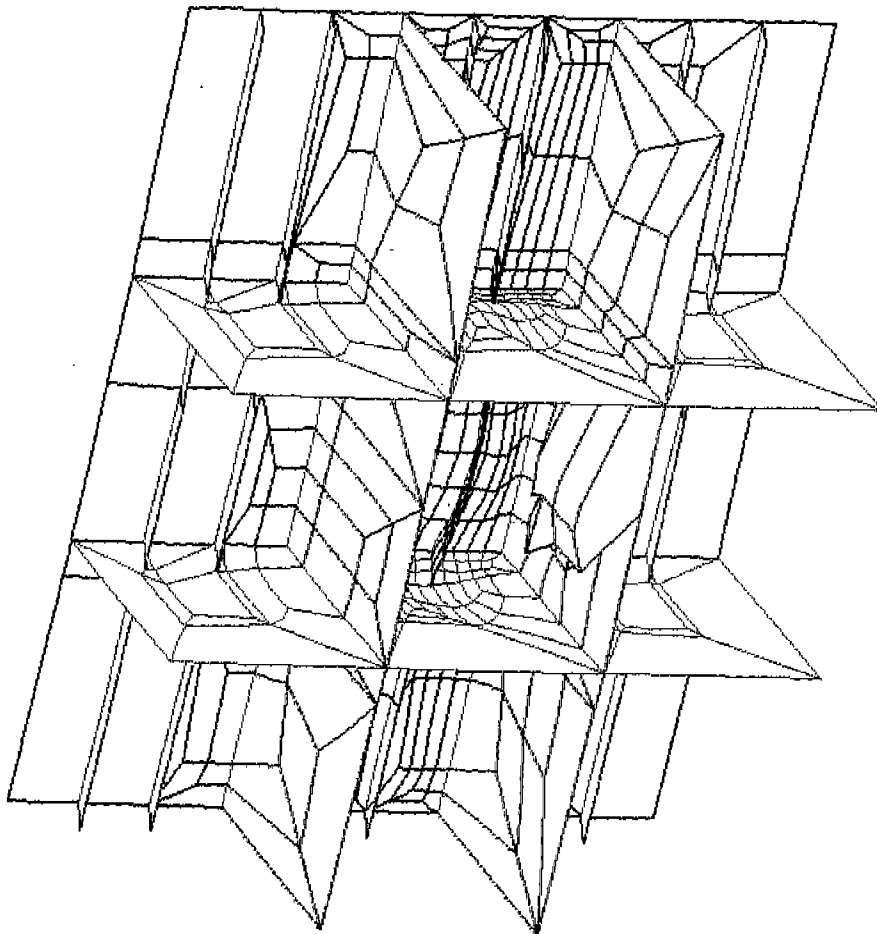


PLASTIC FLAG T=10.0

FIGURE 7.16: Progression of Yield
- Nonlinear Analysis of the ASPPR Redesigned Canted 70° Flat Bar Model

ADINA-PLOT VERSION 4.0.3, 21 SEPTEMBER 1992
M.V. ARCTIC MVA06 LDC ELASTIC-PERFECTLY PLASTIC

ADINA DEFORMED XMIN 6022.
LOAD STEP XUMAX 5833.
TIME 10.00.532 YMIN 150.9
YUMAX 362.2



M.V. ARCTIC - WITHOUT INNER SKIN

FIGURE 7.17: Displaced Shape
- Nonlinear Analysis of the ASPPR Redesigned Canted 70° Flat Bar Model

To facilitate the demonstration of the effects of varying the structural parameters, the conclusions from this analysis are presented in Section 7.5, along with the conclusions from the results of the other models analyzed in the parametric study.

7.4.4 Modified Slenderness Ratios of Flat Bar Sections

To determine the effects of the slenderness ratio of the flat bar section on the response of the panel, the slenderness was increased. The same moment of inertia of the flat bar section redesigned to ASPPR (Section 5.4) was maintained. The new flat bar dimensions were determined as follows:

ASPPR Redesigned Flat Bar Dimensions : 11.81 x 0.709

ASPPR Redesigned Flat Bar Bending Moment of Inertia:

$$I = \frac{(0.709)(11.81)^3}{12} = 97.32 \text{ in}^4 \quad (7.1)$$

Increase the slenderness by increasing the depth of the flat bar section by 25%. Therefore:

$$\text{Depth} = 11.81 * 1.25 = 14.76 \text{ in.}$$

The thickness required to maintain the bending moment of inertia is:

$$\text{thickness} = \frac{(97.82)(12)}{(14.76)^3} = 0.36 \text{ in} \quad (7.2)$$

Therefore, the flat bar section with an increased slenderness ratio has the following dimensions:

375 x 9.1 (mm)
14.76 x 0.36 (in)

To facilitate the comparison of the results of the two flat bar models, the first flat bar model ("less slender" mainframe model from Section 5.4) will be referred to as model 1, and the model analyzed in this section (the "more slender" model) will be referred to as model 2.

The FE model (model 2) is shown in Figure 7.18. The results of the nonlinear analysis are presented in Figures 7.19 to 7.22. This analysis was performed before the stringer grid was modified in model 1 (see Section 5.4.5). Since failure does not occur at the stringer, the errors associated with the irregular mesh at the stringer are expected to be small. Therefore a reanalysis using the modified grid model was not performed.

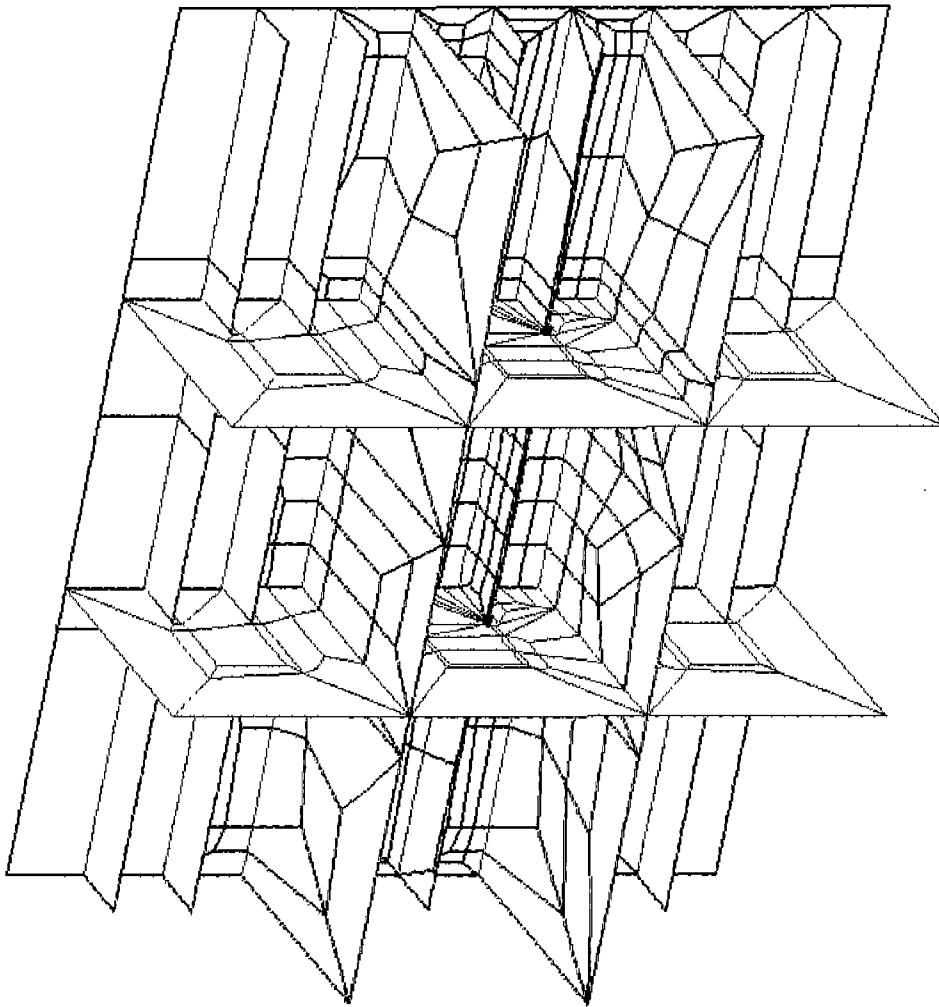
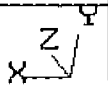
The analysis was performed in two stages. The first stage used four time steps. The response is slightly nonlinear up to step 4 where the analysis failed to converge at a load of approximately 85% of F_{max} . As with the model 1 analysis, with the mainframes modelled as flat bars (Section 5.4), the maximum loaded mainframe, and the region of the stringer that intersects with the top of this mainframe starts to exhibit yielding as the load increases. However, in model 2, the yielding that starts at 59% of F_{max} does not progress across the stringer region between the two frames. The failure which occurred at 85% of F_{max} is due to tripping of the mainframe directly under the maximum applied ice load. This is evident in the lateral displacement of the mainframe. The model 2 mainframe displaces laterally twice the amount of model 1, and trips before the stringer fails.

The second stage of the analysis involved restarting the first stage analysis at time step four with a lateral displacement of one-tenth of the first phase. This analysis, which failed to converge at 88% of F_{max} , provided little additional information about the response since the load level is only slightly above the load level of the first stage. Therefore, the failure mechanism can be predicted from the first stage, and restarting the second stage is not necessary. Also, it took approximately 40 CPU hours (in four days) to complete the stage two run, therefore making it impractical to proceed any further with the analysis.

Figure 7.19 shows the displacements of two points at midspan on the maximum loaded mainframe in the center bay. Node 1112 is a point on the mainframe at the point furthestmost from the hull plating and node 469 is at a point where the frame intersects with the hull plating. The y and z displacements at various applied loads are shown in Figures 7.19(b) and 7.19(c) respectively. Up to failure (for both of these plots), the two points follow the same displacement pattern, indicating that as the load is increased, the hull, and the mainframe displace inward and upward by the same amount.

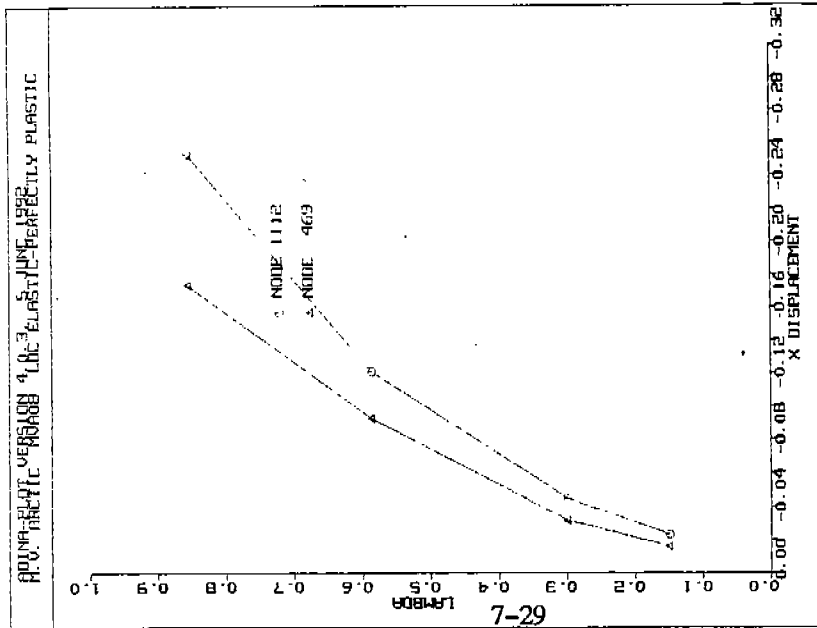
ADINA-PLOT VERSION 4.0.3 7 JUNE 1992
M.V. ARCTIC MVAOB LDC ELASTIC-PERFECTLY PLASTIC

ADINA DEFORMED UMIN 6021.
LOAD STEP QUMAX 5847.
TIME 4.008.277 UMIN 155.9
QUMAX 344.2

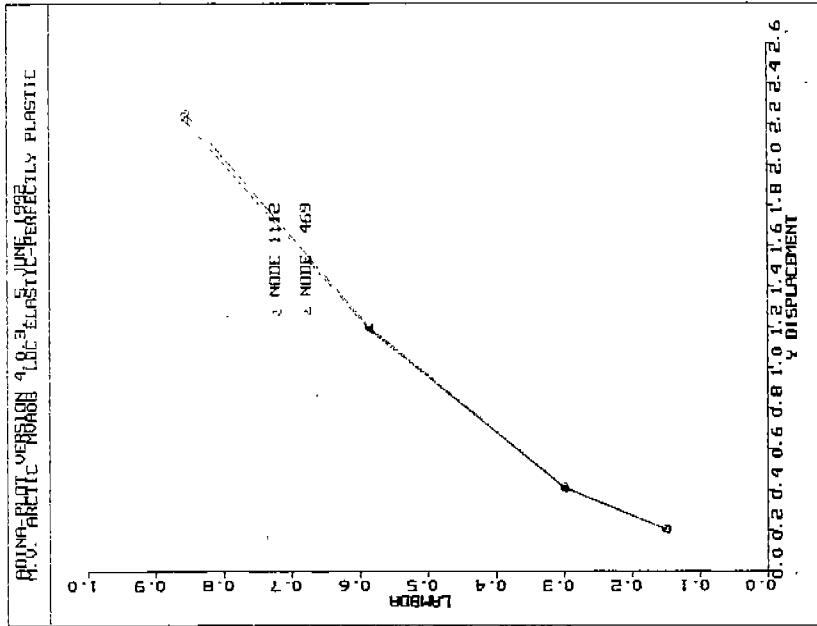


MODEL WITHOUT INNER SKIN

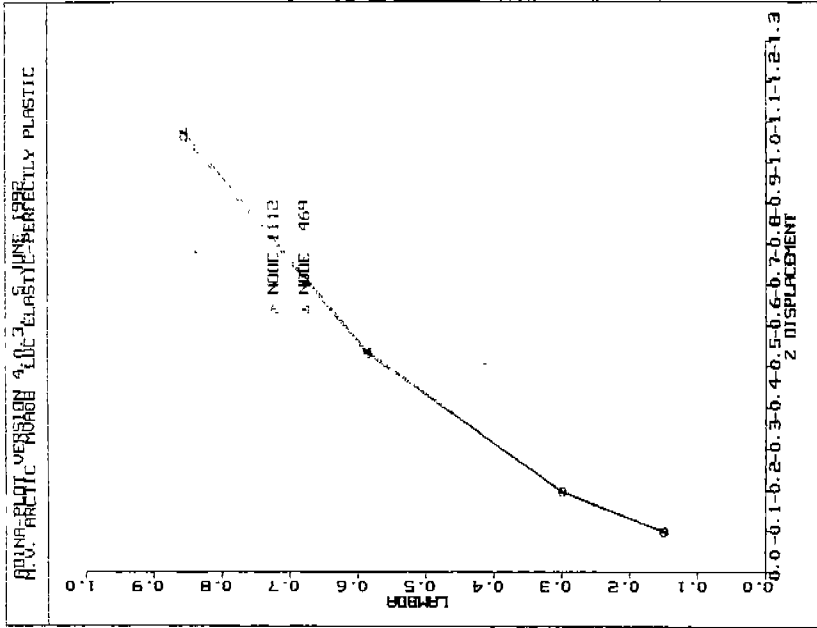
FIGURE 7.18: Redesigned ASPPR FE Model of the Midbody Panel
Using Flat Bars With Increased Slenderness



(a)



(b)



(c)

FIGURE 7.19: Displacement versus Applied Load Curves
 - Nonlinear Analysis of the ASPPR Redesigned Increased Slenderness Flat Bar Model

191

Figure 7.19(a) shows the displacement in the x direction (i.e. in the fore-aft direction). The two points show a slight difference in displacement at time step 1 which increases until the two curves start to rapidly diverge at time step 4 — with a difference in displacement of about 0.08 inches. At the same load level in model 1, this difference in displacement is only 0.04 inches (Figure 5.18), indicating that the mainframe in model 2 is much more likely to trip. This is different from the results of model 1 where the stringer fails before the mainframe trips.

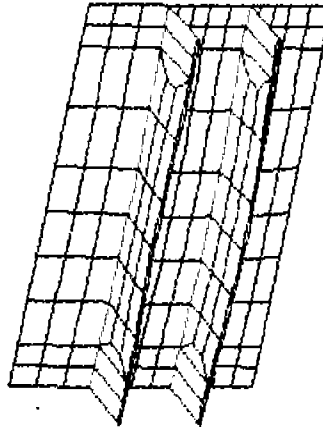
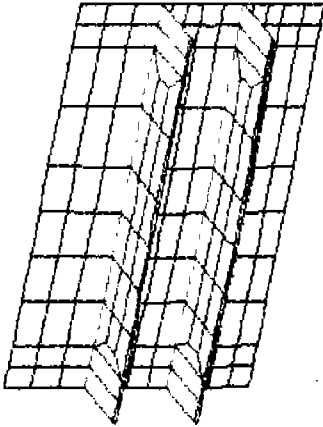
By comparing the progression of yielding between the two models, it is evident that the mainframe is more likely to trip before the stringer fails (in model 2). Figure 7.20(a) shows the progression of plasticity in the top stringer and Figure 7.20(b) shows the plasticity in the mainframes and outer skin of model 2. At time step 4 (85% of F_{max}) the mainframe under the maximum applied load has almost completely yielded, however, the stringer shows slight yielding. At the same load in the model 1 analysis (between steps 7 and 9 of Figure 5.19), the stringers show approximately the same progression of yielding, however, the mainframes show very little plasticity. Because the mainframes yield under lower load levels in model 2, tripping will occur earlier. For model 2, the increase in slenderness in the mainframes is sufficient to cause the mainframes to buckle before failure of the stringers.

Figure 7.21 shows the magnified displaced shape of the outer shell and frames at the center bay from load steps 1 to 4. The mainframe under the local area of load application shows the tripping response. A high magnification factor has been used to identify this. Figure 7.22 shows the displaced shape plots of the stringers. The stringers can be seen to be displaying large out-of-plane displacements at step 4, however comparison of the magnitude of the displaced shape with the scale used in the displaced shape plot of the stringer (at failure) of model 1 (Figure 5.21) shows much less stringer displacement for model 1.

The conclusions from this analysis are compared to the results of the other models (analyzed in the parametric study) in Section 7.5.

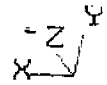
15%

30%



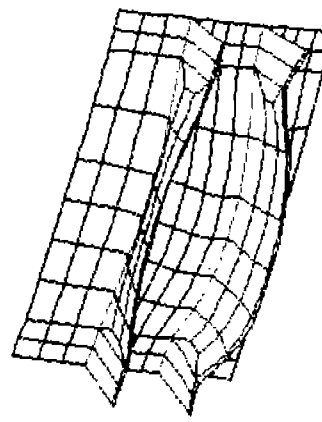
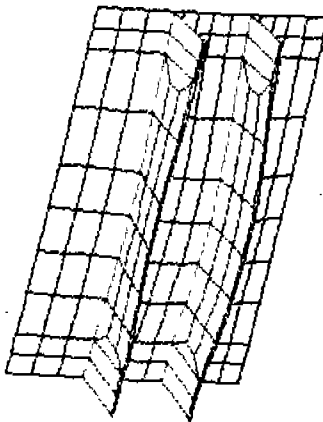
MODEL CENTER PANEL T=1.0

MODEL CENTER PANEL T=2.0



59%

86%



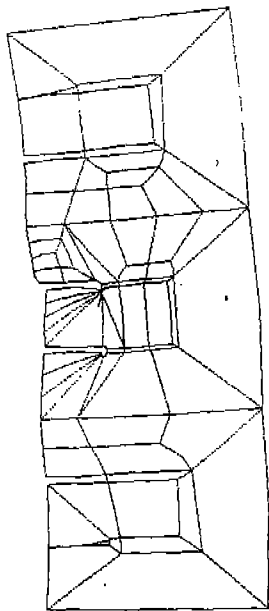
MODEL CENTER PANEL T=3.0

MODEL CENTER PANEL T=4.0

FIGURE 7.21: Center Bay Displaced Shape
 - Nonlinear Analysis of the ASPPR Redesigned Increased Slenderness Flat Bar Model

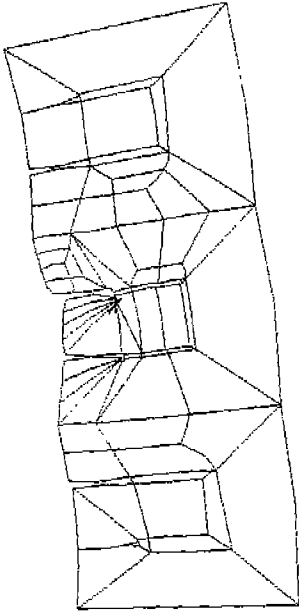
194

59%

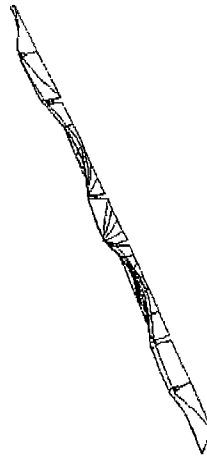


STRINGERS I=3.0

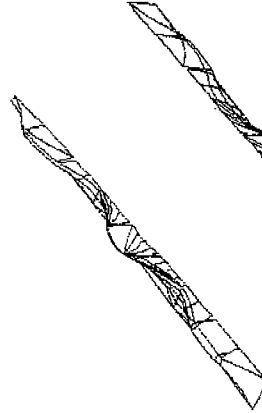
86%



STRINGERS I=4.0



STRINGERS I=3.0



STRINGERS I=4.0

FIGURE 7.22: Stringer Displaced Shape
 - Nonlinear Analysis of the ASPPR Redesigned Increased Slenderness Flat Bar Model

7.4.5 Modified Slenderness Ratios of Canted Flat Bar Sections

The FE model of the modified slenderness 70° canted flat bar model is shown in Figure 7.23. This model was created by modifying the 70° canted flat bar FE model developed in Section 7.4.3. The slenderness was modified by decreasing the frame thickness by 25% from 0.95 in to 0.71 in. It was realized after the analysis was performed that the depth of the frame was not increased to maintain the same moment of inertia in bending. However, the results are still presented as a qualitative indication of the slenderness effects on a canted flat bar.

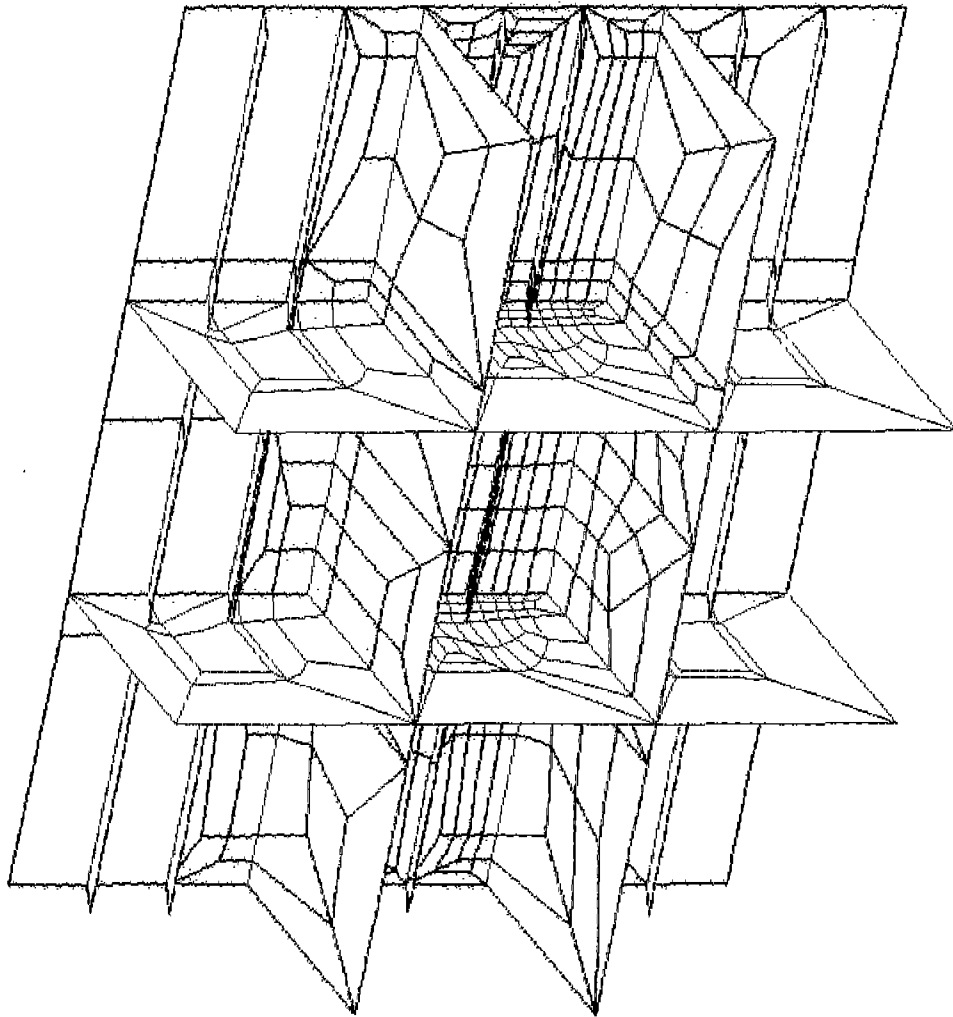
The analysis of the tee and angle models predicted collapse of the mainframes due to bifurcation buckling. The mainframes of the canted flat bar model (analyzed in Section 7.4.3) exhibit a non-bifurcation buckling response. However, the collapse is predicted at the deep webs. The same type of response is also predicted for the modified slenderness canted flat bar model. As shown in Figure 7.24, the gradual change in slope of the load-displacement curves (up to 120% of F_{max}) indicates a steady nonlinear increase in displacement. Above 120% of F_{max} the deep webs have failed and no reasonable conclusions can be made about the response. This is because the deep webs show extensive plasticity at the boundaries that have been assumed to be linear.

Figure 7.25 details the SYY (vertical component) and SXX stresses (longitudinal component) for the overall model without the inner skin. As the load increases to 120% of F_{max} , the compressive component of the bending stresses at the outer shell and in the deep web close to the outer shell increases while the tensile component in the deep webs near the inner skin increases as well. However, above 120% these stress components show insignificant change except locally at the application site of the mainframe with the maximum applied load. The reason for this is shown in Figure 7.26 where the progression of yield through the structure is presented. Above 120% of F_{max} , the top section of both deep webs have yielded. As Figure 7.24 shows, this produces a dramatic decrease in x and y displacement. When the top of the deep webs go plastic, the center bay goes through a global translation in the z direction. This means that the z displacement still increases in the mainframes, but the x and y displacements change very little under the increased load. As discussed earlier, above this load no reasonable conclusions can be made because the deep webs show extensive plasticity close to assumed linear boundaries.

ADINA-PLOT VERSION 4.0.3 6 OCTOBER 1998
M.V. ARCTIC MOA06 LOC ELASTIC-PERFECTLY PLASTIC

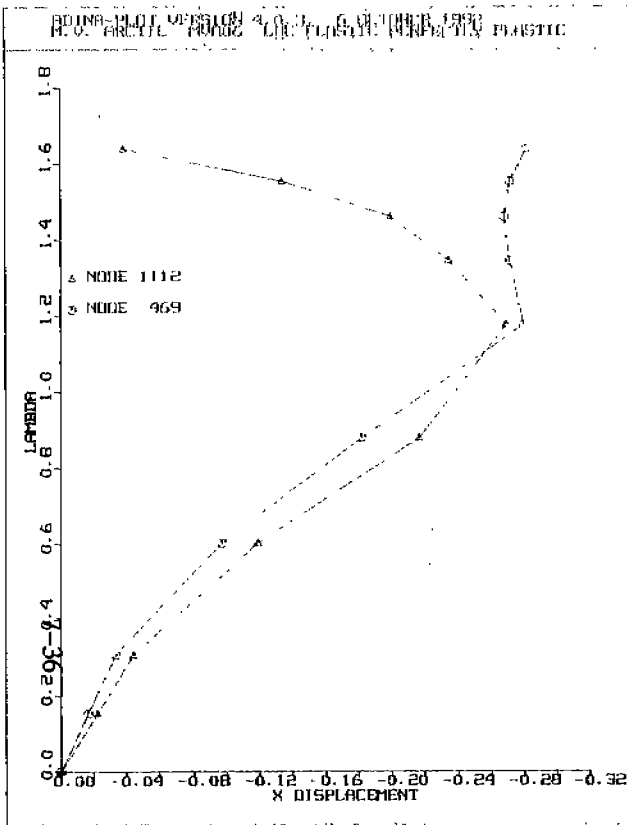
ADINA DEFORMED UNIT 6021
LOAD STEP XUMAX 5849.
TIME 9.0001.30 YUMIN 153.4
YUMAX 339.6

z
x

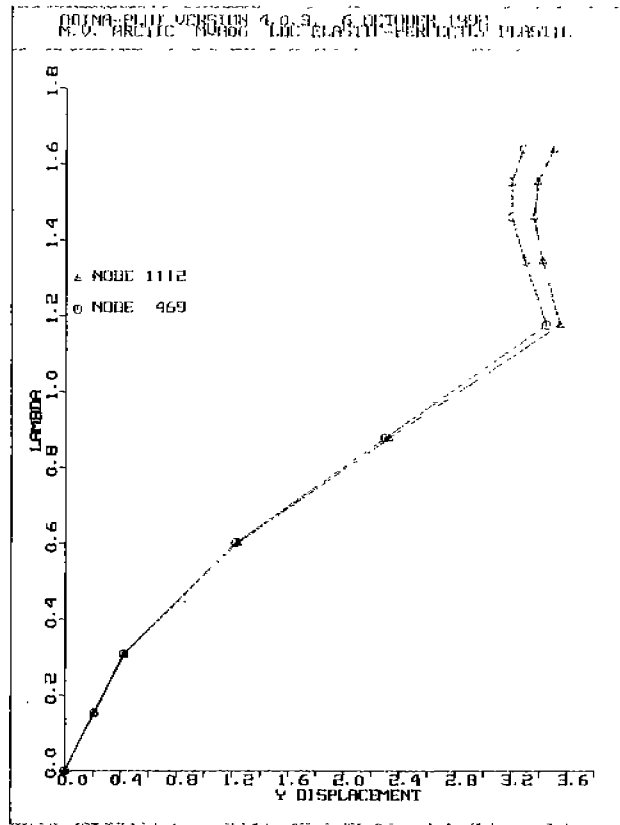


M.V. ARCTIC - WITHOUT INNER SKIN

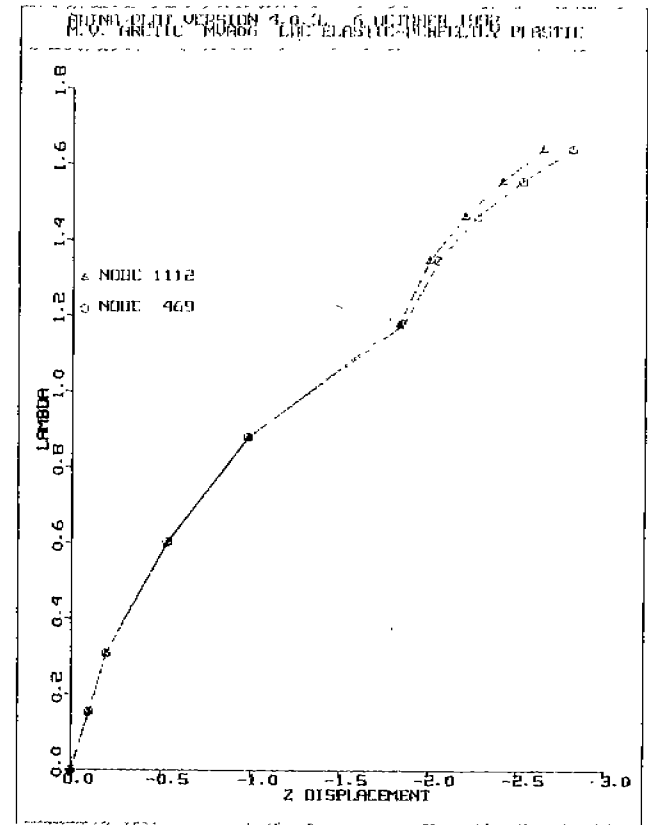
FIGURE 7.23: FE Model of Midbody Panel Using Canted Flat Bars With Increased Slenderness



(a)



(b)



(c)

FIGURE 7.24: Displacement vs. Applied Load Curves
- Nonlinear Analysis of Increased Slenderness 70° Canted Flat Bar Model

861

The displaced shape plot at the highest load is shown in Figure 7.27. This plot shows substantial deformation in the outer skin, at the stringers above and below the center bay, and also at the center section of the aft deep web. Since most of the structure is plastic at this load level, very little can be concluded from the response. This plot is presented only to show the relative displacement of the outer shell and mainframe under the maximum applied load.

The conclusion from this analysis (and the other analyses in this chapter) are presented in Section 7.5 with respect to the effects of modifying the various structural parameters on the response of the midbody panel.

7.5 Summary and Conclusions from the Parametric Study

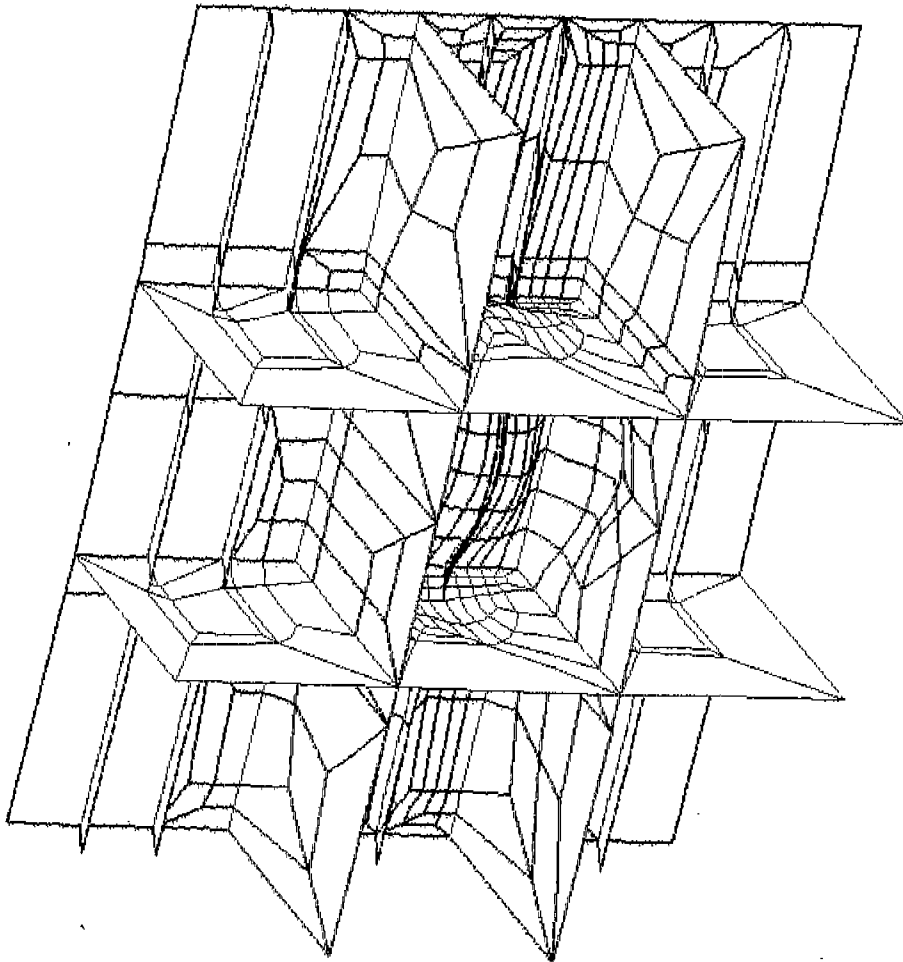
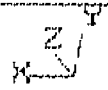
The results from the analyses of the different cross-sections in this chapter are summarized in Table 7.1. The results of the ASPPR redesigned flat bar model (presented in Chapter 5) are also included for comparison purposes.

The predicted values for the start of yield in Table 7.1 are obtained from the plots that show the first incidence of yield. All of these occur in the mainframe under the maximum applied ice load. However, since plots were not produced for every time step, slight variations may exist between the values shown and the actual levels. Based upon this, the onset of yield occurs at approximately the same load level for all midbody analyses.

The start of failure is defined as the initiation of the nonlinear response that produces failure. Since most of the failures are identified by large increases in the frame lateral (x) displacement (especially for tripping of the mainframes), the start of failure is defined mostly by the first occurrence of substantial nonlinearity in the load versus x displacement curves. Except for the slender flat bar model, the start of failure in all models occurs at load levels at or above F_{y0} . Therefore, most cross-

ADINA-PLOT VERSION 4.0.3 6 OCTOBER 1992
M.U. ARCTIC MOA06 LDC ELASTIC-PERFECTLY PLASTIC

ADINA DEFORMED UMIN 6016.
LOAD STEP XUMAX 5832.
TIME 9.000.450 UMIN 164.1
YMAX 361.5



M.U. ARCTIC - WITHOUT INNER SKIN

FIGURE 7.27: Displaced Shape
- Nonlinear Analysis of Increased Slenderness 70° Canted Flat Bar Model

TABLE 7.1: Comparison of Results of Parametric Study

Midbody Main Frame Model	Dimensions (in)	X-Sect Area (in ²)	Load Portion of F_{max}			Mode of Failure
			Start of Yield	Start of Nonlinear* Response	Maximum Load	
Flat Bar**	11.81x0.7087	8.4	0.70	1.30	1.70	Stringer failure
Tee	15.35x0.47+ 2.36x0.47	8.1	0.75	1.25	1.53	Frame tripping
Angle	15.35x2.36 x0.47	8.1	0.75	1.0	1.24	Frame tripping
70° canted flat bar	12.0x0.95	11.4	0.60	1.20	1.80	Web failure
Slender flat bar (+25%)	14.76x0.36	5.3	0.59	0.85	0.85	Frame tripping
Slender 70° canted flat bar	12.0x0.71	8.5	0.60	1.20	1.65	Web failure
* Start of response is associated with a significant change in stiffness.						
** This model was not analyzed in the parametric study. The results are presented in Chapter 5. It is included for comparison purposes.						

F_{max} and 130% of F_{max} , respectively. The lower failure load of the angle section is due to the asymmetry of the frame cross-section. As described in Section 7.4.2, under increasing load, plasticity develops at the intersection of the web and flange of the frame. The loss of material from yielding effectively results in a disconnection between the remaining unyielded material in the web and flange. This disconnection which makes the angle section very unstable, does not develop in the symmetric sections (flat bars and tees). Therefore, they are more stable than the angle section and fail at higher loads.

The ASPPR designed flat bar panel section fails in the stringer due to extreme yielding at the intersection of the frame and the stringer. This happens before tripping occurs. However, when the flat bars are more slender, they fail due to tripping. This occurs because increasing the slenderness of flat bar mainframes results in a decrease in the lateral stiffness as the load is applied and yielding occurs. This produces failure by tripping at lower load levels.

When the flat bars are canted at 70° , model failure occurs at the deep webs rather than the mainframes regardless of the slenderness of the frames. Because the frames are canted, bifurcation buckling does not occur and the lateral rotation of the mainframes is gradual. As the load is increased, the load carrying ability in the deflected mainframes decreases and the load is shed to the stringers and deep webs. With very high ice loads also directly applied to the deep webs, failure occurs in the webs first.

Based upon the summary of the parametric study outlined above, flat bar mainframe sections provide the best stability and can carry the greatest load before failure. Most sections are stable at F_{max} except for very slender flat bars. Increasing the slenderness of uncanted flat bar mainframes reduces the stability of the frames, and the maximum load that the structure can carry. Finally, when flat bars are canted their stability increases, however, the maximum load that the structure can carry does not change significantly.

8. EVALUATION OF THE COMPUTATIONAL IMPACT
OF INCORPORATING STRAIN HARDENING MODULUS

All analyses performed until now have assumed that the nonlinear constitutive relationship for steel is elastic perfectly plastic. An elastic perfectly plastic material property is characterized by curve #1 shown in Figure 8.1. Because the material is perfectly plastic, after yielding occurs the structure has no stiffness to resist the increased load. The flat portion of the curve after the yield point results in continued strain without any further increase in stress (i.e. load).

While this relationship seemed a reasonable approximation to the response of steel, in reality steel has some stiffness after yielding. This stiffness is known as the strain hardening modulus, and is characterized by curve # 2 in Figure 8.1. In this case, after yielding has occurred an increase in strain will produce a small increase in stress.

Since this investigation is primarily interested in predicting the stability of the structure after yielding occurs, using a strain hardening modulus may have an effect on the predicted response. To determine whether this is the case, two analyses were performed. The first analysis utilized the overall model geometry with the mainframes modelled as angle sections. This model, which was previously analyzed as elastic perfectly plastic (see Section 7.4.2), was then analyzed with a strain hardening modulus. The results of the two analyses were compared now to determine the impact of using the strain hardening modulus. The second analysis is basically the same, except that the overall model utilizes mainframes modelled as flat bars (see Section 5.4 for the results from the elastic perfectly plastic analysis). Both models use MAESTRO boundary conditions.

The strain hardening modulus used for the analysis is $0.75 * 10^6$ psi. A precise value could not be found in any reference material; however, discussions with qualified people produced this approximation of the strain hardening modulus. It is approximately equal to 1/40 of the modulus of elasticity ($30.0 * 10^6$ psi). This was considered satisfactory since it is only important here to assess the overall effect of the strain hardening modulus.

8-2

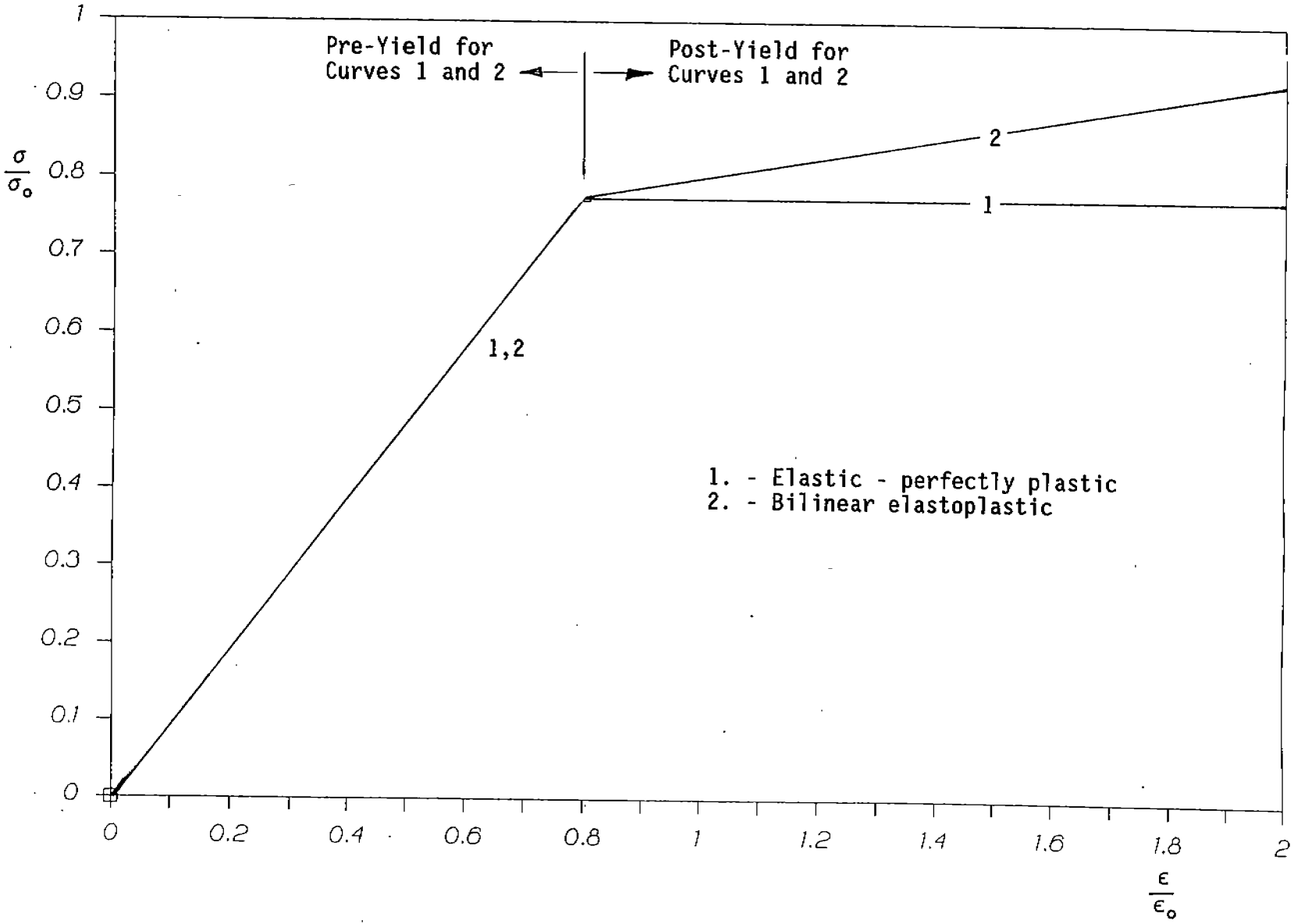


FIGURE 8.1: Types of Modelling Methods for the Nonlinear Material Properties of Steel

206

8.1 Angle Model Using MAESTRO Boundary Conditions

The overall FE model of the M.V. Arctic midbody panel with the mainframes modelled as angle sections is shown in Figure 8.2. The results for the analysis without strain hardening can be found in Section 7.4.2. The load versus x displacement curves for the nonlinear analyses with and without strain hardening are shown in Figure 8.3. The curves for the y and z displacements show insignificant differences, therefore they are not presented. For comparison purposes the model without strain hardening is designated as model # 1. The model with strain hardening is designated as model # 2.

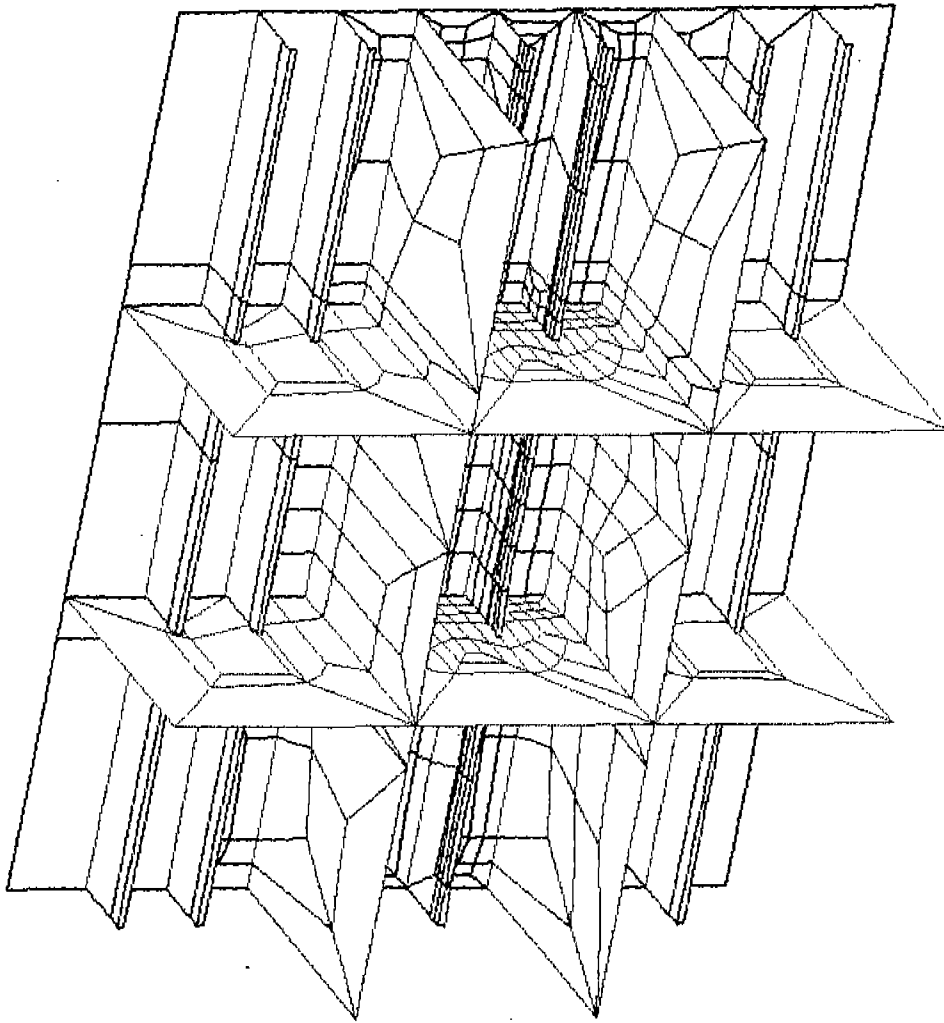
The node at the point of intersection of the web and plating on the mainframe is node #469. At approximately 125% of F_{max} , the lateral displacements for node 469 for either model are approximately the same. Nodes 2739 and 2810 are located on the mainframe flange. The difference in these curves is the slope of the curves between zero and F_{max} .

Model 1 starts to displace in the negative x direction (aft) as the load increases. As detailed in Section 7.4.2, this is due to the increasing slope of the outer skin as it displaces inward slightly forward of the deep web. The outer skin rotation causes the flange of the angle section to move in the aft direction. This happens as plasticity is developing at the intersection of the flange and web of the mainframe. This leaves the frame with little lateral resistance. Model 2 does not exhibit the same response because of the extra lateral strength in the flange due to the strain hardening. The same outer skin rotation effects exist and the onset of plasticity does not change. However, as the material yields it still has a small amount of stiffness and consequently some lateral resistance. Therefore, this material resists this displacement in the negative x direction.

The SYY stress at the center bay of models 1 and 2 is shown in Figure 8.4. At the maximum load (approximately 125% of F_{max}) no significant differences are found between the stress levels and stress distribution of both models.

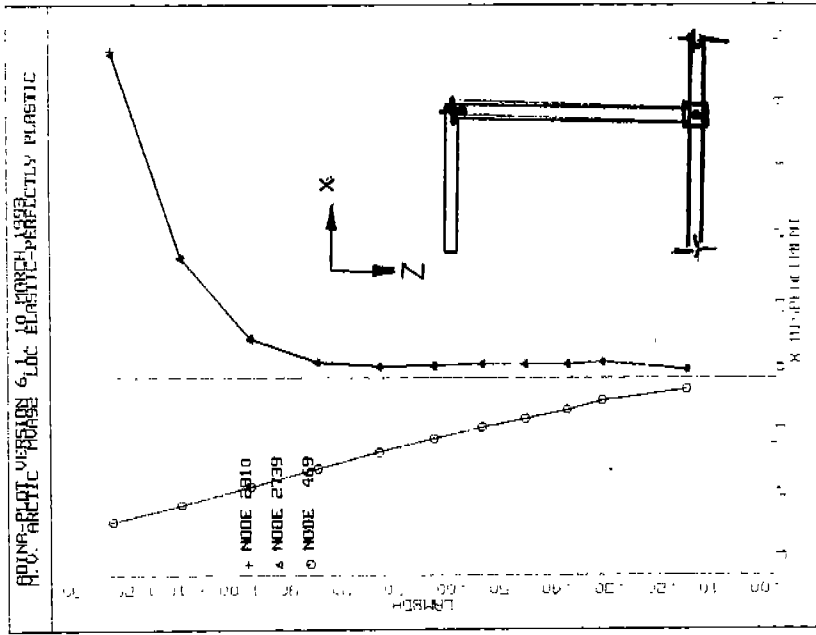
ADINA-PLOT VERSION 4.0.3, 18 SEPTEMBER 1992
M.V. ARCTIC MVA06 LDC ELASTIC-PERFECTLY PLASTIC

ADINA DEFORMED XMIN -6022.
LOAD STEP XMAX 5849.
TIME 11.001.30 YMIN 152.9
YMAX 339.1

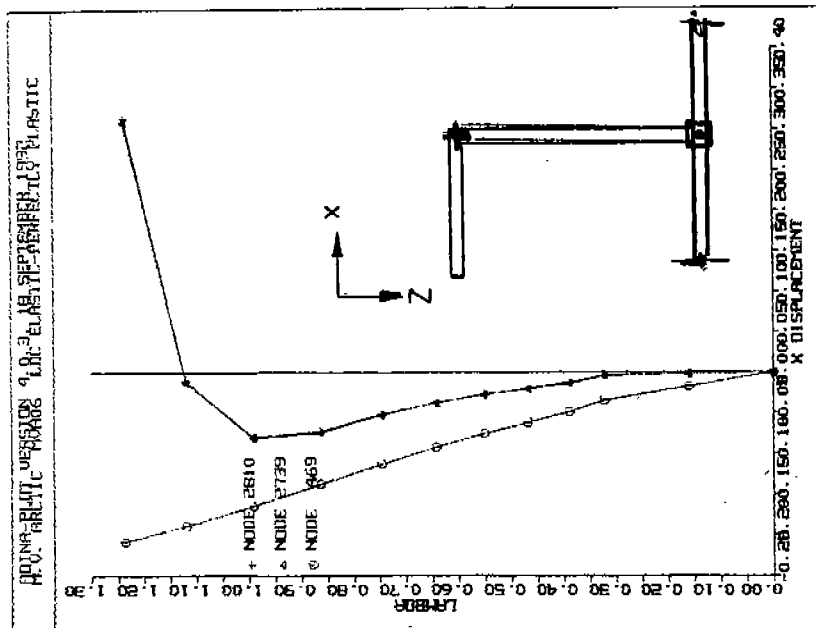


M.V. ARCTIC - WITHOUT INNER SKIN

FIGURE 8.2: Redesigned ASPPR FE Model of the Midbody Panel Using ANGLE Stiffeners



(a) Without Strain Hardening



(b) With Strain Hardening

FIGURE 8.3: X Displacement vs. Applied Load Curves
 - Nonlinear Analysis of ASPPR Redesigned Angle Section With and Without Strain Hardening

8.2 Flat Bar Model Using MAESTRO Boundary Conditions

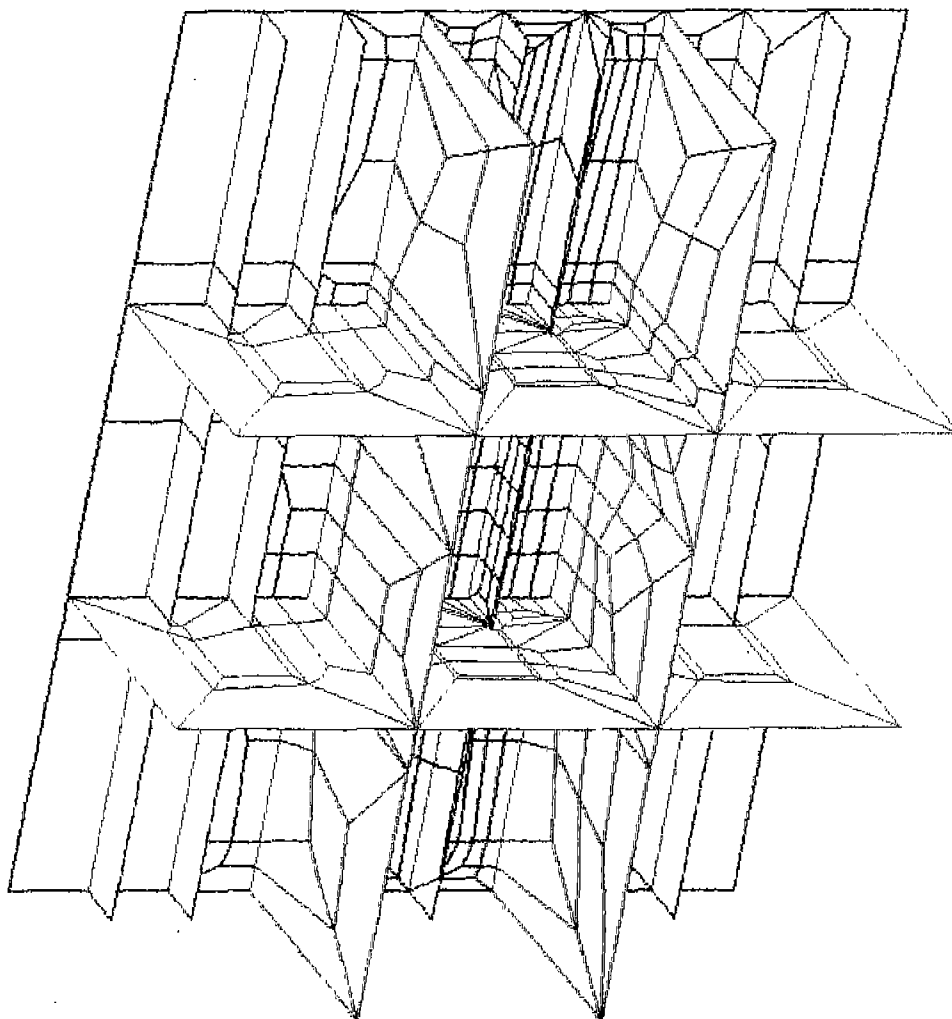
The overall FE model of the M.V. Arctic midbody panel with the mainframes modelled as flat bars is shown in Figure 8.5. The results for the analysis without strain hardening are taken from Section 5.4.5. The load versus x displacement curves for the nonlinear analyses with and without strain hardening are shown in Figure 8.6. The curves for the y and z displacements show insignificant differences and therefore are not presented. For comparison purposes the model without strain hardening is designated as model #1. The model with strain hardening is designated as model #2.

Throughout the load range up to approximately 150% of F_{max} , the lateral displacements of both curves are approximately the same. Above that point the difference in the curves is due to the increased stability of the model 2 structure from the non-zero strain hardening modulus. In the model 1 analysis (see Section 5.4.5), the stringer became very unstable at approximately 168% of F_{max} , and the solution algorithm established equilibrium through unloading. In model 2, the strain hardening modulus provides some stiffness following yielding. Therefore, the solution algorithm is able to establish equilibrium through continued increases in load. However, the analysis is stopped at time step 16 since there is virtually no difference between the two models up to a load of approximately 160% of F_{max} .

The overall SYY stress of models 1 and 2 at time step 15 (160% of F_{max}) are shown in Figure 8.7. This is close to the maximum load. There are notable differences in the stresses. The extra stiffness from the strain hardening modulus in model 2 results in a slower transition from bending stresses to membrane stresses in the outer skin. This is evident in the higher compressive stresses in the outer skin of model 2. However, since model 2 now has some stiffness past the yield point, the stresses in the flat bar mainframes are allowed to increase above the yield stress. This is evident in the band of stress defined by the colour black at the extreme fibre of the maximum loaded mainframe. The stress levels at the corresponding location in model 1 are at the yield point.

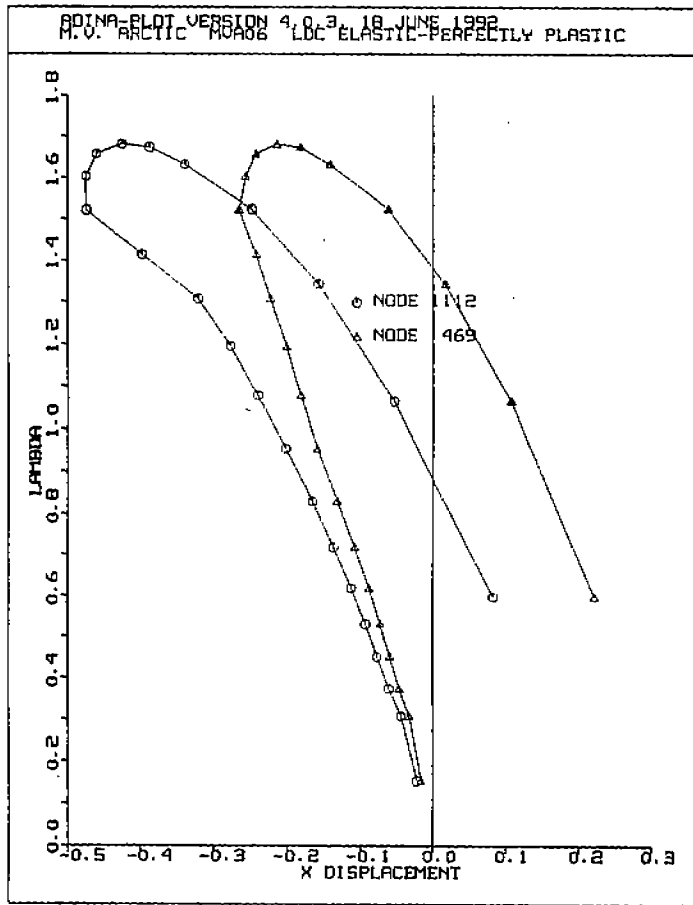
ADINA-PLOT VERSION 4.0.3 8 JUNE 1992
M.V. ARCTIC MVA07 LDC ELASTIC-PERFECTLY PLASTIC

ADINA DEFORMED XUMIN 6023.
LOAD_STEP XUMAX 5851.
TIME 21.00126 YUMIN 149.4
YUMAX 336.1

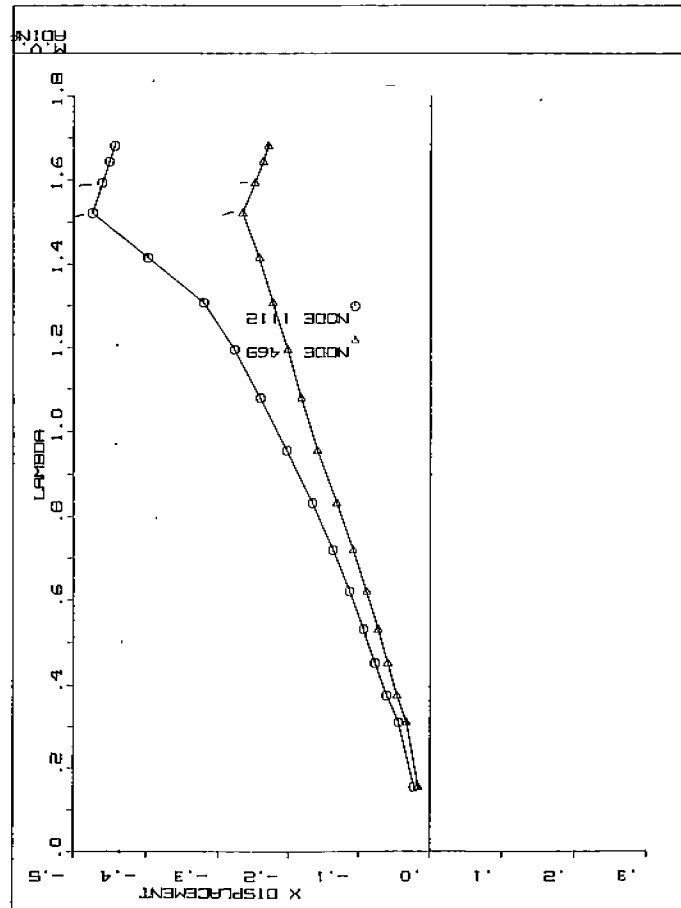


M.V. ARCTIC - WITHOUT INNER SKIN

FIGURE 8.5: FE Model of Redesigned Midbody Structure with Flat Bars



(a) Without Strain Hardening



(b) With Strain Hardening

FIGURE 8.6: X Displacement vs. Applied Load Curve
- Nonlinear Analysis of ASPPR Redesigned Flat Bar Section With and Without Strain Hardening

213

8.3 Summary and Conclusions

The strain hardening modulus has a visible effect on the stresses in the flat bar model and a much less visible effect on the stresses in the angle model. This is due to the fact that the angle model still has some unyielded material in the outer flange. This unyielded material can take additional load. In the flat bar model, all of the material at the outer fibre has yielded. Therefore, an additional load can only be carried through the strain hardening of the flat bar. This strain hardening allows the stresses to increase.

The buckling response (of both models) is not significantly affected by using a strain hardening modulus. In the angle section model buckling occurs as a result of the development of an eccentric ribbon of unyielded material in the flange of the mainframe (see Section 5.3.4). The development of this eccentric section of unyielded material occurs regardless of the use of a strain hardening modulus. Therefore buckling occurs at approximately the same load level for the angle frame model with and without strain hardening. In the flat bar model, failure occurs due to an instability in the stringer following extensive yielding. The use of a strain hardening modulus does not significantly increase the strength of the structure following this yielding. Therefore it does not prevent the instability from occurring at the stringer. It does, however, provide a sufficient increase in strength to enable the solution algorithm to establish equilibrium through increasing loads.

9. STUDY OF BUCKLING SENSITIVITY TO BOUNDARY CONDITIONS AT THE MIDBODY

The nonlinear analyses performed on the M.V. Arctic midbody FE models thus far have all included the global response of the ship. This global response was determined through an analysis of the whole ship using the program MAESTRO and was included in the midbody FE models by applying displacements determined from MAESTRO along the outer boundaries of the FE models.

The overall effect of using the MAESTRO boundary conditions is that it creates overall longitudinal (x) and vertical (y) in-plane compressive stresses of approximately 10,000 psi in the rigid body FE models. To determine the effect of these compressive stresses on the stability of the structure, the sensitivity of the results to alternative boundary conditions is explored.

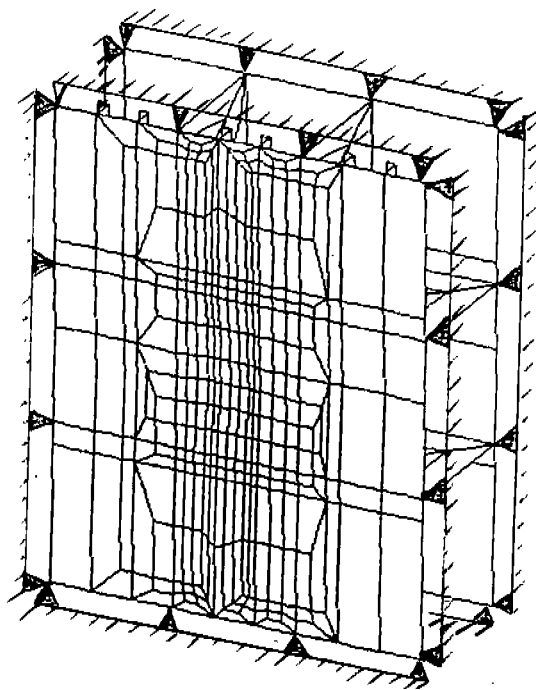
This involves applying various types of boundary conditions, other than the MAESTRO conditions, to the overall (i.e. 3x3 bay) FE model of the M.V. Arctic midbody region. A very localized FE model consisting of the midpanel region (i.e. 1 bay) of the midbody FE model is also created and analyzed to determine the buckling response sensitivity to boundary conditions.

The M.V. Arctic FE model used for this study utilizes mainframes modelled as angle sections. These sections have proven to be the most unstable. Therefore, the differences in stability from using various boundary conditions is expected to be more discernable using the relatively unstable angle model.

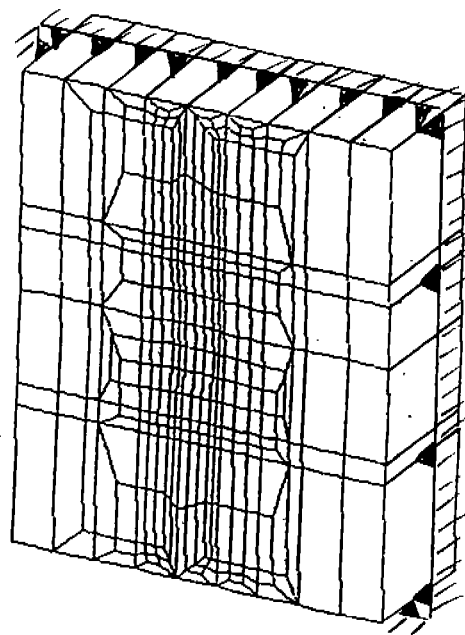
A strain hardening modulus has been included in all of the analyses performed in the boundary condition study.

9.1 Overall Midbody FE Model Boundary Condition Study

The first set of boundary conditions studied involved completely fixing all nodal translations on the outer boundaries of the midbody FE model (i.e. 3x3 bay model) created with angle stiffeners. This boundary condition is shown in the sketch of the midbody FE model plotted in Figure 9.1(a).



(a) Fixed Boundary Conditions



(b) Pinned Boundary Conditions

FIGURE 9.1: Boundary Conditions Used in Sensitivity Study of Midbody FE Model With Angle Stiffeners

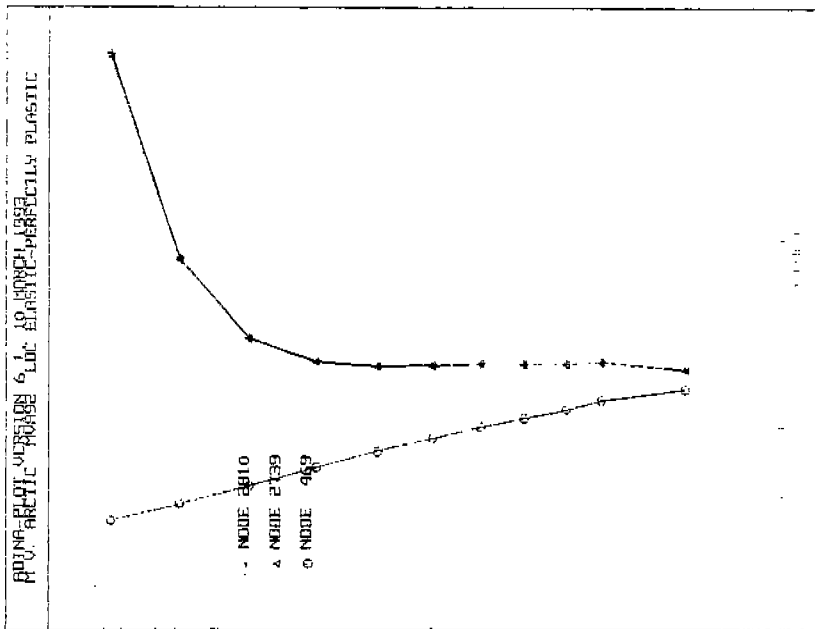
(Note: The shaded triangles showing pinned boundary conditions are for illustration purposes and are not located at all nodes where translations are fixed.)

The resulting load displacement curve for the x component at three nodes along the midspan section of the maximum loaded mainframe is shown in Figure 9.2(b). The load displacement curve for the angle model with MAESTRO boundary conditions is shown in Figure 9.2(a). A similar type of response occurs in both models. The frames start to move laterally at about F_{max} and fail due to tripping. However, the magnitudes of the frame lateral displacements and the load at failure are different.

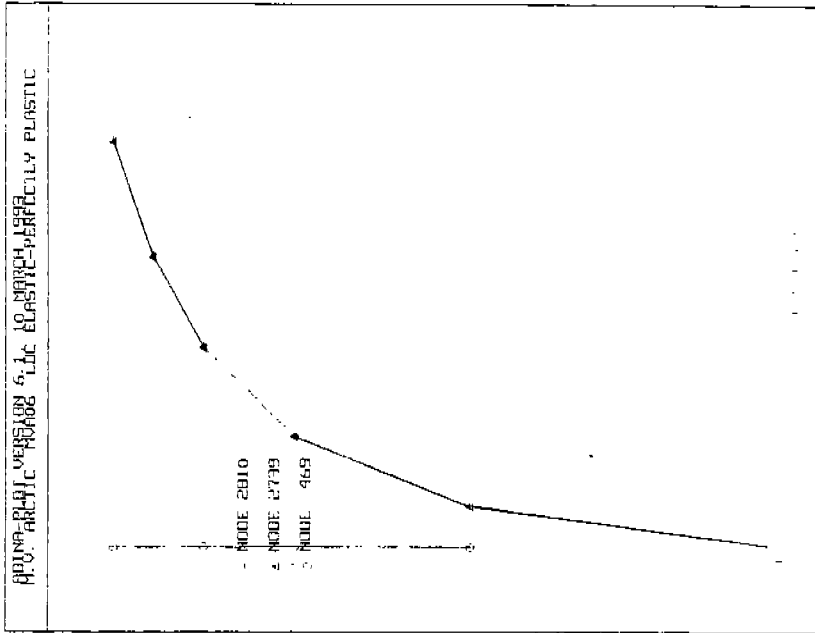
The SYY stresses at the center bay of both models (MAESTRO and fixed boundary conditions) at load levels near and above F_{max} are shown in Figure 9.3. The distribution of stress is very similar in both models. However, the stress levels are quite different. The stresses in the model with fixed boundary conditions are between 10 ksi and 20 ksi less than the stress levels for the model with MAESTRO boundary conditions. This is attributed mostly to the absence of the in-plane compressive stresses resulting from the MAESTRO prescribed displacements.

The final plot from this analysis is a deformed cross-sectional plot of the mainframe at the same elevation (i.e. y coordinates) as the nodes used for the curves of Figure 9.2. Note that this figure is not a graph but is a plot of the actual frame cross-sections at a snapshot in time/loading. The deformed cross-sections for loads of 1.18 and 163% of F_{max} are shown in Figures 9.4(a) and 9.4(b), respectively. A magnification factor of 20 is used to enhance the displaced shapes. This plot shows that the instability appears to be taking the form of buckling. These plots are not available for the corresponding analysis with MAESTRO boundary conditions.

The second set of boundary conditions that were studied for the model is shown in Figure 9.1(b). These constraints approximate pinned boundary conditions and are created by fixing the translations of all boundary nodes along an x-y plane midway through the depth (z) of the model. Because the constraints are at mid-depth two extra stringers (extreme top and bottom) and two extra deep webs (extreme forward and aft) are included in the model. This provides the structural



(a) MAESTRO Boundary Conditions

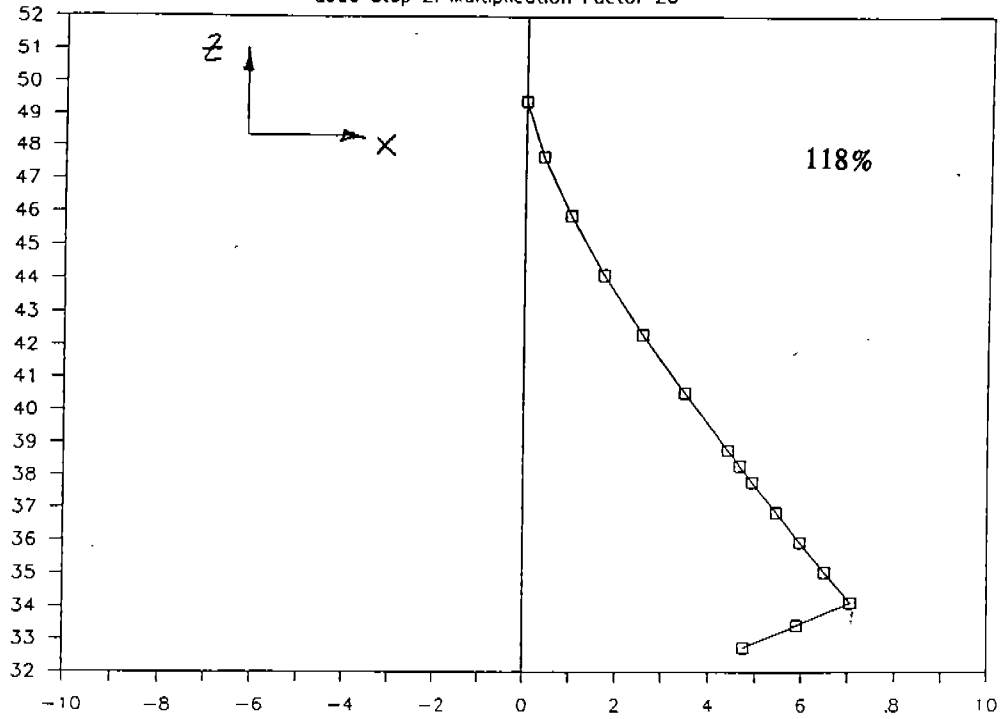


(b) FIXED Boundary Conditions

FIGURE 9.2: X Displacement vs. Load Curves
 - Nonlinear Analysis of ASPPR Redesigned Midbody Model
 Comparing Angle Sections With MAESTRO and Fixed Boundary Conditions

MVA12: Rigid Boundary / Frame 2

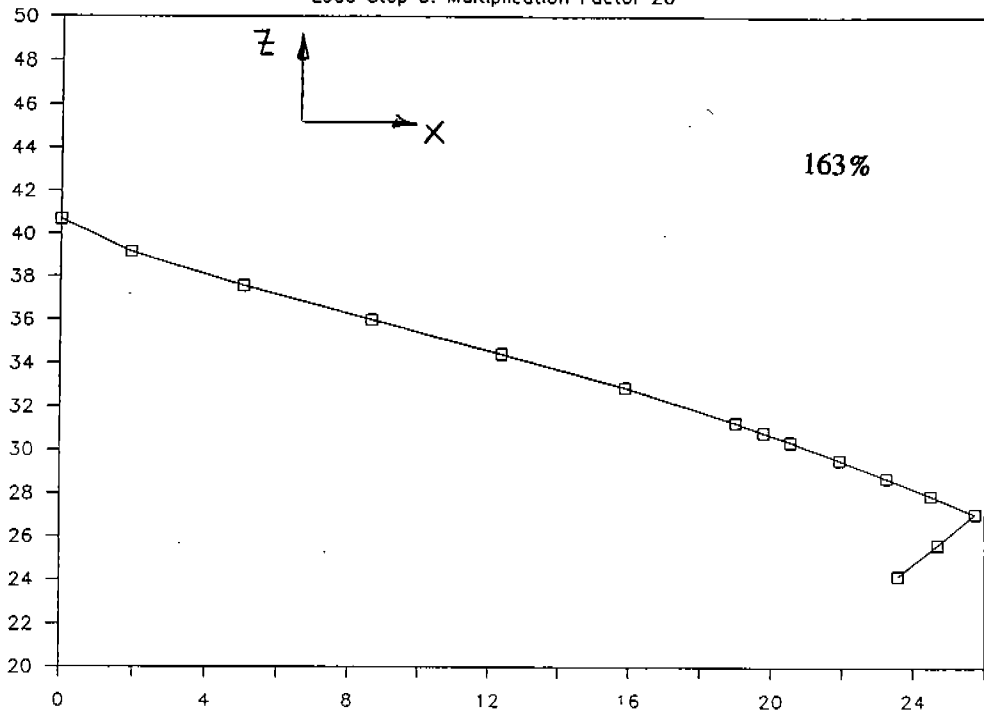
Load Step 2: Multiplication Factor 20



(a)

MVA12: Rigid Boundary / Frame 2

Load Step 5: Multiplication Factor 20



(b)

FIGURE 9.4: Angle Section Deformed Shape
 - Nonlinear Analysis of ASPPR Redesigned Model With Fixed Boundary Conditions
 9-6

connection of the outer and inner skins at the model boundaries. (Note: Because the top-stringer elements are plotted, the elements representing the mainframes are not visible in Figure 9.1(b).)

A displaced shape plot of the same cross-section as shown in Figure 9.4 for fixed boundary conditions is shown in Figure 9.5 for pinned boundary conditions. The deformed shapes for loads of 1.18 and 153% of F_{max} are shown in Figures 9.5(a) and 9.5(b), respectively. A magnification factor of 20 is used to enhance the deformed cross-sections.

The type of instability appears again to be taking the form of buckling. The shape of the deformed cross-section is very similar to that of the previous analysis. At 118% of F_{max} the displacement of both models is approximately 0.35 inches. At the maximum loads (which are slightly different), the lateral displacements are in the range of 1.0 inch.

9.1.1 Summary of Overall Model Boundary Condition Study

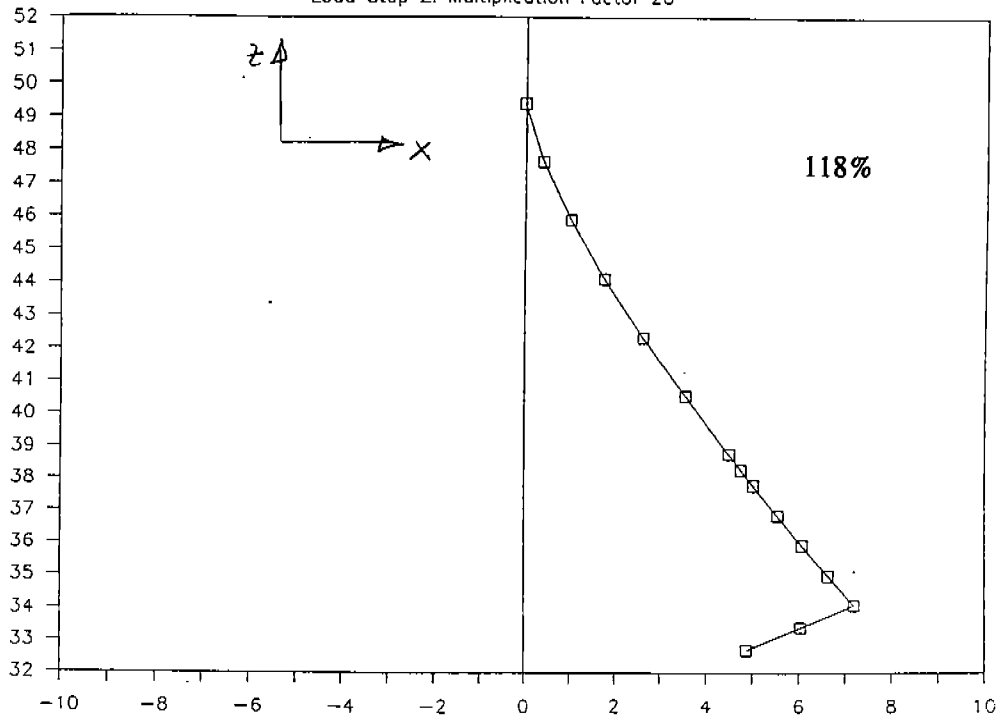
There was no significant difference in the response using the overall model with either fixed or pinned boundary conditions. However, the response using these two boundary conditions differs significantly from the response using MAESTRO boundary conditions. Therefore it is concluded that the overall ship response is important in determining the response and stability of the midbody FE model. Also, because there is no difference between the fixed and pinned conditions, it is concluded that the stability of the mainframe is a local response. The large webs and stringers create a sufficiently rigid boundary condition around the center bay to prevent the boundary conditions along the outer boundaries of the model from significantly affecting the frame response in the center bay.

Based upon this conclusion, the investigation into the effects of boundary conditions was modified. Since the response is local to the center bay, regardless of the outer boundary conditions, a series of analyses was carried out on a model of the center bay.

The results of this part of the investigation are presented in the following section.

MVA12: Pinned Boundary /Cross Section 2

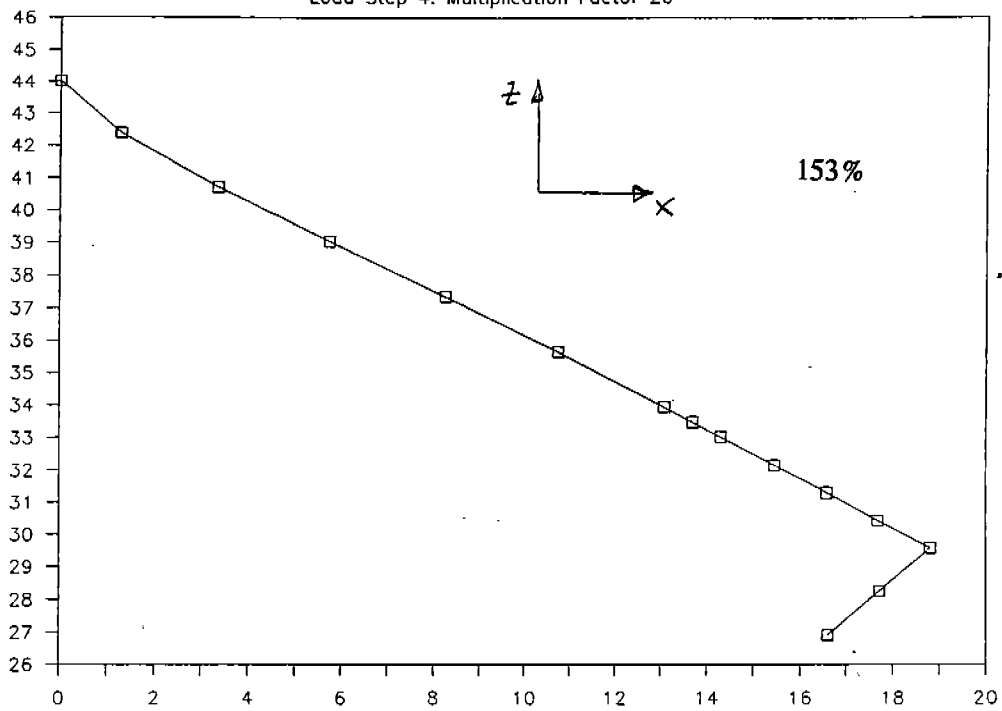
Load Step 2: Multiplication Factor 20



(a)

MVA12: Pinned Boundary /Cross Section 2

Load Step 4: Multiplication Factor 20



(b)

FIGURE 9.5: Angle Section Deformed Shape
 - Nonlinear Analysis of ASPPR Redesigned Model With Pinned Boundary Conditions
 9-8

9.2 Center Bay Model Boundary Condition Study

The FE model of the center bay is a subset of the midbody FE model including only the center bay geometry. The model is shown in Figure 9.6. The model consists of the outer skin and mainframe elements bounded by the center bay deep webs and stringers. The ice pressure load that is applied to the center bay section of the midbody model FE is also applied to the center bay FE model.

The first analysis of the center bay FE model involved fixing the translations and rotations of the outerskin nodes at the top and bottom stringer locations and the forward and aft deep web locations. These boundary conditions are illustrated in the sketch provided in Figure 9.7(a). A plot of the applied load (as automatically determined by ADINA) at each time step is shown in Figure 9.8.

The structure carries increasing loads up to and seemingly past 241% of F_{max} . This increase in load carrying capability is due to the excessive boundary conditions. With the edges completely fixed, the structure eventually supports the load in membrane. Since a strain hardening modulus is used, the model can continue to carry an increasing load after yielding.

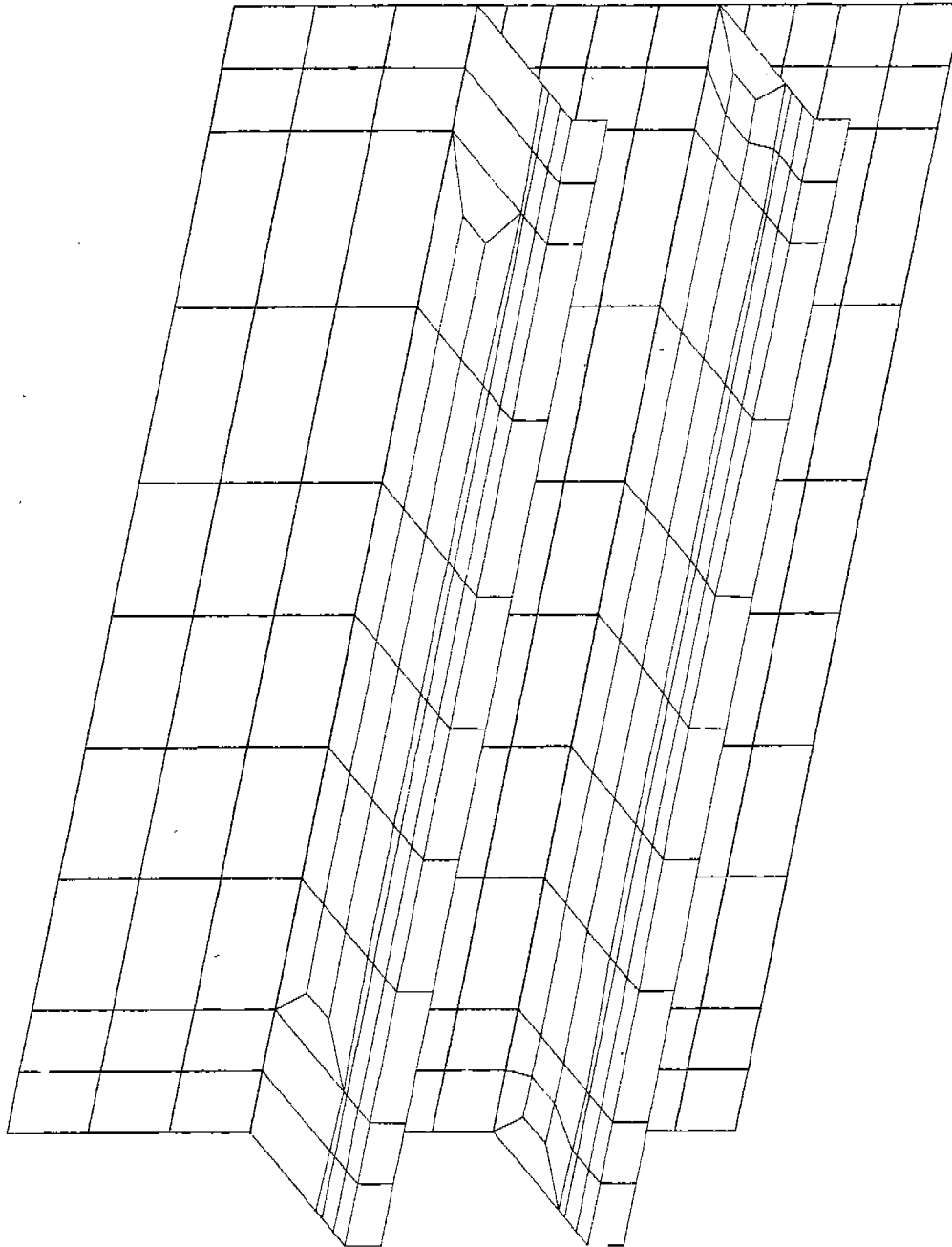
The structure does not appear to become unstable since the load continues to increase throughout the analysis. However, as presented below, an instability does become evident. At a load of 245% of F_{max} the analysis was terminated. Above this point no reasonable results can be predicted.

Plots of the SYY stresses at loads of 118.2% of F_{max} and 133.9% of F_{max} are shown in Figure 9.9. The maximum stresses are very local and are concentrated at the outer fibre of the mainframes. The stress in the mainframe with the maximum applied ice load is much higher than the stresses in the adjacent frame. This is due to the boundary conditions. With total fixity where the frames intersect with the stringers, very little load is transferred from one frame to the other.

The displaced shape of the midspan cross-section of the mainframe under the peak ice load at various load levels is provided in Figure 9.10(a). The development of "buckling" is evident. The overall displaced shape of the two mainframes at 241% of F_{max} is shown in Figure 9.10(b).

ADINA-PLOT VERSION 6.1, 9 JULY 1993
M.V. ARCTIC LDC FIXED BOUNDARY CONDITIONS COMBINED LOAD

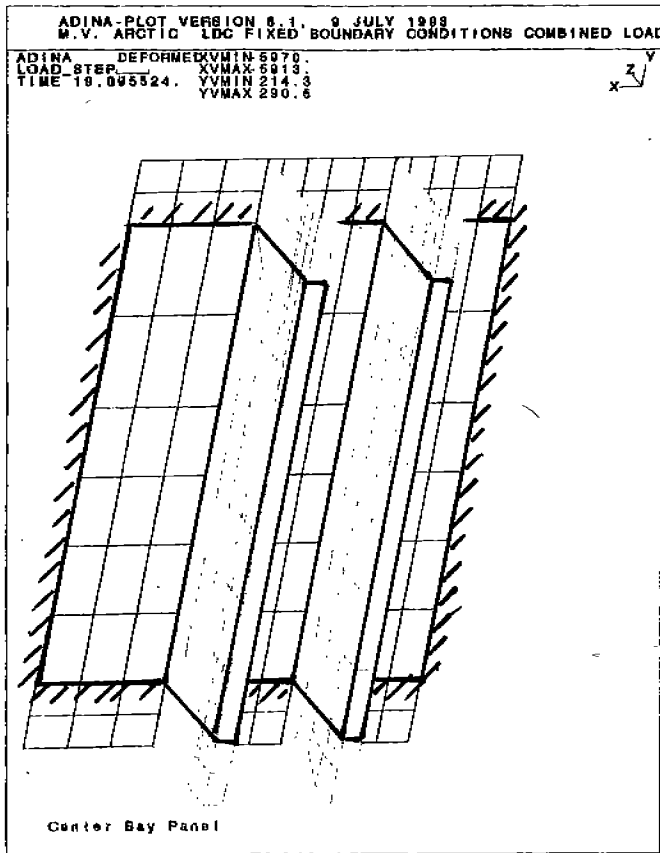
ADINA DEFORMEDXVMIN-5970.
LOAD_STEP_____XVMAX-5913.
TIME 19.005524. YVMIN 214.3
YVMAX 290.5



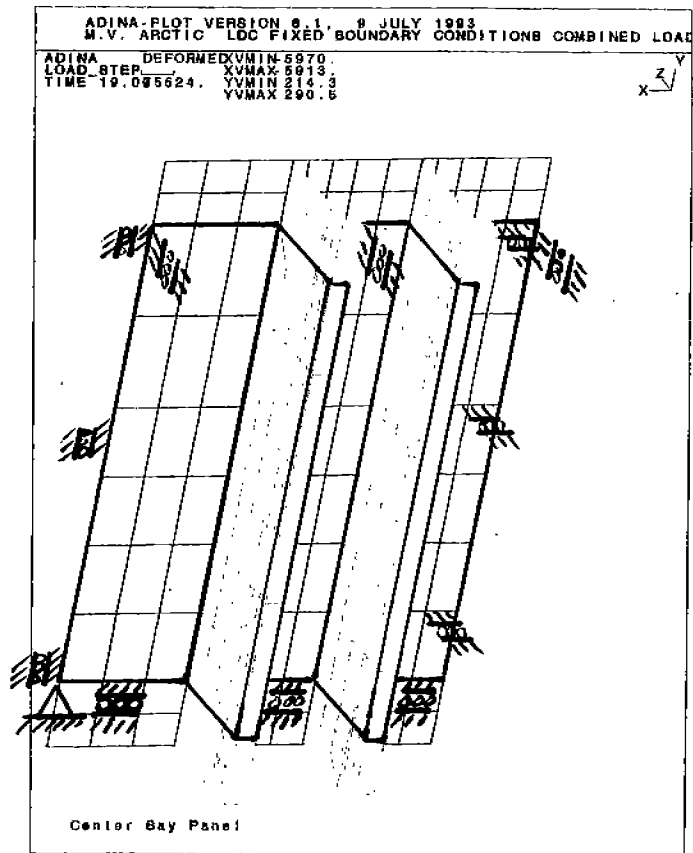
Center Bay Panel

FIGURE 9.6: FE Model of Center Bay Section of Midbody Model
Using the Redesigned ASPPR Angle Section
9-10

9-11



(a) Completely Fixed Boundary Conditions



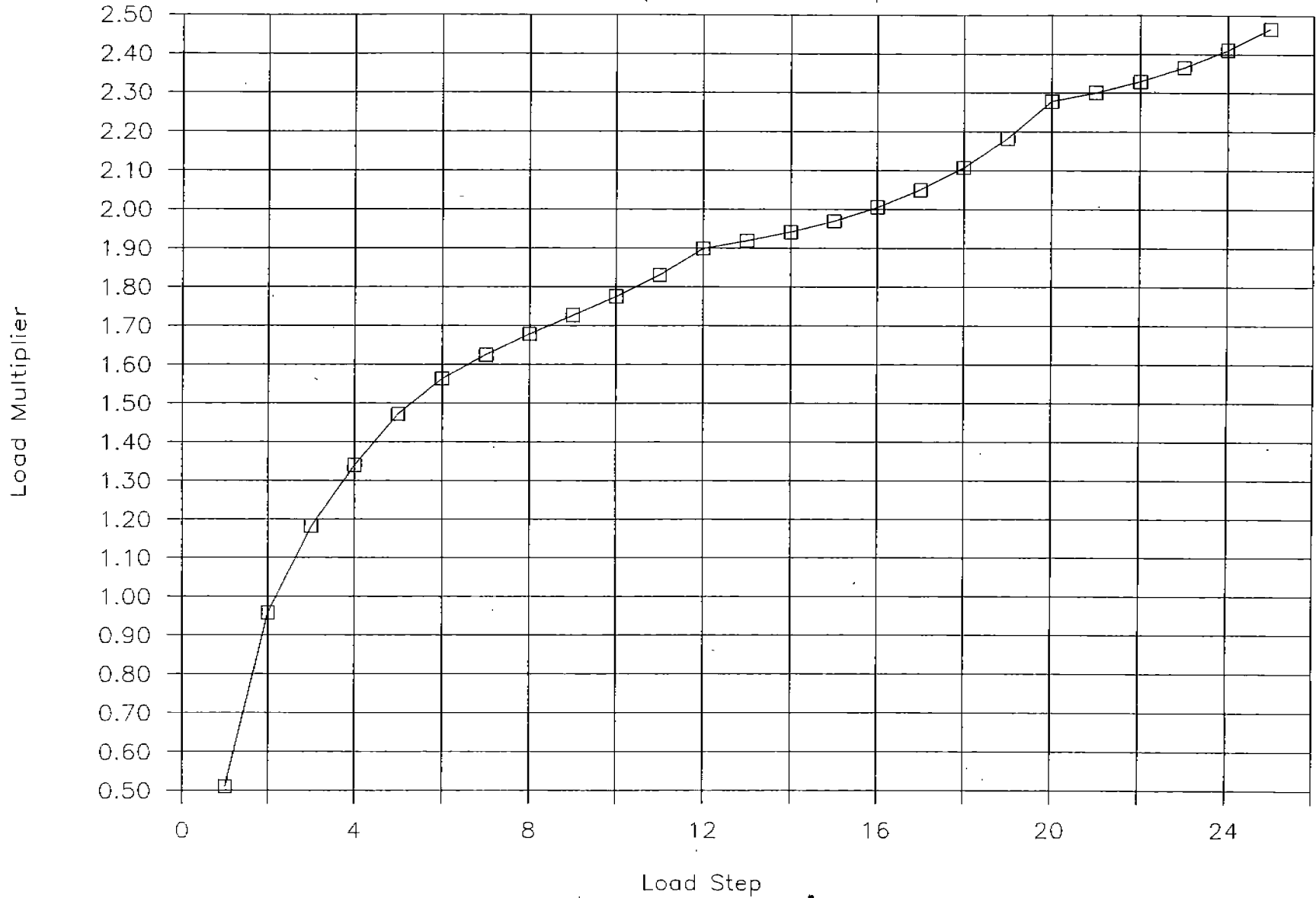
(b) Fixed Rotations Boundary Conditions

FIGURE 9.7: Boundary Conditions Used in the Sensitivity Study of the Midbody Center Bay FE Model

227

Mid Panel Model: Fixed Boundaries

Load Multiplier vs Load Step

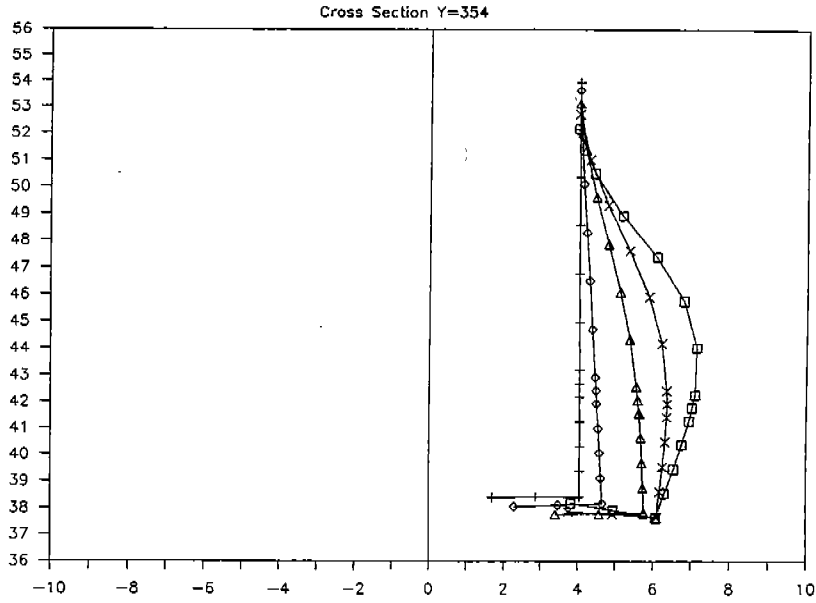


**FIGURE 9.8: Applied Load at Each Time Step
- Nonlinear Analysis of Center Bay FE Model**

9-12

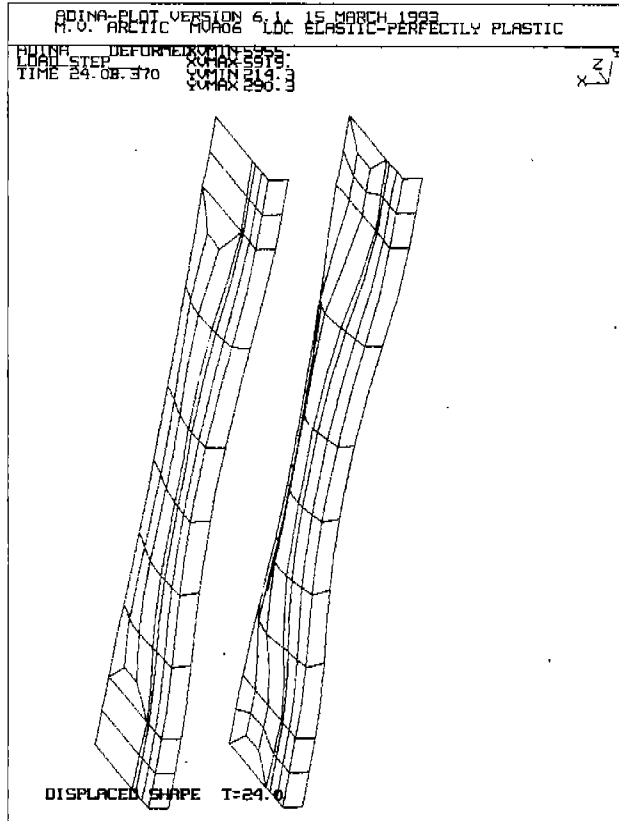
228

Mid-Panel Model: Rigidly Fixed Edges



+ = $0.51 * F_{max}$ ◇ = $1.57 * F_{max}$ △ = $1.83 * F_{max}$ X = $2.00 * F_{max}$ □ = $2.41 * F_{max}$

(a) Cross-Section Displaced Shape Plot



(b) Overall Main Frame Displaced Shape at $2.41 * F_{max}$

FIGURE 9.10: Main Frame Displaced Shape Plots
- Nonlinear Analysis of Center Bay FE Model

The second boundary condition scenario in the analysis of the center bay FE model involved changing the four edges from a completely fixed condition to a fixed rotation condition. Two adjacent edges are free to translate in-plane. This boundary condition scenario is shown in Figure 9.7(b). In-plane compressive loads that produce 10,000 psi stresses in both directions are applied to the edges that are free to translate. The lateral ice load is the same as in the previous analysis.

A plot of the applied load at each time step is shown in Figure 9.11. With an in-plane load and freely translating edges, the structure is capable of carrying load up to 160% of F_{max} . However, above this load the increase in load carrying capacity is very small and the structure seems to become unstable. This instability is demonstrated in the curve shown in Figure 9.12. Above F_{max} , the lateral displacement of the nodes (2739 and 2810) at the midspan cross-section of the maximum loaded mainframe increases substantially. This indicates the presence of buckling.

A plot of the displaced shape of the midspan frame cross-section at various load levels from the analysis with pinned boundary conditions and in-plane loads is provided in Figure 9.13. The development of buckling is evident. The direction and shape of the buckling is very similar to the buckling from the results of the midbody FE model fixed and pinned boundary condition analyses (see Figure 9.4 and 9.5). However, it is quite different from the type of buckling predicted from the center bay model with fixed boundary conditions (see Figure 9.10(a)).

A linear eigenvalue buckling analysis was also performed on this model. The first buckling mode is shown in Figure 9.14. The critical buckling load is 280% of F_{max} . (Note: the plot shows a load factor of 27.8, however the applied load was 10% of F_{max} . Therefore, the buckling load is $.1 * \text{Load Factor} * F_{max}$.) The shape of the buckled mainframe is very similar to that predicted from the nonlinear analysis (see Figure 9.13). The linear buckling load is very high since the stiffness is based upon the initial geometry of the structure with no yielded material. In actual fact, the geometry changes and the stiffness degrades due to plasticity as the load increases. Therefore, the actual buckling load will be much lower, as the nonlinear analyses predict.

Mid-Panel Model: Combined Loads

NO IMPERFECTIONS

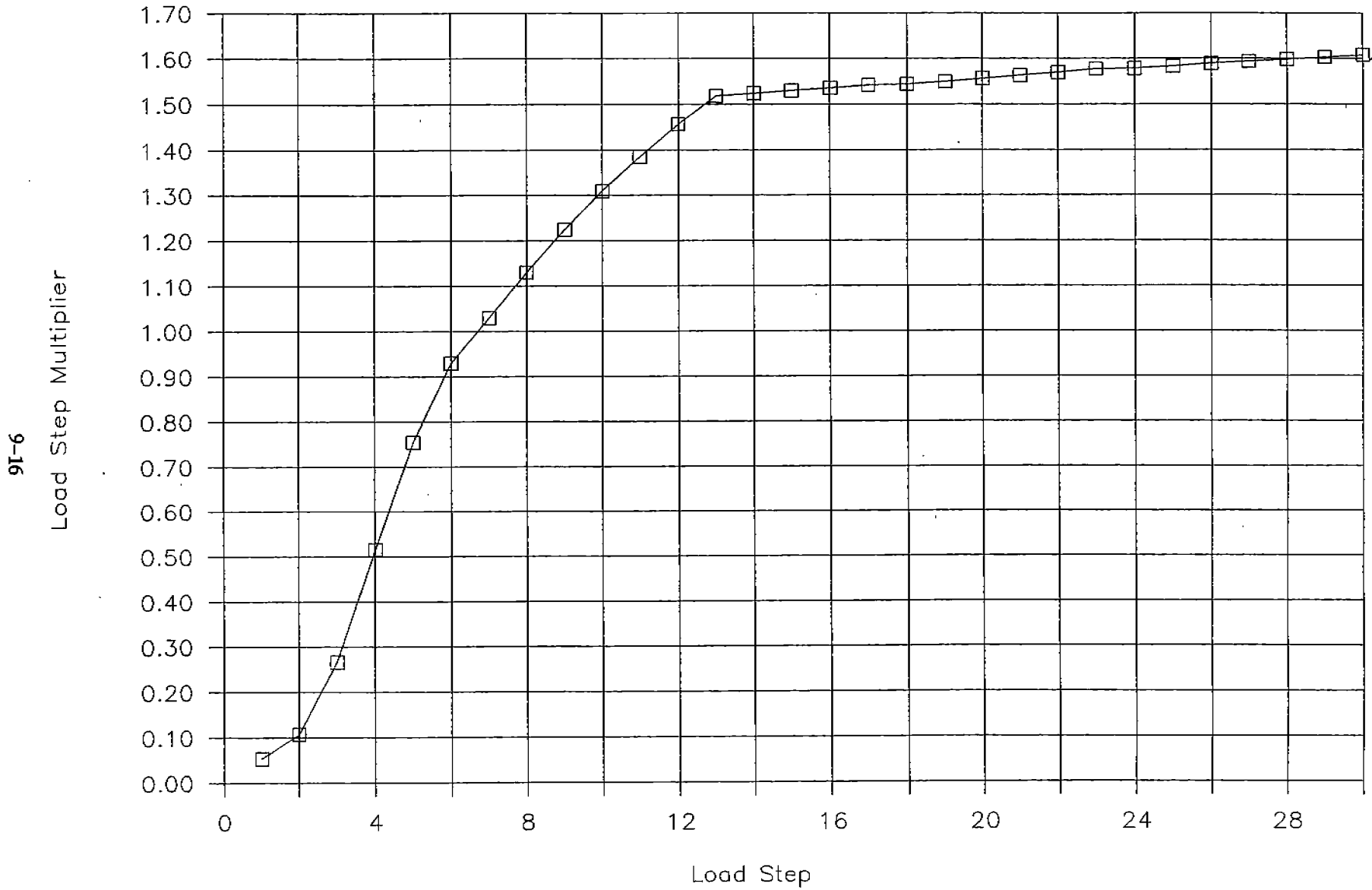


FIGURE 9.11: Applied Load at Each Time Step
- Nonlinear Analysis of Center Bay FE Model With an In-Plane Load

232

Mid Panel Model: Comb Load: No Imperf

Lambda vs X Displacement

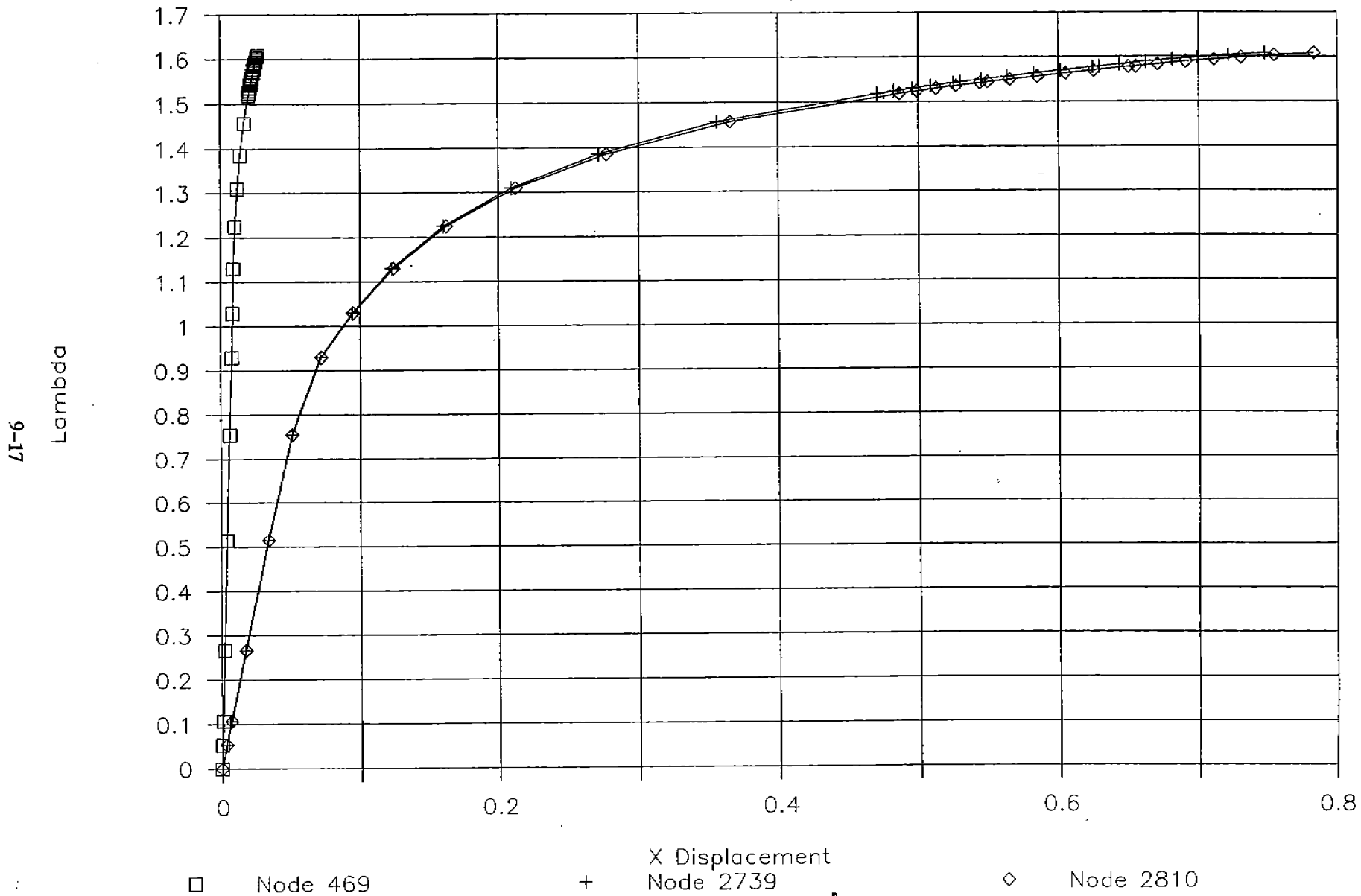


FIGURE 9.12: X Displacement vs. Load at the Midspan of the Main Frame - Nonlinear Analysis of Center Bay FE Model With an In-Plane Load

233

Mid Panel Model: Comb Loads: No Imperf

Comparison of Frame Cross Sections (10)

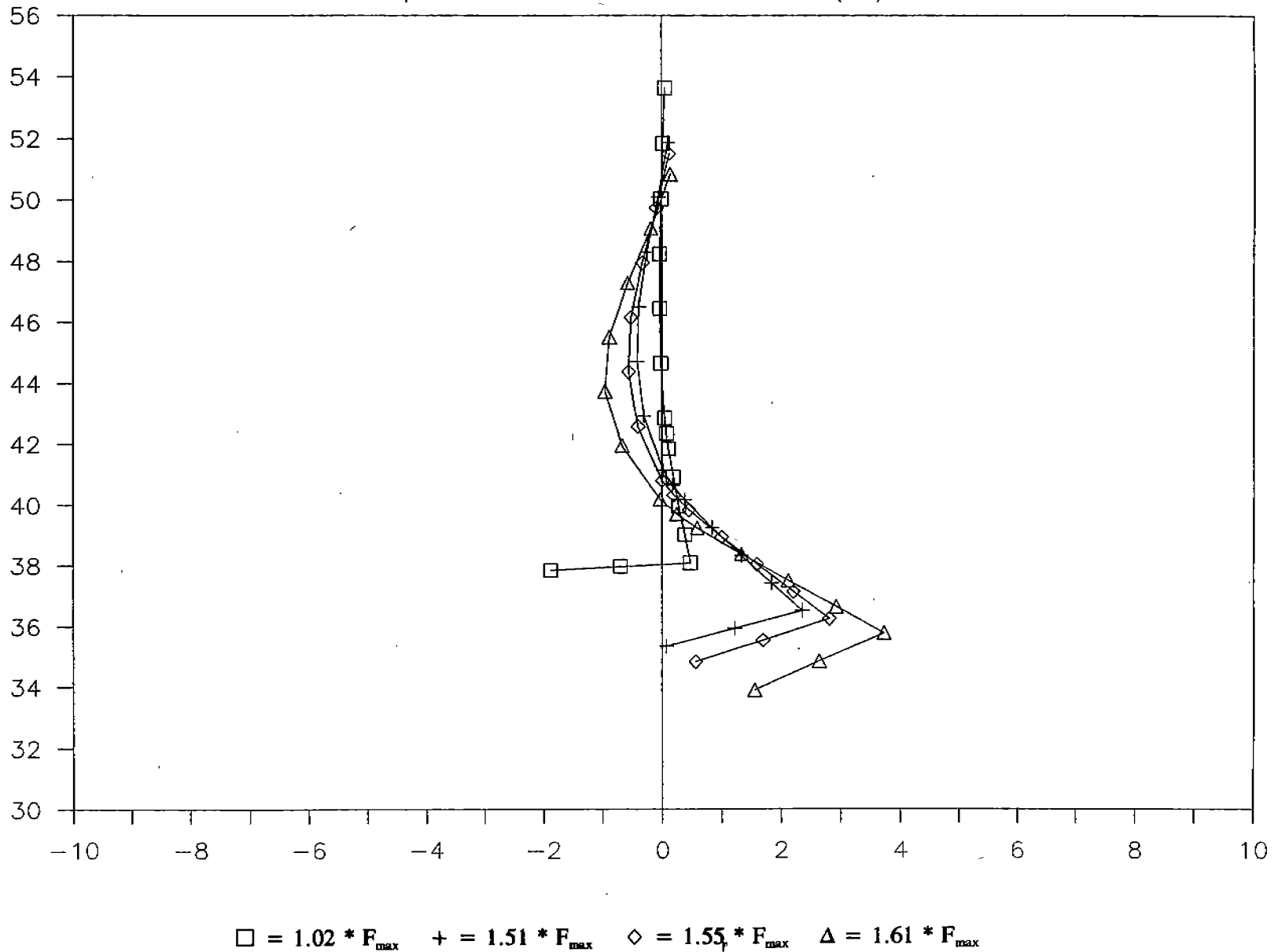
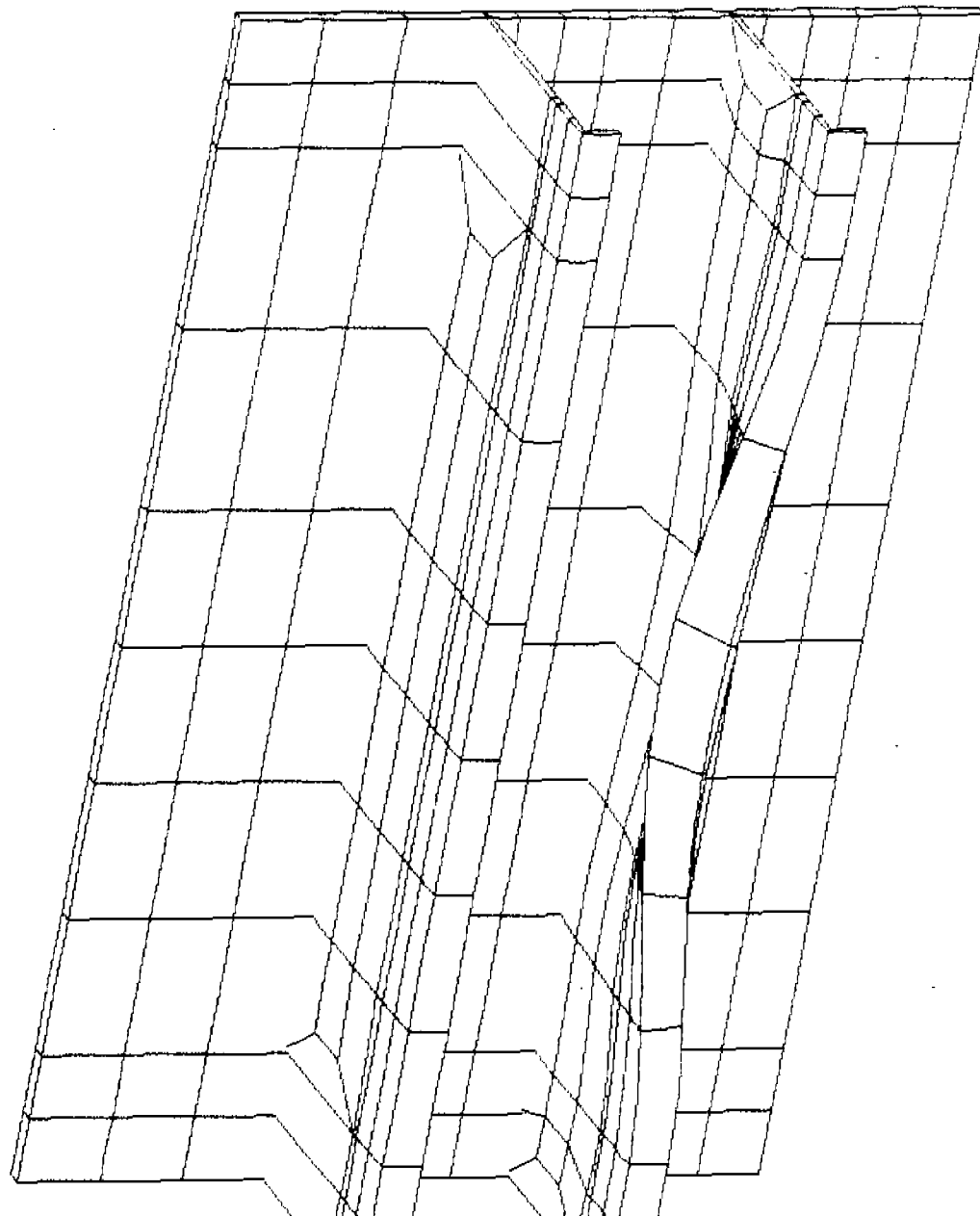
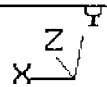


FIGURE 9.13: Main Frame Displaced Shape Plots
 - Nonlinear Analysis of Center Bay FE Model With an In-Plane Load

634

ADINA-PLOT VERSION 6.1, 18 MARCH 1993
Mid/Panel Model With Applied IN-PLANE Loading

ADINA MODE SHAPE MODESHAP 5974.
MODE 1 XUMAX 5911.
LOAD FAC = 27.79 YUMIN 211.5
YMAX 291.0



9.2.1 Summary of Center Bay Model Boundary Condition Study

In-plane compressive loads combined with lateral ice loads produce dramatically different results in the center bay model from the results of an initial model with only the lateral ice load and fixed or pinned boundary conditions. The absence of the in-plane load changes the direction and nature of the buckling response. The boundary conditions are different in the two models in that the model with in-plane loading permits "free" translation of the edges.

The significant conclusion from this brief study is that the accuracy of the results is not influenced much by the local stiffness of the model outside of the center bay. This is evident from the similarity in results of fixed vs. pinned boundaries. However, the local buckling response of the mainframes is critically influenced by the global ship load contribution to the local model. The overall ship response to the applied ice load results is a 10,000 psi (approximate) biaxial compressive stress being set up in the 3x3 bay region of the overall ship model. The boundary condition study shows that this compressive load must somehow be included in the local 3x3 bay model. More significantly, it shows that it doesn't really matter how this effect is included in the model, as long as the bi-axial stress is applied to the region of interest. This is confirmed by the fact that similar results are obtained either by using the 1 bay model with in-plane loads or by using the 9 bay model (i.e. 3x3 bay model) with explicitly defined MAESTRO boundary conditions along all external model boundaries. This is extremely significant since the 1 bay model is much smaller than the 3x3 bay model. Use of the smaller model allows many more runs to be performed in the same time required to run the 3x3 bay model.

To summarize, the in-plane stresses are critical in determining the nonlinear buckling response of the simplified model of the M.V. Arctic midbody. Reasonable results can be obtained if the in-plane stresses are correctly incorporated into the simplified model.

9.3 Summary of Boundary Condition Study

The post-yield buckling response of the mainframes of the M.V. Arctic is a local response which is greatly affected by the global loading contribution of the overall ship response. This response

does not seem to significantly depend upon the boundary conditions of the structure outside the deep webs and stringers that immediately bound the local bay in which the mainframes are located.

The in-plane compressive stresses resulting from the overall ship response are transmitted through the structure outside of the local bay, and greatly affect the post-yield buckling response. Therefore, including the effects of the global ship response is extremely important.

In the bulk of the work undertaken in this project, the in-plane compressive stresses from the global ships response were included through prescribed displacements from an independent analysis of the ship using MAESTRO. However, if these in-plane stresses are fairly constant, they may be determined through simpler methods. They can then be applied to the model as in-plane forces.

9-22

238

10. EVALUATION OF THE EFFECT OF IMPERFECTIONS ON THE MODEL

Imperfections have an effect on the buckling strength of structures. All real structures have some imperfections and these can be in the form of residual stresses or displacement distortions. In ship structures, imperfections are often caused by welding, fabrication and in-service loads. Depending on the response of interest, "imperfections" can also be asymmetries in geometry or loading which cause a response to be nonsymmetric.

In analyzing a structure using the finite element method with a nonlinear solver, some imperfection in the geometry or loading is necessary in order to initiate buckling. That is, if a perfect column were loaded with a compressive load, the column could be loaded indefinitely without seeing any stability problems (i.e. it would not buckle). If the same column were modelled with an imperfection, then a buckling analysis of the column would predict failure at a load level roughly equal to the Euler Buckling load if the response is elastic and the imperfection is small.

The ship hull which we are studying in this project is a stiffened panel structure which consists of a grid formed by transverse deep webs and longitudinal stringers. Between adjacent deep webs are located transverse mainframes. The ice load which we are modelling is applied over a longitudinal distance which spans several deep webs; however, it has a peak load which is concentrated over one of the mainframes. If we consider the response within one bay (bounded by two stringers and two deep webs), the loading is concentrated on one frame and hence the response will be asymmetric with respect to the centerline of the bay. This in itself causes an "imperfection" in the loading which will allow buckling to be numerically predicted.

The analyses which were performed prior to this point in the project did not include any geometric imperfection other than the intrinsic geometric and loading asymmetries described in the previous paragraph. These analyses did predict buckling; however, it is of interest to see how the analyses results will be affected by incorporating geometric imperfections into the model. Various imperfections were incorporated into the model either by using an ADINA option to include a geometric imperfection as a function of previous analysis results or by explicitly modifying the

geometry to include an out-of-plane deflection. This section of the report describes the work undertaken in this area.

10.1 Midpanel Model Using Fixed Rotations with In-plane Load

It was decided to start with a reduced model to conduct this study in order to reduce the execution time of ADINA. The conclusions which can be drawn regarding the effects of imperfections on the response of the smaller model will provide us with insight into the problem prior to performing the runs on the larger model. The model which was used for the study is the midpanel model. This model is described in Section 9.3.

The boundary conditions employed with the midpanel model are fixed rotations at the plate boundaries with an in-plane load applied. The purpose of the in-plane load is to include the effects of the global response of the ship in the local analysis.

The applied loading is a pressure loading as used in the previous analyses. As described in Appendix A, the peak load is concentrated on one of the mainframes and is calculated using the ASPPR recommended procedure.

In the following nonlinear analyses, imperfections were incorporated into the geometry using the option within ADINA to import a displaced shape from a separate file. This displaced shape is used to modify the undeflected geometry, prior to application of the load. The imperfection used for the nonlinear analyses is a buckling mode shape determined by performing a linear eigenvalue buckling analysis. Because the eigenvalue buckling analysis is linear, the buckling mode is calculated for the unloaded geometry and reflects how the structure would buckle if its stiffness were unaffected by material yielding. Of course this is not actually the case; however, the purpose of the linear eigenvalue buckling analysis is to incorporate an imperfection into the model, not to accurately predict buckling. The exact nature of the imperfection should not be critical; however, by using the buckling mode shape as the imperfection (as opposed to a central displacement, etc.), the effect of incorporating an imperfection should be maximized. A magnitude must be supplied for the mode shape as the mode shape is normalized with respect to the point having the largest displacement. The magnitudes used

in the following analyses are a function of the mainframe web thickness and are varied from .25 to 1.0 times the web thickness.

A plot of the buckling mode shape that was used to determine the imperfection is shown in Figure 10.1. The plot shows the deflected shape of the mainframes under the buckling load. The linear buckling load for this mode is predicted at 450% of F_{max} . (The load factor shown in the plot is 45.15. However, a load vector multiplier of 0.1 was used in the analysis. Therefore, the load factor in Figure 10.1 must be multiplied by 0.1 to produce the actual factor of 4.5 or 450%.) This mode shape is from a linear eigenvalue analyses which is based upon a linear geometry, which does not include any degradation of stiffness due to yielding. Therefore, the buckling load predicted using linear eigenvalue buckling is much higher than the actual buckling load where the stiffness will be degraded due to plasticity. The first buckling mode was not used because it corresponded to buckling at the upper extreme edge of the outer skin. This region is outside the applied boundary conditions and is therefore a spurious response.

10.1.1 Nonlinear Analysis of Midpanel Model with Imperfections

The nonlinear analysis was performed, as with the previous analyses, using the arc-length method and incorporating both material and geometric nonlinearities into the solution. The stiffness matrix is reformed at every equilibrium iteration (this is a requirement of arc-length method).

Figure 10.2 shows a plot of the load multiplier (Lambda) versus the load step. The load multiplier is determined automatically using ADINA based upon convergence criteria for the solution. The plot gives an indication of the difficulty which ADINA has with convergence at any given load step. The x scale of the plot is the load step number which has no physical significance; it is the time step of the solution process. A decrease in slope in the plot is an indication of convergence problems. A slope of zero indicates a very unstable geometry which is experiencing changes with no change in applied load. This is sometimes associated with buckling. A negative slope indicates that the applied load is too large to establish equilibrium. This is often associated with buckling or snap-through problems where there is a large change in stiffness.

ADINA-PLOT VERSION 6.1, 18 MARCH 1993
Mid/Panel Model With Applied IN-PLANE Loading

ADINA MODESHAPE XUMIN 5974.
MODE 2 XUMAX 5911.
MODE 2 YUMIN 211.5
LOAD FAC = 45.14 YUMAX 291.0

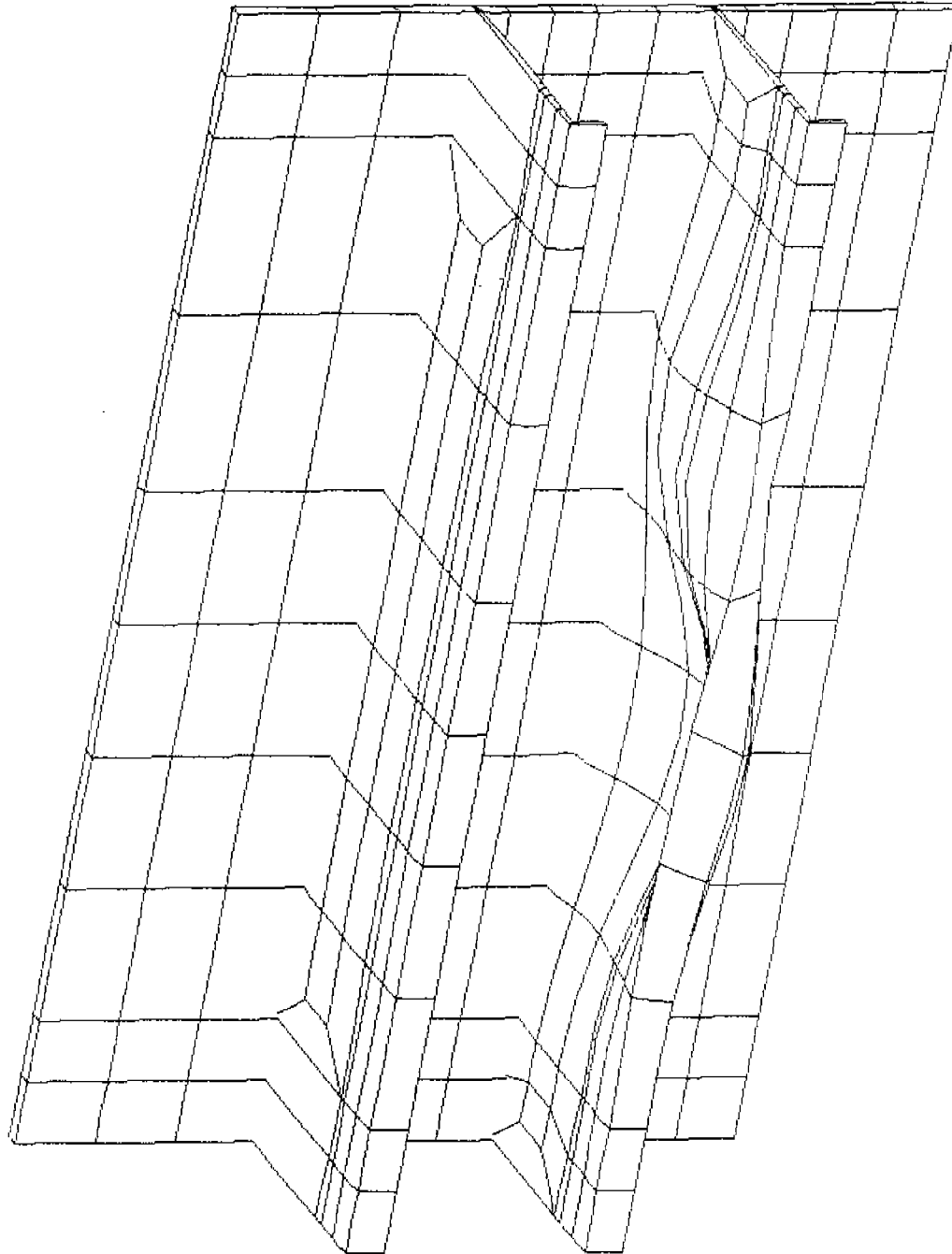
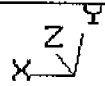
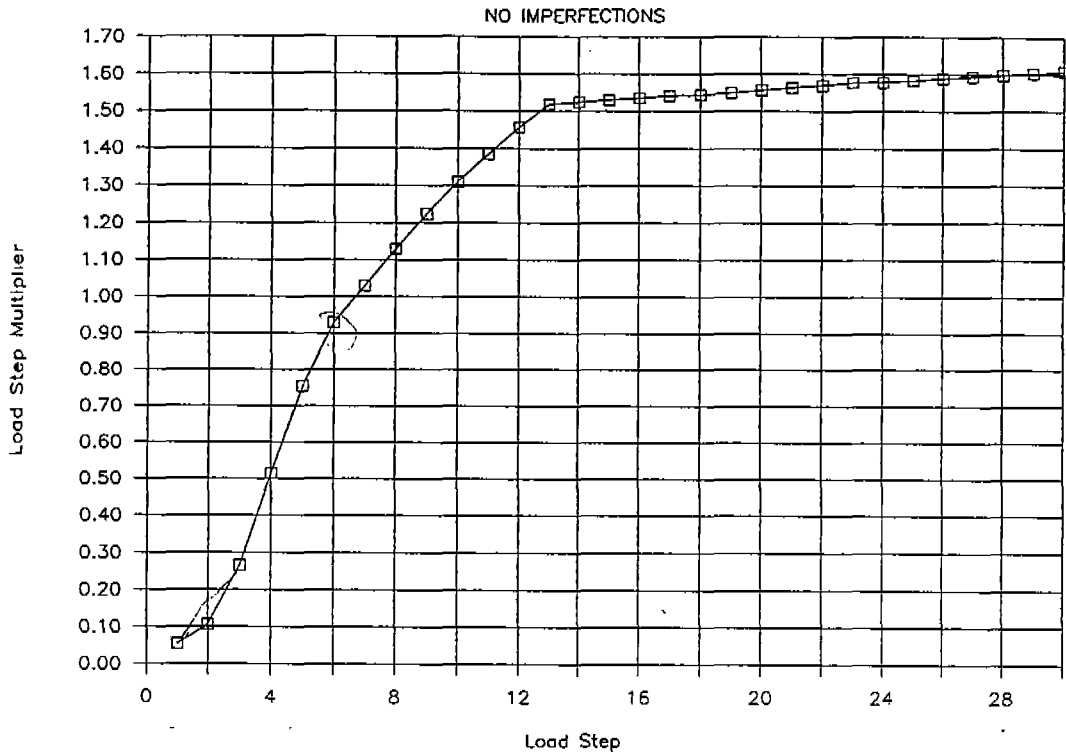


FIGURE 10.1: Second Buckling Mode Shape
- Nonlinear Analysis of Mid Panel Model Using Fixed Rotations and an In-Plane Load

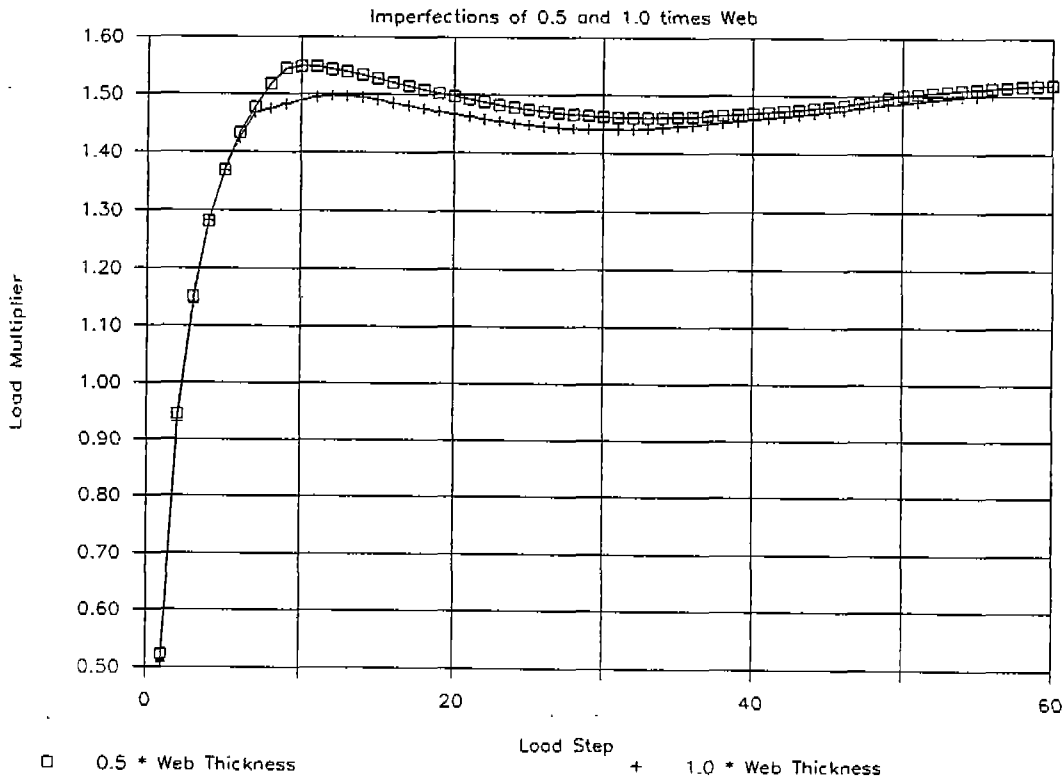
242

Mid-Panel Model: Combined Loads



(a)

Load Multipliers: Mid Panel Model



(b)

**FIGURE 10.2: Load Fraction vs. X Displacement
- Nonlinear Analysis of Midpanel Model With Imperfections**

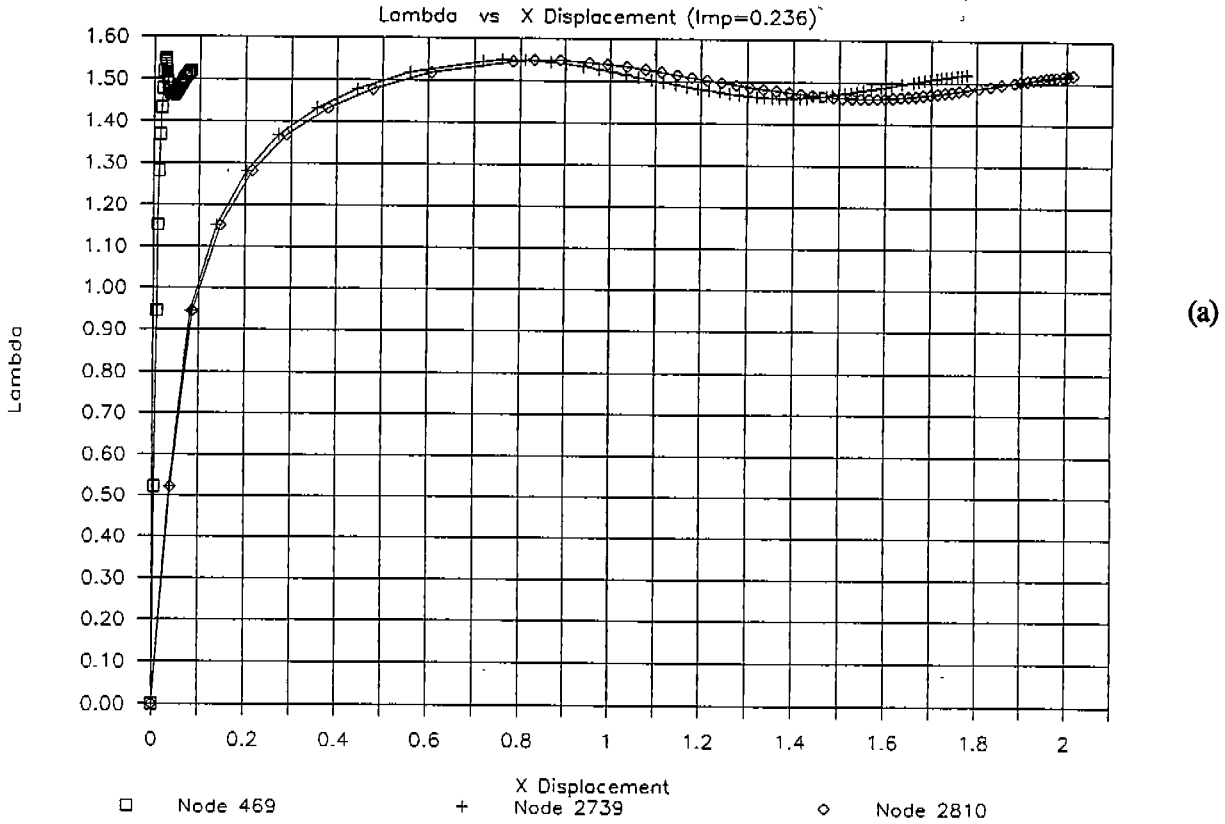
Figure 10.2(b) shows Lambda versus load step for two magnitudes of imperfection, 0.5 and 1.0 times the web thickness. For both curves, Lambda can be seen to increase nonlinearly with load step up to a point where the slope takes an abrupt change. The point of this change of slope is about 1.55 for an imperfection magnitude of 1.0 and about 1.5 for an imperfection magnitude of 0.50. Following this point of load application, the two curves show the same trend and seem to come together at about 40 to 50 time steps. It is important not to put too much physical significance on this plot and it is sufficient to say that the two solutions show similar loading characteristics and both seem to indicate buckling problems at about 145% of F_{max} .

Figure 10.2(a) shows Lambda versus Load Step for the same model with no imperfections. The x scale is different in the two plots, however, the response can be seen to be very similar. The abrupt change in slope associated with the loss of stiffness in the frame can be seen to occur at about 150% of F_{max} as was observed for the two curves which included imperfections. The main difference between the two curves is that the curve generated for the model with no imperfections is seen to show close to a constant slope after the large change in stiffness at 150% of F_{max} . Although the response was not taken any further, it is thought that the constant slope will continue to increase. This is indicative of a now stable structure which supports the applied load through plate membrane action rather than through the bending stiffness of the frames. The mainframe now contributes little to the solution.

Figure 10.3(a) shows a plot of x displacement (longitudinal) versus applied load for an imperfection of .236 * the web thickness. At a load level of about 150% of F_{max} the mainframe can be seen to buckle, showing a large increase in lateral deflection (about two inches) for no increase in load. Figure 10.3(b) shows the same plot for a model with no imperfection. The response can be seen to follow a similar trend approaching an asymptote at about 160% of F_{max} , however, the lateral displacement is significantly less when no imperfection is included in the model.

It would be interesting to carry the analysis out to the point where the frames have buckled completely and the incremental load is completely carried by the plating; however, this was not possible. The solution times and manpower requirements involved in taking the analysis further are prohibitive.

Mid Panel Model: Combined Load + Imperf



Mid Panel Model: Comb Load: No Imperf

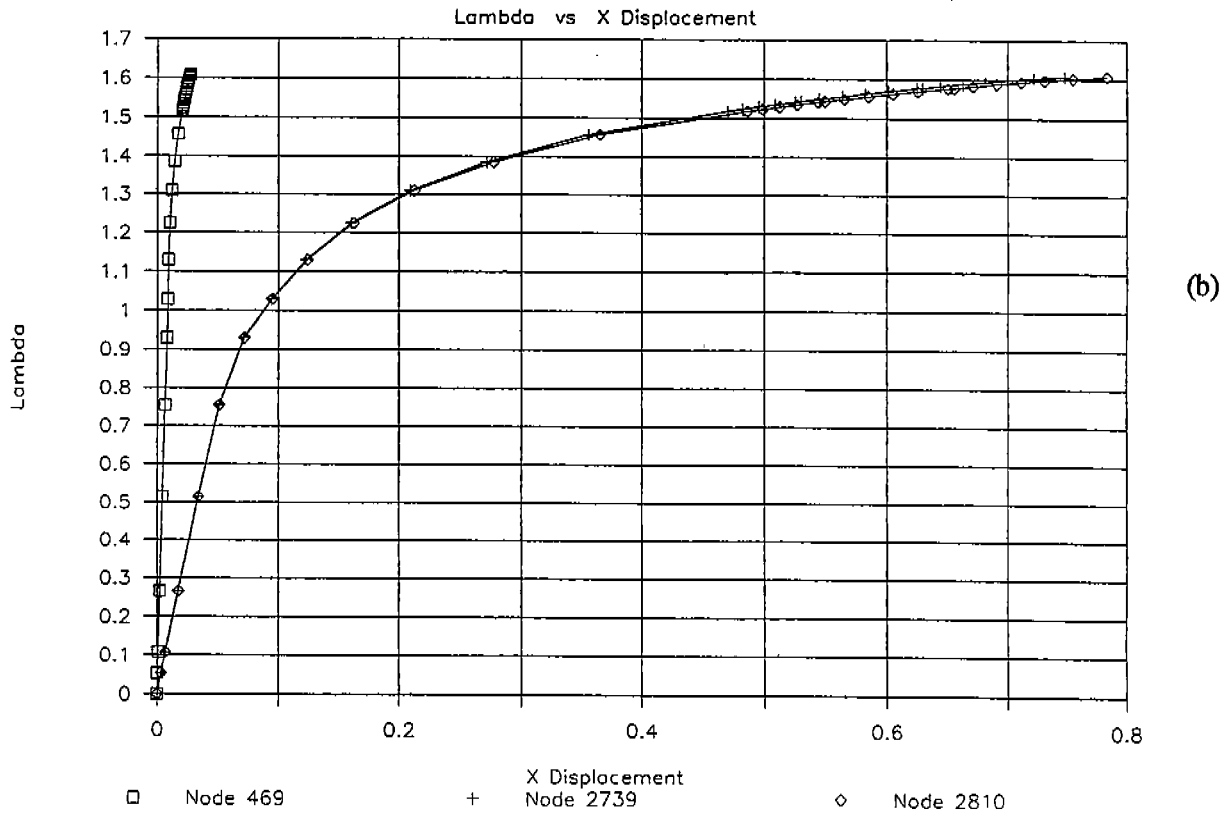


FIGURE 10.3 Load Step Multiplier for Midpanel Model With Imperfections
10-7

245

Figure 10.4 shows a plot of the deflected cross-section of the maximum loaded mainframe at midspan with and without imperfections. The cross-section is shown for the load level of 152% of F_{max} corresponding to load step 8 with imperfections and load step 13 without imperfections. The two cross-sections can be seen to be very similar with the buckled shape being slightly more pronounced for the model with imperfections but equally well predicted for the model without imperfections.

In conclusion, it appears that the buckling load level can be accurately predicted using a model with or without imperfections; however, the model with imperfections shows a more complete buckling. The solution can be seen to reach the maximum load level sooner with imperfections. This results in a decrease in execution time to get to the same point in the analysis. It is important to note, however, that the buckling load is well predicted with both models.

10.2 Overall Model Using Fixed Rotations With In-plane Load

The analysis of the midpanel FE model performed in the previous section concluded that the buckling response was not extremely sensitive to imperfections. The most significant effect from using imperfections is the development of a more complete buckled state. To more confidently establish whether or not this conclusion is valid for the midbody scantlings of the M.V. Arctic, a similar imperfection sensitivity analysis was then performed on the overall midbody FE model.

The study was carried out by analyzing the midbody model with and without an imperfection. To keep analysis times at a reasonable level, the runs were performed using in-plane compressive loads to simulate the effects of the MAESTRO boundary conditions. It was discovered that the arc length method takes considerably longer to iterate to a solution when using prescribed displacements than when using totally constrained degrees-of-freedom. As presented in Chapter 9, in-plane compressive loads produce a very similar buckling response to that obtained using MAESTRO prescribed displacements.

The boundary conditions that are used involve fixing the rotations at the outer boundaries. Two edges are free to translate in-plane where the vertical (y-direction) and longitudinal (x direction) in-plane compressive loads are applied. The lateral ice loads are the same as for all other analyses.

Mid Panel Model: Frame Cross Section

With and Without Imperfections (mf=10)

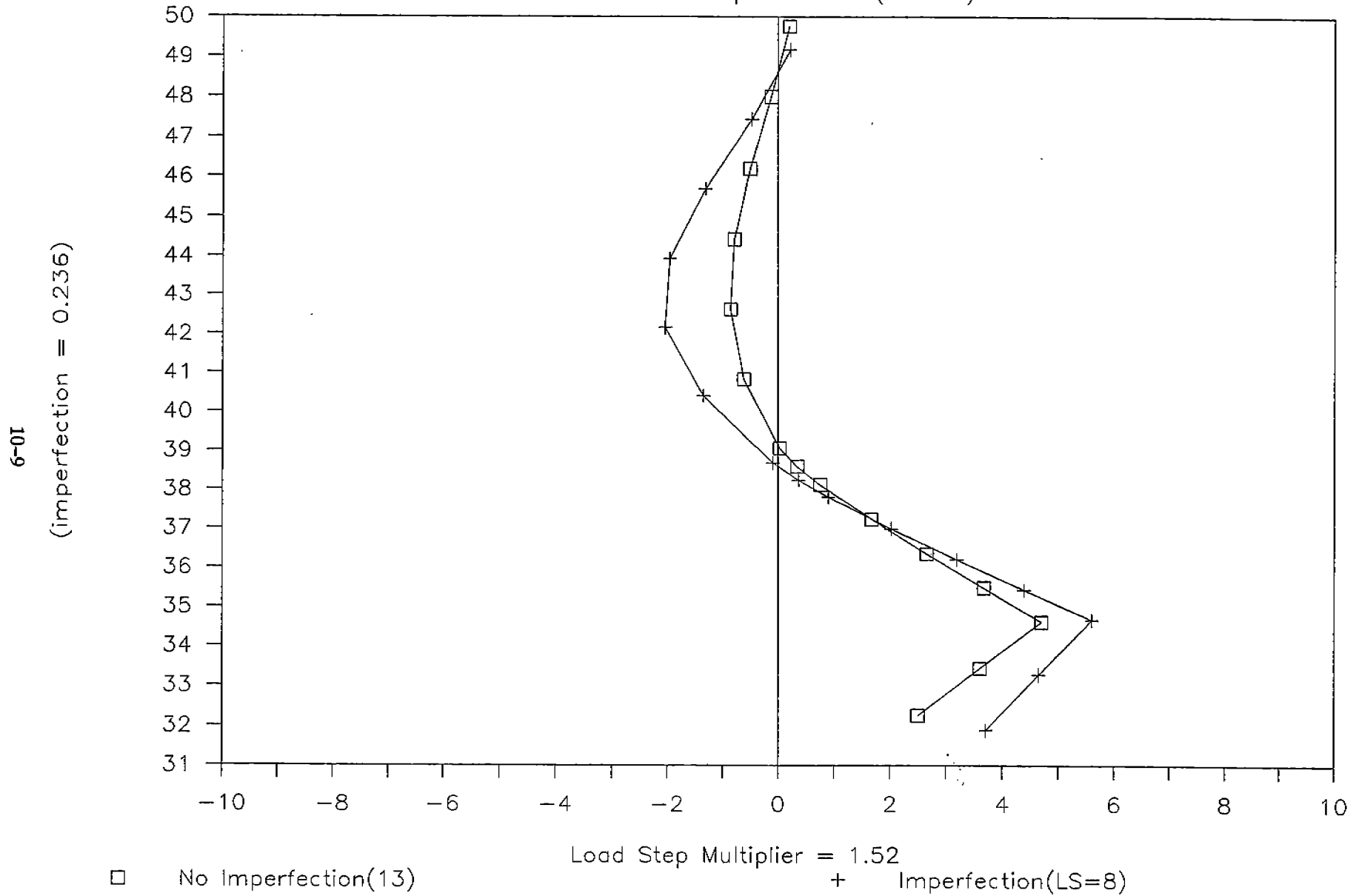


FIGURE 10.4: Comparison of Main Frame Deflected Cross-Sections With and Without Imperfections

Lhe

The results of the two analyses are shown in Figures 10.5 to 10.7. As with the midpanel FE model, the response differs very little between models with and without imperfections (derived from a linear buckling analysis).

Figure 10.5 shows curves of displacement (x, y, and z) versus load step for the analysis without imperfections. Figure 10.6 shows the load versus displacement curves for the analysis with imperfections. Very little difference is found in the plots from the two analyses. A large increase in lateral (x) frame displacement occurs at approximately F_{max} in both analyses. These results are also similar to the analysis of the same model with MAESTRO boundary conditions (see Figure 8.3(b)).

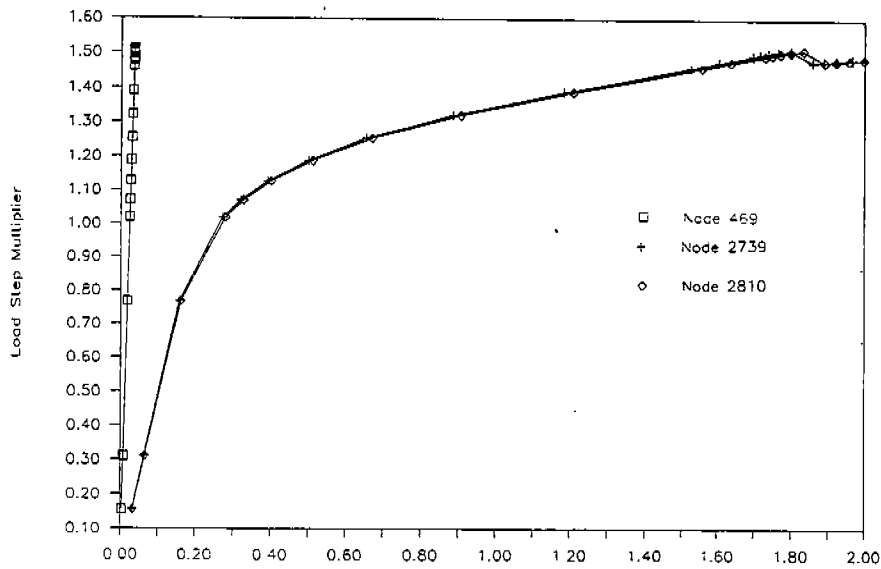
Figure 10.7 shows a plot of the midspan deflected cross-section of the maximum loaded mainframe with and without imperfections at approximately 140% of F_{max} . The deflected shapes and maximum displacements are very similar with and without imperfections. There is a slight difference in the rotation of the flange with respect to the web. In the model without imperfections the flange maintains its position in relationship to the web. In the model with imperfections, the flange rotates towards the web. This is due to the rotation imposed upon the flange from the applied imperfection.

10.3 Residual Stress Effects due to Welding

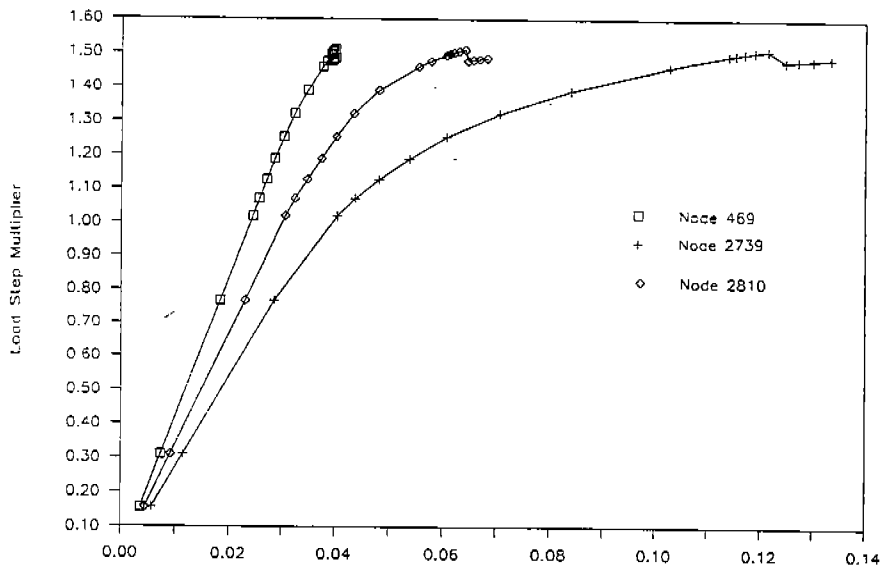
The work initially proposed on evaluating the effect of imperfections due to welding could not be carried out because the time required was devoted to the areas previously discussed. However, the determination of residual stresses in the plating from welding was performed. The results of this work are presented in Appendix C.

10.4 Summary of Imperfection Study

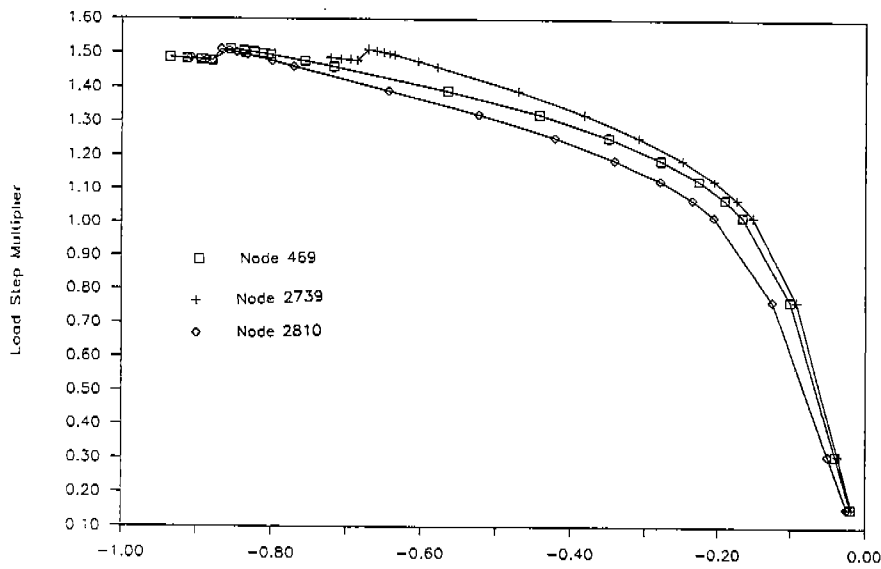
The use of imperfections derived from a linear eigenvalue buckling analysis does not produce any significant changes in the nonlinear response of the mainframes in the midbody FE model of the M.V. Arctic. Instabilities appear at approximately the same load levels with and without imperfections. The response and maximum loads after the development of the instability are also very similar.



(a) X Displacement

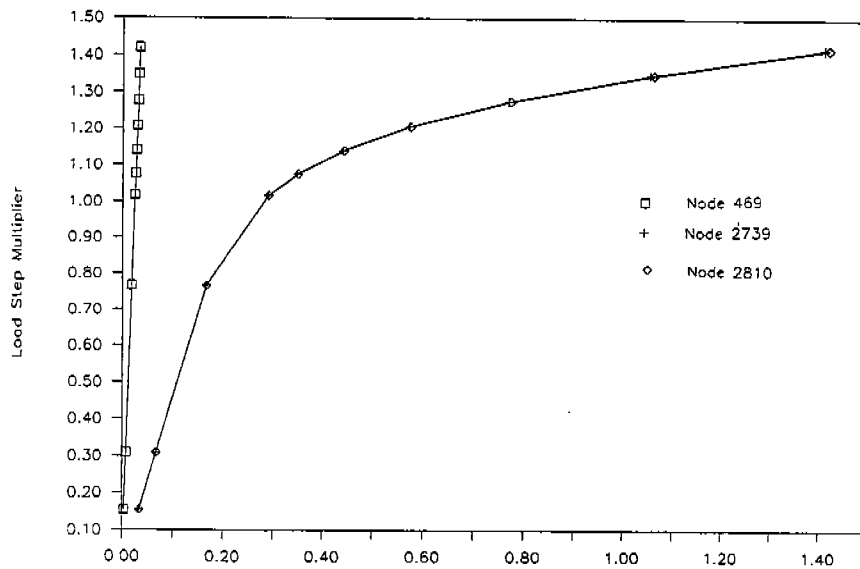


(b) Y Displacement

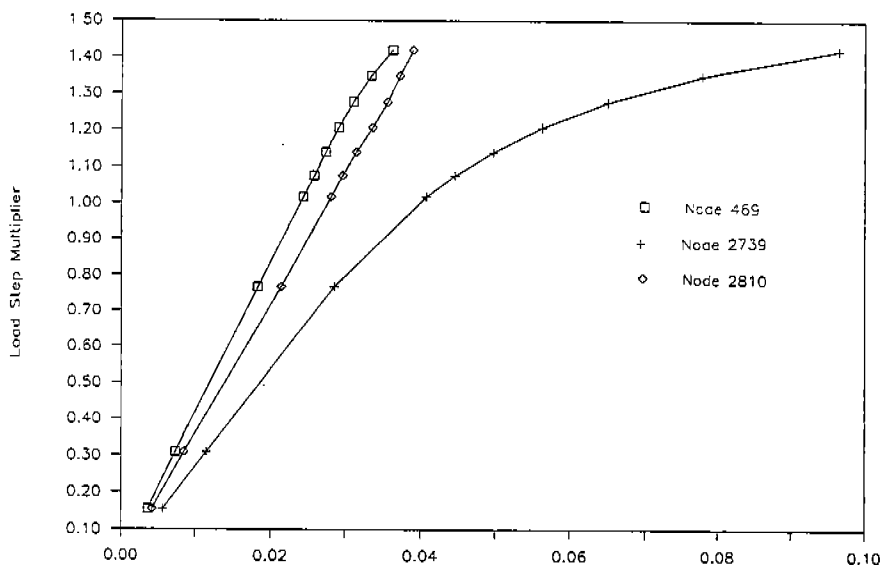


(c) Z Displacement

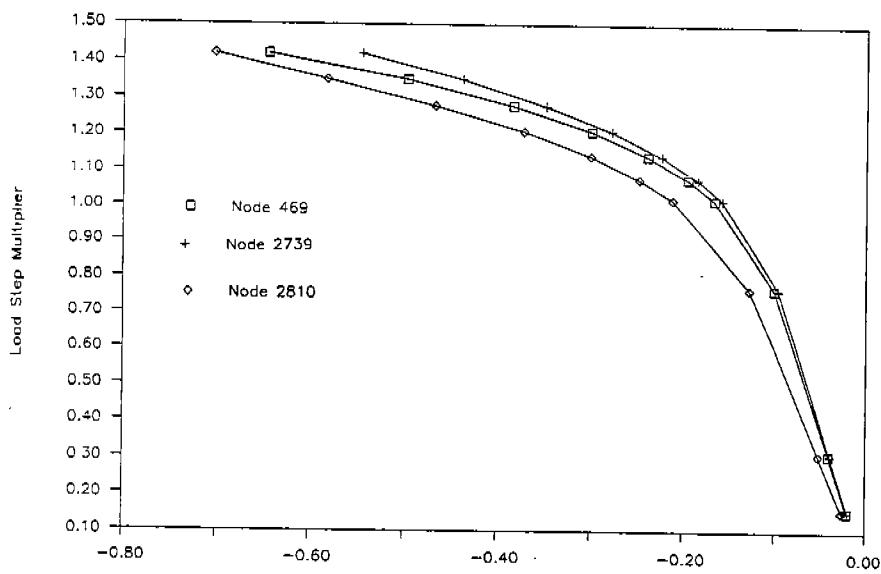
FIGURE 10.5: Load Fraction Versus Displacement - Nonlinear Analysis of the Midbody FE Model Without Imperfections



(a) X Displacement

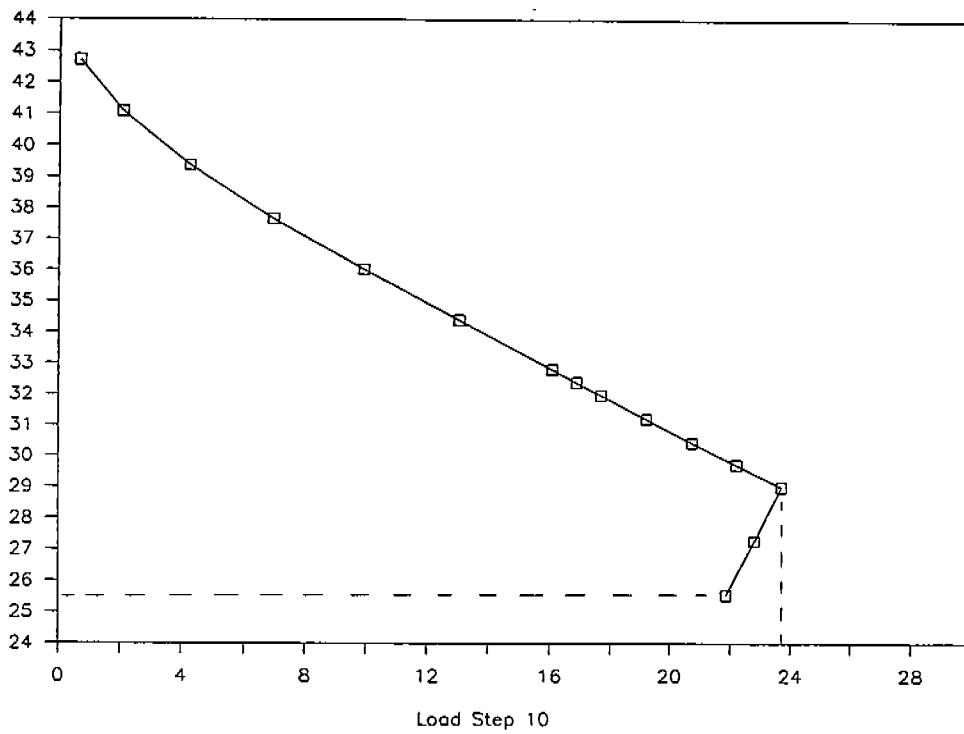


(b) Y Displacement

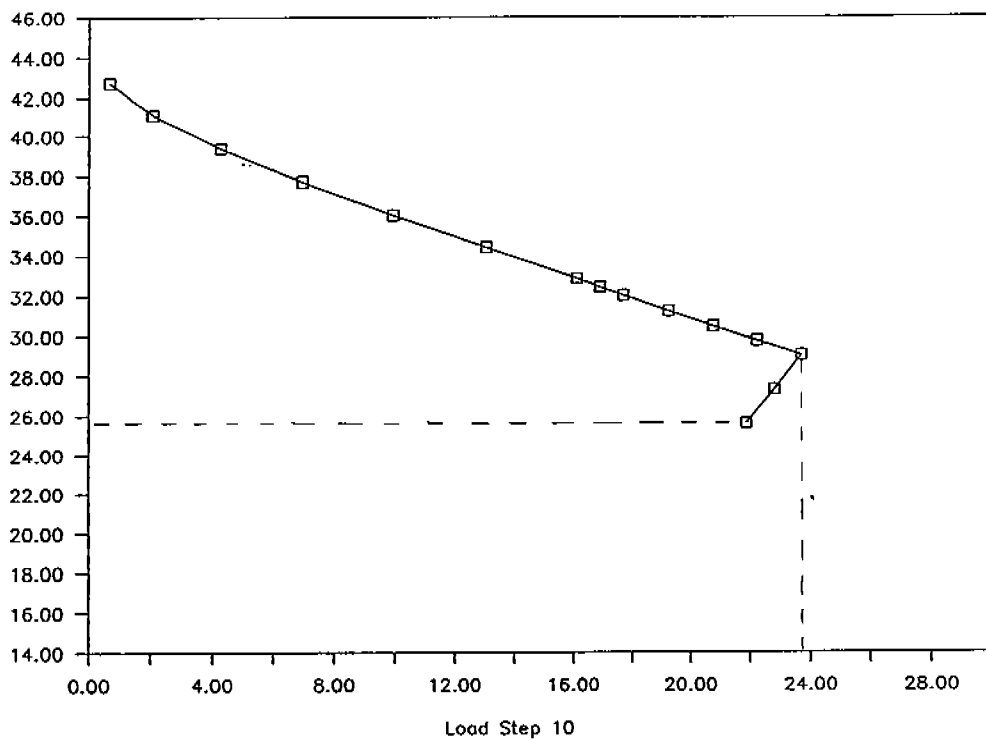


(c) Z Displacement

FIGURE 10.6: Load Fraction Versus Displacement - Nonlinear Analysis of the Midbody FE Model With Imperfections



(a) Without Imperfections



(b) With Imperfections

FIGURE 10.7: Comparison of Midbody FE Model Main Frame Deflected Cross-Sections With and Without Imperfections

11. SUMMARY, CONCLUSIONS AND RECOMMENDATIONS

This investigation has studied the effects of yielding on the stability of the structure of the M.V. Arctic. Two regions of the ship (the midbody and bow) were initially chosen, redesigned according to the ASPPR rules, and analyzed using nonlinear finite element methods.

The analyses of the midbody and bow predicted very different responses in the two regions of the ship. The analyses of the bow model predicted the initiation of yield at 70% of F_{max} with a large decrease in stiffness occurring at 80% of F_{max} . Following this, the model experienced extensive yielding. At 105% of F_{max} , the panel is almost completely yielded without any indication of instability. The midbody model predicted yielding to initiate at approximately the same load level as the bow model, however, the midbody structure was able to carry substantially more load (than the bow) and buckling failure occurred at a stringer location at approximately 130% of F_{max} .

The failure of the bow at a much lower load level than the midbody is due to several factors. The stiff boundary conditions at the bow result in a faster progression of yield. This results in a bow structure that is much less stiff than the midbody structure at the same load level. Also, the inertial effects used in the bow analysis introduce an additional compressive force in the structures that is not present in the midbody.

These analyses were performed to determine which region provided the most potential for further study of the M.V. Arctic. Based upon the results of the analyses of the midbody region (Chapter 5) and the bow region (Chapter 6), the midbody region was chosen for further study. The main reason behind this choice is that the midbody region provided an area which was easier to study and which more clearly displayed the mainframe instabilities that are of interest in this investigation.

The next phase of the investigation was a parametric study of the midbody region. This study was carried out to determine the effects of varying certain structural parameters on the plastic stability of the structure. These parameters included: type of mainframe stiffener, slenderness ratios, strain hardening, imperfections, and residual stresses.

Based upon the results of using different mainframe sections, it is concluded that symmetric mainframe sections (flat bars and tees) provide the best stability and carry the greatest load before failure. However, asymmetric sections such as angle sections and canted flat bar sections are still stable up to F_{max} . The most unstable section was very slender flat bars. Increasing the slenderness of flat bars reduces both the stability and the load carrying capability of the structure. Therefore, except for very slender flat bars, all models designed to the revised ASPPR are capable of carrying a load as great as F_{max} without failure due to buckling. In all cases yielding has occurred prior to the application of F_{max} .

There was very little change in the response of the midbody models with and without strain hardening effects. The use of a strain hardening modulus results in an increase in stresses past the yield strength since the tangent modulus is non-zero. However, it has very little effect on the buckling response.

The same conclusion is made from the study of the effect of imperfections on the stability of angle section mainframes. The imperfections that were used in this study were applied to the maximum loaded mainframe, and were derived from a linear eigenvalue buckling analysis. As indicated in the literature study, the effect of imperfections on the stability of ship structure is one of the least understood areas. This seems mostly due to an incomplete understanding of the types of imperfections that actually occur in ships. While using a simple buckling mode shape may not accurately represent an actual frame imperfection, the sensitivity of the response to an imperfection (real or not) can be measured. In this case, the imperfection has little effect on the buckling response. Instabilities appear at approximately the same load levels (with and without imperfections). The response subsequent to the initiation of the instability is very similar up to the maximum loads.

From a modelling consideration, the most important conclusions regarding the study of the midbody FE model are with respect to the boundary conditions and the global ship response. The post-yield buckling response of the mainframes of the M.V. Arctic is a local response that is not significantly affected by the stiffness of the surrounding structure, but is greatly affected by the loads which are transmitted to the local structure due to the global response of the surrounding structure. Specifically, the local bay response does not seem to significantly depend upon the stiffness of the

structure outside the deep webs and stringers that immediately bound the local bay on which the mainframes are located. It was discovered that changing the boundary conditions at the outer boundaries of the FE model did not significantly alter the buckling response.

However, the response of the local bay is greatly affected by the response of the surrounding structure. The in-plane compressive stresses, which are transmitted through the structure outside of the local bay, affect the post-yield buckling response. Including the effects of the global ship response is very important. In this investigation, the in-plane compressive stresses from the global ship response were included through prescribed displacements from an independent analysis of the ship using MAESTRO. However, if these in-plane stresses are fairly constant, they may be determined through simpler methods. The stresses can then be transformed and applied to the model as forces.

In general, the results show that all mainframe sections designed to the proposed ASPPR regulations remain stable up to the design ice load of F_{max} . However, this conclusion is based upon the analysis results where the level of support is based upon the existing scantlings. The dimensions of the deep webs, stringers, and inner skin of the existing M.V. Arctic were used in the FE analysis. The level of support in ice-breakers designed for the proposed ASPPR does not include an inner skin, and the stiffness of the deep web structure can be blended into the mainframes to reduce the number of levels of support. One of the most significant conclusions of this investigation is that the center bay structure is not affected by the stiffness of the surrounding structure. This was mostly due to the high stiffness of the deep webs and stringers that surround the center bay. If the deep webs or stringers change, this conclusion may not be valid. Therefore, it is recommended that an investigation be carried out using all scantlings designed for the proposed ASPPR. As with the present study, the global ship effects should be included in the response.

The type of mainframe section that seems to be of most interest with respect to possible use in the design of ships scantlings is the flat bar. This section is most likely the least expensive to fabricate and it proved to be very stable except for highly slender sections. It is recommended that the continued investigation outlined above be carried out using flat bar sections.

It is also recommended that more work be done on the effects of slenderness on the stability of flat bar mainframes. The present investigation only studied two different sections. This is insufficient to firmly establish the sensitivity of stability to slenderness ratios. This work should be performed on the model discussed above.

Finally, it is recommended that the study into the effects of residual stresses on the plastic stability of ship scantlings be completed. This work was started during this initial investigation, but, it was not possible to finish the study. These stresses add another component of stress to an already complicated stress zone. Based upon the fact that stresses from the overall ship response affect the buckling response, it is also important to determine whether residual stresses affect the stability of ship scantlings.

REFERENCES

1. Hughes, Owen F., Ship Structural Design — A Rationally-Based, Computer-Aided Optimization Approach, The Society of Naval Architects and Marine Engineers, New Jersey, (1988).
2. Iyengar, N.G.R., Structural Stability of Columns and Plates, Ellis Horwood Limited, West Sussex, England, (1988).
3. Smith, C.S., Influence of Local Compressive Failure on Ultimate Longitudinal Strength of a Ship Hull, International Conference on Practical Design in Shipbuilding (PRADS 77), Tokyo, (1977).
4. Smith, C.S., et al., Strength of Stiffened Plating Under Combined Compression and Lateral Pressure, The Royal Institute of Naval Architects, (1991).
5. Caridis P.A. and Frieze, P.A., Flexural-torsional Elastic-plastic Buckling in Flat Stiffened Plating Using Dynamic Relaxation. Part 1: Theory, Thin-Walled Structures, Vol. 6(6), pp. 453-81, (1988).
6. Tanaka, Y. and Endo, H., Ultimate Strength of Stiffened Plates with Their Stiffeners Locally Buckled in Compression, Journal of the Naval Architects of Japan, Vol. 164, Nov. (1988).
7. Bhat S.U., and Wierbicki, T., On the Plastic Tripping of Flatbar Stiffeners, Thin-Walled Structures, Vol. 7, pp. 281-300, (1989).
8. Smith, C.S., et al., Strength and Stiffness of Ship Plating Under In-plane Compression and Tension, The Royal Institute of Naval Architects, (1987).
9. Caridis, P.A., The Local Behaviour of Flat Stiffened Plating Under Uniaxial Edge Compression, Department of Naval Architecture, University of Glasgow, (1987).
10. Dow, R.S. and Smith, C.S., Effects of Local Imperfections on Compressive Strength of Long Rectangular Plates, Journal Construction Steel Research, Vol. 4, pp. 51-76, (1984).
11. Kakol, W., Stability Analysis of Stiffened Plates by Finite Strips, Thin-Walled Structures, Vol. 10 pp. 277-297, (1990).
12. Graves-Smith, T.R., Developments in Thin-Walled Structures-3, Elsevier Applied Science Publishers Ltd., (1987).
13. Mansour-Tehrani, F. and Graves-Smith, T.R., A Mixed-Mode Method for Analyzing the Buckling of Partially Prismatic Thin-Walled Structures, Thin-Walled Structures, Vol. 12, pp. 1-16, (1991).
14. Carlsen, C.A., A Parametric Study of Stiffened Plates in Compression, The Structural Engineer, Vol. 58B, No. 2, June, (1980).

15. Guran, A. and Shirazi-Adl, A., Some Remarks Concerning the Post-Buckling Behaviour of Compressible Columns, Impact and Buckling of Structures, ASME Annual Meeting, (1990).
16. VASGEN, A Finite Element Model Generation Program for VAST, Version 6.0, Martec Limited, Halifax, Nova Scotia, (1992).
17. ADIDAT, A Program to Translate VAST Geometry Files in ADINA Files, Martec Limited, (1991).
18. ADINA, Version 6.0, A Finite Element Program for Automatic Dynamic Incremental Nonlinear Analysis, K.J. Bathe, ADINA Engineering Inc., Watertown, MA, USA, (1991).
19. Bathe, K.J. and Dvorkin, E.N., "On the Automatic Solution of Nonlinear Finite Element Equations", J. Computers and Structures, Vol. 17, No. 5-6, pp. 871-879, (1983).
20. ADINA Verification Manual - Nonlinear Problems, ADINA Engineering Inc., Watertown, MA, USA, (1990).

APPENDIX A

**CASPPR ICE LOAD DETERMINATION FOR THE
BOW AND MIDBODY REGIONS OF THE M.V. ARCTIC**

CASPPR ICE LOAD DETERMINATION FOR THE BOW AND MIDBODY REGIONS OF THE M.V. ARCTIC

A. Midbody Region

For this project, we are trying to apply a methodology, developed for designing individual elements of ship's structure, to a grillage.

The first step is to calculate the overall extent of the ice load patch. The rules specify the horizontal and vertical extent (HP and VP) of the load, based on the displacement and power of the ship under consideration. For the M.V. Arctic, HP and VP are:

$$\begin{aligned} \text{HP} &= 2.15(D^{0.9} + D^{0.68} \times P^{0.33})^{0.5} \\ &= 15.6 \text{ metres (where } D = 38 \text{ thousand tonnes, } P = 11 \text{ MW)} \\ \text{VP} &= \text{HP}/8 \\ &= 1.95 \text{ metres} \end{aligned}$$

From the rules, the design pressure load, PAV, over the whole ice load patch is 4.5 MPa.

This value of PAV is for a CAC1 ship, applied in the bow region. It must be reduced by the class factor and area factor before it can be applied to the structure. For a CAC4 ship, the class factor is 0.4 and for the midbody area, the area factor is 0.5. Therefore, the value of PAV is:

$$\begin{aligned} \text{PAV} &= \text{PAV} \times 0.4 \times 0.5 \\ &= 0.9 \text{ MPa} \end{aligned}$$

The shape of the load, as described in the background report to the rules, is triangular over the longitudinal extent of the mesh. The vertical height of the load is VP, and the height is 2 x PAV.

For the M.V. Arctic:

Length of load is 51.18 feet (15.6 metres).
Vertical height of load is 1.95 metres.
Peak of triangular distribution is 2 x 0.9 or 1.8 MPa.

At this point, we have described the area to which the load is applied, the magnitude of the load, and the manner in which it is distributed over the area. There is a further step which must be considered. This is the load which acts on a main frame. According to the rules, within the overall load patch, there are some load peaks higher than PAV and some lower. The overall average is PAV. Recognizing the nature of the ice load, and that an individual frame may experience a load higher than PAV, a further refinement to the load application is required.

A.1 Main Frame Load

The local load acting on a main frame is determined as follows:

$$\begin{aligned} DPT_{mf} &= S_{mf}/HP \\ &= 0.026 \end{aligned}$$

Referring to Table 2 in CASPPR, the value of PAV_{mf} is equal to 10.16 MPa. This value must be reduced by the class and area factors, for a new value of 2.03 MPa.

This pressure is superimposed on the existing PAV, and is centered on a main frame within the mesh. It is important to ensure the overall total load on the structure remains the same.

Currently the total load is:

$$\begin{aligned} F &= 0.5 \times (2 \times PAV) \times L \times H \\ &= 0.5 \times (2 \times 0.9) \times 15.6 \times 1.95 \\ &= 27.38 \text{ MN} \end{aligned}$$

where L is the longitudinal extent and H the vertical extent.

The pressure to be applied to the main frame is 2.03 MPa, in a triangular distribution. Therefore, within one main frame space, the load is:

$$\begin{aligned} F_{mf} &= 0.5 \times (2 \times 2.03) \times 0.41 \times 1.95 \\ &= 1.62 \text{ MN} \end{aligned}$$

To maintain the same total load, the load applied to the main frame must be subtracted from the total calculated earlier, and a new effective height of the load distribution can then be calculated.

$$\begin{aligned} F_{\text{new}} &= F - F_{\text{mf}} \\ &= 27.38 - 1.62 = 25.76 \text{ MN} \end{aligned}$$

The height of this portion of the load, now spread over a length of (15.6 - 0.41) or 15.19 metres is:

$$\begin{aligned} 25.76 &= 1/2 (1.95)(P_{\text{new}}) (15.6 - .41) \\ P_{\text{new}} &= 1.74 \text{ MPa} \end{aligned}$$

The CASPPR ice load for the midbody (as calculated) region is shown in Figure A.1.

A.2 Bow Region

The same methodology used to calculate the midbody ice loads is used to calculate the bow ice loads. This derivation is outlined below:

Footprint

$$\begin{aligned} \text{HP} &= 2.15 (D^{0.7} + D^{.68} \times P^{0.33})^{0.5} \\ &= 2.15 (38^{0.7} + 38^{.68} \times 11^{0.33})^{0.5} \\ &= 15.6 \text{ m} \\ \text{VP} &= \text{HP}/8 = 1.95 \text{ m} \end{aligned}$$

$$\text{Frame spacing} = 12" = 0.30 \text{ m}$$

Design Parameter

$$\begin{aligned} \text{DPT} &= S/\text{HP} \\ &= \frac{0.30}{15.6} = 0.019 \\ \text{PAV} &= 10.64 \text{ MP} \end{aligned}$$

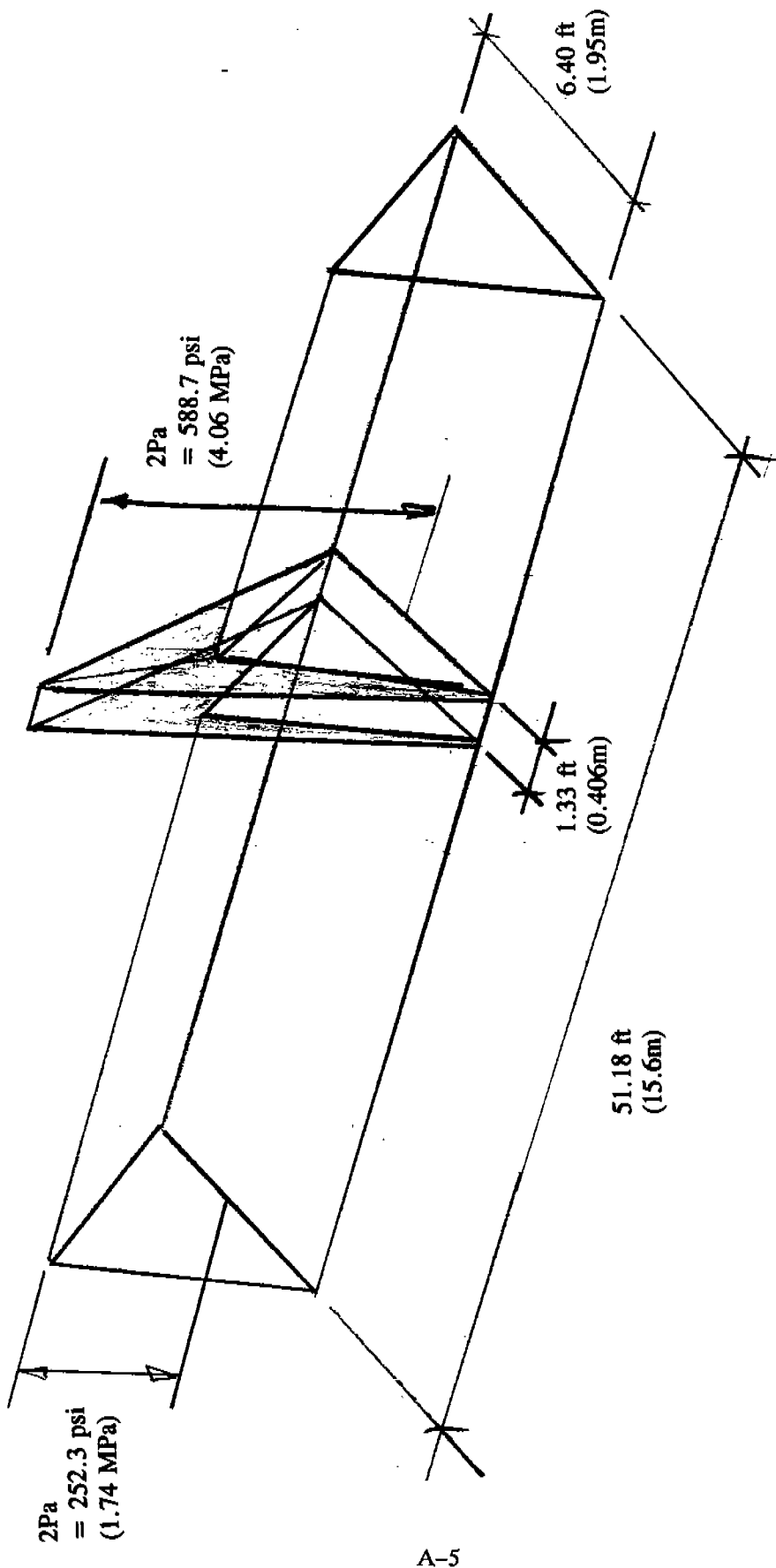


FIGURE A.1: ASPPR Determined Ice Loads at the Midbody Region of the M.V. Arctic

4.4

Modify PAV for the class factor and area factor

Area factor for bow = 1.0

Class factor (CAC4) = 0.4

$$(PAV)_{\text{main frame}} = (PAV) \times 1.0 \times 0.4 = \underline{4.26 \text{ MPa}}$$

Design Pressure over Total Footprint

$$(PAV)_{\text{total}} = 4.5 \times 3.0 \times 0.4 = \underline{1.8 \text{ MPa}}$$

Total force acting on the footprint:

$$\begin{aligned} F_{\text{tot}} &= (PAV)_{\text{tot}} \times HP \times VP \\ &= 1.8 \times 15.6 \times 1.95 \\ &= 54.76 \text{ MN} \end{aligned}$$

Force on the main frame:

$$\begin{aligned} F_{\text{mf}} &= (PAV)_{\text{main frame}} \times \text{Fr. spacing} \times VP \\ &= 4.26 \times 0.3 \times 1.95 \\ &= 2.49 \text{ MN} \end{aligned}$$

Force distributed over remainder of patch:

$$\begin{aligned} F_{\text{rem}} &= F_{\text{tot}} - F_{\text{mf}} \\ &= 54.76 - 2.49 = 52.27 \text{ MN} \end{aligned}$$

Height of triangular distribution:

Over main patch: Height = 3.44 MPa
Over main frame: Height = 8.51 MPa

The CASPPR ice loads for the bow region (as calculated are shown in Figure A.2.

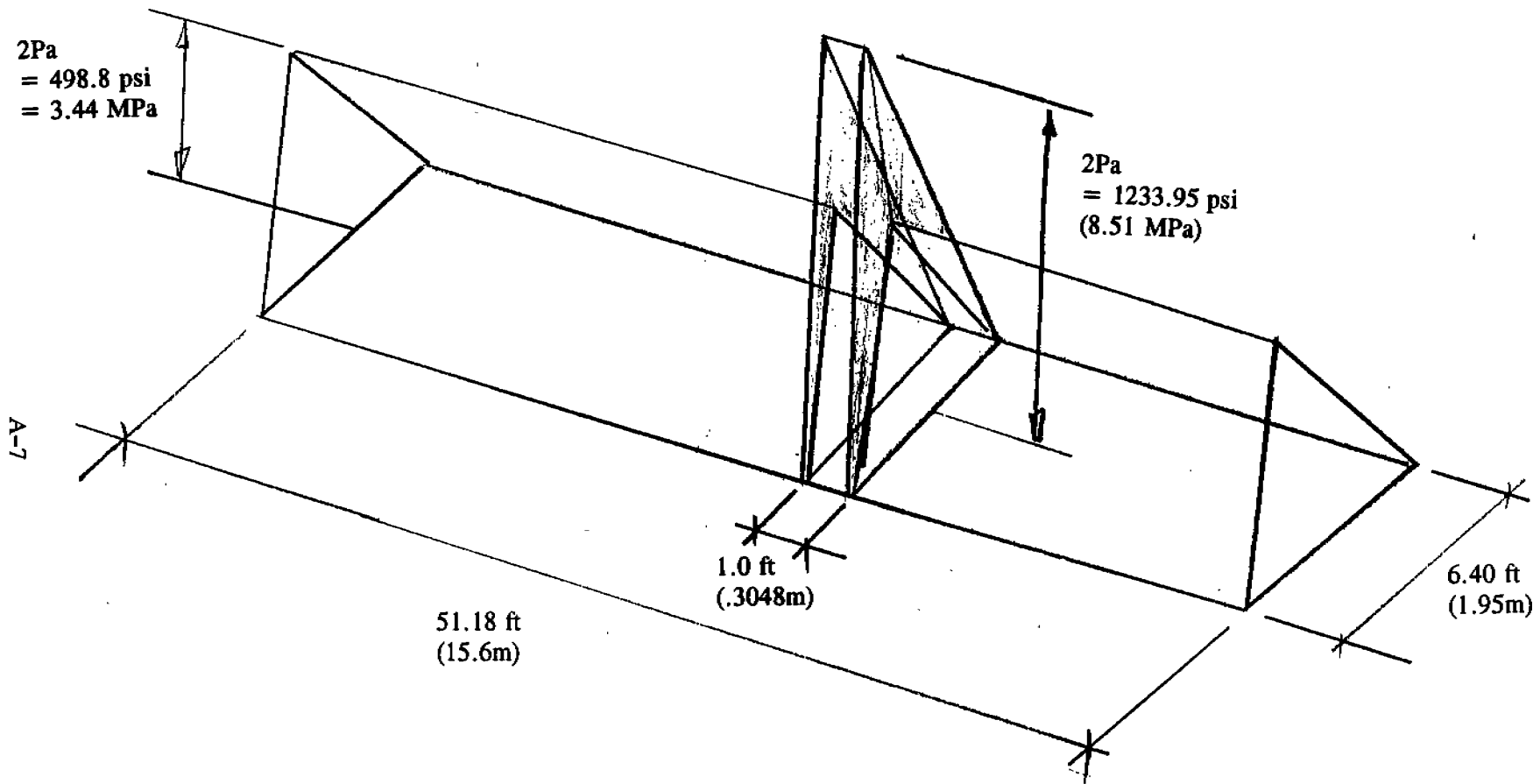


FIGURE A.2: ASPPR Determined Ice Loads at the Bow Region of the M.V. Arctic

265

APPENDIX B
BENCHMARK AND TEST PROBLEMS

BENCHMARK AND TEST PROBLEMS

This appendix contains a listing of the files necessary to perform the ADINA test problem #1 covered in Section 4.5 of the main body of the report. These listings were copied from the ADINA verification manual.

EXAMPLE B.40

ANALYSIS OF SNAP THROUGH OF AN ARCH STRUCTURE

Objective:

To perform a postbuckling analysis of an arch structure using the load-displacement control method [1].

Physical Problem:

An assemblage of two identical bars subjected to an apex load is considered (see Fig. B.40 (a)).

Finite Element Model:

From symmetry, the arch structure is modeled using one 2-node truss element as shown in Fig. B.40 (a).

Solution Results:

The analytical solution for the load-deflection relationship is [2]:

$$P = 2kL \left[-1 + \frac{1}{\left[1 - 2 \frac{\Delta}{L} \sin 15^\circ + \left(\frac{\Delta}{L}\right)^2\right]^{\frac{1}{2}}} \right] \left(\sin 15^\circ - \frac{\Delta}{L}\right)$$

The obtained numerical solution is given in Fig. B.40 (b) and an excellent comparison with the analytical solution is observed.

User Hints:

- If a static solution is attempted by using either the modified Newton iteration, full Newton iteration or BFGS method, the displacement response can be traced only to $\Delta = 1.1$. Beyond this region the program execution is terminated because the arch stiffness matrix is not positive definite.

References:

- [1] Bathe, K.J. and Dvorkin, E.N., "On the Automatic Solution of Nonlinear Finite Element Equations", Computers and Structures, Vol. 17, No.5-6, pp. 871-879, 1983.
- [2] Bathe, K.J., Finite Element Procedures in Engineering Analysis, Prentice Hall, 1982.

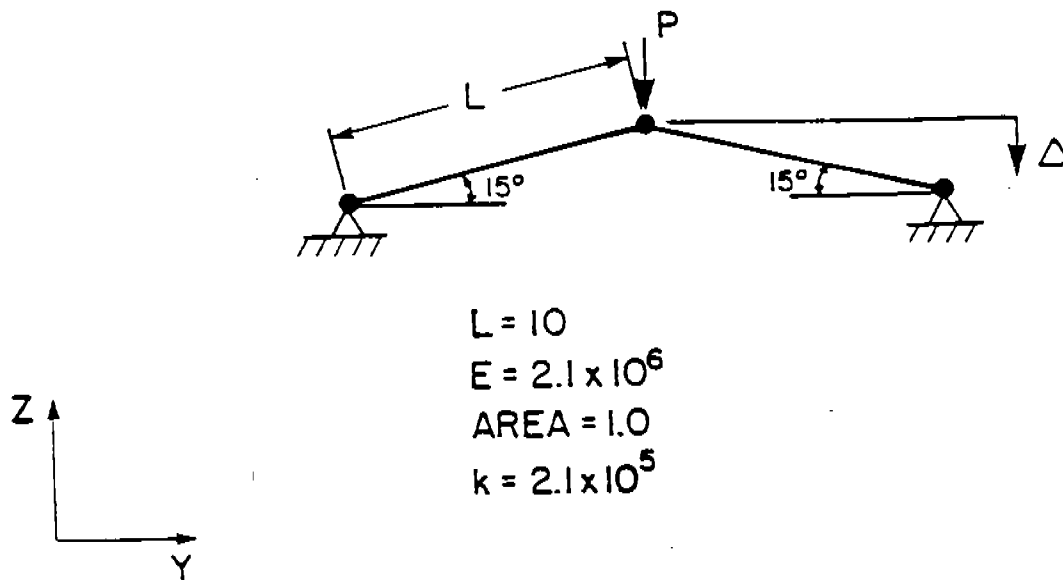


Figure B.40 (a)

(THIS PAGE INTENTIONALLY LEFT BLANK)

```

*      A D I N A - I N      3 . 0      I N P U T      F I L E
*
* B.40 ANALYSIS OF SNAP THROUGH OF AN ARCH STRUCTURE
*
FILEUNITS LIST=8 LOG=7 ECHO=7
FCONTROL HEADING=UPPER ORIGIN=UPPERLEFT
CONTROL PLOTUNIT=PERCENT HEIGHT=1.25
*
DATABASE CREATE
*
HEAD 'B.40 ANALYSIS OF SNAP THROUGH OF AN ARCH STRUCTURE'
*
MASTER IDOF=110111 NSTEP=100 DT=1.0 REACTION=YES
KINEMATICS DISPL=LARGE STRAIN=SMALL
AUTOMATIC-LDC NODE=2 DIR=3 DISPL=-1.0E-01,
          DISPM=5.5 CONT=YES
PRINTOUT VOLUME=MAXIMUM IPRIC=0 IPRIT=0 IPDATA=3 CARDIMAGE=NO
PORTHOLE FORMATTED=YES FILE=60
*
SYSTEM 1 CYLINDRICAL
COORDINATES / ENTRIES  NODE  R  THETA
                          1   0.   0.
                          2  10.  15.
*
MATERIAL 1 ELASTIC E=2.1E06
EGROUP 1 TRUSS
ENODES / ENTRIES  EL  N1  N2
                          1   1   2
EDATA / ENTRIES  EL  AREA
                          1  1.0
*
FIXB DIR=3 / 1
LOADS CONCENTRATED
      2  3  -0.5
*
FRAME
MESH NODES=11 ELEMENT=1 BCODE=ALL
EVECTOR VAR=PFORCE OUTPUT=ALL
*
ADINA
END

```

* ADINA - PLOT 4.0 INPUT FILE

* B.40 ANALYSIS OF SNAP THROUGH OF AN ARCH STRUCTURE

*
FILEUNITS LIST=8 LOG=7 ECHO=7
FCONTROL HEADING=UPPER ORIGIN=UPPERLEFT
CONTROL PLOTUNIT=PERCENT HEIGHT=1.25

* DATABASE COMMANDS TO LOAD OR OPEN THE ADINA-PLOT DATABASE

*
DATABASE CREATE FORMATTED=YES
*DATABASE OPEN

*
FRAME

MESH ORIGINAL=1 DEFORMED=0 NOD=11 EL=1 BCODE=ALL SUBFRAME=2211,
MARGIN=YES

EVECTOR VAR=PFORCE OUTPUT=ALL

*
NPOINT APEX NODE=2

LIST NPOINT

RESULTANT DISPLACEMENT '-<Z-DISPLACEMENT>'

LIST RESULTANT

*
USERDATA ANALYTICAL DISPLACEMENT LOAD P

0.05000	0.1369E+04	/	0.10000	0.2663E+04	/	0.15000	0.3882E+04
0.20000	0.5029E+04	/	0.25000	0.6104E+04	/	0.30000	0.7108E+04
0.35000	0.8042E+04	/	0.40000	0.8907E+04	/	0.45000	0.9705E+04
0.50000	0.1044E+05	/	0.55000	0.1110E+05	/	0.60000	0.1171E+05
0.65000	0.1225E+05	/	0.70000	0.1272E+05	/	0.75000	0.1314E+05
0.80000	0.1350E+05	/	0.85000	0.1381E+05	/	0.90000	0.1405E+05
0.95000	0.1424E+05	/	1.00000	0.1438E+05	/	1.05000	0.1447E+05
1.10000	0.1450E+05	/	1.15000	0.1449E+05	/	1.20000	0.1443E+05
1.25000	0.1432E+05	/	1.30000	0.1417E+05	/	1.35000	0.1398E+05
1.40000	0.1374E+05	/	1.45000	0.1346E+05	/	1.50000	0.1315E+05
1.55000	0.1280E+05	/	1.60000	0.1241E+05	/	1.65000	0.1199E+05
1.70000	0.1154E+05	/	1.75000	0.1105E+05	/	1.80000	0.1054E+05
1.85000	0.1000E+05	/	1.90000	0.9440E+04	/	1.95000	0.8852E+04
2.00000	0.8242E+04	/	2.05000	0.7611E+04	/	2.10000	0.6962E+04
2.15000	0.6296E+04	/	2.20000	0.5615E+04	/	2.25000	0.4921E+04
2.30000	0.4214E+04	/	2.35000	0.3498E+04	/	2.40000	0.2773E+04
2.45000	0.2041E+04	/	2.50000	0.1305E+04	/	2.55000	0.5657E+03
2.60000	-0.1750E+03	/	2.65000	-0.9152E+03	/	2.70000	-0.1653E+04
2.75000	-0.2388E+04	/	2.80000	-0.3116E+04	/	2.85000	-0.3837E+04
2.90000	-0.4549E+04	/	2.95000	-0.5250E+04	/	3.00000	-0.5939E+04
3.05000	-0.6613E+04	/	3.10000	-0.7271E+04	/	3.15000	-0.7912E+04
3.20000	-0.8533E+04	/	3.25000	-0.9132E+04	/	3.30000	-0.9709E+04
3.35000	-0.1026E+05	/	3.40000	-0.1079E+05	/	3.45000	-0.1129E+05
3.50000	-0.1175E+05	/	3.55000	-0.1219E+05	/	3.60000	-0.1260E+05
3.65000	-0.1297E+05	/	3.70000	-0.1330E+05	/	3.75000	-0.1360E+05
3.80000	-0.1386E+05	/	3.85000	-0.1407E+05	/	3.90000	-0.1425E+05
3.95000	-0.1438E+05	/	4.00000	-0.1446E+05	/	4.05000	-0.1450E+05
4.10000	-0.1449E+05	/	4.15000	-0.1443E+05	/	4.20000	-0.1432E+05
4.25000	-0.1416E+05	/	4.30000	-0.1394E+05	/	4.35000	-0.1367E+05
4.40000	-0.1334E+05	/	4.45000	-0.1295E+05	/	4.50000	-0.1251E+05
4.55000	-0.1200E+05	/	4.60000	-0.1143E+05	/	4.65000	-0.1080E+05
4.70000	-0.1010E+05	/	4.75000	-0.9337E+04	/	4.80000	-0.8507E+04

```
4.85000 -0.7609E+04 / 4.90000 -0.6642E+04 / 4.95000 -0.5605E+04
5.00000 -0.4496E+04 / 5.05000 -0.3315E+04 / 5.10000 -0.2061E+04
5.15000 -0.7316E+03 / 5.20000 0.6731E+03 / 5.25000 0.2154E+04
5.30000 0.3713E+04 / 5.35000 0.5350E+04 / 5.40000 0.7066E+04
5.45000 0.8863E+04 / 5.50000 0.1074E+05 / 5.55000 0.1270E+05
5.60000 0.1474E+05 / 5.65000 0.1687E+05 / 5.70000 0.1908E+05
5.75000 0.2137E+05 / 5.80000 0.2375E+05 / 5.85000 0.2622E+05
5.90000 0.2877E+05 / 5.95000 0.3142E+05 / 6.00000 0.3415E+05
*
```

```
AXIS 1 0.0 0.0 0.0 0.0 6.0 'DISPLACEMENT, APEX'
```

```
AXIS 2 0.0 0.0 0.0 -15000 25000 'LAMBDA'
```

```
GRAPH DISPLACEMENT APEX LAMBDA NULL SYMBOL=1 OUTPUT=ALL,
SUBFRAME=2111 XAXIS=1 YAXIS=2
```

```
UGRAPH ANALYTICAL SYMB=2 XAXIS=-1 YAXIS=-2 OUTPUT=ALL SSKIP=10
```

```
TEXT XP=50 YP=70 COLOR=GREEN STRING='<1> ADINA'
```

```
TEXT XP=50 YP=66 COLOR=GREEN STRING='<2> ANALYTICAL SOLUTION'
```

```
*
```

```
ZLIST VARIABLES=Y-REACTION Z-REACTION DISPLACEMENT
```

```
*
```

```
* CHECK LISTING
```

```
*
```

```
CONTROL EJECT=NO LINPAG=10000
```

```
FILEUNITS LIST=9
```

```
PLIST APEX VAR=Z-DISPLACEMENT Z-PREScribed_FORCE
```

```
*
```

```
END
```

APPENDIX C
RESIDUAL STRESS IN T-BUTT WELDMENT

RESIDUAL STRESS

in

T - BUTT WELDMENT

by

Leslie T. Russell, Ph.D., P.Eng.

May 19, 1992



1.0 INTRODUCTION

The stress which remains in a body after all external loads are removed is known as residual stress. This stress is also known by other names such as locked in stress, internal stress, etc. Residual stress in a body may be caused by different actions performed on the body. Residual stress due to grinding is found to be localized and normally is contained in a layer close to the surface, while the residual stress due to distortion of the metal in processes such as shearing and rolling is more extensive. Any action which causes plastic distortion of the body may result in residual stress. The action of welding which causes the metal in a limited area to become molten during the process results, on cooling, in residual stress. It is this stress, caused by welding, which is the subject of this investigation.

The present investigation is concentrated on the effect of welding in a ship structure and the resultant creation of residual stress. The focus is on the welding of parts of the structure which can be described as T - butt weldments.

In particular it is the purpose of this investigation to establish the residual stress in the area of the fillet weld of the structure shown in Figure 1.

2.0 STRUCTURE SPECIFICS

The size of the material used in the calculation of the residual stress is representative of the plates proposed for the use in the M. V. Arctic. The thickness of the various plates is between 11 mm and 19 mm and for this thickness it is noted in the literature that the variation of the residual stress through the plate thickness is small and can therefore be ignored. For plates of greater thickness this variation of the residual stress cannot be ignored. The yield stress of the plate material is understood to be 34,000 psi.

The weld size used throughout the structure varies in relation to the plate thickness and in the area of concern is between 3/16 inch and 3/8 inch. The yield stress of the weld material is 44,000 psi.

3.0 METHOD OF ANALYSIS

Nagaraja¹ and Masubuchi² have shown that the residual stress produced in the creation of a T - butt weldment through the fillet welding process is not substantially different from the residual stress produced by the butt welding of two plates and the edge welding of a single plate. The residual stress produced in the butt welding of two plates produces essentially

the same stress as the stress produced in the flange of a T - butt weldment. Likewise the residual stress produced in the edge welding of a plate produces essentially the same stress as found in the web of the T - butt weldment after welding. The distribution of the residual stress in both the butt welding of two plates and the edge welding of the single plate has been established and it is this technique which has been used in this investigation to predict the residual stress distribution in the weldment component.

4.0 DETERMINATION OF RESIDUAL STRESS DISTRIBUTION

The calculation of the residual stress in any structure is by its very nature not exact. The values must be considered to be the best estimate which can be found through calculation and if greater accuracy is required this must be determined through experimental methods.

The prediction of the stresses for the configuration shown in Figure 1 is based on the work of Nagaraja¹ and Masubuchi² and is presented in non-dimensional form in order that the estimation of stresses may be used in other configurations and also in numerical form for the structure shown in Figure 1. It is noted that the main stress produced in the weldment shown is tension in the direction of the weld. The stress produced in the direction normal to the weld direction is also tension but is small in comparison to the longitudinal stress. According to Masubuchi this stress is sufficiently small that it can be ignored.

The prediction for the residual stress is given in the curves which follow. It should be noted that the distorted shape could be of major concern if buckling is to be considered and that this shape may be of greater significance in the determination of buckling than the residual stress arising because of the welding procedure.

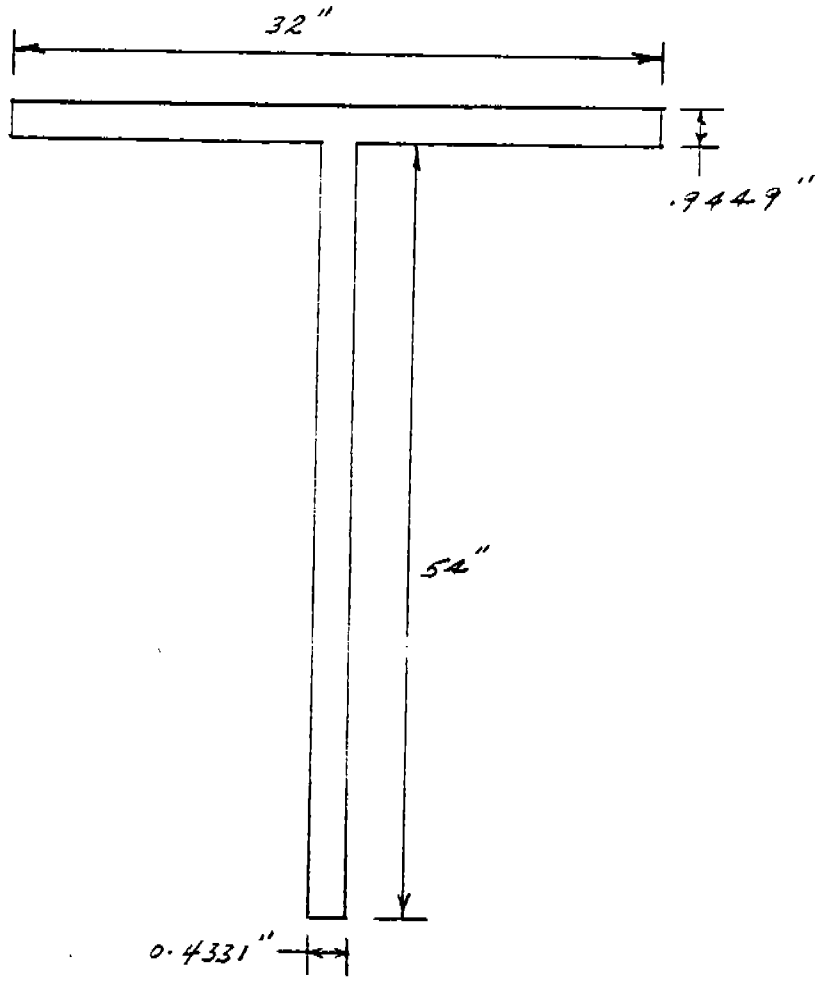
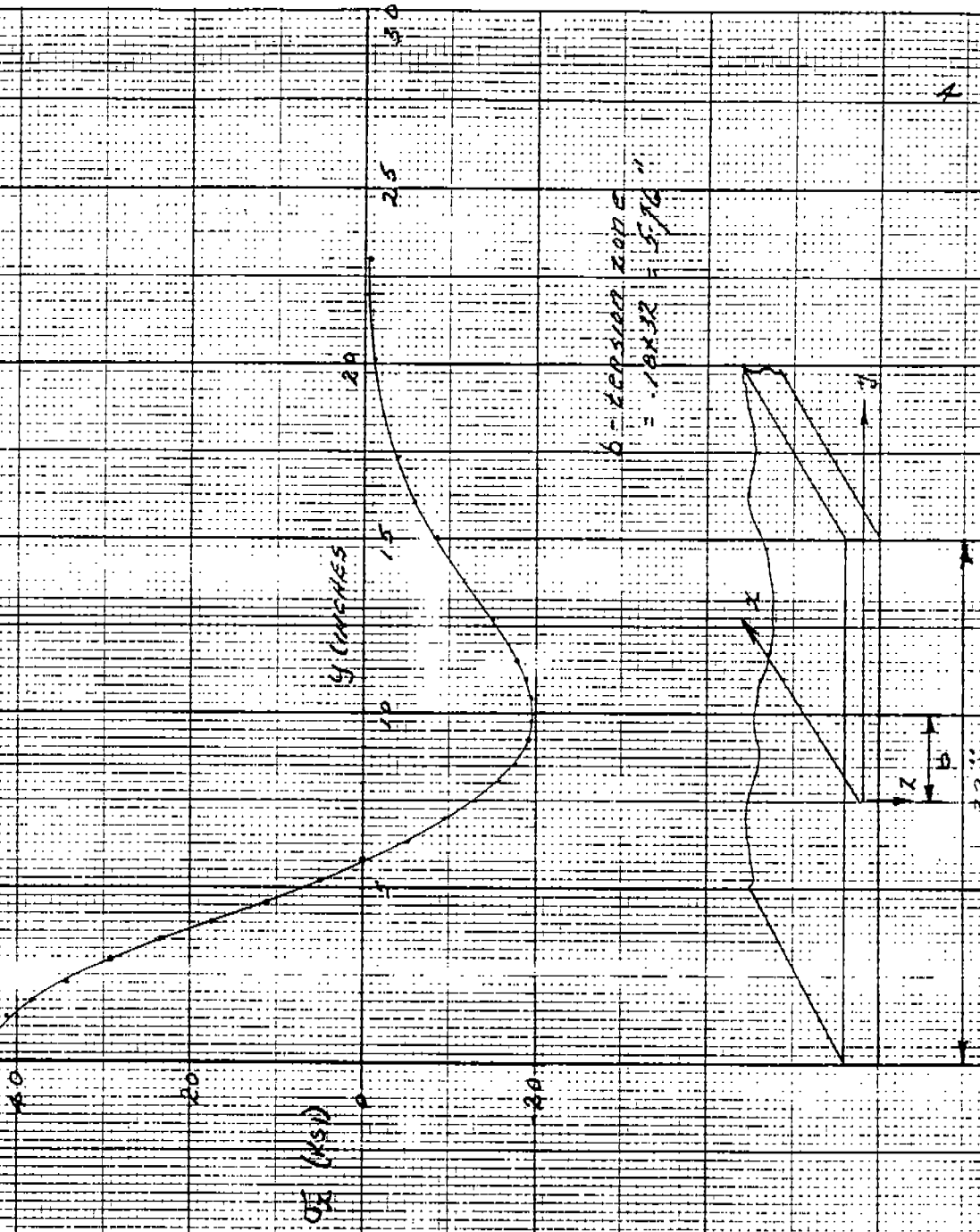


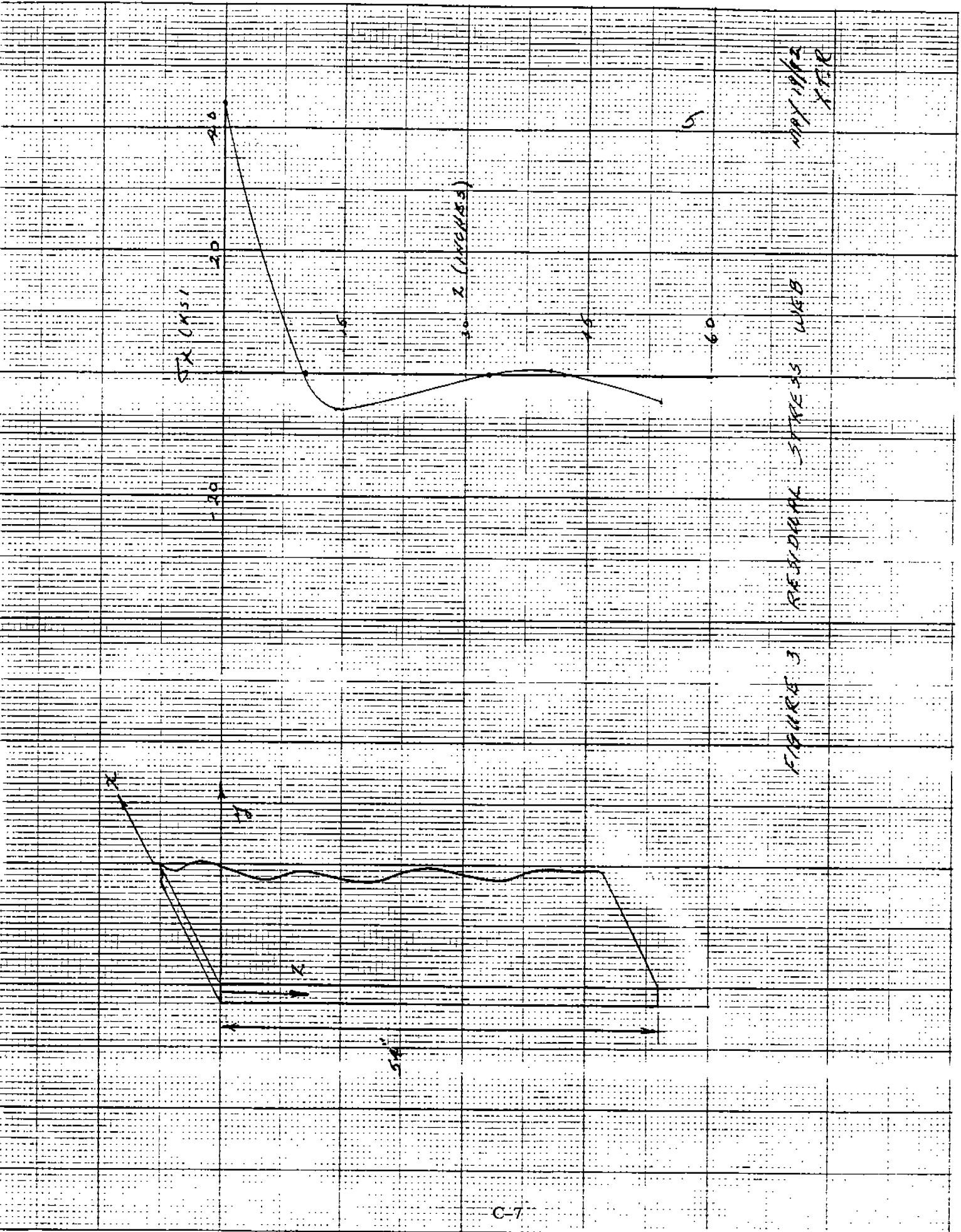
Figure 1 T - BUTT WELDMENT



$b = \text{PER SIDE } 2.00 \text{ IN}$
 $= 1.8 \times 32 = 5.76 \text{ IN}$

FIGURE 2. RESIDUAL STRESS FRANGE

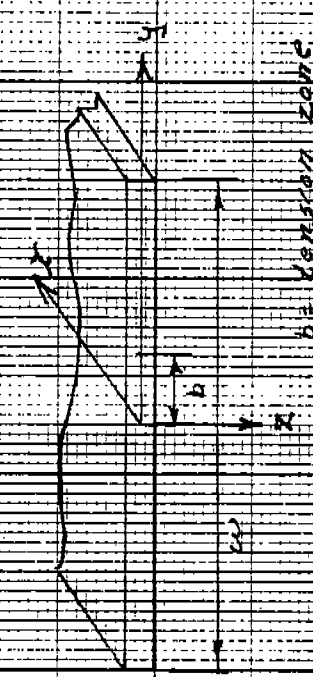
MAY 1972
A. J. R.



MAY 1962
TTR

FIGURE 3 RESIDUAL STRESS WEB

C-T



b = TRANSITION ZONE

σ_y = yield stress, weld metal

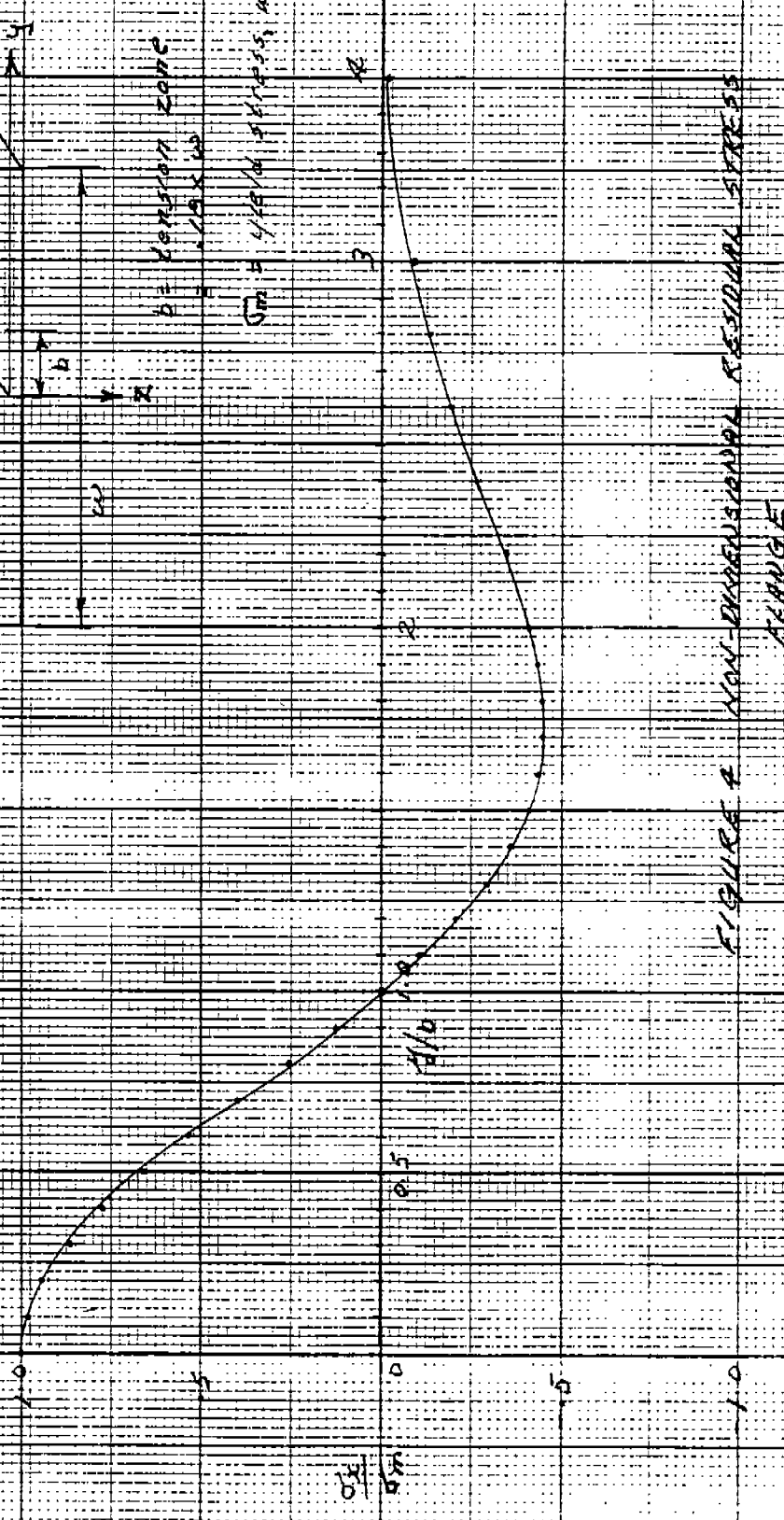
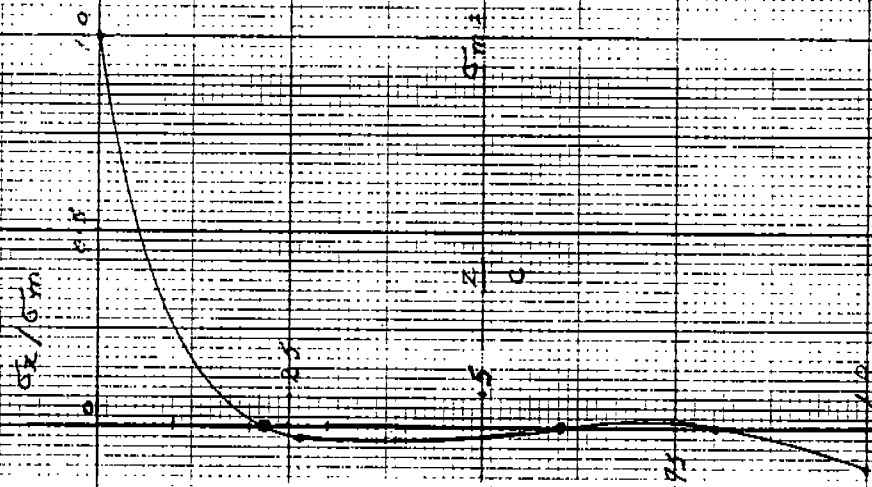
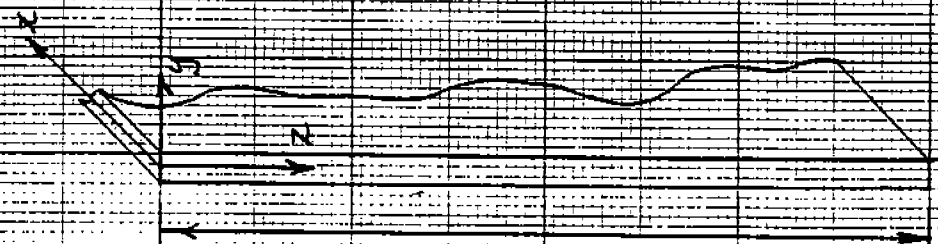


FIGURE 4 NON-DIMENSIONAL RESIDUAL STRESS CHANGE



SMALL YIELD STRESS, WELD METAL

FIGURE 5. HIGH-DIMENSIONAL RESIDUAL STRESS

WMEB

C-9

5.0 REFERENCES

1. Nagaraja Rao, N. R., Estuar, F. R., and Tall, L., " Residual Stress in Welded Shapes", Welding Research Supplement, pp 295-s - 306s, July 1964.
2. Masubuchi, K., "Analysis of Welded Structures", Pergamon Press, 1980.

COMMITTEE ON MARINE STRUCTURES

Commission on Engineering and Technical Systems

National Academy of Sciences – National Research Council

The COMMITTEE ON MARINE STRUCTURES has technical cognizance over the interagency Ship Structure Committee's research program.

**John Landes, University of Tennessee, Knoxville, TN
Howard M. Bunch, University of Michigan, Ann Arbor, MI
Bruce G. Collipp, Marine Engineering Consultant, Houston, TX
Dale G. Karr, University of Michigan, Ann Arbor, MI
Andrew Kendrick, NKF Services, Montreal, Quebec
John Niedzwecki, Texas A & M University, College Station, TX
Barbara A. Shaw, Chairman, Pennsylvania State University, University Park, PA
Robert Sielski, National Research Council, Washington, DC
Stephen E. Sharpe, Ship Structure Committee, Washington, DC**

DESIGN WORK GROUP

**John Niedzwecki, Chairman, Texas A&M University, College Station, TX
Bilal Ayyub, University of Maryland, College Park, MD
Ovide J. Davis, Pascagoula, MS
Maria Celia Ximenes, Chevron Shipping Co., San Francisco, CA**

MATERIALS WORK GROUP

**Barbara A. Shaw, Chairman, Pennsylvania State University, University Park, PA
David P. Edmonds, Edison Welding Institute, Columbus, OH
John F. McIntyre, Advanced Polymer Sciences, Avon, OH
Harold S. Reemsnyder, Bethlehem Steel Corp., Bethlehem, PA
Bruce R. Somers, Lehigh University, Bethlehem, PA**

CS
11/11/83

RECENT SHIP STRUCTURE COMMITTEE PUBLICATIONS

Ship Structure Committee Publications - A Special Bibliography

- SSC-384 Post-Yield Strength of Icebreaking Ship Structural Members C. DesRochers, J. Crocker, R. Kumar, D. Brennan, B. Dick, S. Lantos 1995
- SSC-383 Optimum Weld-Metal Strength for High Strength Steel Structures R. Dexter and M. Ferrell 1995
- SSC-382 Reexamination of Design Criteria for Stiffened Plate Panels by D. Ghose and N. Nappi 1995
- SSC-381 Residual Strength of Damaged Marine Structures by C. Wiernicki, D. Ghose, N. Nappi 1995
- SSC-380 Ship Structural Integrity Information System by R. Schulte-Strathaus, B. Bea 1995
- SSC-379 Improved Ship Hull Structural Details Relative to Fatigue by K. Stambaugh, F. Lawrence and S. Dimitriakis 1994
- SSC-378 The Role of Human Error in Design, Construction and Reliability of Marine Structures by R. Bea 1994
- SSC-377 Hull Structural Concepts For Improved Producibility by J. Daidola, J. Parente, and W. Robinson 1994
- SSC-376 Ice Load Impact Study on the NSF R/V Nathaniel B. Palmer by J. St. John and P. Minnick 1995
- SSC-375 Uncertainty in Strength Models for Marine Structures by O. Hughes, E. Nikolaidis, B. Ayyub, G. White, P. Hess 1994
- SSC-374 Effect of High Strength Steels on Strength Considerations of Design and Construction Details of Ships by R. Heyburn and D. Riker 1994
- SSC-373 Loads and Load Combinations by A. Mansour and A. Thayamballi 1994
- SSC-372 Maintenance of Marine Structures: A State of the Art Summary by S. Hutchinson and R. Bea 1993
- SSC-371 Establishment of a Uniform Format for Data Reporting of Structural Material Properties for Reliability Analysis by N. Pussegoda, L. Malik, and A. Dinovitzer 1993
- SSC-370 Underwater Repair Procedures for Ship Hulls (Fatigue and Ductility of Underwater Wet Welds) by K. Grubbs and C. Zanis 1993
- SSC-369 Reduction of S-N Curves for Ship Structural Details by K. Stambaugh, D. Lesson, F. Lawrence, C-Y. Hou, and G. Banas 1993
- SSC-368 Probability Based Ship Design Procedures: A Demonstration by A. Mansour, M. Lin, L. Hovem, A. Thayamballi 1993
- SSC-367 Fatigue Technology Assessment and Strategies for Fatigue Avoidance in Marine Structures by C. C. Capanoglu 1993

hbl (hbl)

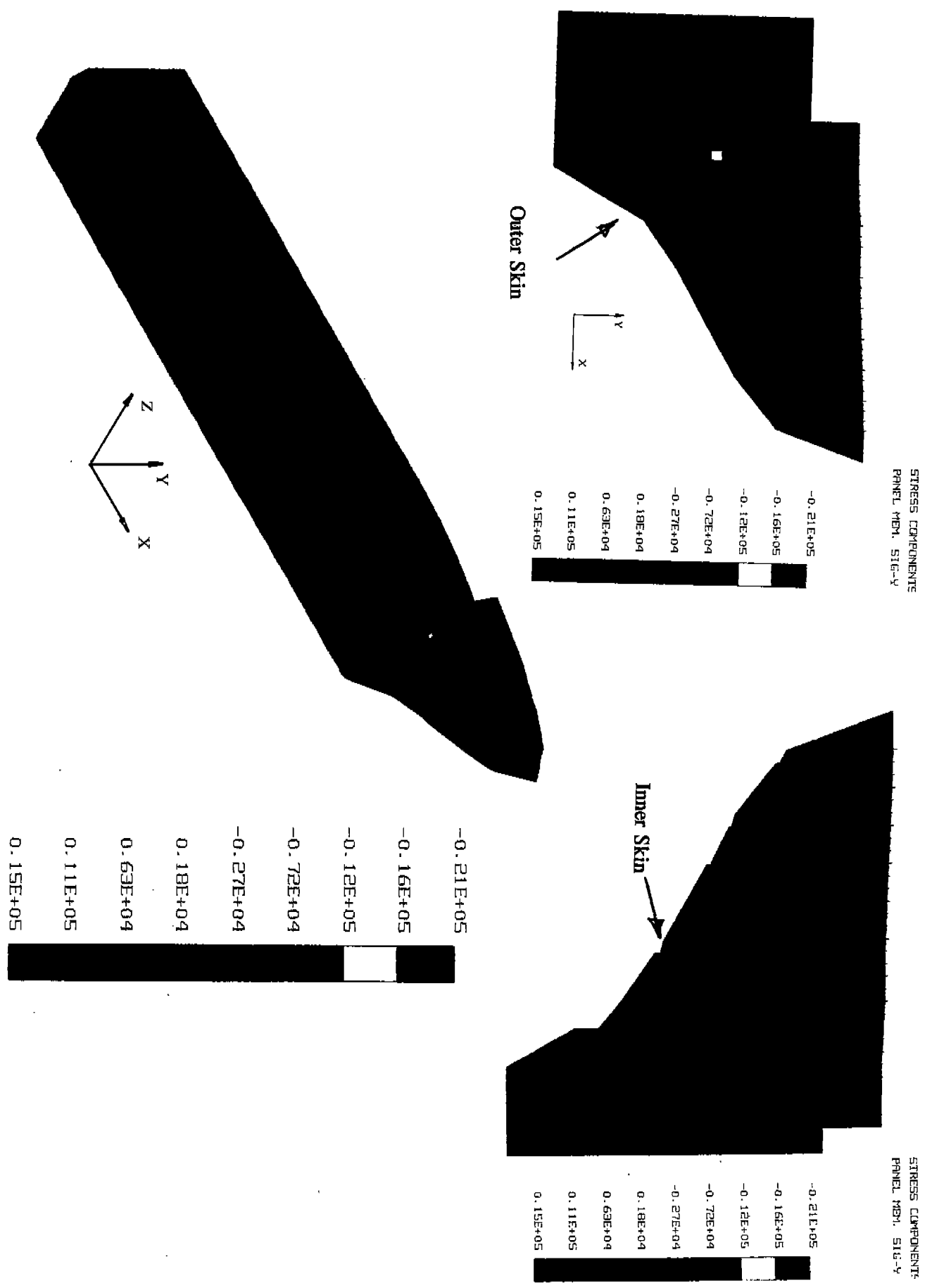


FIGURE 6.8: Vertical Stress in the Outer and Inner Shells — MAESTRO Analysis

143 (CP)

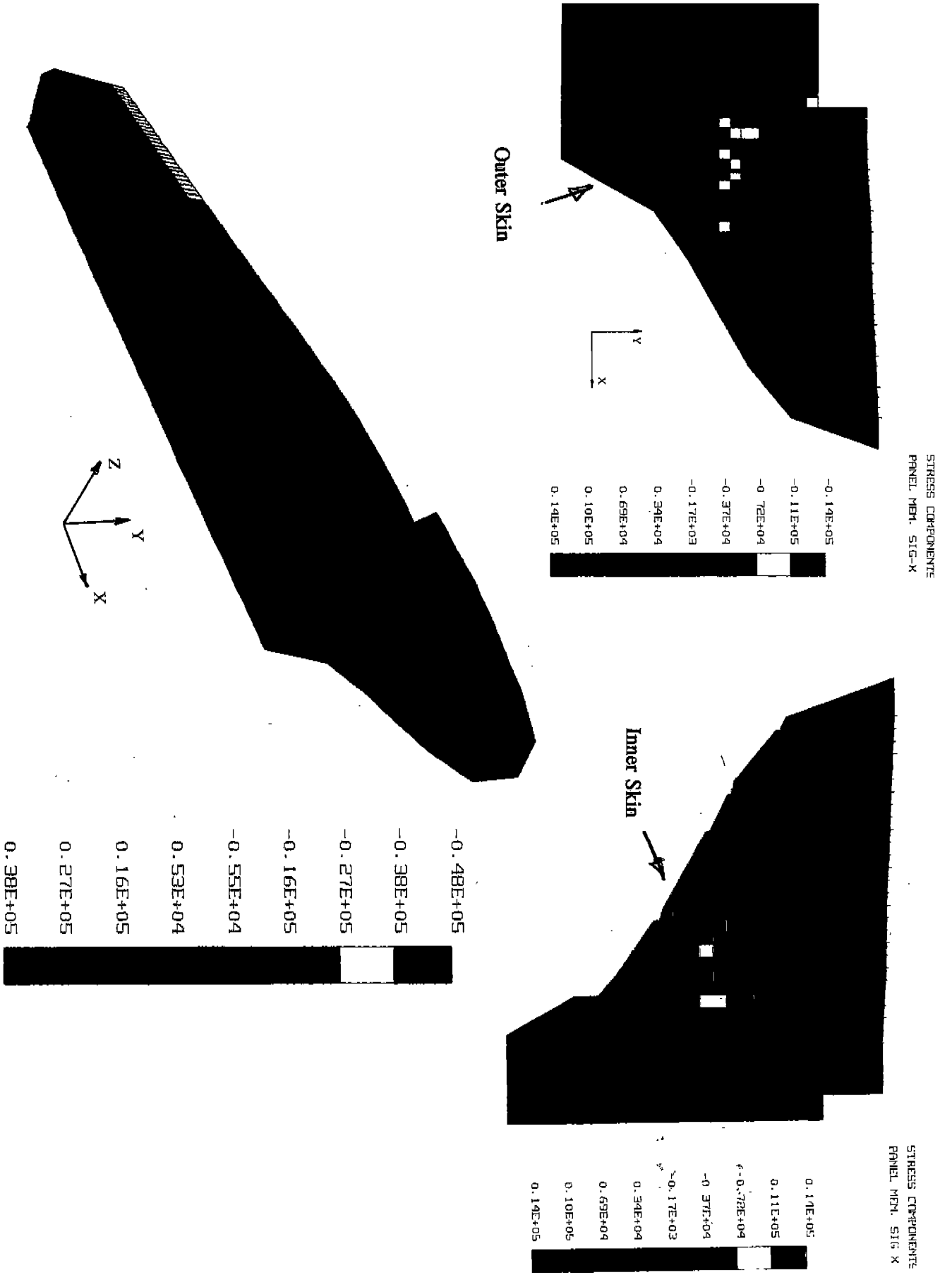
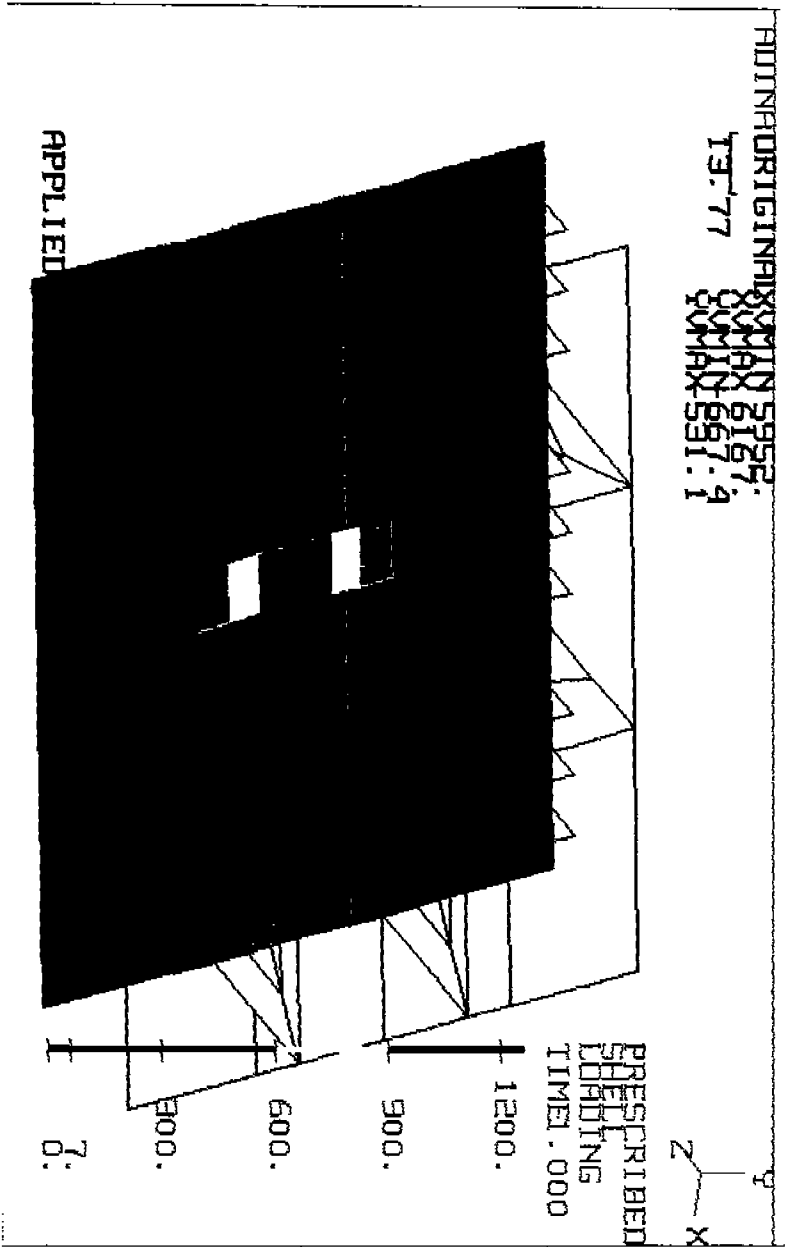


FIGURE 6.7: Longitudinal Stress Distribution in Outer and Inner Shells — MAESTRO Analysis

151



Note: Pressure is in PSI

FIGURE 6.11: Applied Load on ADINA Model

152

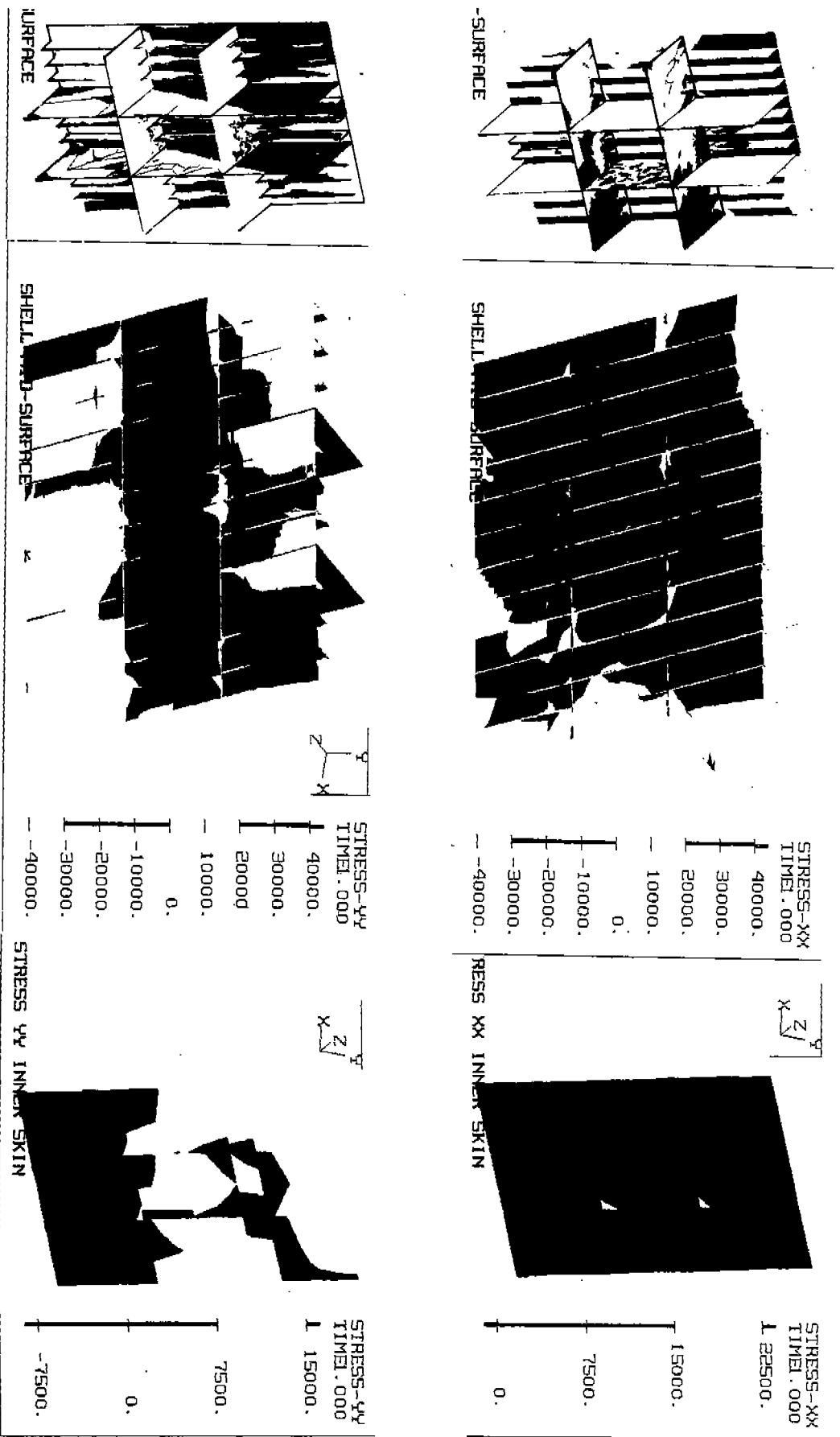


FIGURE 6.12: Linear Analysis Results for Bow Panel

661

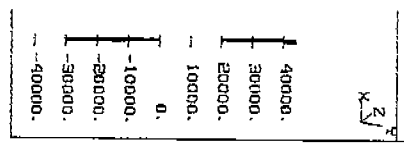
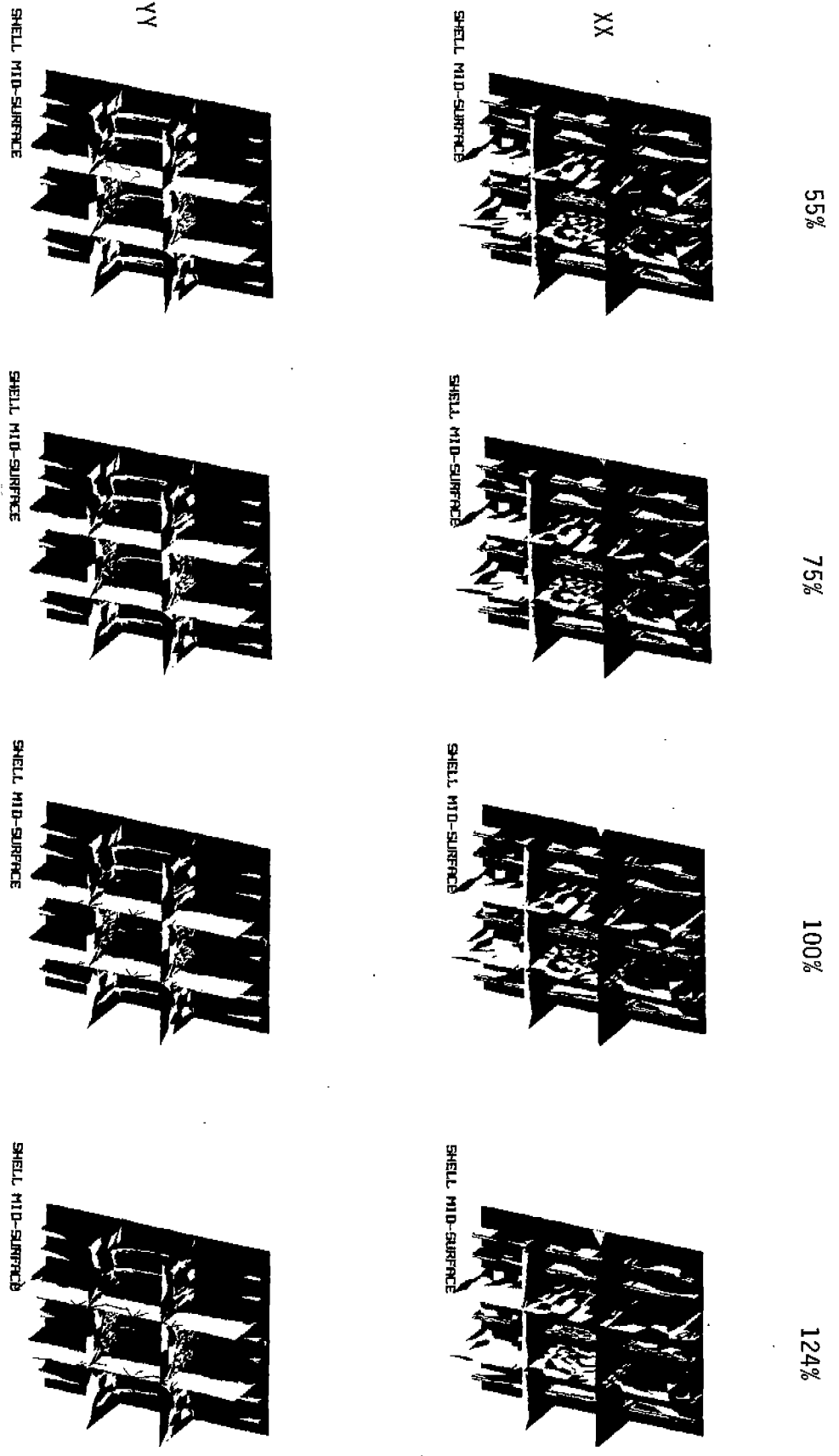


FIGURE 7.10: Overall SXX and SY Y Stresses
 - Nonlinear Analysis of the ASPPR Redesigned Angle Section Model

LSI

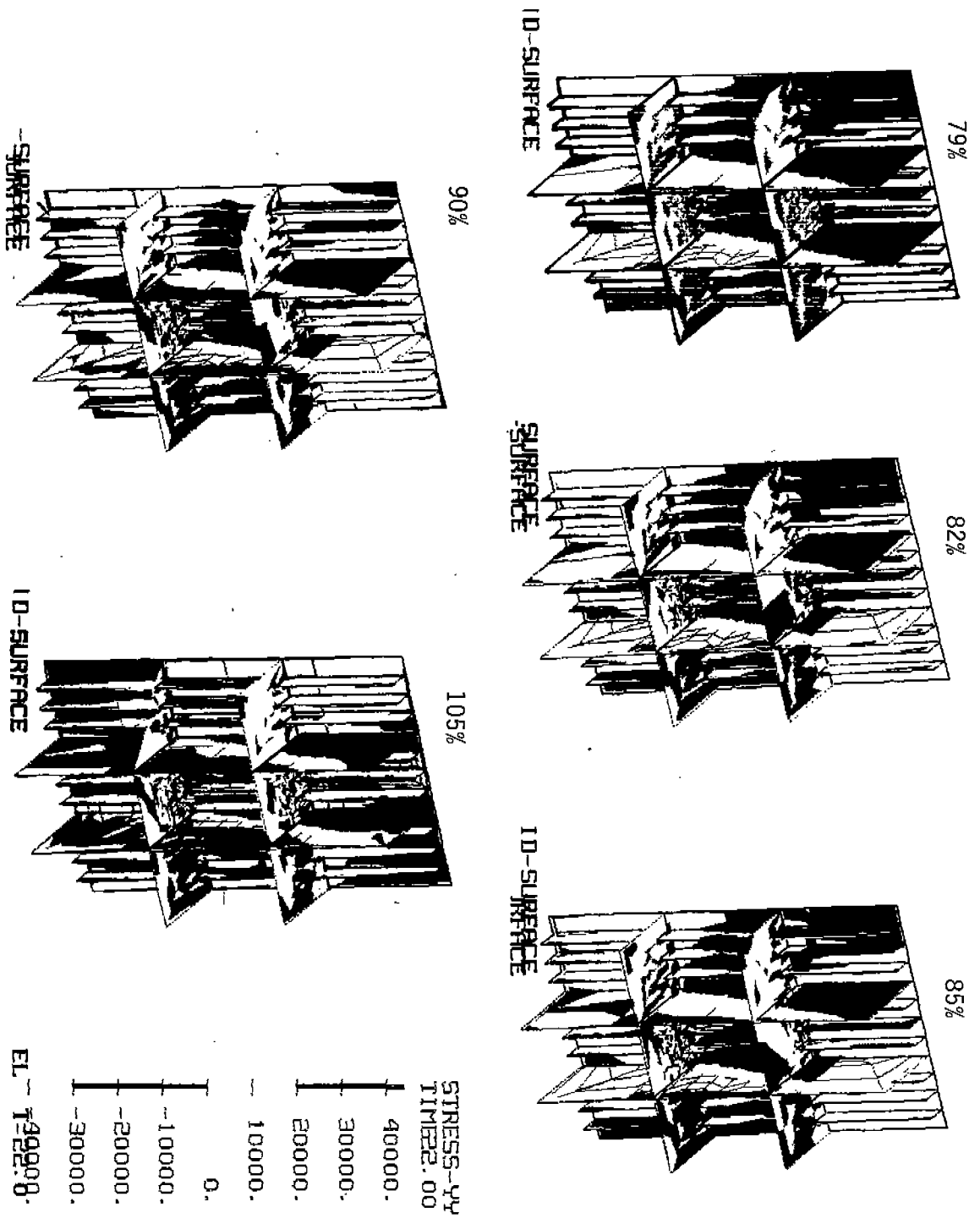
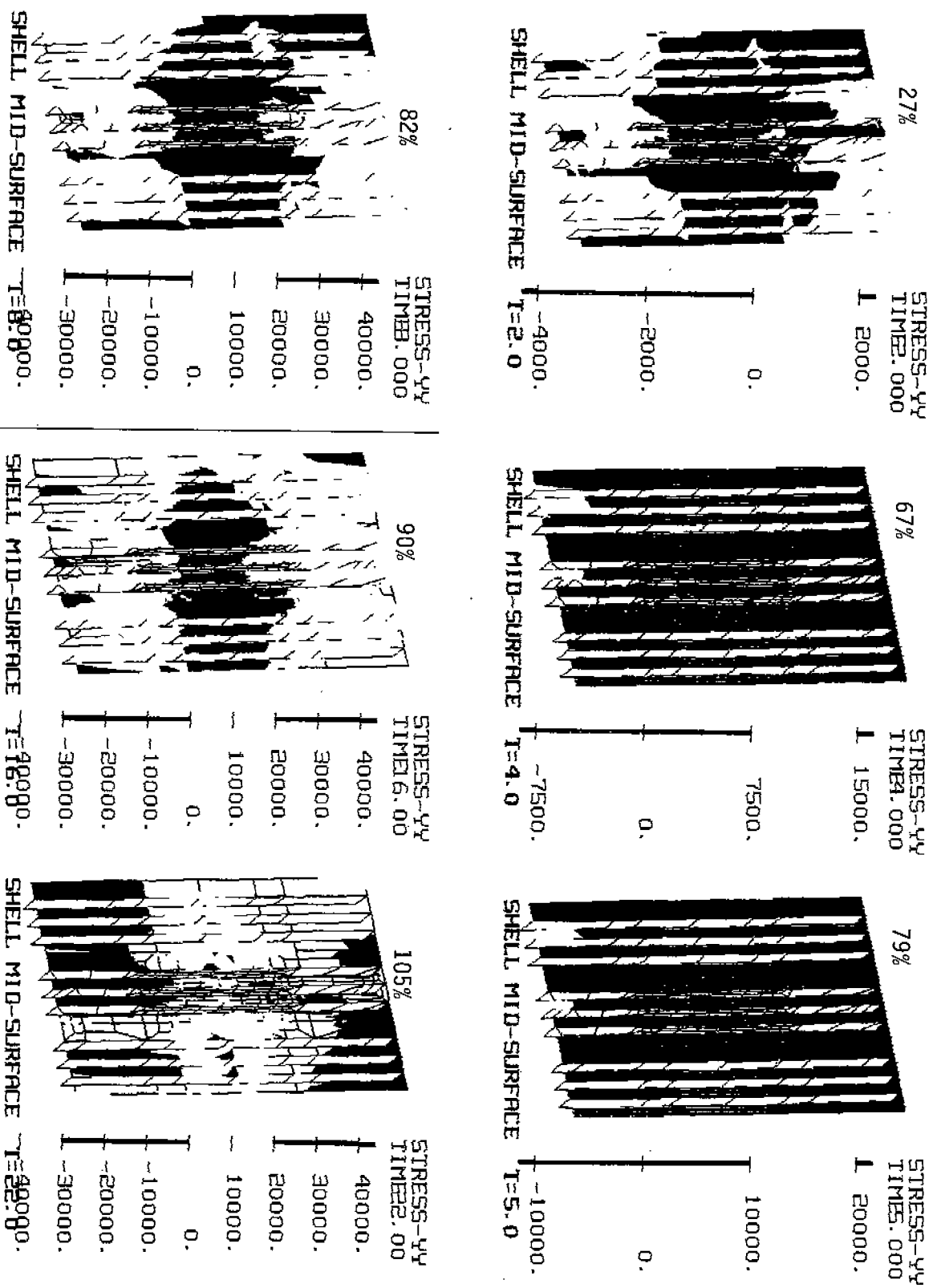


FIGURE 6.14: SYX Stress Contours in Panel Structure



158

FIGURE 6.15: SYX Stress in Outer Shell Plating

FIGURE 7.11: Center Bay SYX Stresses - Nonlinear Analysis of the ASPPR Redesigned Angle Section Model

MODEL CENTER PANEL_T=9.0 MODEL CENTER PANEL_T=11.0



124%

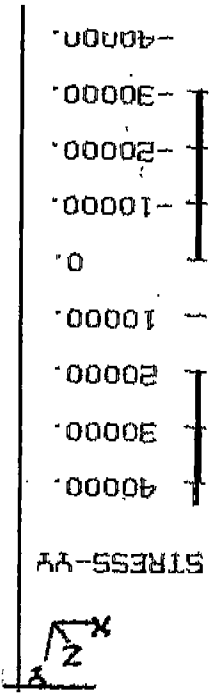
100%

MODEL CENTER PANEL_T=7.0 MODEL CENTER PANEL_T=5.0



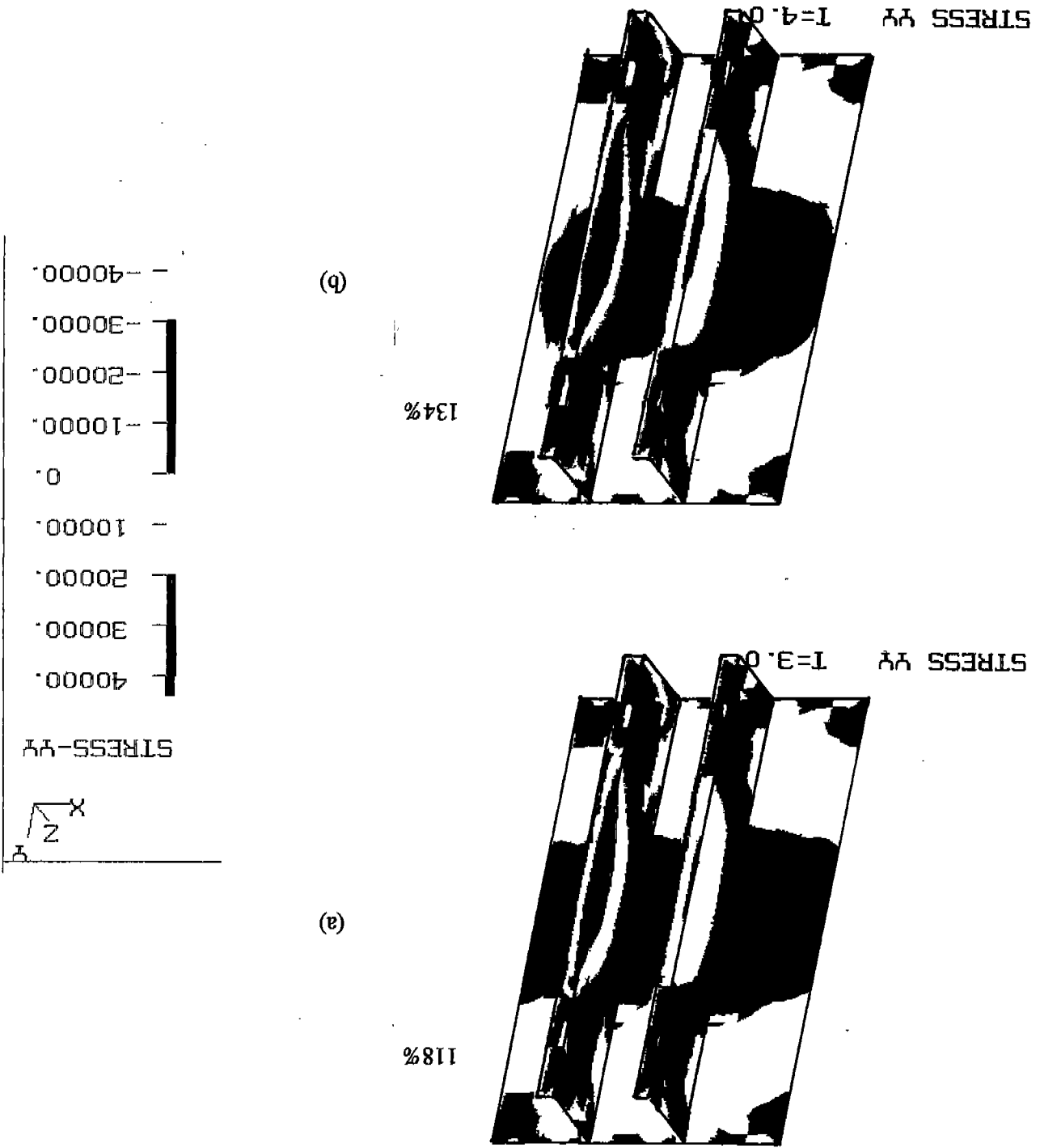
75%

55%



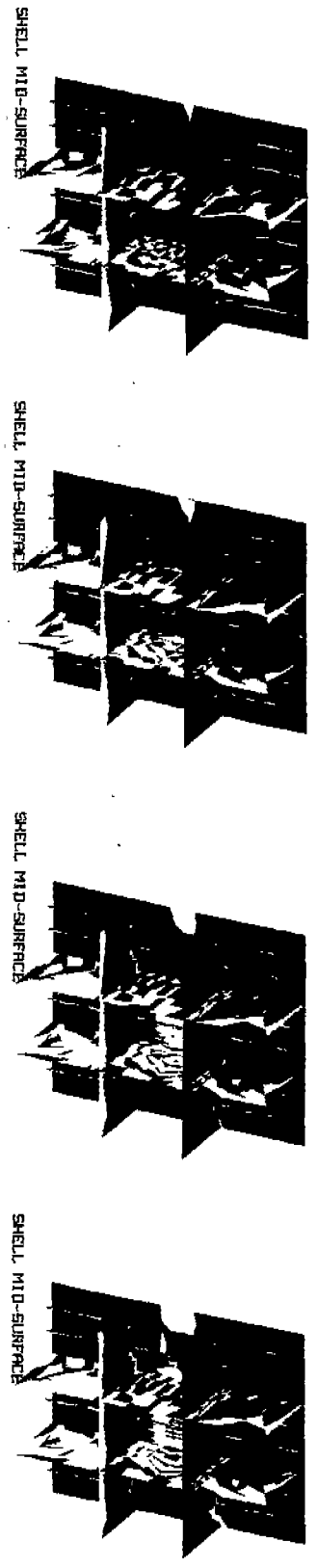
bec

FIGURE 9.9: SYX at Various Load STEPS - Nonlinear Analysis of Center Bay FE Model



60% 120% 145% 162%

XX



YY

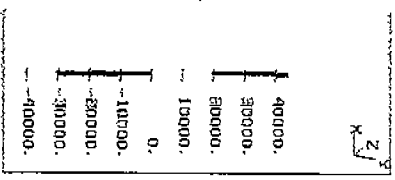
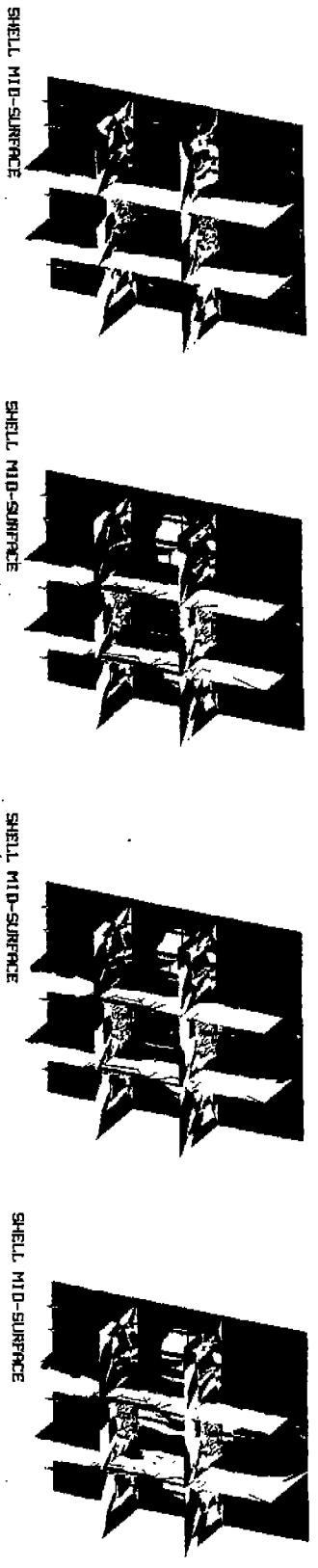


FIGURE 7.25: Overall SXX and SY Y Stresses
 - Nonlinear Analysis of Increased Slenderness 70° Canted Flat Bar Model

FIGURE 7.26: Progression of Yield - Nonlinear Analysis of Increased Slenderness 70° Canted Flat Bar Model

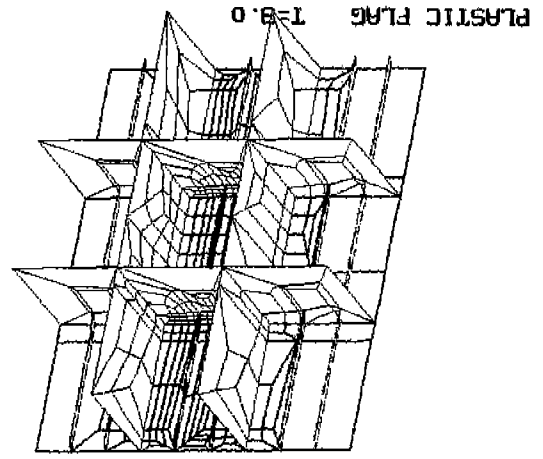
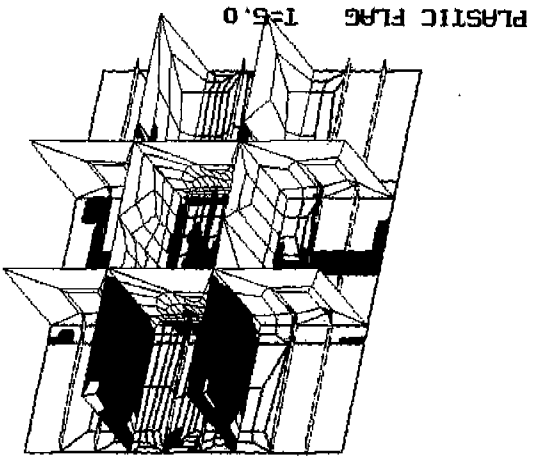
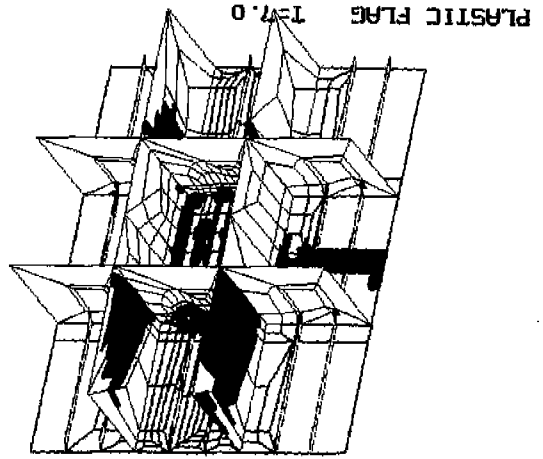
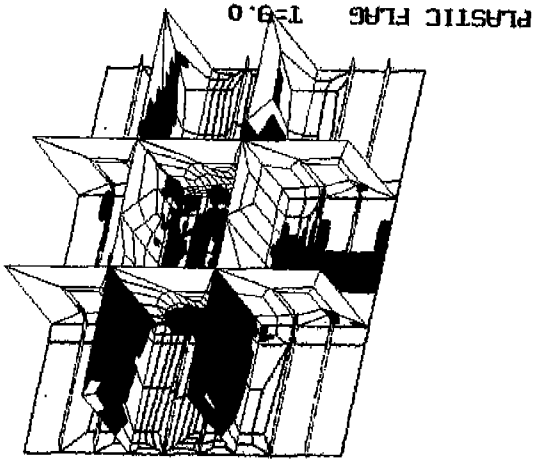
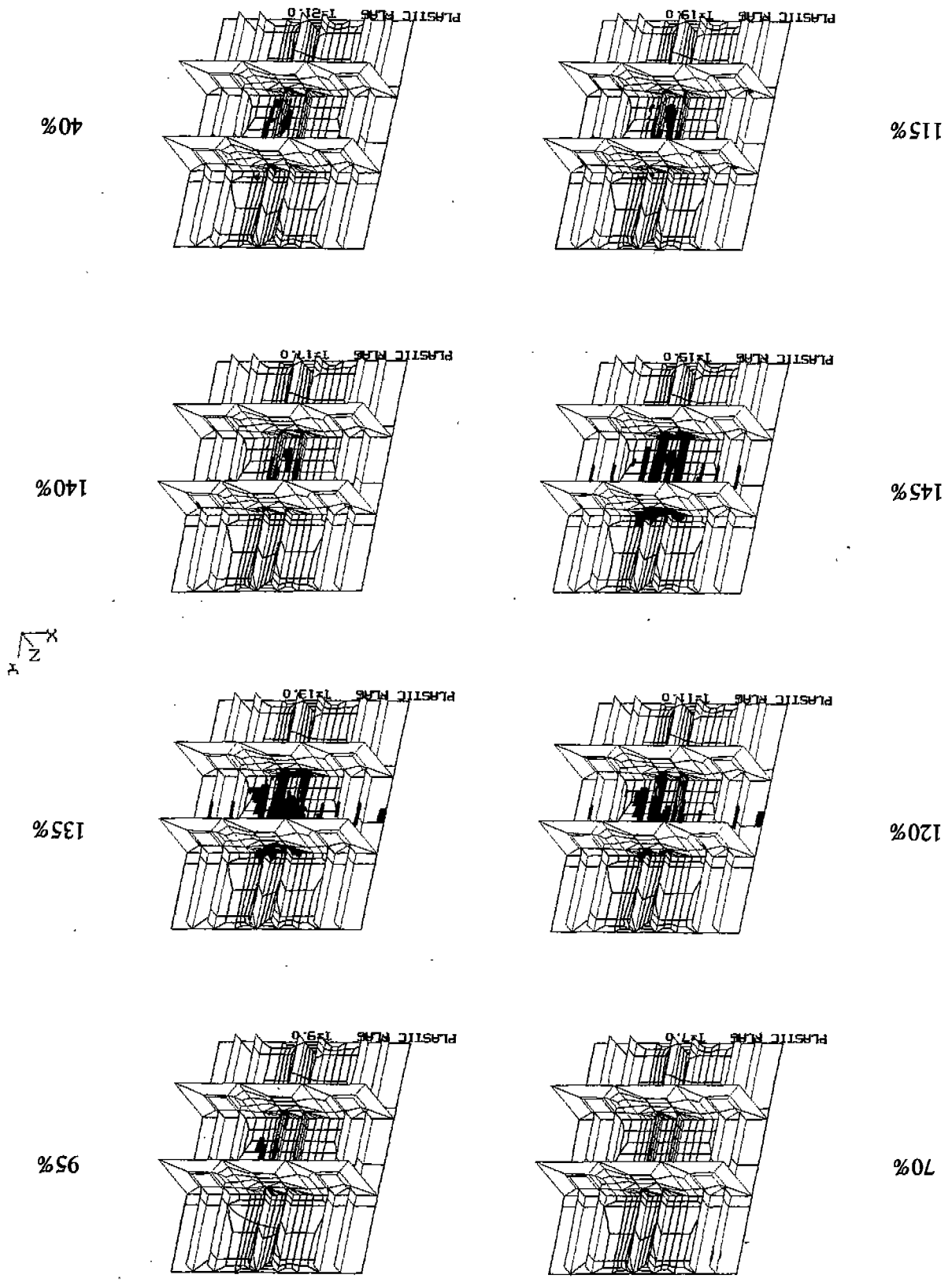


FIGURE 5.19: Progression of Yield at Various Percentages of F_{max} - Nonlinear Analysis of ASPPR Redesigned Midbody Structure

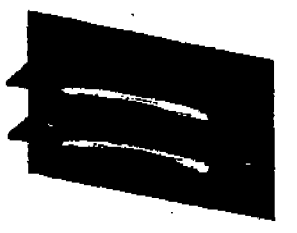


811

(11)



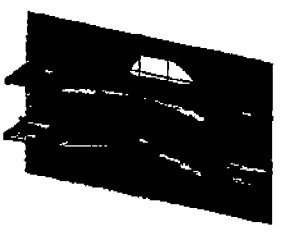
MODEL CENTER PANEL - T=9:0



MODEL CENTER PANEL - T=9:0



MODEL CENTER PANEL - T=10:0



MODEL CENTER PANEL - T=12:0



MODEL CENTER PANEL - T=14:0



MODEL CENTER PANEL - T=15:0



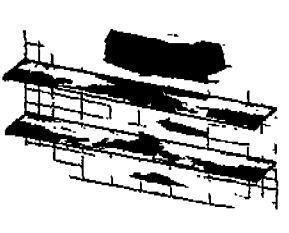
MODEL CENTER PANEL - T=16:0



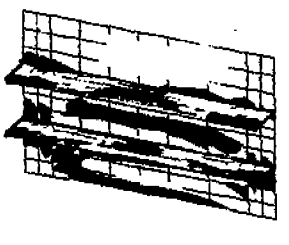
MODEL CENTER PANEL - T=17:0



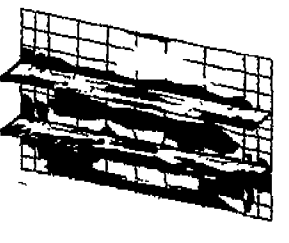
MODEL CENTER PANEL - T=18:0



MODEL CENTER PANEL - T=19:0



MODEL CENTER PANEL - T=20:0



MODEL CENTER PANEL - T=22:0

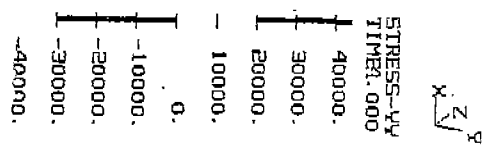


FIGURE 5.24: Displaced Shape of the Center Bay at Various Load Levels - Nonlinear Analysis of ASPPR Redesigned Midbody FB Model

170

FIGURE 7.4: Overall SYY Stress at Various Load Levels - Nonlinear Analysis of the ASPPR Redesigned TEB Section Model

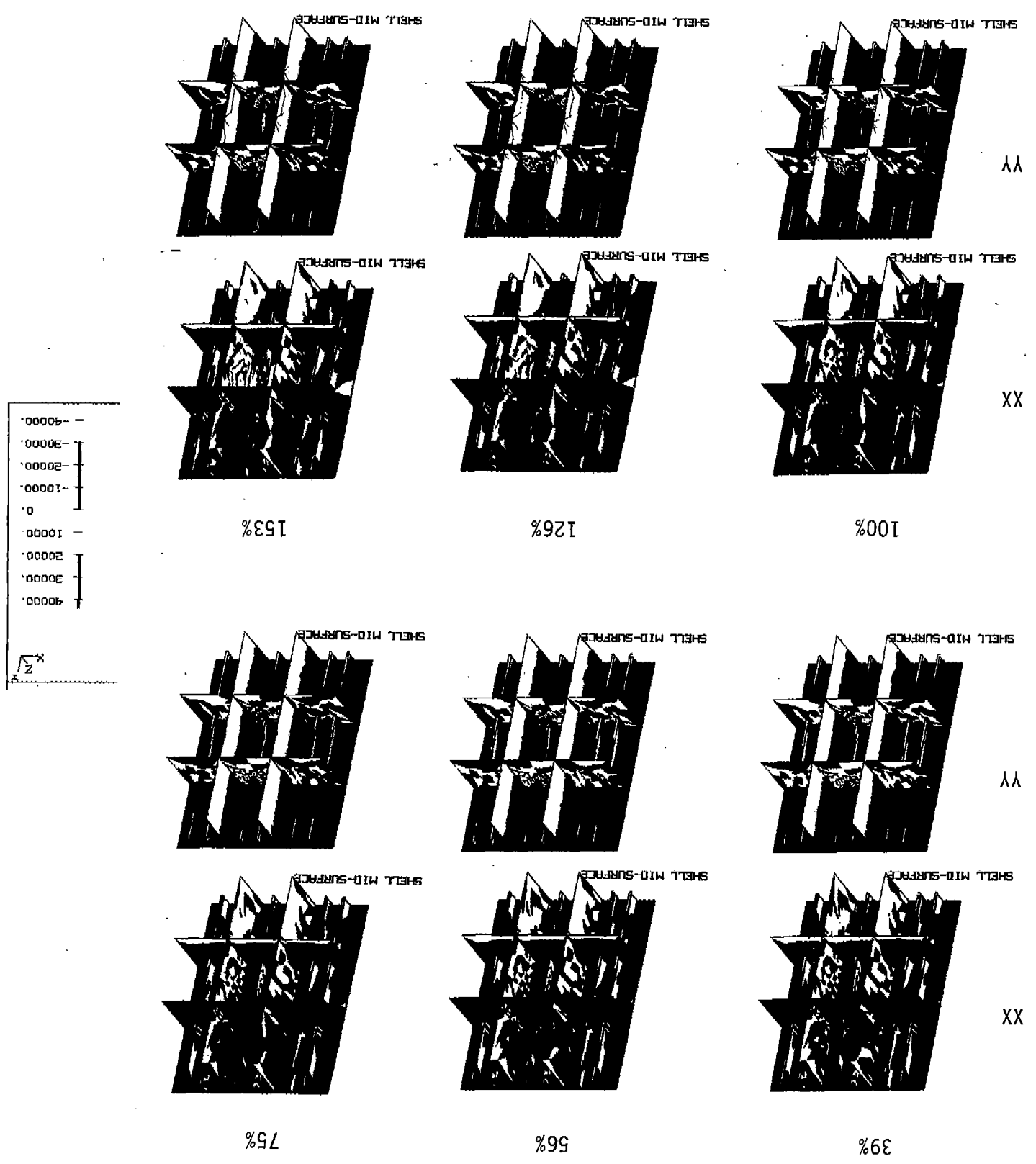


FIGURE 5.27: Progression of Yield - Nonlinear Analysis of ASPPR Redesigned FH Model With Modified Stringer Mesh

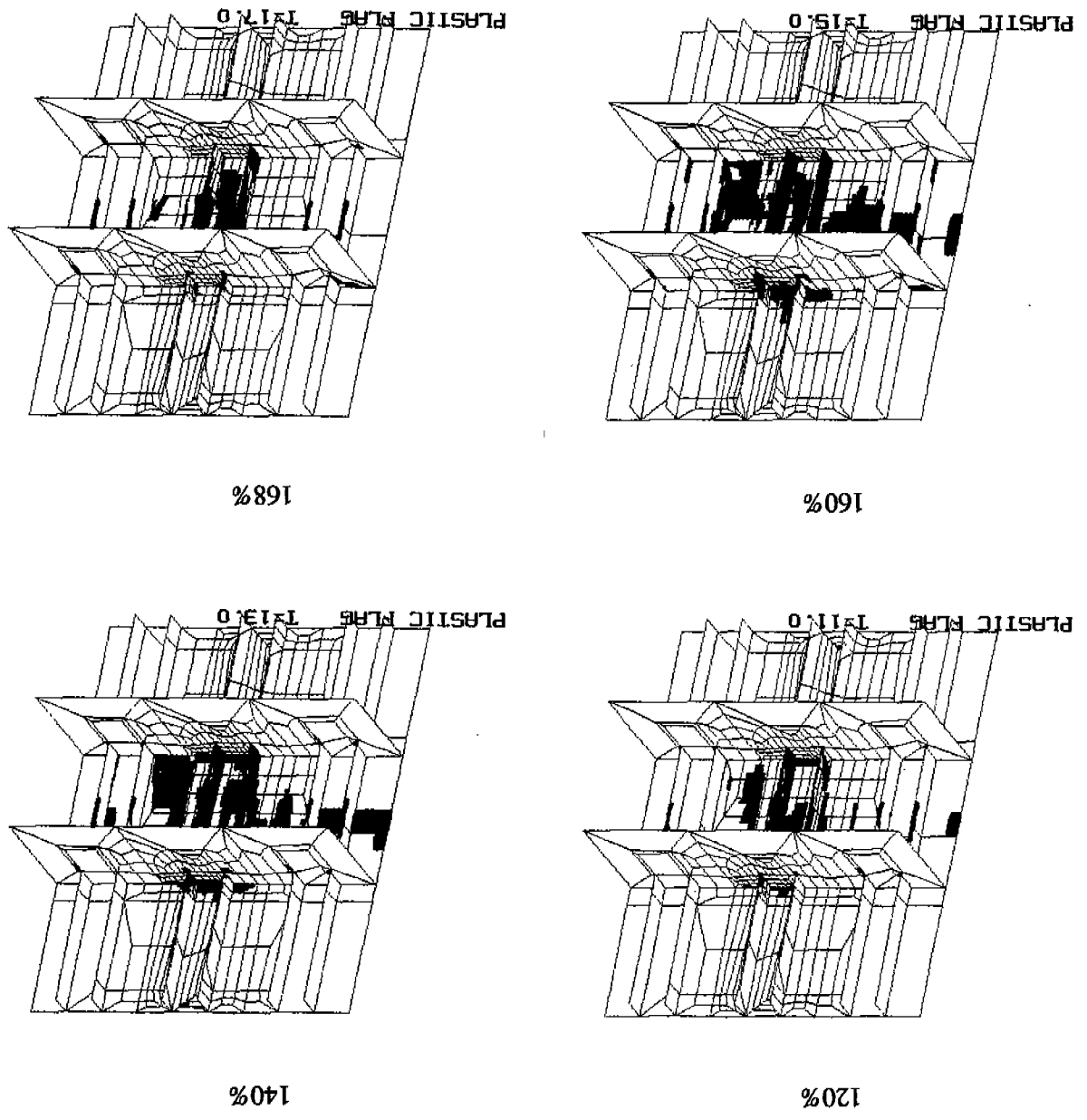
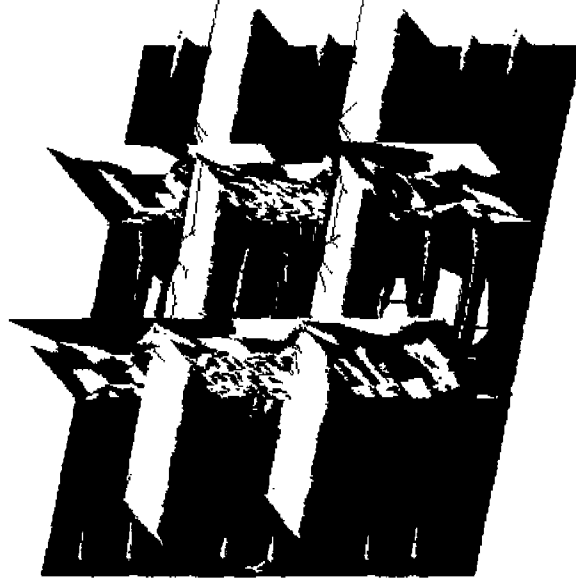


FIGURE 8.7: Overall SYY Stresses - Nonlinear Analysis of ASPFR Redesigned Flat Bar Section With and Without Strain Hardening

(b) With Strain Hardening

SYY SHELL MID-SURFACE I=13.0



(a) Without Strain Hardening

SYY SHELL MID-SURFACE I=15.0

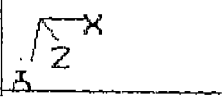
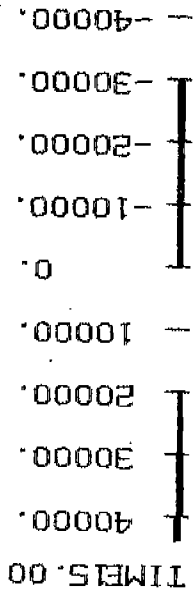
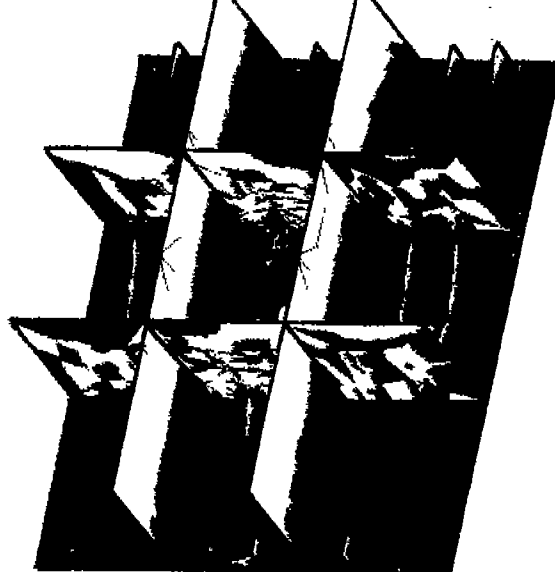
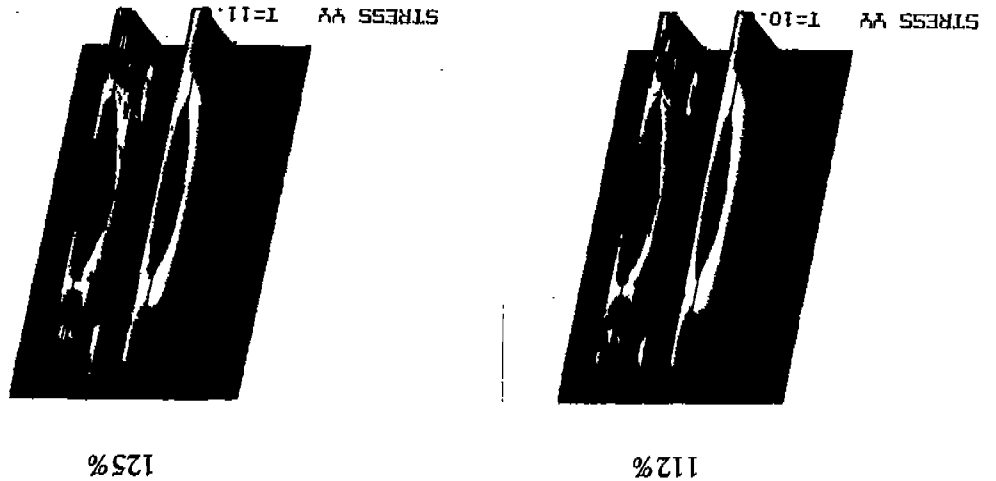
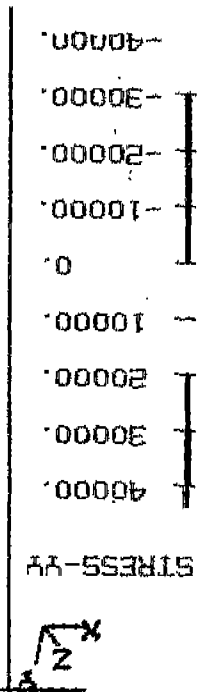
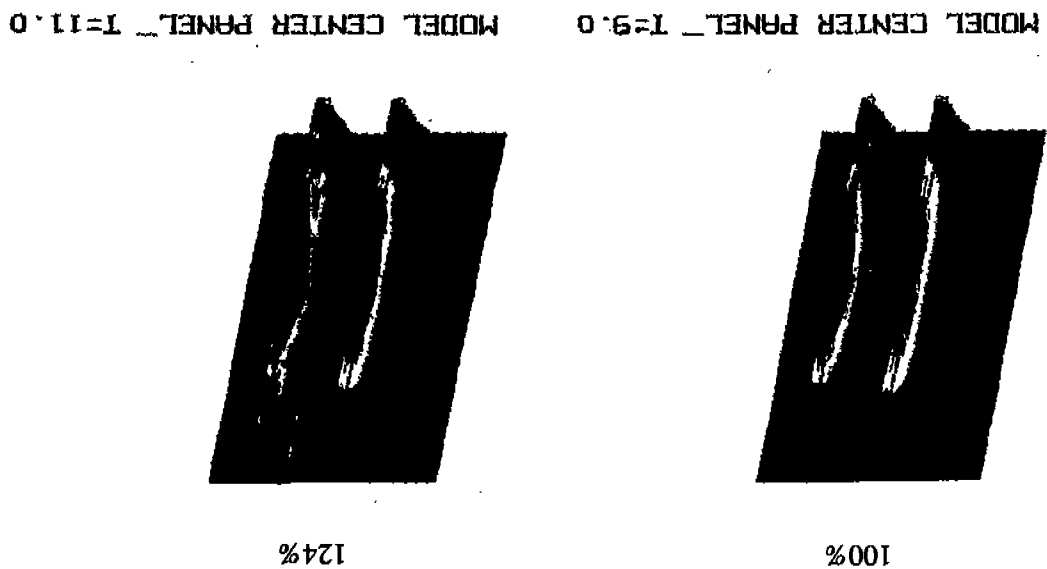


FIGURE 8.4: SYX at Center Bay - Nonlinear Analysis of ASPFR Redesigned Angle Section With and Without Strain Hardening

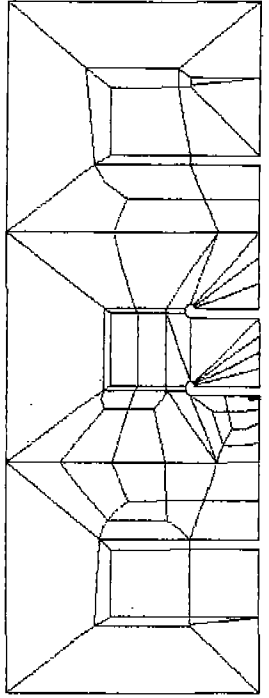
(b) With Strain Hardening



(a) Without Strain Hardening

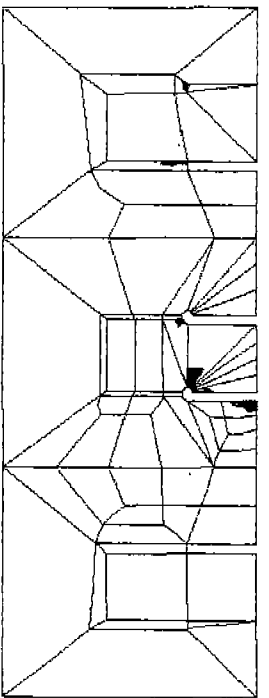


59%



PLASTIC FLAG T=3.0

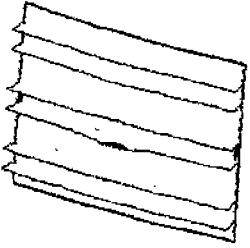
86%



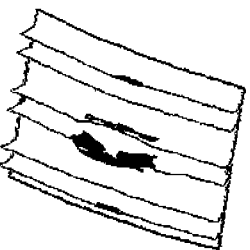
PLASTIC FLAG T=4.0

(a)

x
z



PLASTIC FLAG T=3.0



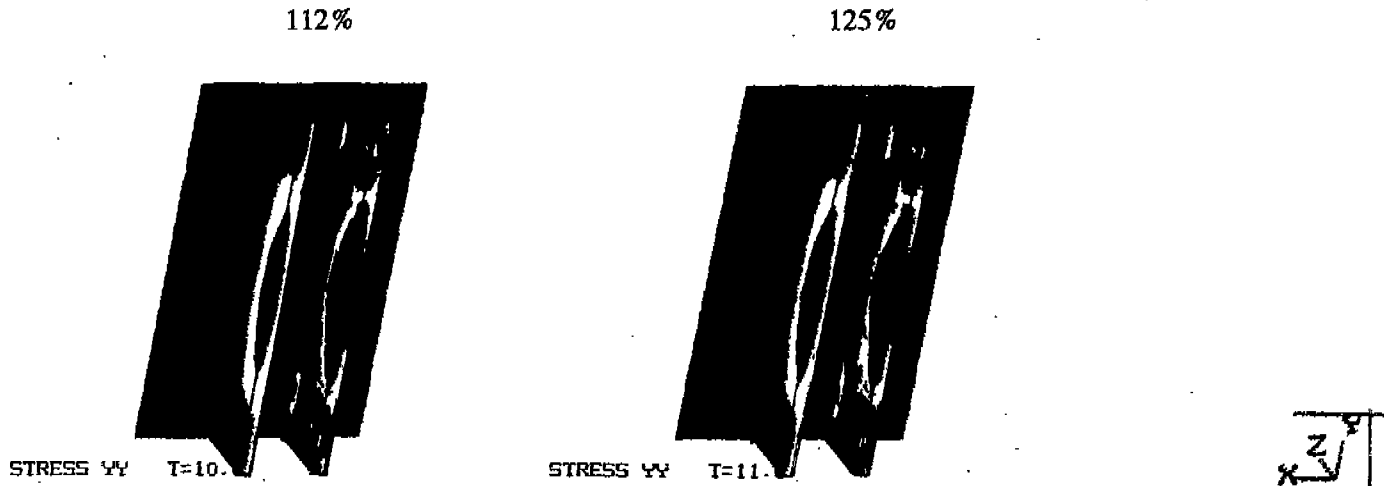
PLASTIC FLAG T=4.0

x
z

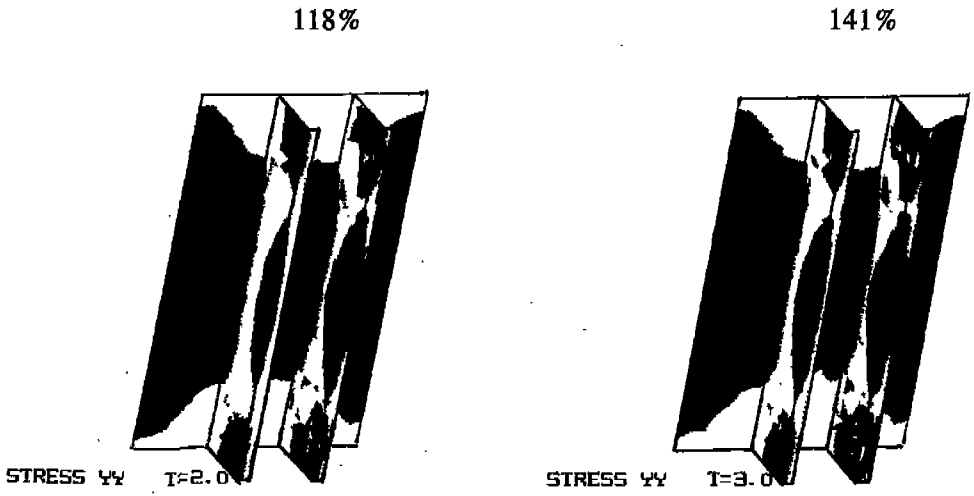
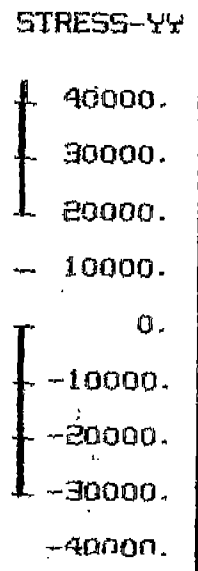
(b)

193

FIGURE 7.20: Progression of Yield
- Nonlinear Analysis of the ASPPR Redesigned Increased Slenderness Flat Bar Model

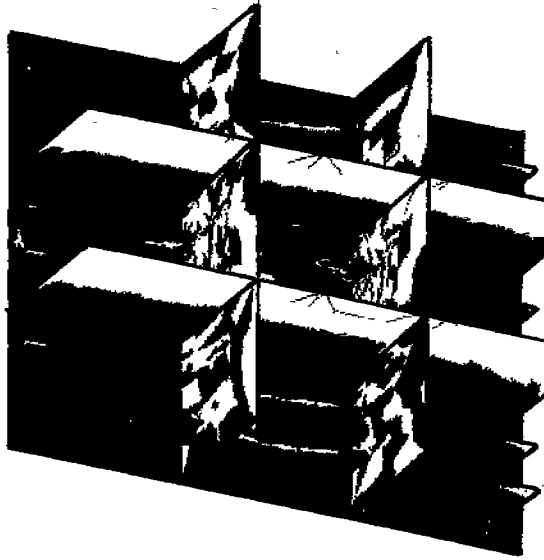


(a) MAESTRO Boundary Conditions

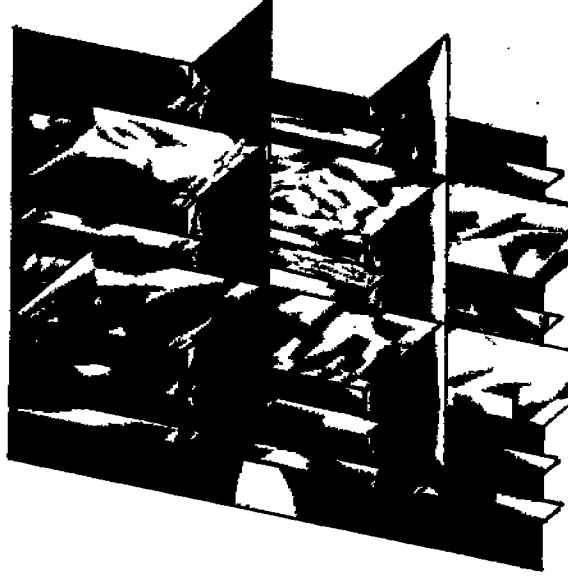


(b) FIXED Boundary Conditions

FIGURE 9.3: SYY Stresses on the Center Bay
 - Nonlinear Analysis of ASPPR Redesigned Midbody Model
 Comparing Angle Sections With MAESTRO and Fixed Boundary Conditions



SYX SHELL MID-SURFACE Y=15.0



SYX SHELL MID-SURFACE Y=15.0

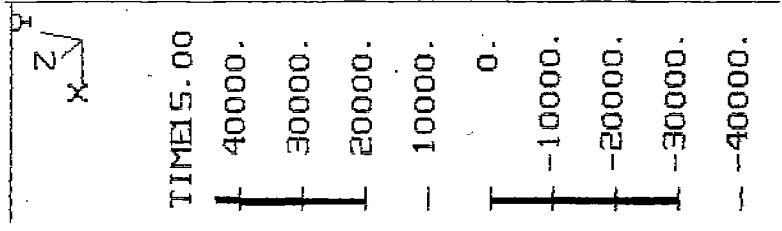


FIGURE 5.22: SYX Stress at 140% of F_{max}
 - Nonlinear Analysis of ASPPR Redesigned Midbody FE Model

125

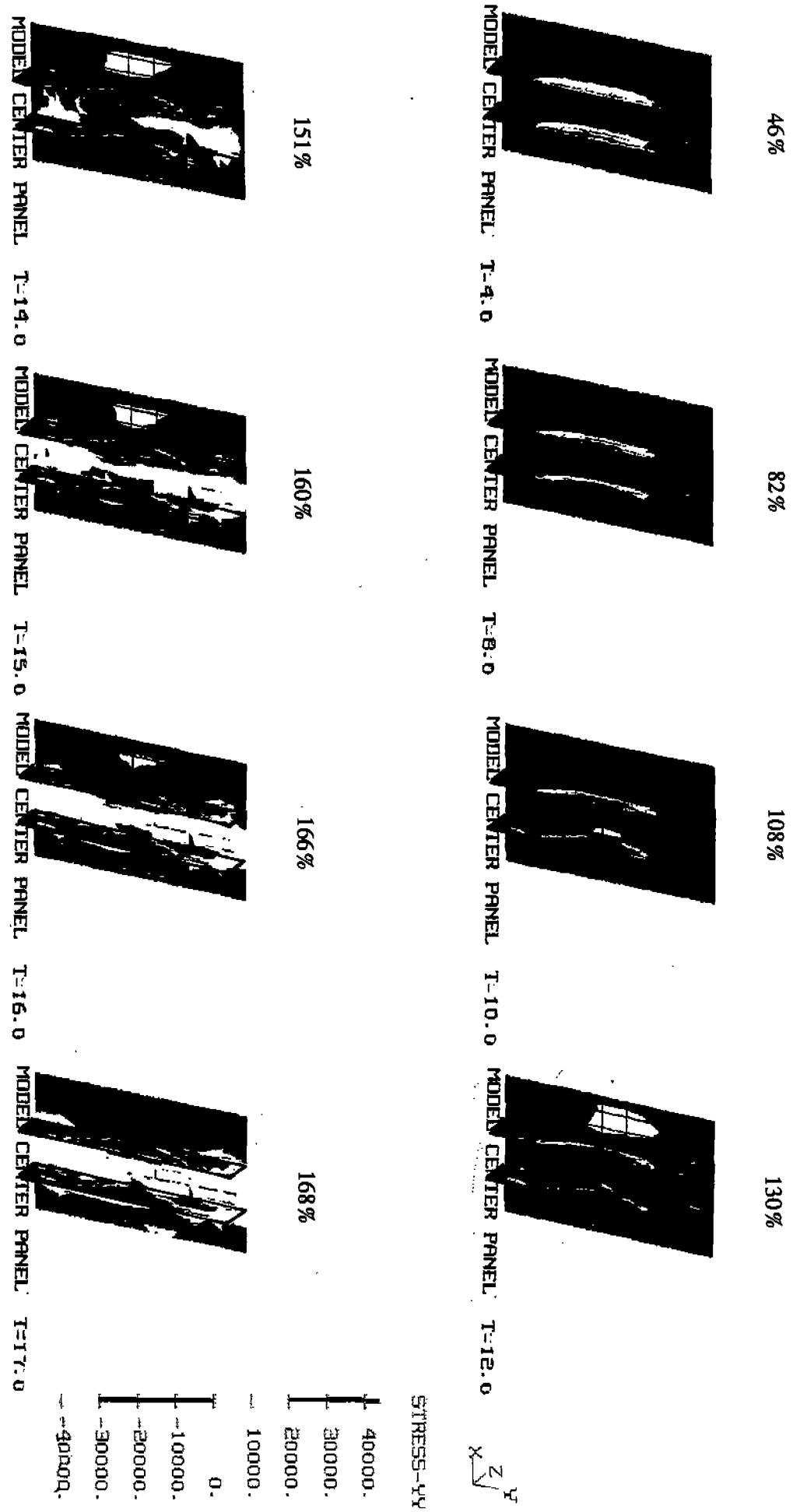
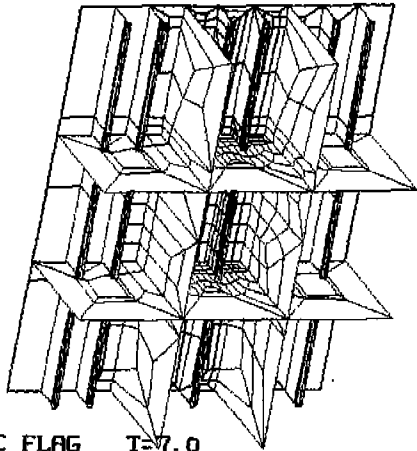


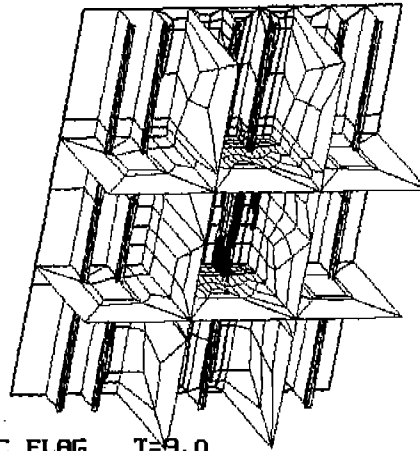
FIGURE 5.29: SYX on the Center Bay at Various Load Levels
- Nonlinear Analysis of ASPPR Redesigned FE Model With Modified Stringer Mesh

75%



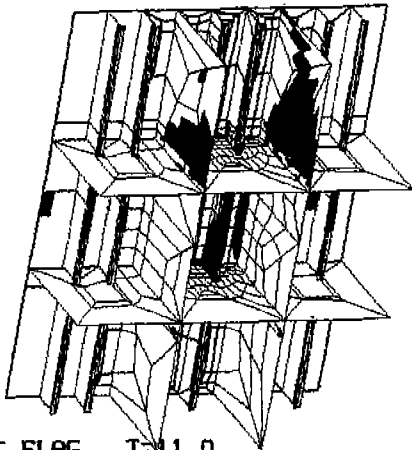
PLASTIC FLAG T=7.0

100%



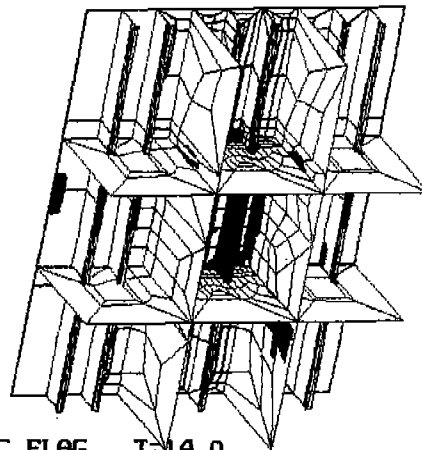
PLASTIC FLAG T=9.0

126%



PLASTIC FLAG T=11.0

153%



PLASTIC FLAG T=14.0



FIGURE 7.6: Progression of Yield
- Nonlinear Analysis of the ASPPR Redesigned TEE Section Model

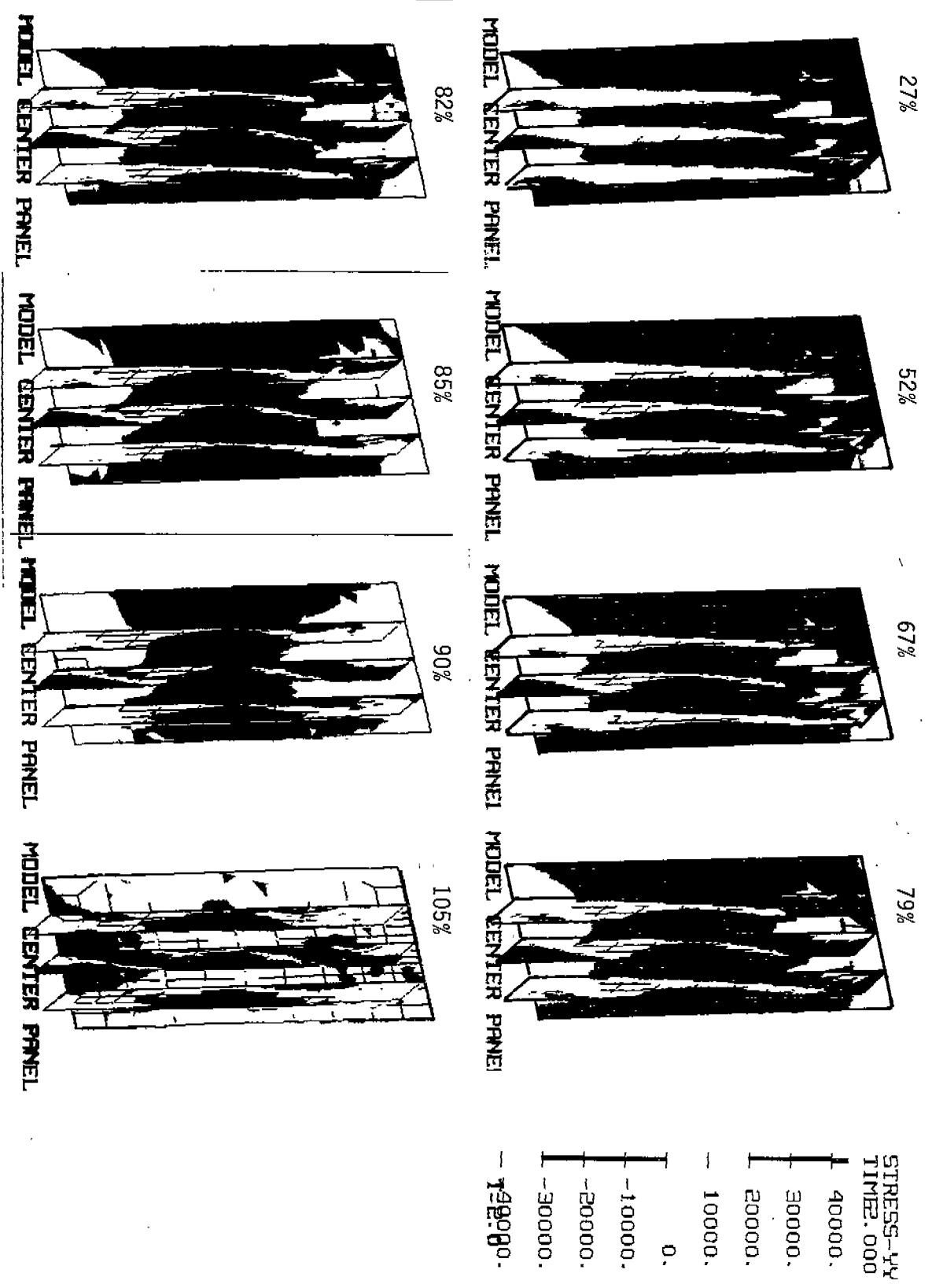


FIGURE 6.17: SY Y Stress in Main Frames at Center Bay

90%

138%

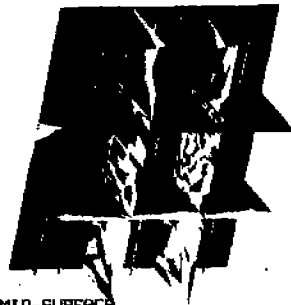
161%

178%

XX



SHELL MID-SURFACE



SHELL MID-SURFACE

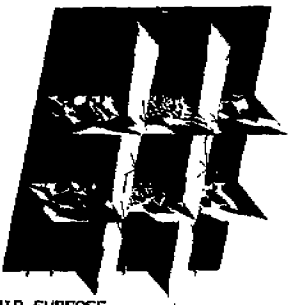


SHELL MID-SURFACE

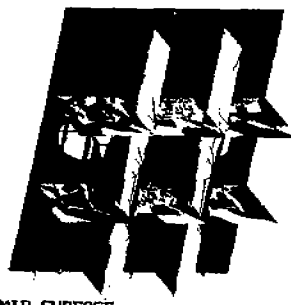


SHELL MID-SURFACE

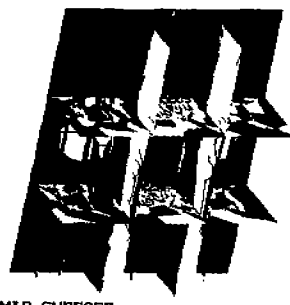
YY



SHELL MID-SURFACE



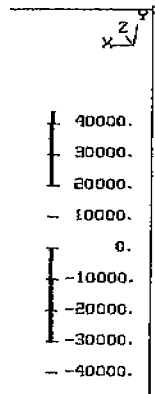
SHELL MID-SURFACE



SHELL MID-SURFACE



SHELL MID-SURFACE

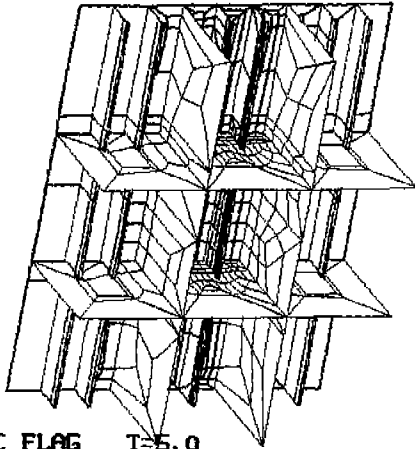


185

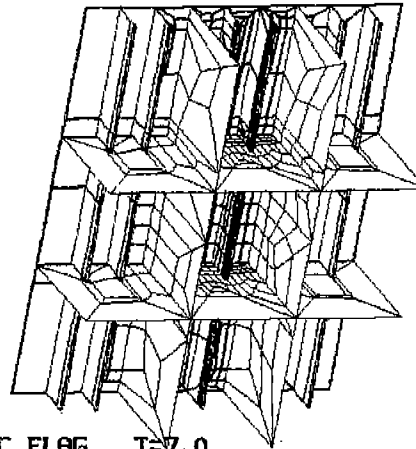
FIGURE 7.15: Overall SXX and SYY Stresses
 - Nonlinear Analysis of the ASPPR Redesigned Canted 70° Flat Bar Model

55%

75%



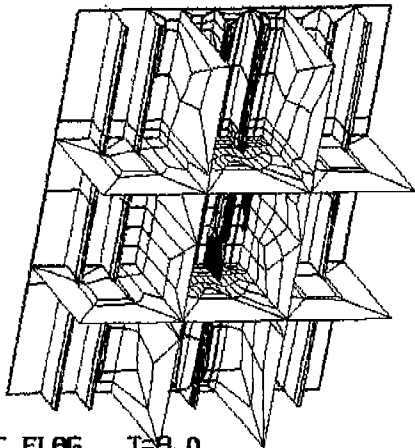
PLASTIC FLAG T=5.0



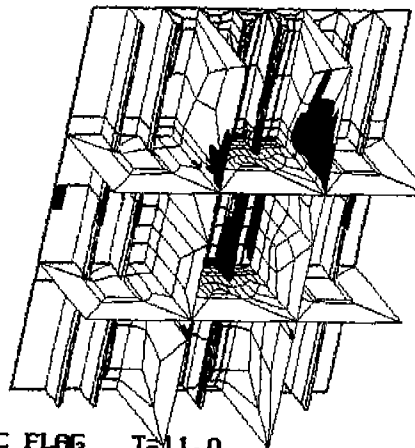
PLASTIC FLAG T=7.0

100%

124%



PLASTIC FLAG T=9.0



PLASTIC FLAG T=11.0

FIGURE 7.12: Progression of Yield
- Nonlinear Analysis of the ASPPR Redesigned Angle Section Model

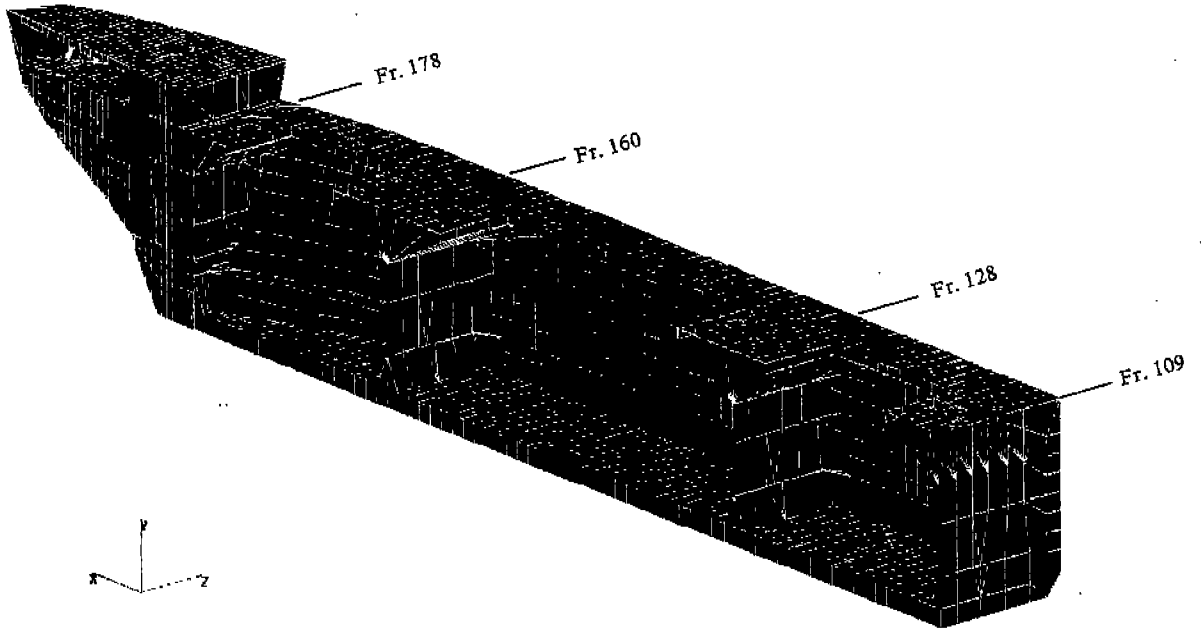
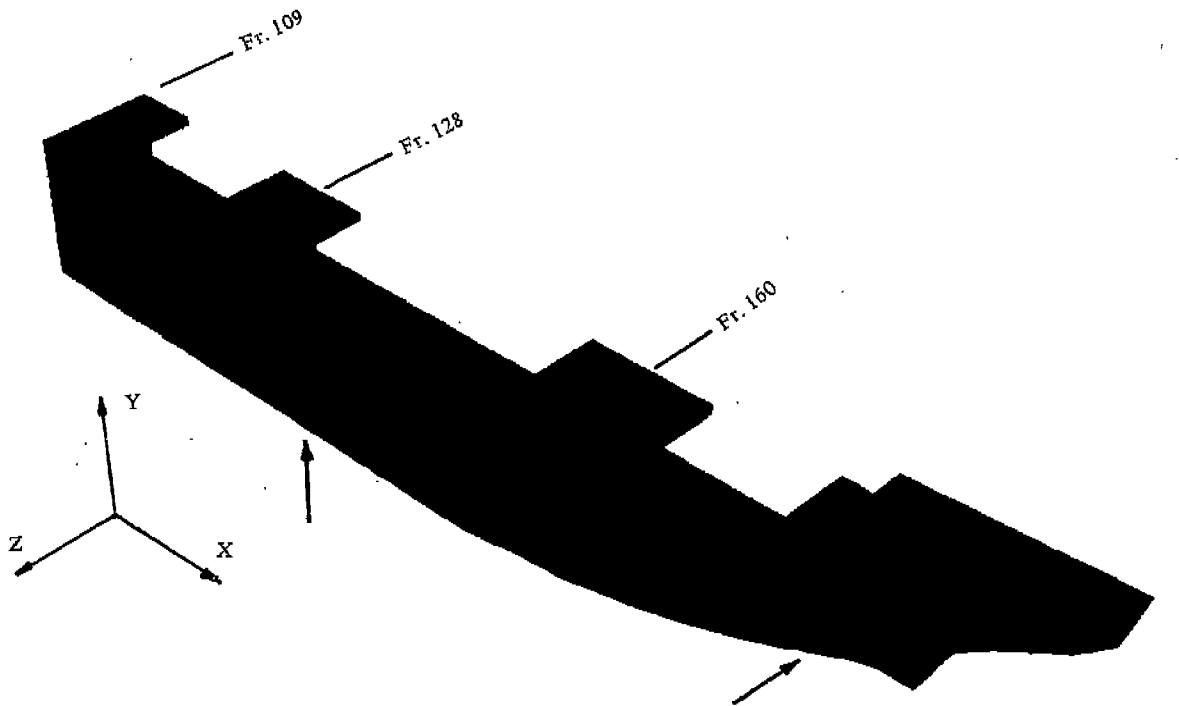


FIGURE 5.1: MAESTRO Model of the M.V. ARCTIC (Showing the Main Bulkheads Locations)

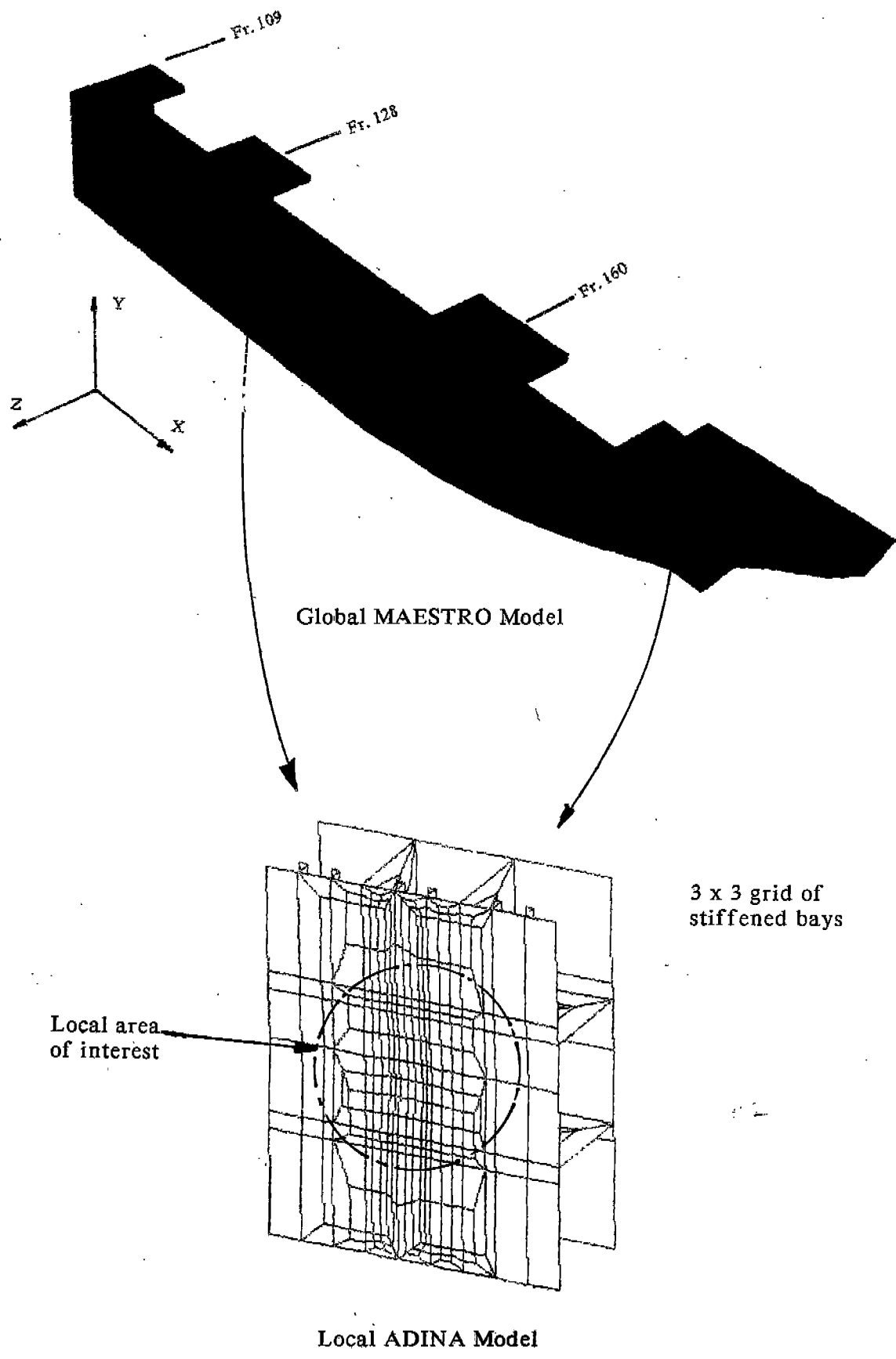
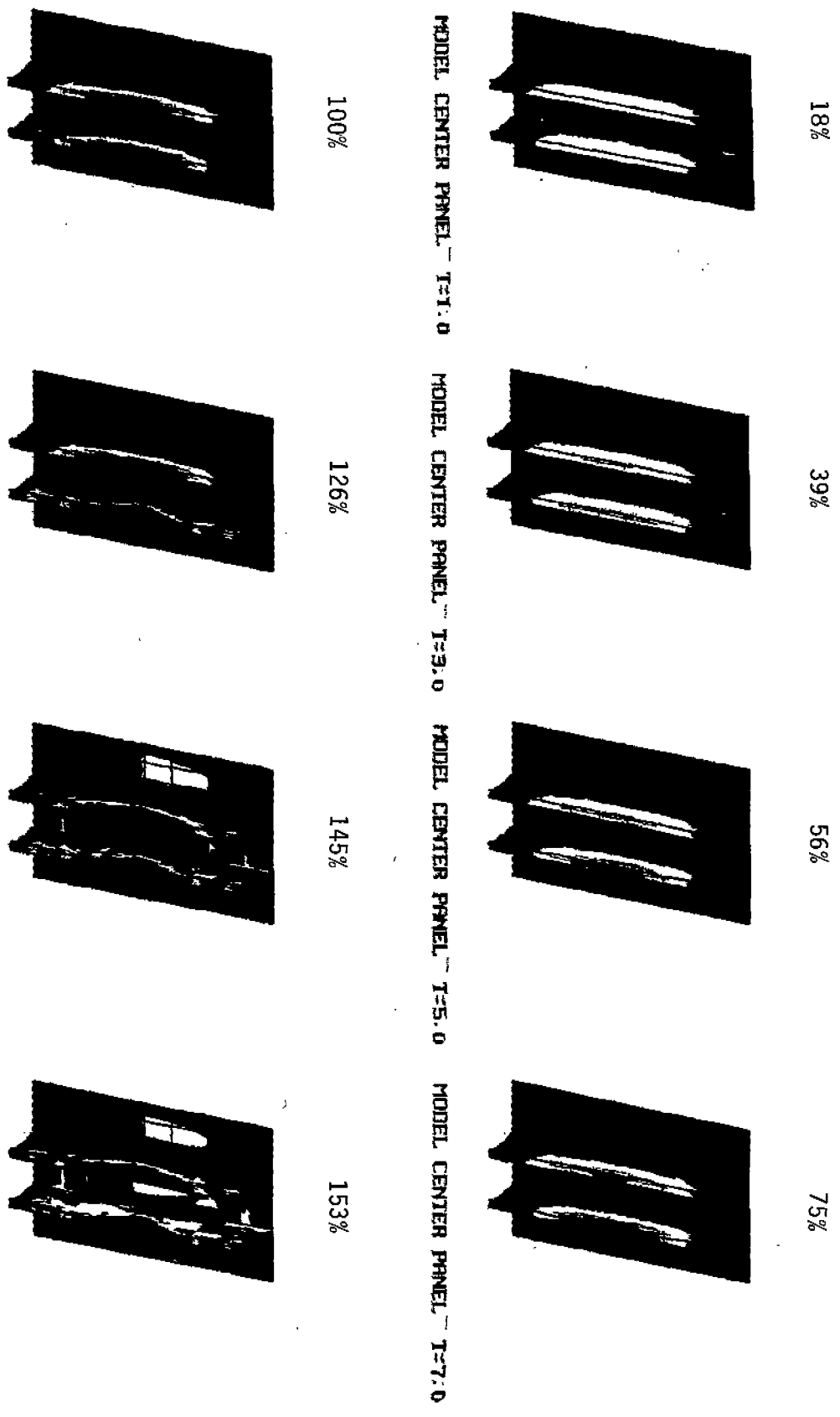


FIGURE 4.2: Location of Midbody and Bow FE Models on the MV Arctic



MODEL CENTER PANEL T=9.0 MODEL CENTER PANEL T=11.0 MODEL CENTER PANEL T=13.0 MODEL CENTER PANEL T=14.0

171

FIGURE 7.5: Center Bay SYX Stress at Various Load Levels
 - Nonlinear Analysis of the ASPPR Redesigned TEB Section Model

159

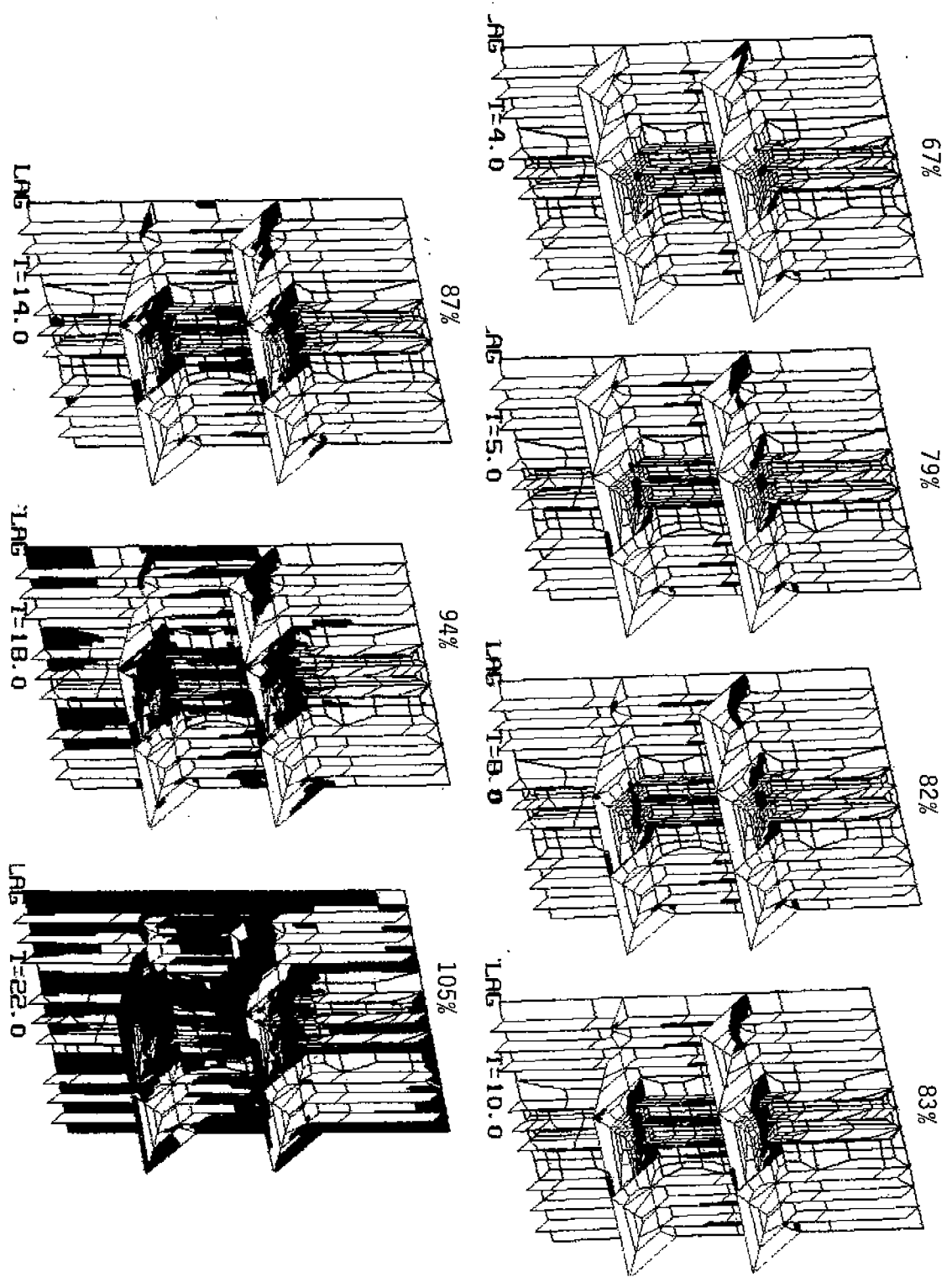
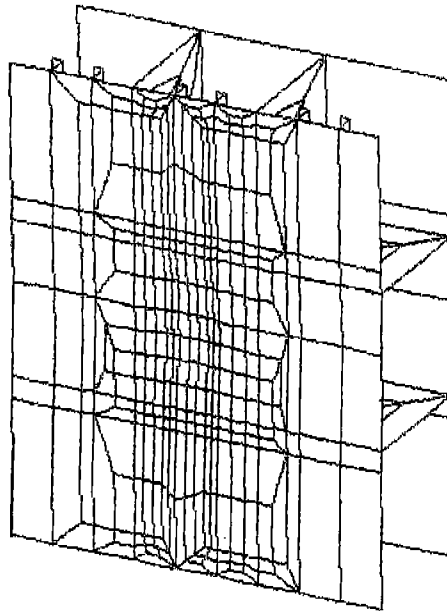
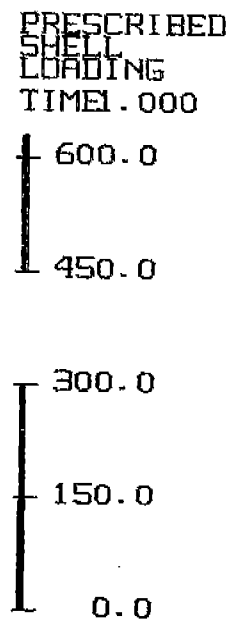
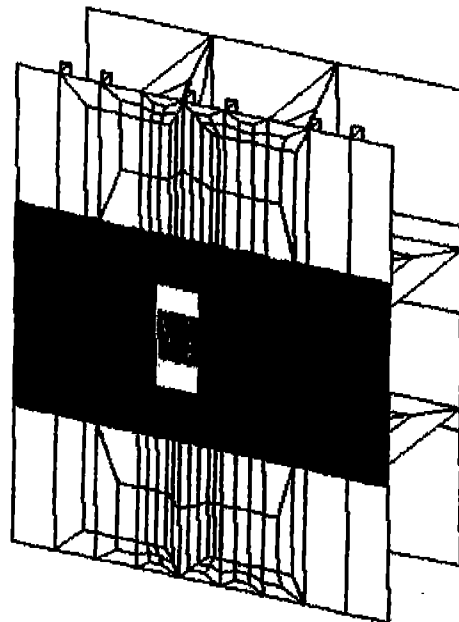
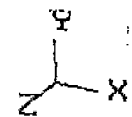


FIGURE 6.16: Progression of Yielding Through the Structure



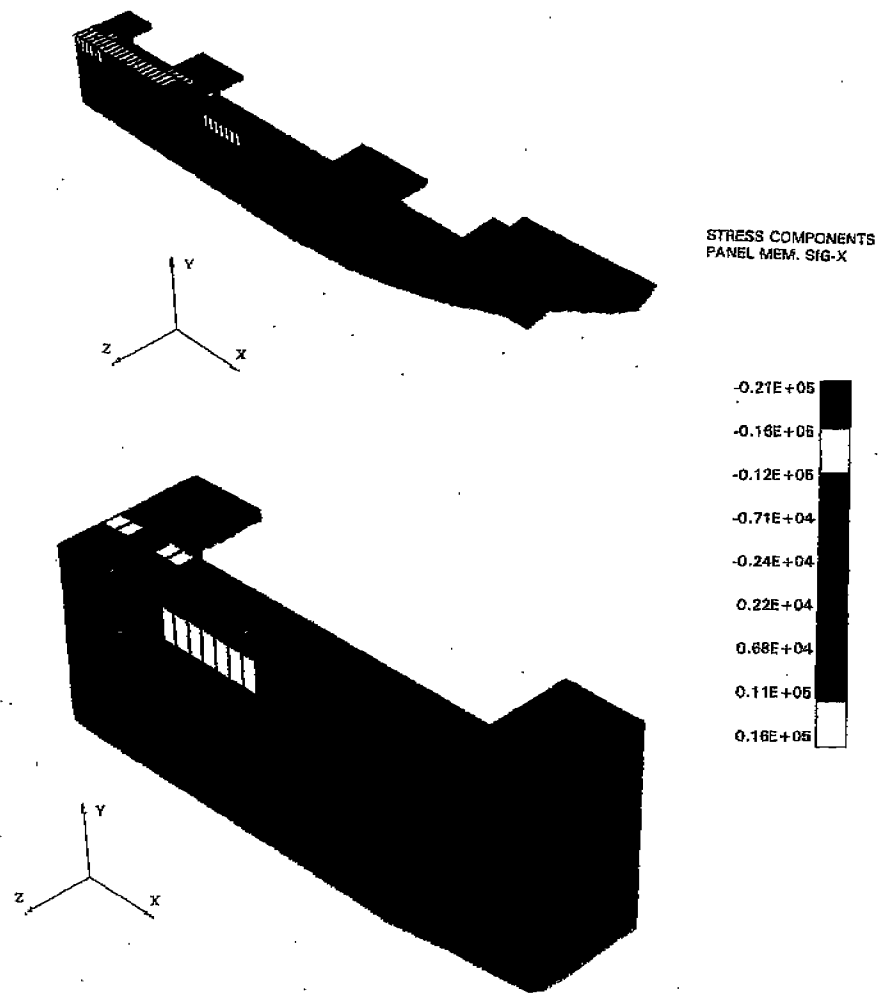
(a) Finite Element Model of Midbody



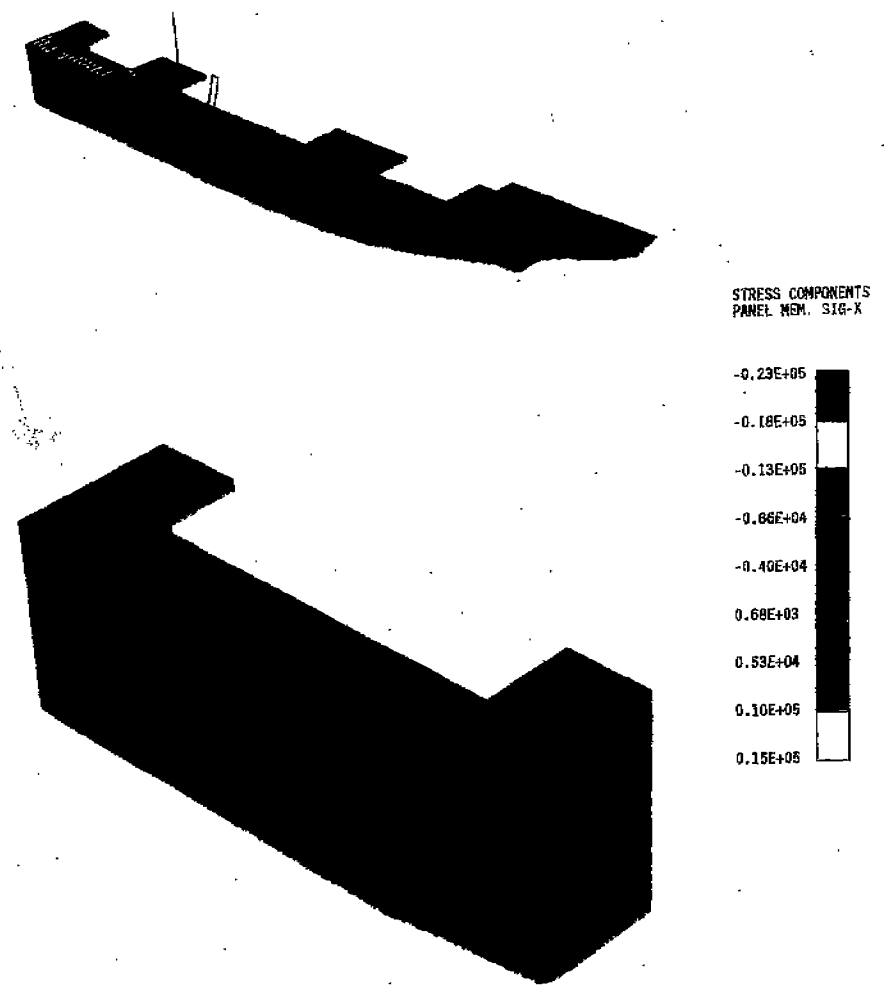
Note: Pressure is in PSI

(b) ASPPR Ice Load

FIGURE 5.9: Finite Element Model of M.V. Arctic Existing Midbody Structure Showing ASPPR Load



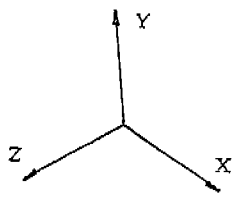
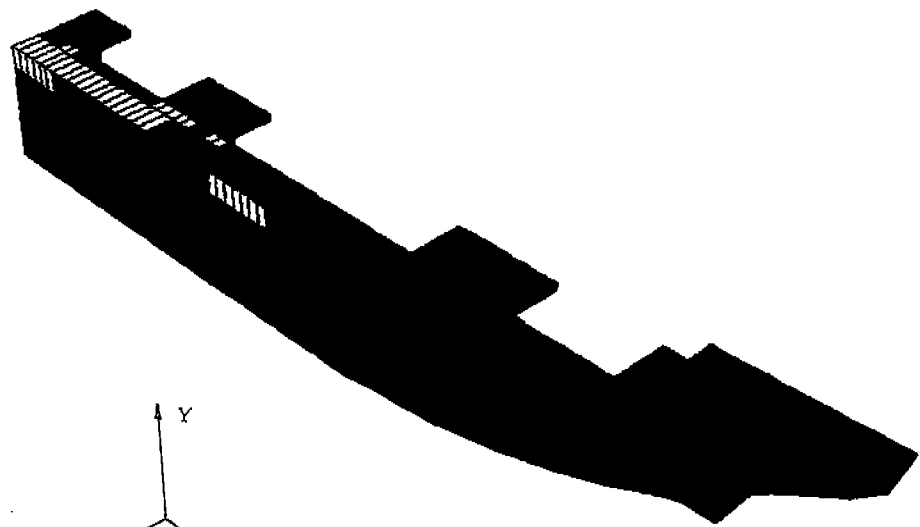
(a) Symmetric Boundary Conditions



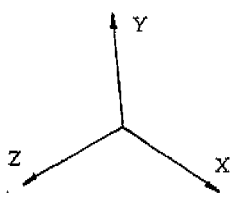
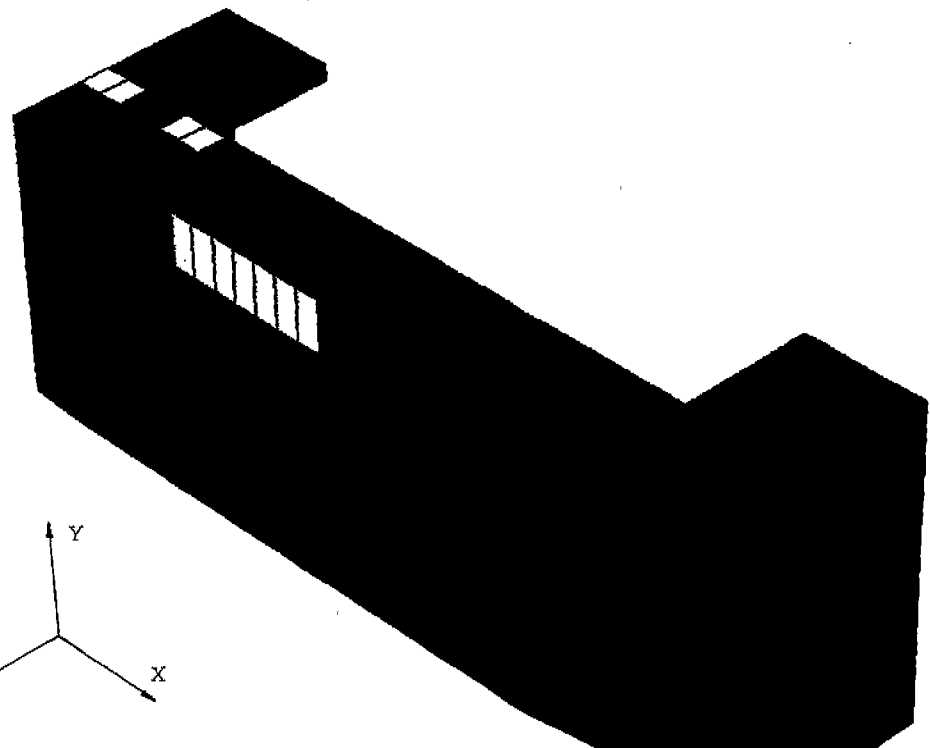
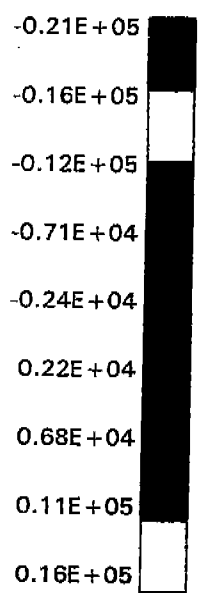
(b) Antisymmetric Boundary Conditions

FIGURE 4.6: SXX Stress Plots for Symmetric and Antisymmetric Boundary Conditions

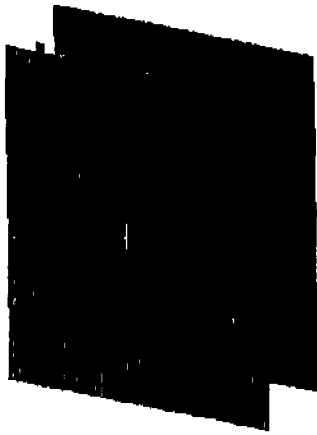
64



STRESS COMPONENTS
 PANEL MEM. SIG-X

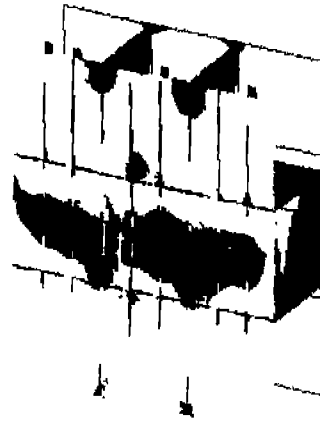


30%

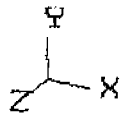


SHELL MID-SURFACE T=2.0

80%



SHELL MID-SURFACE T=4.0



STRESS-YY

16000.

8000.

0.

-8000.

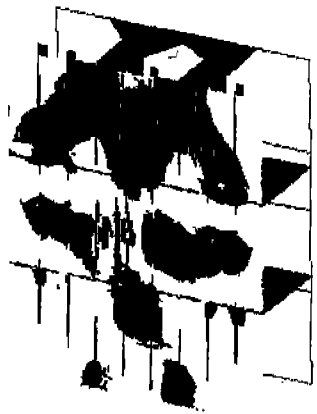
-16000.

-24000.

-32000.

-40000.

98%



SHELL MID-SURFACE T=6.0

103%



SHELL MID-SURFACE T=8.0

FIGURE 5.16: SYY Stress Distribution at Various Percentages of F_{max}
- Nonlinear Analysis of Existing Midbody FE Model

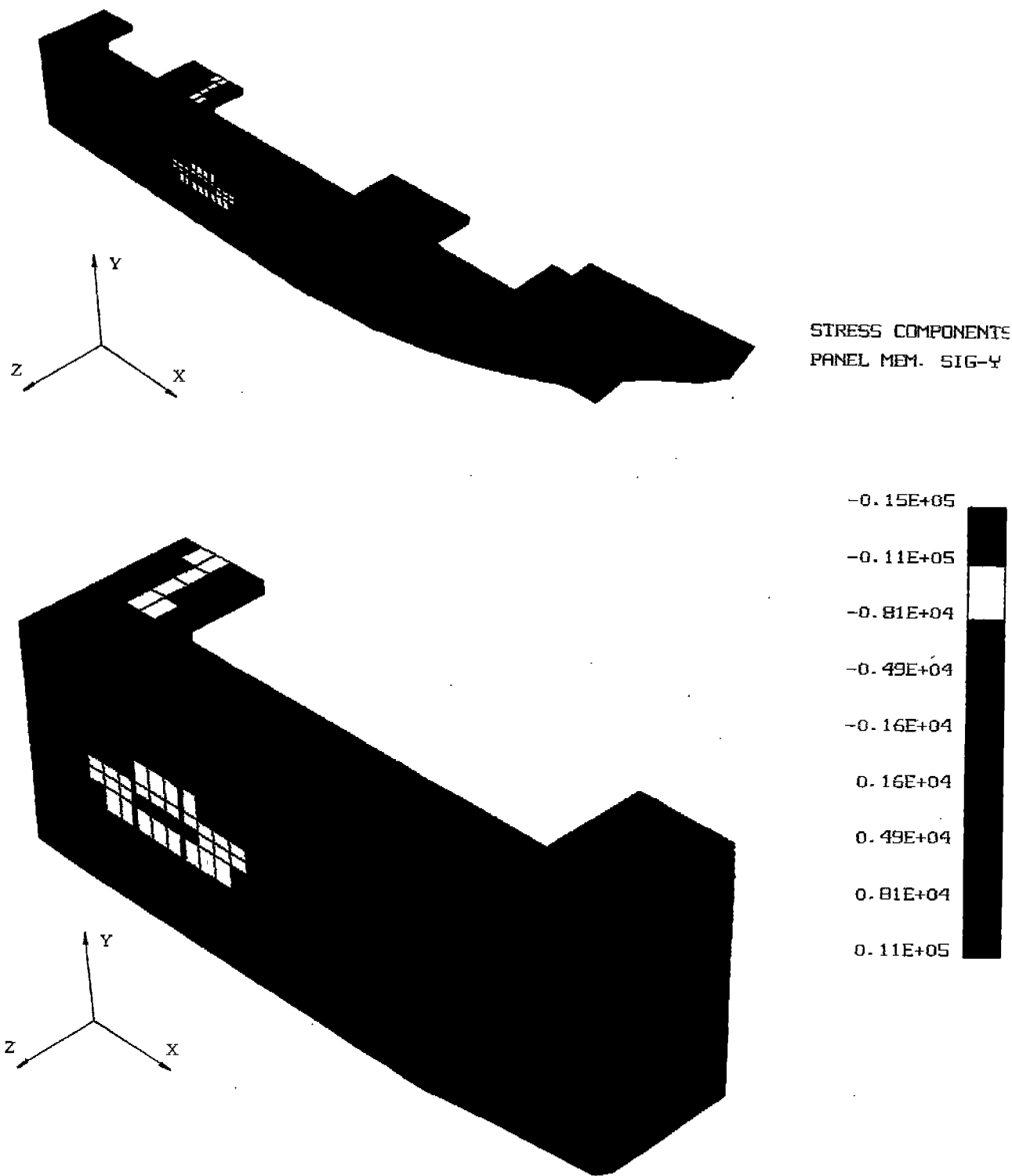
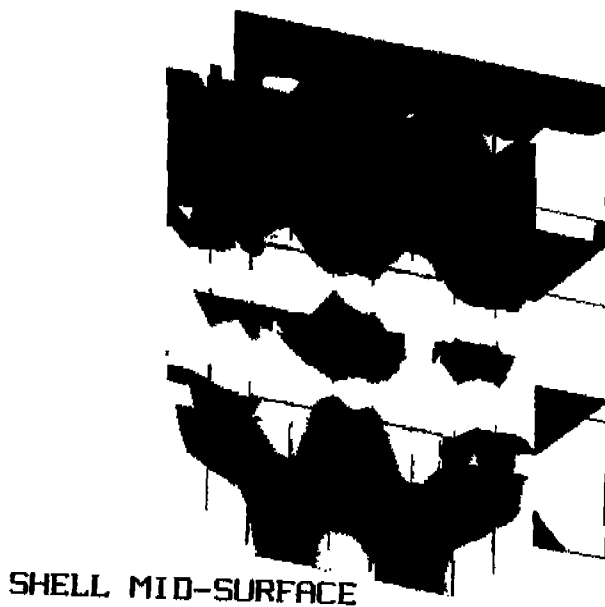


FIGURE 5.8: Transverse Stress Distribution due to Still Water Bending Moment and Ice Loads Acting at the Midbody

89



(a) SXX Stress Distribution



(b) SYY Stress Distribution

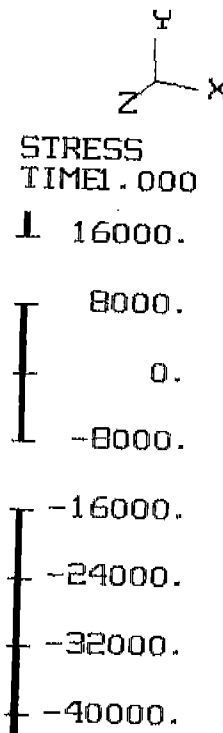


FIGURE 5.10: Stress Distribution from the Linear Analysis of the Existing Midbody FE Model

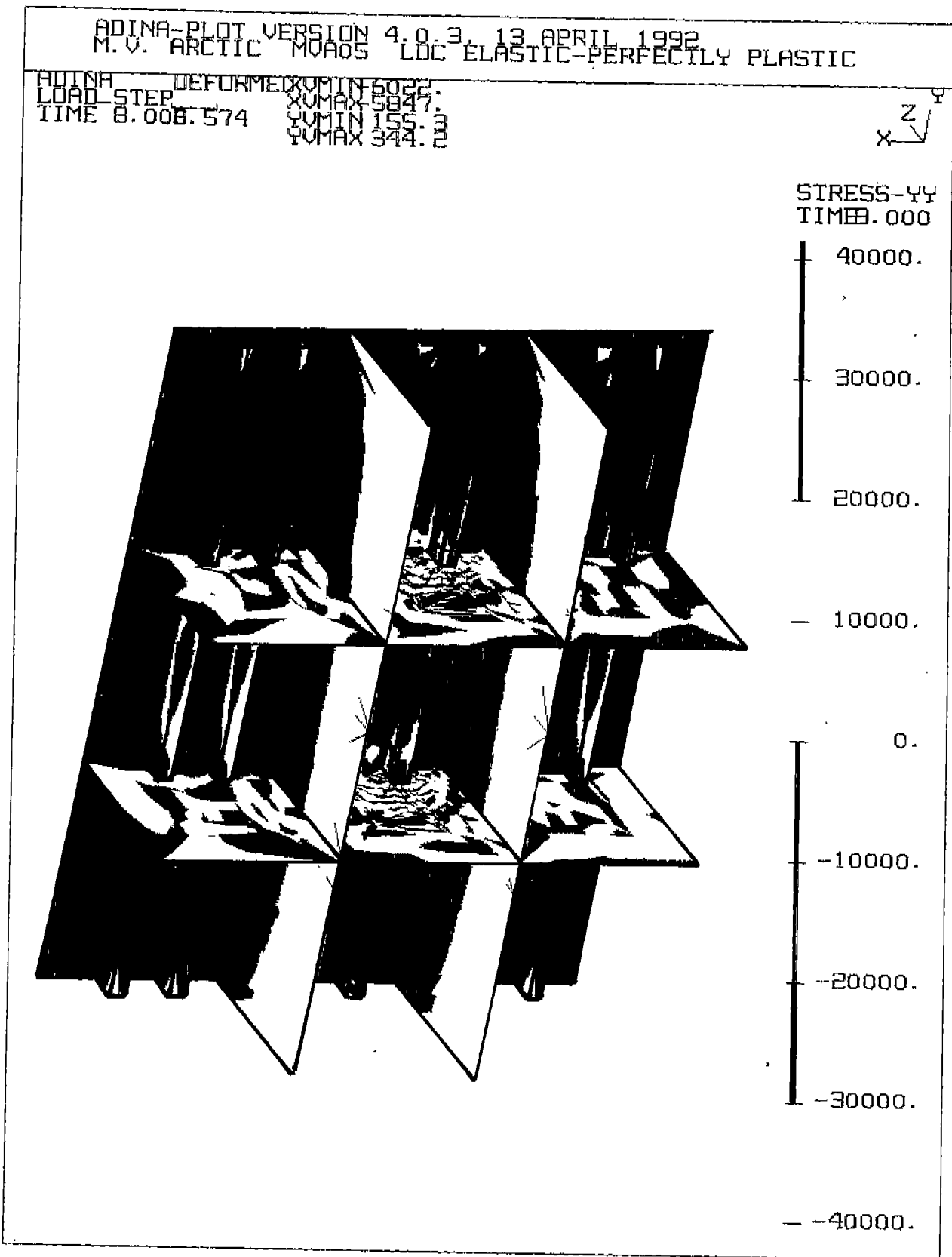
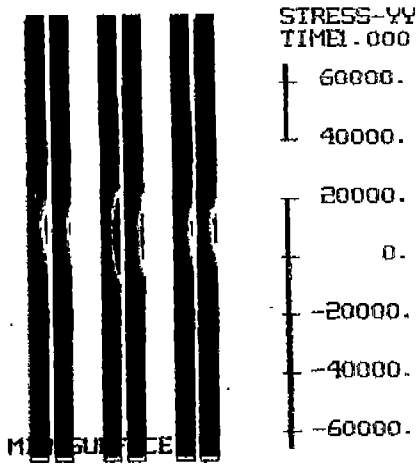


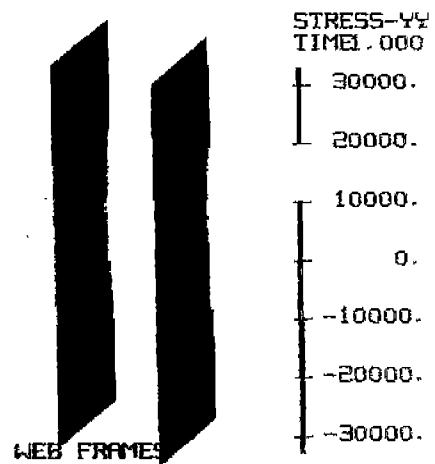
FIGURE 5.13: SYY Stress Near F_{max}
- Nonlinear Analysis of the Existing Midbody FE Model

PLIINH ORIGINAL DEFORMED Y
 LOAD STEP TIME 1.0008.39 18.39 Z X



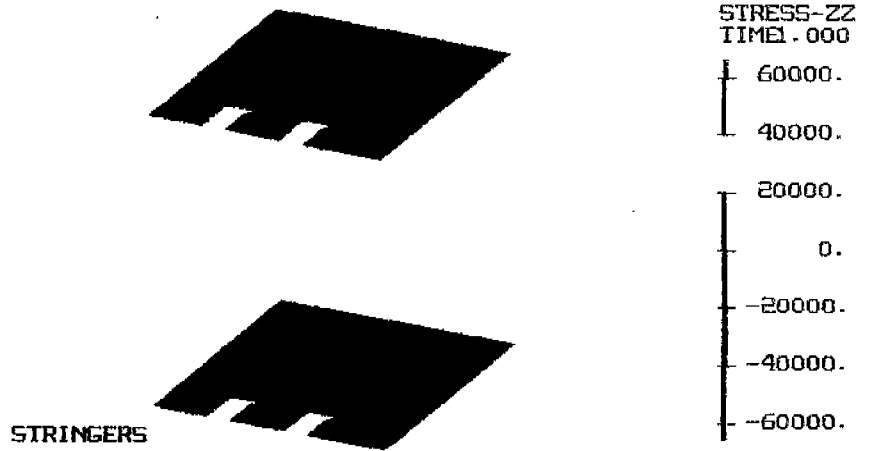
(a) SYX in Main Frames

PLIINH DEFORMED ORIGINAL Y
 LOAD STEP TIME 1.0008.918 XUMAX 58 XUMIN 90 XUMAX 70



(b) SYX in Deep Webs

PLIINH DEFORMED ORIGINAL Y
 LOAD STEP TIME 1.0008.958 XUMAX 58 XUMIN 90 XUMAX 70



(c) SZZ in Stringers

FIGURE 5.11: Scantling Stresses from the Linear Analysis of the Existing Midbody FE Model